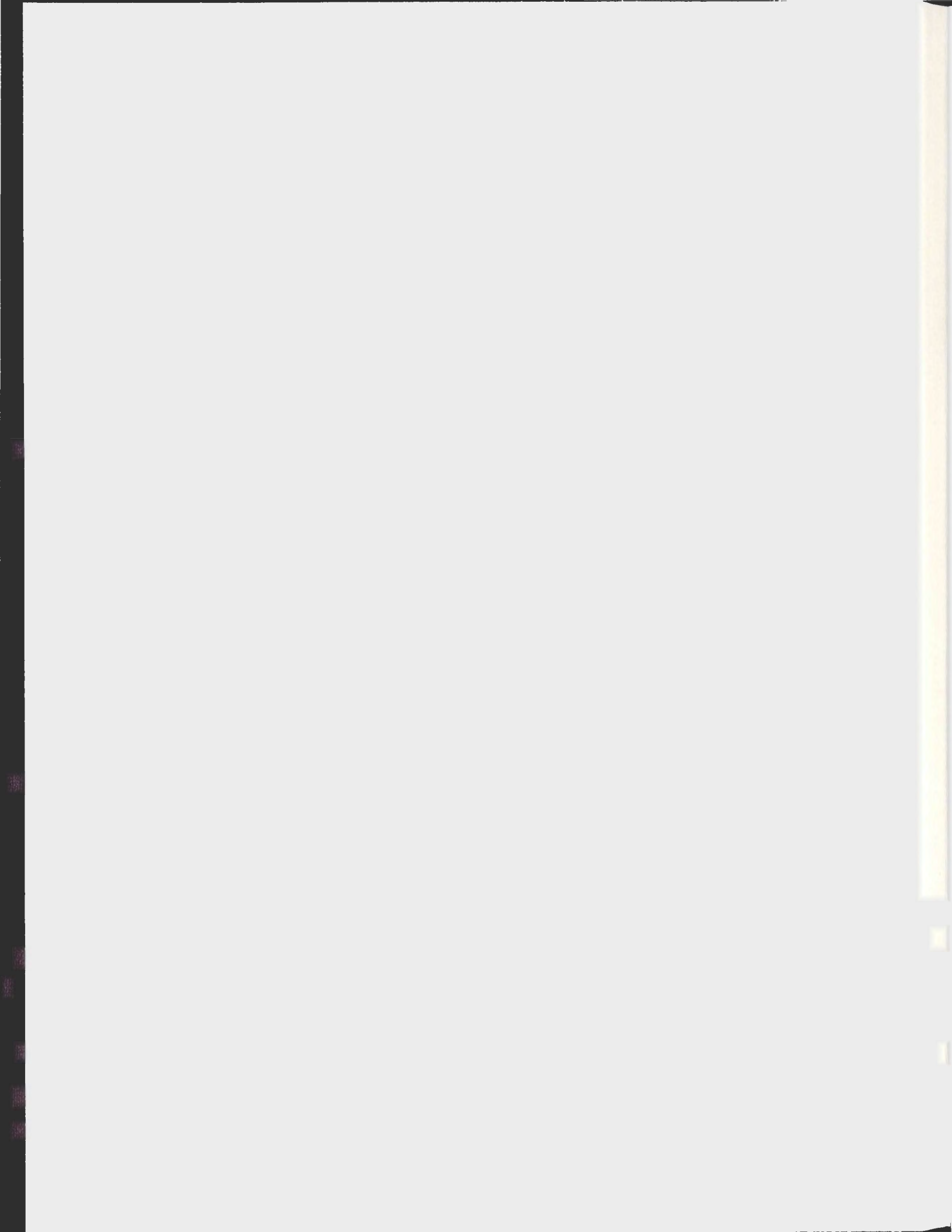


MESOZOIC TECTONIC AND STRATIGRAPHIC
EVOLUTION OF THE ORPHAN BASIN, WITH SPECIAL
EMPHASIS ON REGIONAL CORRELATIONS WITH
FLEMISH PASS AND NORTHERN JEANNE D'ARC
BASINS, GRAND BANKS OF NEWFOUNDLAND

BURCU GACAL-İŞLER



**Mesozoic Tectonic and Stratigraphic Evolution of the Orphan Basin, with Special
Emphasis on Regional Correlations with Flemish Pass and Northern Jeanne d'Arc
Basins, Grand Banks of Newfoundland**

by

Burcu Gacal-İşler

A thesis submitted to the School of Graduate Studies
in partial fulfillment of the requirements for the degree of

Master of Science

Department of Earth Sciences

Memorial University of Newfoundland

May 2009

ABSTRACT

The tectonic framework and depositional settings of the Orphan Basin are studied using ~25,000 km of 2-D seismic reflection profiles and stratigraphic data from nine key exploration wells. The evolution of the region is recorded in five seismic distinct stratigraphic units (Z, A, B, C, X), each separated from one another by widespread regional markers U1-U4, representing prominent unconformities. Exploration well data showed that Units Z, A, B, C and X are correlated with the Pre-Cambrian/Paleozoic basement, ?Triassic/Jurassic, Early Cretaceous, Late Cretaceous and Tertiary successions, respectively. Similarly, the well data showed that U1, U2, U3 and U4 markers are correlated with the Top Paleozoic, Top Jurassic, Mid-Cretaceous and Base Tertiary Unconformities, respectively. The well data further showed that the seismic Units A, B+C, and X are broadly correlated with three regional tectonic episodes, where each episode includes a period of extension, followed by a period of protracted uplift associated with sectoral break-up, and a period of sustained thermally-driven subsidence.

On the basis of stratigraphic and structural architecture of the successions imaged between the Top Paleozoic Unconformity and the Base Tertiary Unconformity, the study area is divided into five tectonic provinces: the Western and Southwestern Basin Margin, the Eastern Basin Margin, the White Sail Fault Zone, the West Basin and Ridge Province, and the East Basin. The Bonavista and White Sail Fault Zones were developed during the ?Jurassic (may be as early as Triassic if evaporates are present in the Orphan Basin), as prominent basin-bounding faults. Several large faults paralleling the White Sail Fault

Zone also developed during this time. The extensional tectonic activity continued in the study area throughout the Cretaceous, but slowly culminated in the late Cretaceous / Early Tertiary as indicated by the absence of growth strata within the Tertiary succession associated with the faults, and tip points of these faults being situated in the Early Tertiary successions.

The seismic data documents that faults in the northern and northeastern segment of the Orphan Basin display greater growth, rotation and tilting of the mid-Late Cretaceous successions than those observed in the western and southern segment of the basin. These observations together with the large fan-shaped fault splays of the White Sail Fault Zone collectively suggest that the Flemish Cap probably experienced a progressive clockwise rotation of 25°-35° during the Late Jurassic – Late Cretaceous. This rotation and extrusion of the Flemish Cap is largely accommodated by the Cumberland Belt Fault Zone in the south and the Charlie Gibbs Transfer Zone in the north.

ACKNOWLEDGEMENT

This thesis is the outcome of an amazing voyage during which I have been inspired and supported by many people. I wish to take this opportunity to express my gratitude and appreciation to those incredible individuals who have enriched my journey in several ways.

First of all, I would like to express my sincere appreciation to my supervisors, Ali E. Aksu and E. Michael Enachescu who kindly accommodated me in this project. Their great support, encouragement and advices were necessary to finish this thesis. I would like to thank Jeremy Hall and Kim Welford for their constructive discussions early in this study.

Financial support for this project was provided by Pan-Atlantic Petroleum Systems Consortium (PPSC), and Natural Sciences and Engineering Research Council of Canada (NSERC). I acknowledge contributions of data and software support from the Landmark Graphics®, the Geologic Survey of Canada – Atlantic Basin Database, the Canada Newfoundland and Labrador Offshore Petroleum Board, the Stratalog (Calgary and Alberta) and the HIS Energy.

Many thanks to Peter Bruce for his much-needed help and Dan Vasiliu and Clyde Clements for their technical support which made this project more efficient and enjoyable.

I would like further express my greatest gratitude to Ali E. Aksu, for sharing his wisdom and knowledge, for his endless assurance, never-ending enthusiasm. He is not only an excellent mentor but also a great support in my daily life. His amazing work ethic and dedication will always be admired. Without his excellent contribution and courage this thesis would not have been possible.

I would like to express my sincere thanks too to my former supervisor Cüneyt Akal (Can), for making me love research and appreciate the significance of hardwork and patience in science and lastly for being such a great friend.

All present and former colleagues and friends, our coffee breaks and lunchtime talks often helped me see things in a new light and gave me much needed energy at times when I was feeling overwhelmed. No further away than a couple of keyboard commands, a phone call or a short letter, all my Turkish friends thank you for always being there for me.

I owe my deepest gratitude to my father Hasan and mother Sabber for all the opportunities and support they have given me over the years, and for their belief in me that I could do whatever I set my mind to. This journey would have simply been impossible without you. Finally and very specially, I say thank you to my husband, Bursin, whose love, patience and support, not to forget sleepless nights have contributed to the completion of this thesis.

Table of Contents

Abstract	ii
Acknowledgements	iv
List of Figures	xii
List of Tables	xx
Chapter 1. Introduction	
1.1. Preamble	1
1.2. Regional Geological Settings	1
1.3. The Physiography of the Eastern Canadian Continental Margin	4
1.4. Geologic Evolution of the Atlantic Canadian Continental Margin	9
1.4.1. Late Triassic - Early Jurassic (Tethys Rift Stage)	15
1.4.2. Late Jurassic - Early Cretaceous (North Atlantic Rift Stage)	16
1.4.3. Aptian - Albian (Labrador Rift Stage)	17
1.4.4. Late Cretaceous - Paleocene (East Greenland Rift Stage)	18
1.5. Stratigraphy of the Jeanne d'Arc Basin	19
1.6. Thesis Objectives	33
Chapter 2. Data Set and Methodology	
2.1. Data Set	38
2.1.1. Borehole Data	38

2.1.2. Seismic Data	38
2.2. Methods	41
2.2.1. Seismic Stratigraphy	43
2.2.2. Fault Mapping	47
2.2.3. Mapping Techniques	47
2.2.4. Synthetic Seismograms	49
2.2.5. Time-Depth Conversion	50
2.3. Software Used	51
2.3.1. <i>SeisWorks</i> TM	51
2.3.2. <i>StratWorks</i> TM	51
2.3.3. <i>SynTool</i> TM	51
Chapter 3. Stratigraphy	
3.1. Exploration Well Data	53
3.1.1. Hare Bay E-21	55
3.1.2. The Baie Verte J-57	59
3.1.3. Bonavista C-99	61
3.1.4. Blue H-28	62
3.1.5. Linnet E-63	66

3.1.6. Bonanza M-71	68
3.1.7. Kyle L-11	70
3.1.8. Baccalieu I-78	73
3.1.9. Mizzen L-11	75
3.1.10. Great Barrasway F-66	77
3.2. Summary Stratigraphy across the Study Area	78
3.3 Seismic Stratigraphy	78
3.3.1 Regional Seismic Markers Representing Unconformity Surfaces	85
3.3.1.1 Unconformity - U1: surface capping Unit Z	85
3.3.1.2 Unconformity - U2: Surface Capping Unit C	90
3.3.1.3 Unconformity - U3: Surface Capping Unit B	93
3.3.1.4 Unconformity - U4: Surface Capping Unit A	100
3.3.2 Seismic Units	103
3.3.2.1 Unit Z (Paleozoic and Precambrian Basement)	103
3.3.2.2 Unit C (Jurassic / ? Late Triassic)	103
3.3.2.3 Unit B (Early Cretaceous)	107
3.3.2.4 Unit A (Late Cretaceous)	110
3.3.2.5 Unit X (Tertiary)	113

Chapter 4. Tectonic Architecture of the Study Area

4.1. Introduction	116
4.2. Western and Southwestern Basin Margin Province	116
4.3. Eastern Basin Margin Province	133
4.4. White Sail Fault Zone Province	144
4.5. West Basin and Ridge Province	158
4.5.1. Northern Portion of the West Basin and Ridge Province	160
4.5.2. Southern Portion of the West Basin and Ridge Province	179
4.6. East Basin Province	181
4.6.1. Northern Portion of East Basin Province	181
4.6.2. Central Portion of the East Basin Province	188
4.6.3. Southern Portion of the East Basin Province	197
4.7. Possible Strike-Slip Faults within the Orphan Basin	206

Chapter 5. Interpretation and Discussion

5.1. Regional Tectonic Evolution	207
5.1.1. Phase I	208
5.1.1.1. Rifting (Late Triassic – Early Jurassic)	208
5.1.1.2. Uplift and Erosion (Early Jurassic)	218

5.1.1.3. Postrift (Early Jurassic – mid-Jurassic)	220
5.1.2. Phase II	224
5.1.2.1. Rifting (Late Jurassic – Early Cretaceous)	224
5.1.2.2. Uplift and Erosion (mid-Valanginian – mid-Aptian)	226
5.1.2.3. Postrift (Early Cretaceous – Valanginian to Aptian)	229
5.1.3. Phase III	229
5.1.3.1. Rifting (mid-Cretaceous – Albian to Aptian)	229
5.1.3.2. Postrift (Late Cretaceous – Paleocene)	231
5.2. Tectonic Model of the Flemish Cap Rotation	233
5.3. Regional Paleogeography and Sedimentary Evolution	238
5.3.1 Phase I	238
5.3.1.1. Rifting (Late Triassic – Early Jurassic)	238
5.3.1.2. Uplift and erosion (Early Jurassic)	241
5.3.1.3. Postrift (Early Jurassic – mid-Jurassic)	241
5.3.2. Phase II	243
5.3.2.1. Rifting (Late Jurassic – Early Cretaceous)	243
5.3.2.2. Uplift and Erosion (mid-Valanginian – mid-Aptian)	244
5.3.2.3. Postrift (Early Cretaceous – Valanginian to Aptian)	245

5.3.3. Phase III	246
5.3.3.1. Rifting (mid-Cretaceous – Albian to Aptian)	246
5.3.3.2. Postrift (Late Cretaceous – Paleocene)	250
Chapter 6. Implications for Petroleum Systems	
6.1. Foreword	251
6.1.1. Evolution of the Petroleum System	252
6.2. Potential Reservoir Rocks in Orphan and Flemish Pass Basins	253
6.3. Types of Hydrocarbon Traps	254
6.4. Distribution and Maturity of the Source Rock	254
6.5. Recommendations for Future Work	255
Chapter 7. Conclusions	
Conclusions	258
References	263
Appendix A	285
Appendix B	289

List of Figures

Chapter 1

- Figure 1.1.** Distribution of sedimentary basins offshore Newfoundland and the inset map shows the regional framework for the Orphan Basin in relation to the Flemish Pass and Jeanne d'Arc Basins, the Orphan Knoll, and Flemish Cap.....2
- Figure 1.2.** (A) Detailed bathymetric chart of the Grand Banks of Newfoundland and (B) 3-D Block diagram of the Orphan Basin showing morphological structures of the seafloor.6
- Figure 1.3.** Appalachian tectono-stratigraphic zones within the island of Newfoundland.....11
- Figure 1.4.** Four diagrams illustrating various stages in the evolution of the northern Atlantic Ocean.....13
- Figure 1.5.** Schematic chart depicting the relationship between geological time, rifting stages, deformation style and orientation.14
- Figure 1.6.** Lithostratigraphic chart of the Jeanne d'Arc and Orphan Basins.20
- Figure 1.7.** Bathymetry map of Northern Grand Banks of Newfoundland.21
- Figure 1.8.** Generalized lithostratigraphic chart for the Upper Cretaceous and the lower part of the Paleogene stratigraphic succession in the Jeanne d'Arc Basin.31

Chapter 2

- Figure 2.1.** Basemap of the study area.....39
- Figure 2.2.** Example of GSI 2000-2003 2D seismic dip line.42
- Figure 2.3.** Schematic cross-section showing depositional sequences, sequence boundaries and typical internal reflection termination patterns.45
- Figure 2.4.** Types of reflection configurations and seismic reflection patterns of prograding clinoforms46
- Figure 2.5.** Schematic profiles and a well showing the technique used in seismic stratigraphy...48

Chapter 3

Figure 3.1. Index map showing 2D seismic profiles, locations of exploration wells drill in Orphan Basin and environs, portions of various seismic reflection profiles shown in figures in this chapter.....	54
Figure 3.2. Summary lithostratigraphic logs of exploration wells Hare Bay E-21, Baie Verte J-57 and Bonavista C-99.	56
Figure 3.3. Lithostratigraphic chart of the Jeanne d’Arc and Orphan Basins.	58
Figure 3.4. Summary lithostratigraphic logs of exploration wells Blue H-28, Linnet E-63 and Bonanza B-27.	64
Figure 3.5. Summary lithostratigraphic logs of exploration wells Kyle L-11, Baccalieu I-78 and Mizzen L-11.	71
Figure 3. 6. North to south summary lithostratigraphic correlation between nine key exploration wells in study area.	79
Figure 3.7. Regional composite seismic reflection profile A.	80
Figure 3.8. Regional composite seismic reflection profile B.	81
Figure 3.9. Regional composite seismic reflection profile C.	82
Figure 3.10. Regional composite seismic reflection profile D.	83
Figure 3.11. Regional composite seismic reflection profile E.	84
Figure 3.12. Multichannel seismic reflection profile Or0-118 showing examples of onlap, offlap, downlap and erosional truncation.	86
Figure 3.13. Multichannel seismic reflection profile showing examples of onlap, offlap, downlap and erosional truncation.	87
Figure 3.14. Time-structure map of the regional marker (unconformity) U1.	89
Figure 3.15. Multichannel seismic reflection profile Or1- 106 showing the mild truncation of the Unit C (? Triassic-Jurassic) and the gentle downlap of the overlying Unit B (Early Cretaceous) at the regional marker U2 (Cenomanian Unconformity).	91

Figure 3.16. Multichannel seismic reflection profile Or0- 118 showing the truncation of the Unit C (?Triassic-Jurassic) and the gentle downlap of the overlying Unit B (Early Cretaceous) at the regional marker U2(Cenomanian Unconformity).	92
Figure 3.17. Time-structure map of the regional marker (unconformity) U2.	94
Figure 3.18. Multichannel seismic reflection profile OR0-114 showing the convergence of regional unconformities U1 (Top Paleozoic Unconformity) and U2 (Top Jurassic-Tithonian Unconformity) over the crests of large ridges in West Orphan Basin.	95
Figure 3.19. Multichannel seismic reflection profile OR0-114 showing the apparent conformable character of the regional marker U3 (Mid-Cretaceous Unconformity) in the central portion of a basin within the eastern portion of the study area.	97
Figure 3.20. Time-structure map of the regional marker (unconformity) U3.	98
Figure 3.21. Multichannel seismic reflection profile Or0- 102 showing the convergence of regional unconformities U1(Top Paleozoic), U2(Top Jurassic) and U3(Mid-Cretaceous) over the crests of large ridges in western Orphan Basin.	99
Figure 3.22. Multichannel seismic reflection profile Or0- 106 showing the character of the regional unconformity U4 (Base Tertiary) along the eastern margin of the Orphan Basin.	101
Figure 3.23. Time-structure map of the regional marker (unconformity) U4.	102
Figure 3.24. Isopach map of Unit C (?Triassic-Jurassic) showing the thickness variations in ms twt.	106
Figure 3.25. Isopach map of Unit B (Early Cretaceous) showing the thickness variations in ms twt.	108
Figure 3.26. Isopach map of Unit A (Late Cretaceous) showing the thickness variations in ms twt.	111
Figure 3.27. Isopach map of Unit X -Tertiary (water bottom to Base Tertiary Unconformity) showing the thickness variations in ms twt.	115

Chapter 4

Figure 4.1. Location map of the study area showing major bathymetric elements in the north-central portion of the Grand Banks of Newfoundland.	117
Figure 4.2. Map of the study area, showing the distribution of five tectonic provinces.	118
Figure 4.3. Map of the study area showing the distribution of major faults.	119
Figure 4.4. Multichannel seismic reflection profile N81-140 showing the western margin of the study area.	121
Figure 4.5. Map of the Orphan Basin and surroundings, showing the locations of seismic profiles and exploration wells used in this study.	122
Figure 4.6. Multichannel seismic reflection (ORO-114) profile showing the Eastern Bounding Fault of the Bonavista Fault Zone and its splays.	123
Figure 4.7. Multichannel seismic reflection (ORO-122) profile showing the Eastern Bounding Fault and its splays of the Bonavista Fault Zone.	124
Figure 4.8. Multichannel seismic reflection (ORO-121) profile showing the western margin of the study area.	126
Figure 4.9. Map of the study area showing the distribution the basin and ridge structures.	127
Figure 4.10. Multichannel seismic reflection (ORO-101) profile showing the southwestern margin of the study area.	129
Figure 4.11. Multichannel seismic reflection (ORO-103) profile showing the southwestern margin of the study area.	130
Figure 4.12. Multichannel seismic reflection (ORO-117) profile showing the southwestern margin of the study area.	131
Figure 4.13. Multichannel seismic reflection (OR0-114) profile showing the eastern margin of the study area.	134
Figure 4.14. Multichannel seismic reflection (OR0-106) profile showing the northeastern margin of study area.	135

Figure 4.15. Multichannel seismic reflection (OR0-118) profile showing the northeastern margin of study area.	137
Figure 4.16. Multichannel seismic reflection (OR0-114) profile showing the northeastern margin of study area.	138
Figure 4.17. Multichannel seismic reflection (OR0-120) profile showing the northeastern margin of study area.	141
Figure 4.18. Multichannel seismic reflection (FP99-1040) profile showing the northeastern margin of study area.	142
Figure 4.19. Multichannel seismic reflection (FP99-1100) profile showing the well-developed tilted and rotated fault blocks bounded by major faults N4 and N5.	143
Figure 4.20. Multichannel seismic reflection (OR0-102) profile showing a significant growth at the Mid-Cretaceous Marker.	145
Figure 4.21. Multichannel seismic reflection (OR0-104) profile showing two major listric faults; TF1 and TF2 and their synthetic and antithetic splays.	146
Figure 4.22. Multichannel seismic reflection (OR0-114) profile defining a prominent ridge morphology/structure is delineated by two fault pairs/groups with opposite sense of dip.	150
Figure 4.23. Multichannel seismic reflection (OR0-118) profile showing the well imaged fault zone which shows the TF1 fault appears to sole into the TF2 fault at depth.	151
Figure 4.24. Multichannel seismic reflection (OR0-124) profile demonstrates key components in the central portion of the White Sail Fault Zone.	154
Figure 4.25. Multichannel seismic reflection (OR2-109) profile showing the major faults of the White Sail Fault Zone and their synthetic and antithetic minor faults.	155
Figure 4.26. Multichannel seismic reflection (OR0-111) profile showing the solitary continuation of the imbricate fault fan as a normal-sense extensional fault.	157
Figure 4.27. The isopach map (in milliseconds twt) of the total Mesozoic strata.	159
Figure 4.28. Multichannel seismic reflection (OR0-106) profile showing northern part of the West Basin and Ridge Province.	161

Figure 4.29. Multichannel seismic reflection (OR0- 114) profile showing the major structures of the northern part of the West Basin and Ridge Province.	162
Figure 4.30. Multichannel seismic reflection (OR0-122) profile showing the structures of the central part of the West Basin and Ridge Province.	163
Figure 4.31. Multichannel seismic reflection (OR0-118) profile showing Ridge R2 and its intervening basin a2.	166
Figure 4.32. Multichannel seismic reflection (OR0-124) profile showing the prominent ridge R4 and major depocenter basin a4.	173
Figure 4.33. Multichannel seismic reflection (ORO-110) profile showing the subbasin a4a...175	
Figure 4.34. Multichannel seismic reflection (OR0-112) profile showing an asymmetrical subbasins a4b anda4a and their western boundary ridges R5 and R6.....	176
Figure 4.35. Multichannel seismic reflection (OR0-132) profile showing the southern part of the West Basin and Ridge Province.	180
Figure 4.36. Multichannel seismic reflection (OR0-136) profile showing the southernmost part of the West Basin and Ridge Province.	182
Figure 4.37. Multichannel seismic reflection (OR1-108) profile showing the prominent structures of the northern portion of the East Basin Province.	183
Figure 4.38. Blow-up of multichannel seismic reflection (OR1-108) profile showing the architecture of ridges R8 and R9, and their relationship to faults F10 and F11.	185
Figure 4.39. Multichannel seismic reflection (OR1-106) profile showing the prominent basin a10 and ridge R10.....	187
Figure 4.40. Multichannel seismic reflection (OR1-110A) profile showing basin a10.....	189
Figure 4.41. Multichannel seismic reflection (OR2-108) profile showing the central part of the East Basin Province.	190
Figure 4.42. Multichannel seismic reflection (OR1-120) profile showing major ridge R11, and depocenter a13 of the East Basin Province.	193

Figure 4.43. Multichannel seismic reflection (OR1-120) profile showing major depocenter basin a10 of the East Basin Province.	196
Figure 4.44. Multichannel seismic reflection (OR0-122) profile showing ridge R6 that defines the eastern margin of the White sail Fault Zone, the major depocenter basin a13 and ridge R11 in the East Basin Province.	199
Figure 4.45. Multichannel seismic reflection (OR0-122) profile showing major basins a10 and a11 and ridges R8 and R12 in the East Basin Province.	201
Figure 4.46. Multichannel seismic reflection (OR0-118) profile showing major basin a11 and ridges R12 and R13 in the East Basin and the East Basin Margin Provinces.	203
Figure 4.47. Multichannel seismic reflection (OR0-1128) profile showing the prominent fault fan situated at the southeastermost corner of the Orphan Basin.	205
 Chapter 5	
Figure 5.1. Schematic cross sections showing (A) the structure of the conjugate Grand Banks–Galicia margin pair. (B) regional seismic reflection profile C, across the Orphan and Flemish Pass basins.	209
Figure 5.2. Depth converted regional composite seismic reflection profile A.	214
Figure 5.3. Depth converted regional composite seismic reflection profile B.	215
Figure 5.4. A) The schematic structural model showing the presence of two crustal scale, sinistral, strike-slip transfer zones, Cumberland Belt Transfer Zone and Charlie Gibbs Transform Zone, B) The angular relations between structures.	217
Figure 5.5. Depth converted regional composite seismic reflection profile C.	221
Figure 5.6. Depth converted regional composite seismic reflection profile D.	222
Figure 5.7. Depth converted regional composite seismic reflection profile E.	223
Figure 5.8. Multichannel seismic reflection (OR0-102) profile showing growth.....	227
Figure 5.9. Multichannel seismic reflection (OR0-104) profile showing growth.....	228
Figure 5.10. Schematic reconstruction model of the separation of the Flemish Cap from Orphan Basin.....	234

Figure 5.11. A. Paleogeographic maps of the north Atlantic East Coast Margin.....239
Figure 5.11.B,C. Paleogeographic maps of the north Atlantic East Coast Margin.....240
Figure 5.11.D,E. Paleogeographic maps of the north Atlantic East Coast Margin.....249

List of Tables

Table 2.1. Summary table of the wells showing the location, datum and total depth information.....40

CHAPTER 1. INTRODUCTION

1.1. Preamble

The primary purpose of this thesis is to construct a stratigraphic, chronological and tectonic framework of the Mesozoic sediments in the Orphan Basin which will allow (i) the correlation of regional unconformities between the Orphan, Jeanne d'Arc and Flemish Pass Basins and (ii) the determination of temporal and spatial changes in seismic stratigraphic units within the context of evolving structures so that the petroleum systems throughout the region (the Orphan, Flemish Pass and Jeanne d'Arc Basins) can be better understood.

1.2. Regional Geological Settings

The Orphan Basin is situated on the eastern Canadian continental margin, north of the Grand Banks of Newfoundland and west of Orphan Knoll (Fig. 1.1). The Orphan Knoll is a fragment of continental crust which is a large fault-bounded block detached from North Atlantic during continental rifting (Keen and Beaumont, 1990; Fig. 1.1). The Orphan Basin covers ~160 000 km², and includes the shelf in the west (200-500 m water depth), the upper slope in the center (500-1500 m water depth) and the lower slope in the east (1500-3000 m water depth). It is bounded to the east by the continental-oceanic crust boundary, to the west by the Bonavista Peninsula, to the north by the Charlie Gibbs Transform Zone and to the south by the Cumberland Belt Transfer Zone (Fig. 1.1; Smee, 2003; Enachescu et al. 2005).

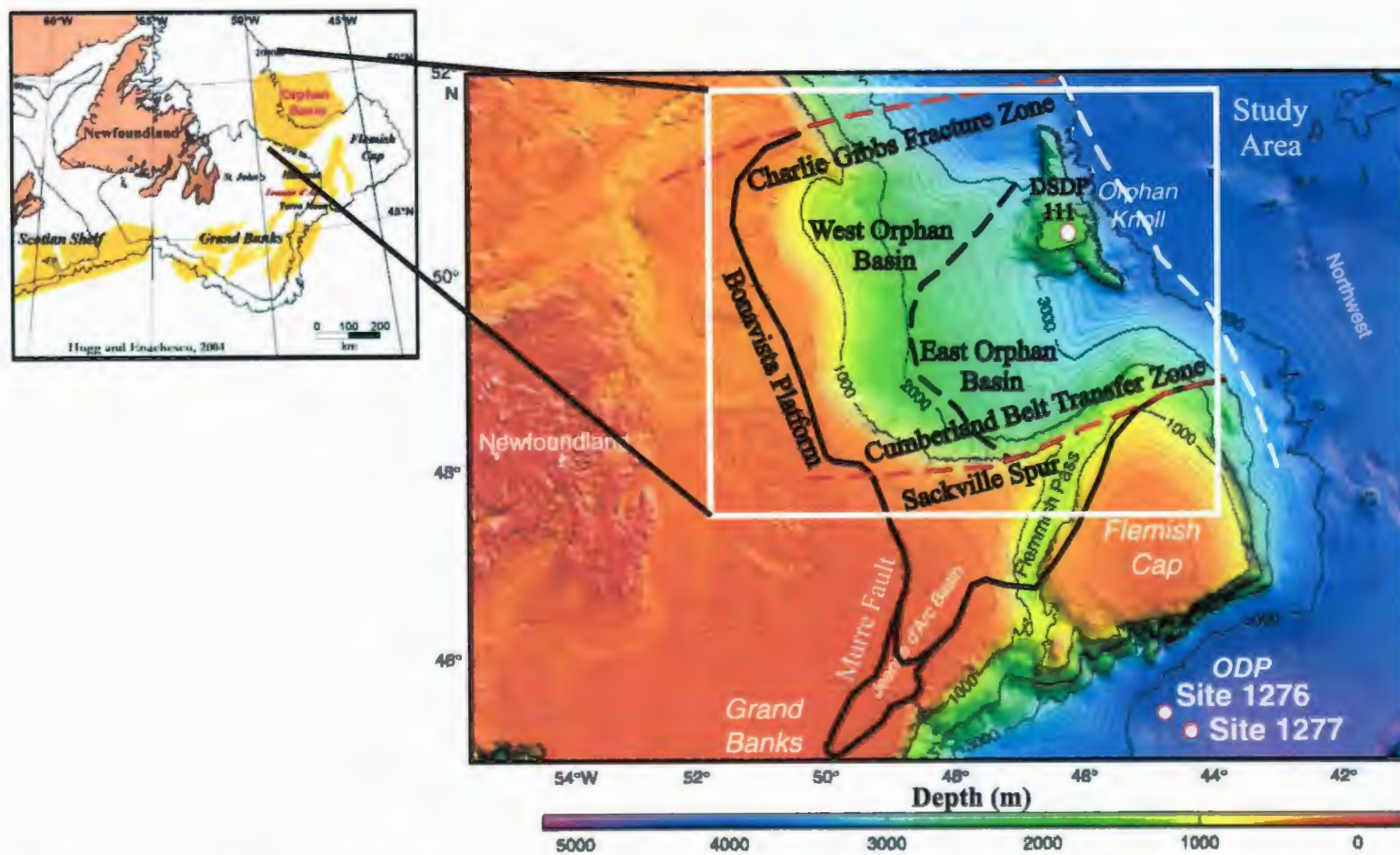


Figure 1.1. Distribution of sedimentary basins offshore Newfoundland (modified from Enachescu and Hogg, 2004). Inset map shows the regional framework for the Orphan Basin in relation to the Flemish Pass and Jeanne d'Arc Basins, the Orphan Knoll, and Flemish Cap. Tectonic Framework from Enachescu et al., 2004. Bathymetry and ODP, DSDP sites from Tucholke et al., 2004. Water depth is in meters.

The Orphan Basin lies along the Atlantic-type rifted margin and it is one of the intra-continental rift basins formed during the Mesozoic within the Pangea supercontinent (Tankard and Welsink, 1989; Keen et al., 1990). The pre-rift Precambrian metamorphic basement and the Paleozoic platform deposits are related to the Appalachian Orogeny (Enachescu et al., 2005). During the Mesozoic multi-episode rift phases, synrift sedimentary rocks were highly faulted in response to extensional stresses. Following the rifting phases, rapid subsidence caused the basin to become deeper (Srivastava, 1978; Keen et al., 1987; Grant and McAlpine, 1990; Smee et al., 2003; Enachescu et al., 2004a, and b). During the Tertiary and Quaternary the region was covered by a moderately thick veneer of clastic deposits which were notably thinner in the east. The rifted region of the Orphan Basin can be divided into two morpho-tectonic domains (1) the East Orphan Basin and (2) the West Orphan Basin (Fig. 1.1; Enachescu et al., 2005). The eastern part of the Orphan Basin is deeper (1500-3000 m) and was initially formed during the Late Triassic-Early Jurassic rift stage whereas, the eastern and western parts of the West Orphan Basin evolved during the Late Jurassic -Early Cretaceous and mid-Cretaceous, respectively (Enachescu et al., 2005)

The Flemish Pass Basin is a north trending bathymetric trough located east of the Jeanne d'Arc Basin (DeSilva, 2000). It is separated from the Orphan Basin by the Cumberland Belt Transfer Zone, which is positioned approximately on the northern Flemish Cap-Sackville Spur bathymetric lineament (Fig. 1.1; Enachescu, 1987; Enachescu et al., 2005). The Jeanne d'Arc Basin covers more than 10,000 km² and is bounded in the west by the Murre and Mercury Faults, and in the east by the Voyager

Fault. The basin is divided into two segments by the Egret Fault (Fig. 1.1; Enachescu, 1987; Deptuck 2003). Salt tectonism played an important role in modifying basin structure and deforming the Late Cretaceous and Tertiary strata (Enachescu, 1987 and 1988; Tankard and Welsink, 1987; Grant and Mc Alpine, 1990; Deptuck, 2003).

Because of its common Late Jurassic-Early Cretaceous tectonic history with the Jeanne d'Arc Basin, the Flemish Pass and the Porcupine Basins (western offshore Ireland), the Orphan Basin attracted recent exploration interest (Enachescu et al., 2005). As new hydrocarbon discoveries are made in deep basin environments, the Orphan Basin is becoming a region of interest for the oil and gas industry. As a consequence, the basin is densely covered by multi-channel seismic 2D and 3D surveys, one deep exploration well was drilled in 2006 and several wells are planned for its eastern part.

This thesis aims to correlate several older exploration wells drilled during an earlier exploration phase (Koning et al., 1988) with a large, modern 2-D reflection seismic grid. The thesis further aims to correlate seismic sequences from the Orphan Basin, the Flemish Pass and Jeanne d'Arc Basins so that the Mesozoic successions in the region can be better understood.

1.3. The Physiography of the Eastern Canadian Continental Margin

The eastern Canadian continental margin is defined by four large morphological elements: the continental shelf, the slope, the rise and the abyssal plain.

The Laurentian Channel defines the border between the Scotian shelf and the southeast Newfoundland shelf. The southeastern part of the Newfoundland shelf is dominated by the Grand Banks of Newfoundland which includes a series of shallow banks, 25-100 m -deep, such as the St. Pierre, Green and Whale Banks. The Grand Banks of Newfoundland covers an area $\sim 280,000 \text{ km}^2$ and is separated from the Island of Newfoundland by the Avalon Channel (Fig. 1.2.A.). The Flemish Cap is located east of the Grand Banks of Newfoundland. The Flemish Pass ($>1000\text{m}$ deep) separates the Flemish Cap from the Grand Banks of Newfoundland. The Northeast Newfoundland shelf is 190-200 km wide, but contains a considerably deeper zone. The morphology of the shelf ($< 200 \text{ m}$ water depth) is dominated by 1) the two large banks, 200-400 m deep the Belle Isle and Funk Island Banks, and 2) three prominent, 200-400 m-deep transverse troughs, called the Marginal Channel, the Notre Dame Channel and the Trinity Trough (Warren, 1976; Shaw, 2006). The morphology of the inner Labrador shelf is characterized by a deep shore-parallel trough, the Labrador Marginal Trough, and several transverse troughs and also deep channels (Fig. 1.2.A). The outer shelf includes shallow banks, such as the Hamilton, Harrison, Nain and Saglek Banks (Grant, 1972).

Around the Grand Banks, the shelf break is 200 m deep; however on the Tail of the Banks it is as shallow as 80 m (Piper, 2005). The shelf break is cut back by several large canyon heads (Piper, 2005). From southern Flemish Pass northward to the Orphan Basin, the shelf break increases up to 300-350 m. On the Labrador Margin, the shelf-slope break occurs at about 300 m water depth, but it is approximately 400-500 m

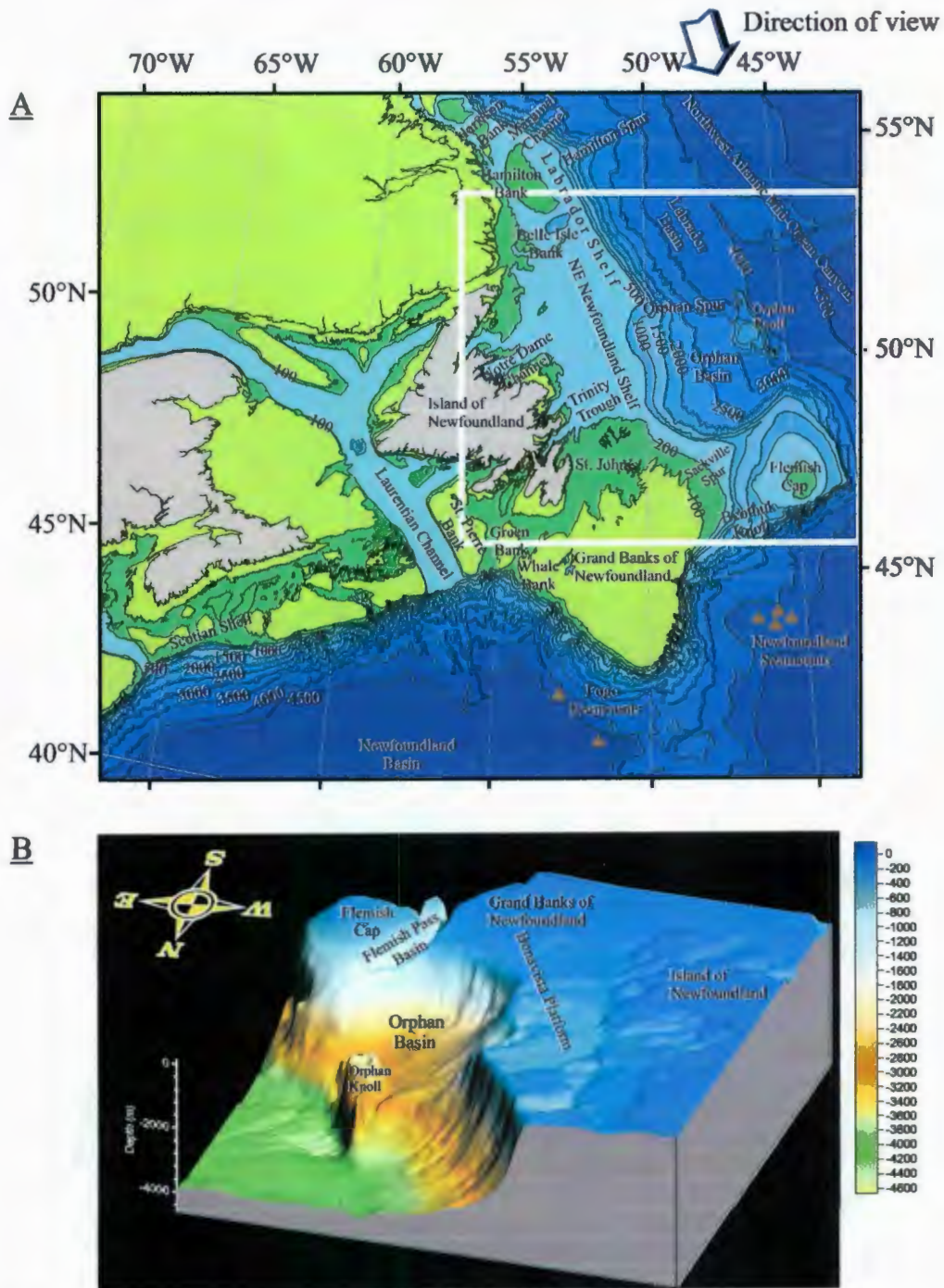


Figure 1.2. (A) Detailed bathymetric chart of the Grand Banks of Newfoundland (after King et al., 2001). (B) 3-D Block diagram of the Orphan Basin showing morphological structures of the seafloor. Vertical exaggeration is 2 times. White box represent the location of 3-D block diagram. Brown triangles show the location of seamounts.

deep at the mouth of transverse troughs and transverse channels (Fig. 1.2.A; e.g., off Hudson Strait; Hesse, 1992).

The slope of the Grand Banks of Newfoundland is dissected by numerous submarine canyons and channels, which have been the main transporting agent of sediments across the slope and rise (Fig. 1.2.A; Piper, 2005). The seabed morphology of the southernmost of the Flemish Cap, around the Beothuk Knoll, shows the undulations associated with current controlled deposition/erosion (Fig. 1.2.A; Grant, 1972). The northwest Flemish Cap is bordered by the Sackville Spur (Kennard et al. 1990) which is the one of the three major sediment drifts on the continental slope associated with Late Tertiary bottom current activity. The other two are the Hamilton Spur and Orphan Spur. These drifts have been formed in regions where there is a sudden drop in the velocity of the south-flowing Western Boundary Undercurrent along the Canadian eastern continental margin (Myers and Piper 1988; Piper, 2005). The Orphan Basin is situated between the Sackville Spur, Trinity Trough, Flemish Cap and the high block named Orphan Knoll (Fig. 1.2.A, B). The seabed morphology of the Orphan Basin is relatively flat, with undissected gentle slopes leading towards the abyssal depth between Orphan Knoll and Flemish Cap (Fig. 1.2.A, B). Water circulation in the Orphan Basin is dominated by two south-flowing currents: the deeper Western Boundary Undercurrent and the surface Labrador Current. The Labrador Current hugs the Orphan Basin slope at 300-700 m water depth (Swallow and Worthington, 1969; Aksu and Hiscott, 1992). The Western Boundary Undercurrent flows over the remainder of the slope and rise. Between

the Orphan Spur and Hamilton Spur the continental slope has a relatively undissected morphology, but the northern parts of the slope becomes progressively more dissected by submarine canyons and channels, feeding submarine fans. (Fig. 1.2.A).

The rise along the eastern Canadian continental margin is generally influenced by processes on the adjacent slope. The continental rise around the Grand Banks of Newfoundland to the northeast Flemish Cap has a generally less dissected morphology (>2400-2600 m deep) than the continental slope, and includes several seamounts (Fig. 1.2.A; e.g. Fogo and Newfoundland Seamounts). The northeast Flemish Cap has a dissected morphology (Fig. 1.2.A, B). Smooth continental rise of northern Flemish Cap gently slopes towards the eastern Orphan Basin (Fig 1.2.B). The Orphan Basin has smooth rise (2500-3000 m) morphology except for the undulations around the Orphan Knoll. The Orphan Knoll has a shallower rise in the southern (<1800 m) and northern parts (<2400 m) and suddenly deepens to the abyssal plain (4000 m) side in the northeast parts (Fig. 1.2.A, B). The Northeast Newfoundland continental rise can be divided into two parts: the southeastern part covers the Orphan Basin rise, the Orphan Knoll and the Flemish Cap rise and has a smooth morphology, whereas the northwestern part that includes the southern Labrador Basin displays a dissected morphology with numerous submarine canyons and channels (Fig. 1.2.A). North of the Hamilton Spur, the continental rise has increasingly dissected seabed morphology because several channels are cutting the rise. The rise leads into the Northwest Atlantic Mid-Ocean Canyon.

The Newfoundland Basin extends ~ 200 km to the southeast from the Grand Banks continental slope. The water depth ranges from 2000 to 5000 m (Tucholke et al.,

1989). The Northwest Atlantic Mid-Ocean Canyon is 3800 km long and plays a very prominent role in the abyssal plains morphology and sediment transportation. This channel starts from Hudson Strait through the Labrador Sea to the northern part of the Sohm Abyssal Plain (Fig. 1.2.A; Chough and Hesse, 1976 and 1980).

1.4. Geologic Evolution of the Atlantic Canadian Continental Margin

The development of the Atlantic Canada can be best explained within the context of the Wilson Cycle of ocean opening and closing. The region covers two collisional orogens, a modern continental margin and the North Atlantic Ocean which is still in the opening stage of the last cycle (Williams, 2003).

The Paleozoic and Precambrian tectonic evolution of the North Atlantic Ocean was preceded by early Paleozoic Iapetus (proto-Atlantic) and Neoproterozoic Uranus (proto-Iapetus) oceans whose cycles led to the generation of the collisional Appalachian (600-300 Myr) and Grenville (1300-950 Myr) orogenies, respectively (Williams et al., 1999). The closing of Uranus Ocean and Grenvillian Orogeny resulted in the assembly of the Neoproterozoic supercontinent Rodinia (McMenamin and McMenamin, 1990; Williams et al., 1999). The closing of the Iapetus Ocean, known as an Appalachian Orogeny led to the assembly of the Pangea, a late Paleozoic supercontinent (Williams, 2003). The North Atlantic Ocean developed in the middle of the supercontinent Pangea which began to rifted apart ~200 Ma ago (Williams et al., 1999, Loudon, 2002). The Appalachian Orogen formed associated with the closure of the Iapetus Ocean and resulted the juxtaposition of the Laurentian and Gondwanan borderlands in a series of successive

events (Fig. 1.3; Williams 1979, 1995; Williams and Hatcher 1983; Chian et al., 1998). The island of Newfoundland and its adjacent offshore areas represent five tectono-stratigraphic zones : the Humber, Dunnage, Gander, Avalon and Meguma Zones (Fig., 1.3; Williams et al., 1999). The Humber Zone shows a record of the opening and closing phases of the Iapetus Ocean and the vestiges of the Laurentian continent (Williams, 1979; Keen et al., 1990; Chian et al., 1998). The Dunnage Zone represents the remnants of the Iapetus oceanic crust and the Gander and Avalon terranes represent the Gondwana and Avalonia margins (Williams 1979; Chian et al., 1998). The Dunnage Zone is divided into the Notre Dame, the Exploits and the Dashwoods subzones, with the Red Indian Line representing a major terrain boundary between the Exploits and Notre Dame subzones (Fig., 1.3; Williams et al., 1988).

The assembling of these terrains occurred after two major tectonic events. The first event is the collision of the Humber Zone continental margin and the Dunnage Zone oceanic rocks (Fig. 1.3). During this event, the Dunnage and Gander Zones were also active with southeastward transport of oceanic crust and mantle (Williams, 2003). The Avalon Zone and its interaction with western zones (Fig. 1.3; e.g. Gander Zone) resulted in the development of subvertical strike-slip faults known as the Dover and Hermitage Bay Faults (Stockmal and Waldran, 1990; Williams, 2003; van der Velden et al., 2004).

The margin on the east coast of Newfoundland and Labrador consists entirely of Precambrian age basement rocks (Keen et al., 1990). The Mesozoic and Cenozoic sediments onlap, or are deposited in fault bounded basins developed within the Paleozoic

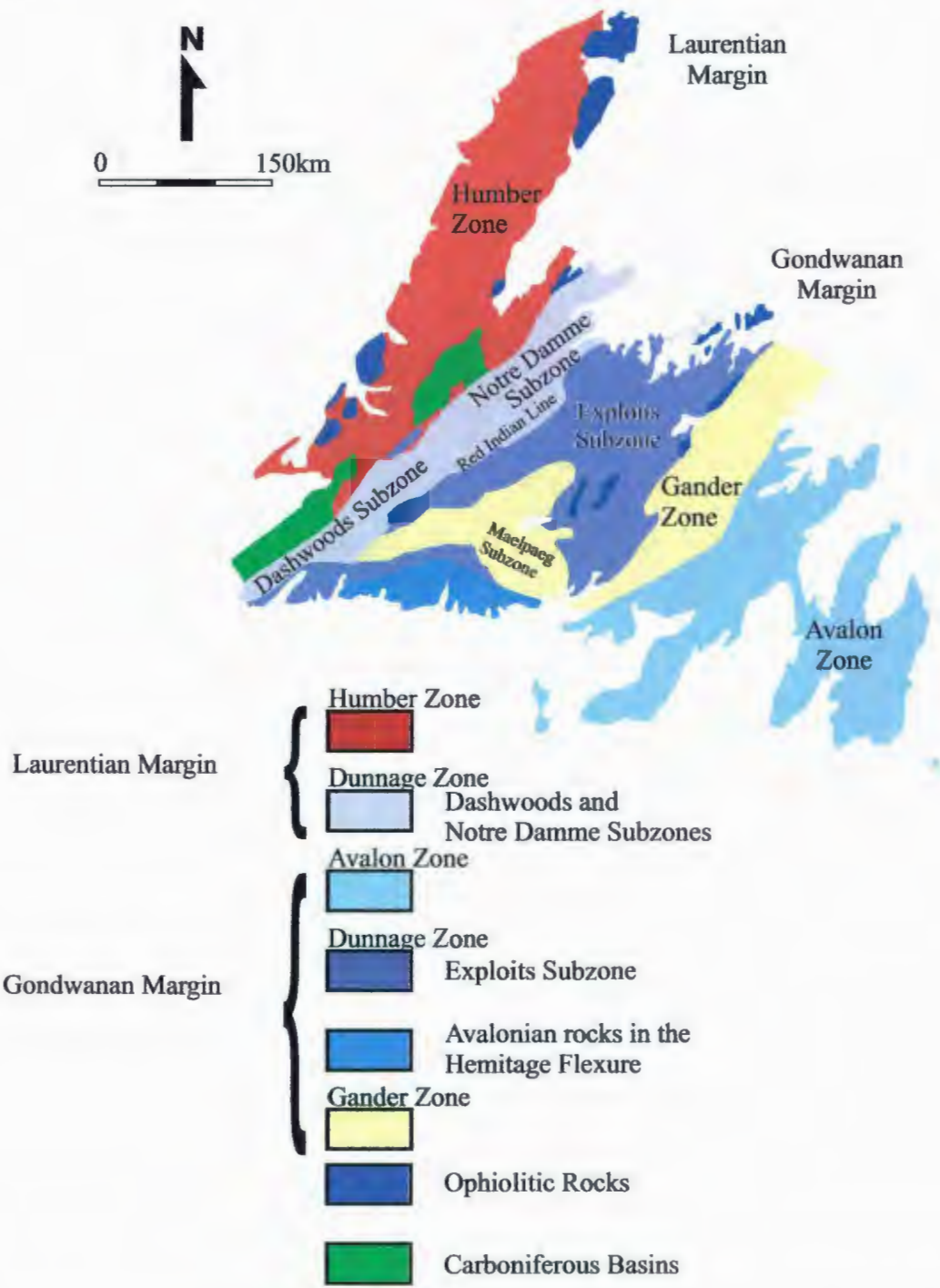


Figure 1.3. Appalachian tectono-stratigraphic zones within the island of Newfoundland (modified from Williams et al., 1988).

and Precambrian rocks of the Appalachian orogen and crystalline rocks of the Canadian Shield (Grant and McAlpine, 1990).

The Mesozoic extension is generally influenced by two distinct styles of tectonism: 1) the Avalon-Meguma terrain arcuate boundary is reactivated and reflected in left-lateral shear basins such as Fundy and Whale Basins and 2) the deformation of half graben by dip-slip extension occurred when old structures became reactivated within the interior of these terrains, such as the Scotian, Jeanne d'Arc and Orphan Basins (Tankard and Welsink, 1989). However, some of these faults intersect the older Appalachian structural grain (eg; the Mercury and Bonavista Faults; Enachescu, 1988, 1992).

The Atlantic Canadian continental margin developed during four main rift stages: 1) Late Triassic-Early Jurassic (Tethys rift stage); 2) Late Jurassic-Early Cretaceous (North Atlantic rift stage); 3) Aptian-Albian (Labrador rift stage) and 4) Late Cretaceous-Paleocene (east Greenland rift stage; Figs., 1.4, 1.5; Enachescu, 1987; Tankard and Welsink, 1987; Sinclair, 1988; Grant and McAlpine, 1990; Enachescu et al., 2005). During each rifting stage the crust underwent stretching, followed by northerly progressing continental break-up and separation which included extension, resulting in horizontal displacement of continental crust via normal listric faults, vertical tectonics, resulting in uplift and subsidence of the crust, and northerly propagating sea floor spreading and emplacement of oceanic crust (Fig. 1.5; Falvey, 1974; McKenzie, 1978; Falvey and Middleton, 1981; Bally, 1983; Deptuck, 2003; Enachescu et al., 2005). During repeated phases of rifting, the continental crust and the lithosphere thinned and

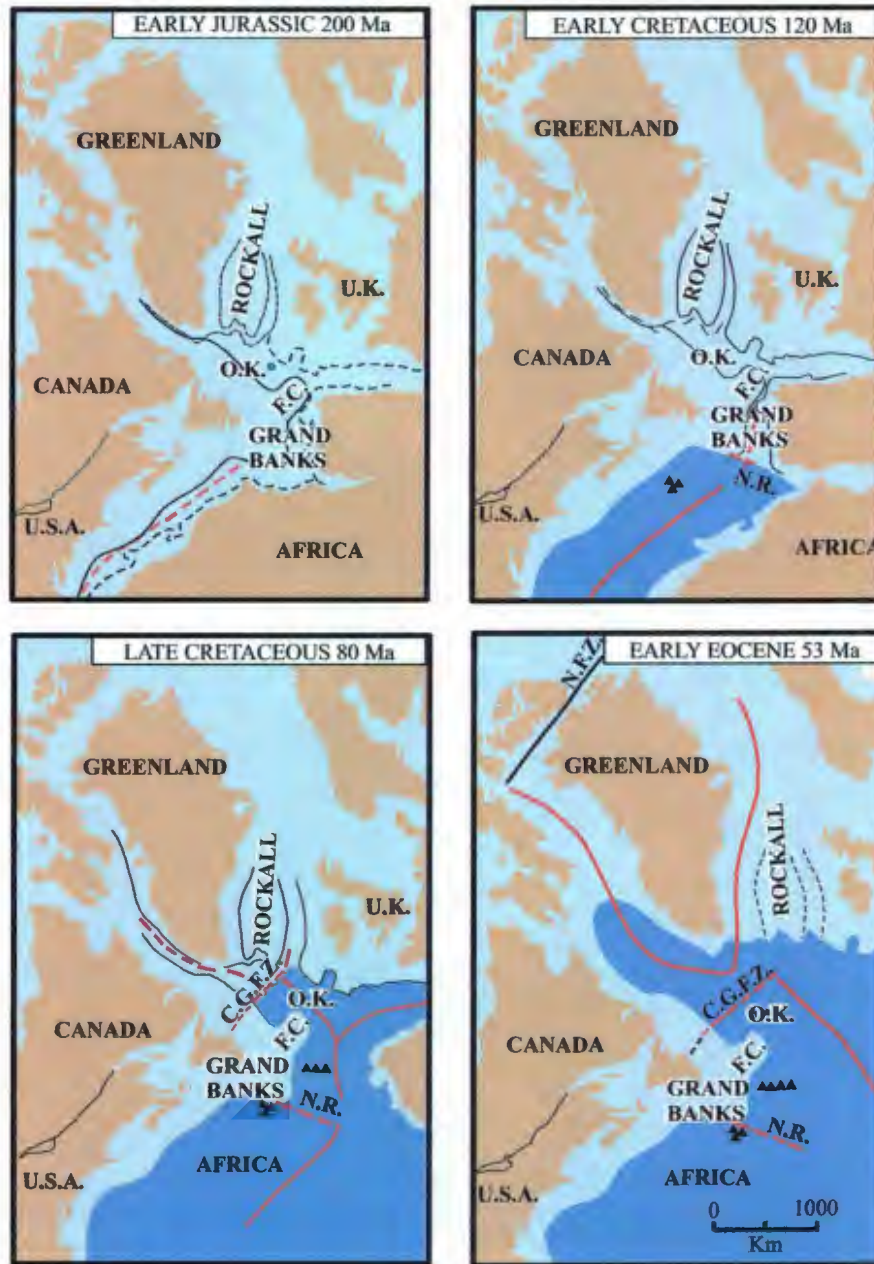


Figure 1.4. Four diagrams illustrating various stages in the evolution of the northern Atlantic Ocean (from Keen and Beaumont, 1990). Dark blue color represents oceanic crust. Dashed red lines represents fracture zones. Continuous red lines represent active spreading centers (mid-ocean ridge). O.K. Orphan Knoll; F.C. Flemish Cap; N.R. Newfoundland Fracture Zone; C.G.F.Z. Charlie Gibbs Fracture Zone. Triangles are seamounts.

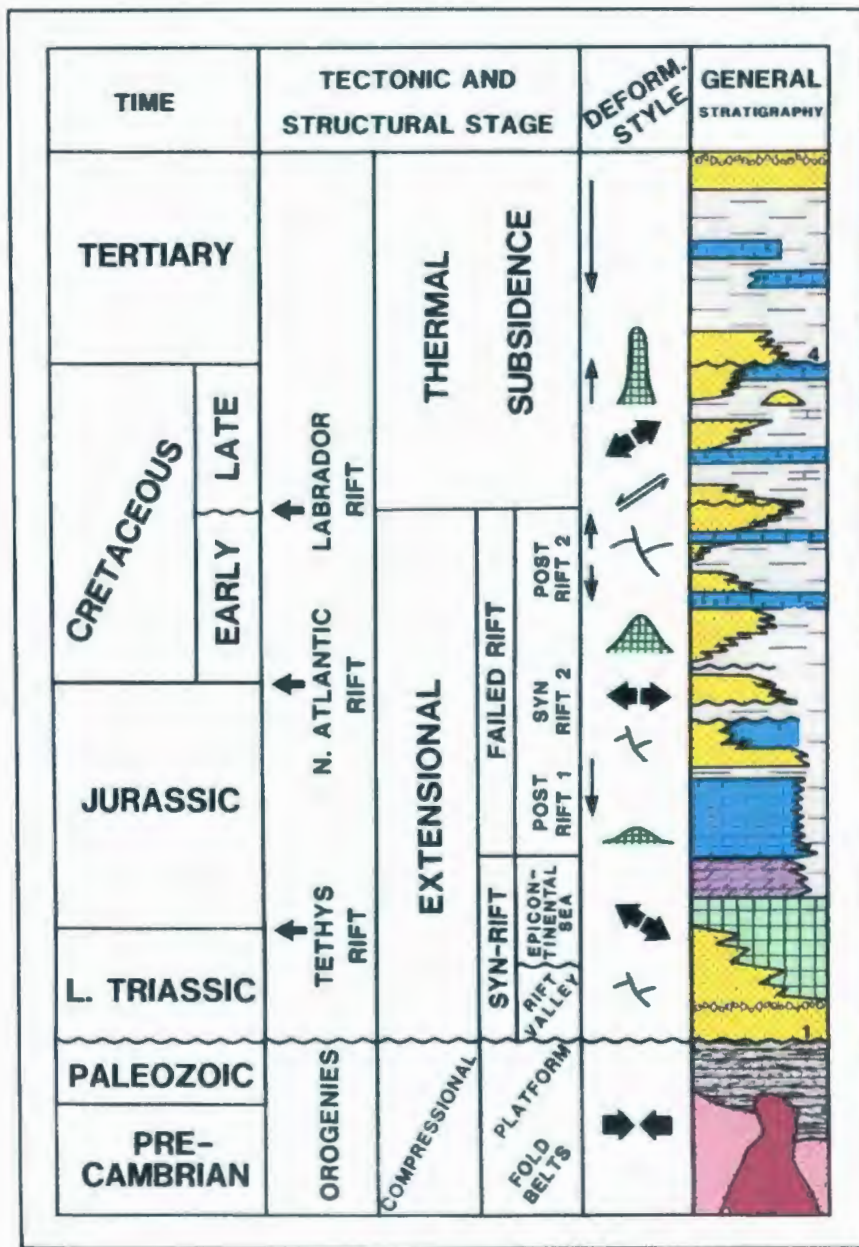


Figure 1.5. Schematic chart depicting the relationship between geological time, rifting stages, deformation style and orientation. Also shown is the simplified stratigraphy for the offshore Newfoundland continental margin. Modified from Enachescu (1987).

heated, which subsequently cooled down and subsided to form a complex set of divergent margin basins (Enachescu, 1987; Louden, 2002). The development of the Atlantic continental margin is also characterized by four periods of subsidence and two main periods of regional inversion caused by the rotation of the extensional vector (e.g. Enachescu, 1987; Tankard and Welsink, 1989; Grant and McAlpine, 1990; Sinclair, 1995; Louden, 2002; Enachescu, et al., 2005).

1.4.1. Late Triassic - Early Jurassic (Tethys Rift Stage – Scotian Margin/ Northern Africa):

The evolution of the North Atlantic Ocean began with the intra-continental Late Triassic rifting resulting in the formation of rift basins from Florida to the Grand Banks and continuing to Northwest Europe (Fig. 1.4; Enachescu, 1987 and 1988; Tankard and Balkwill, 1989). The extension in the Scotian margin was oriented NW-SE and resulted in a series of fault-controlled half graben and basement ridges. At this stage, while the West Orphan Basin was still an elevated part of the continent, the east side of the basin began to form simultaneously with the formation of the Jeanne d'Arc and Flemish Pass Basins. The East Orphan Basin was therefore connected to the Grand Banks basins to the south and Porcupine Basin to the north and also was bordered landward by the basin bounding fault identified as the White Sail Fault zone (Enachescu et al., 2005). During the Late Triassic - Early Jurassic, synrift subsidence led to the deposition of red beds and evaporites (Chadwick, 1985b; Enachescu 1986 and 1987; Tankard and Welsink, 1987; Grant et al., 1988; Wilson et al., 1989; Hiscott et al., 1990; Louden, 2002).

During the mid-Jurassic, the African and North American continental margins began to separate between Nova Scotia and Morocco, thus the central North Atlantic Ocean began to form (Fig. 1.4; Enachescu et al., 2005). To the north, the Grand Banks of Newfoundland only experienced epeirogenic subsidence until the Late Jurassic, as the rifting phase was aborted in the north beyond the Newfoundland Fracture Zone (Enachescu, 1988; Grant and McAlpine, 1990). During the thermal subsidence stage following the Tethys rifting shallow marine shales and limestones were deposited in the extensional basins of the Newfoundland margin.

1.4.2. Late Jurassic - Early Cretaceous (North Atlantic Rift Stage – Western Grand Banks/ Iberia):

Following a prolonged thermal subsidence, the second phase of rifting developed during the Late Jurassic - Early Cretaceous, with continental stretching focused between Newfoundland-Iberia and northwestern Europe (Fig. 1.4). The orientation of the extensional vector progressively rotated from an initial NW-SE direction to an E-W direction, causing transtensional movements of the earlier faults (Enachescu et al., 2005). The earlier formed basins were enlarged and some of them were reshaped with transfer faults and inversion (Enachescu, 1987; Sinclair, 1988; Enachescu et al., 2005).

During the second rifting phase, the Grand Banks of Newfoundland and the East Orphan Basin were tectonically active, received coarse clastic sediments and continued to deepen. Basins along the European margin, such as the Porcupine and Rockall Basins, were still connected to the North Atlantic Margin. A Kimmeridgian shallow sea

developed extending from the southern Grand Banks into northern Europe where the organic-rich shales were deposited (Smee et al., 2003; Enachescu et al., 2004 a, b, c, and 2005). Arms of this sea possibly stretched to the northwest into the proto-Labrador Sea rift (Sonderholm et al., 2003; Enachescu et al., 2005).

1.4.3. Aptian - Albian (Labrador Rift Stage – Greenland/Labrador and Northeast Newfoundland Shelf/ Northwestern Europe)

The separation between the Grand Banks of Newfoundland and Iberia started in the Berriasian, continued in the Albian and lasted into the Aptian with the detachment of the Flemish Cap from the Galicia Bank (Fig. 1.4; Enachescu et al., 2005). In the Early Cretaceous, a prominent triple junction developed northeast of the Flemish Cap, with arms extending toward the south separating the Grand Banks from Iberia, toward the east into the Bay of Biscay and toward the northwest (Sibuet et al., 2007; Enachescu et al., 2005). The Orphan Basin was still active during this rifting stage and was exposed to extension and minor transtension (Enachescu et al., 2005). The rifting of the East Orphan Basin continued but the principal extension moved westward of the White Sail Fault Zone. Intense rifting in the West Orphan Basin created a series of parallel ridges and troughs. Orphan Basin deepened during the subsequent thermal subsidence phase. At the end of the Albian, the Orphan Basin started to separate from its Irish conjugate basins (Fig. 1.4). Extension continued throughout the early Late Cretaceous, when the West Orphan Basin was still connected to the newly formed Labrador basins (Enachescu et al., 2005). At the end of this stage, final continental crust break up took place around the

Grand Banks of Newfoundland, associated with regional uplift and the onset of continental drift. After the regional inversion, marked by a major Albian/Aptian (Mid-Cretaceous or Avalon) unconformity, the Labrador stage rifting was terminated (Koning et al., 1988; Enachescu et al., 2005).

1.4.4. Late Cretaceous –Paleocene (East Greenland Rift Stage Labrador/Greenland and Greenland/ Northern Europe)

During the Late Cretaceous and early Tertiary the separation of Labrador from Greenland, and of Greenland from northern Europe was accompanied by extensive volcanism along west Greenland (Louden, 2002). During the Late Cretaceous, seafloor spreading in the Labrador Sea started in its southern part and then moved to the north in the Early Eocene. The seafloor spreading ended in the Late Eocene (Fig. 1.4; Louden, 2002; Enachescu, 2006).

During the rifting and drifting processes, the western parts of the West Orphan Basin were still tectonically active. Extension and transtensional deformation reactivated the basin troughs and ridges until approximately the Paleocene (Enachescu et al., 2005). The continuation of basin movements and development of block rotation were possibly induced by strike-slip activity on the northern Charlie Gibbs transfer fault and Dover Fault during the Paleocene (Enachescu et al., 2004c and 2005). After the ceasing of rifting in the Early Tertiary, the Orphan Basin and its bathymetric highs such as Orphan Knoll experienced rapid subsidence (Enachescu et al., 2005).

1.5. Stratigraphy of the Jeanne d'Arc Basin

The Jeanne d'Arc Basin is one of several fault-bounded basins located in the Grand Banks of Newfoundland. The sedimentation in the basin was associated with multiple rifting phases during the Mesozoic. The stratigraphic framework is based on results from exploration wells and seismic sequence studies (Jansa and Wade, 1975; Enachescu, 1986, 1987, 1988; Sinclair, 1988; Tankard and Welsink, 1987, 1988, 1989; Tankard and Balkwill, 1989; Hiscott et al., 1990; Grant and McAlpine, 1990; McAlpine, 1990; Deptuck, 2003). The formal lithostratigraphy is summarized below.

The Eurydice Formation consists of reddish siltstones and shales containing scattered anhydrite nodules and rare feldspathic sandstones (Fig. 1.6; Jansa and Wade, 1975). The red clastics of the Eurydice Formation are approximately 98-185 m thick in the southwestern portion of the Jeanne d'Arc Basin. The upper boundary of this formation is the base of the Osprey or Argo formations. Because the evaporites and associated siliciclastics of the Osprey and Argo formations are absent in some wells (Figs. 1.6, 1.7; e.g., Murre G-67), the Eurydice Formation is in places unconformably overlain by the Iroquois Formation (McAlpine, 1990).

The Osprey Formation includes halite rich evaporite sequence interbedded with reddish shale. The formation also contains minor dolomitic mudstones, siltstone and rare sandstone beds (Fig. 1.6). Due to the presence of argillaceous impurities, the color of the halite is often pinkish (Jansa et al., 1977; McAlpine, 1990). The Osprey Formation is 882 m thick. The red shales of the Eurydice Formation commonly interfinger with the

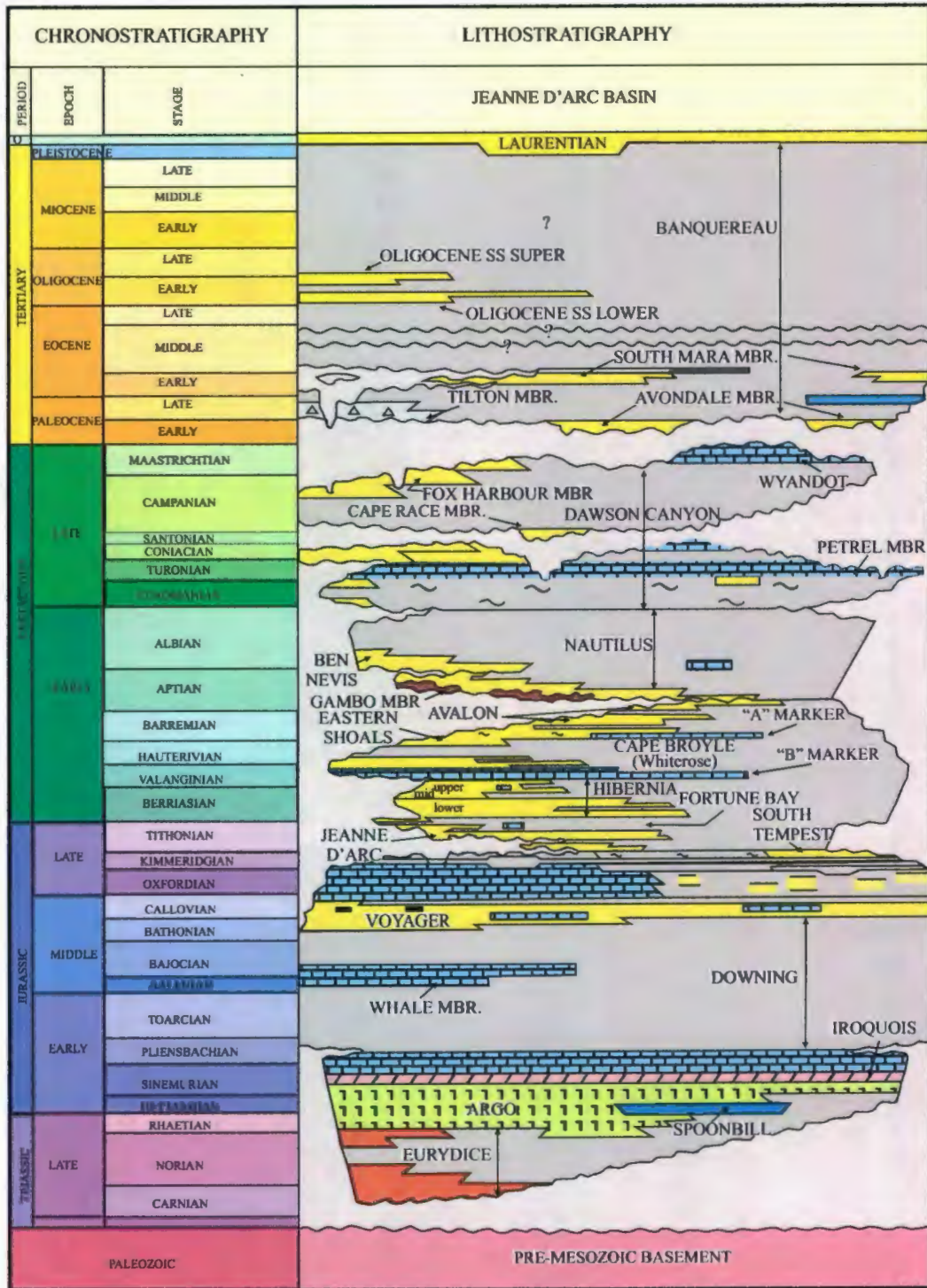


Figure 1.6. Lithostratigraphic chart of the Jeanne d'Arc and Orphan Basins (modified after Sinclair (1988) and C-NLOPB (2003)).

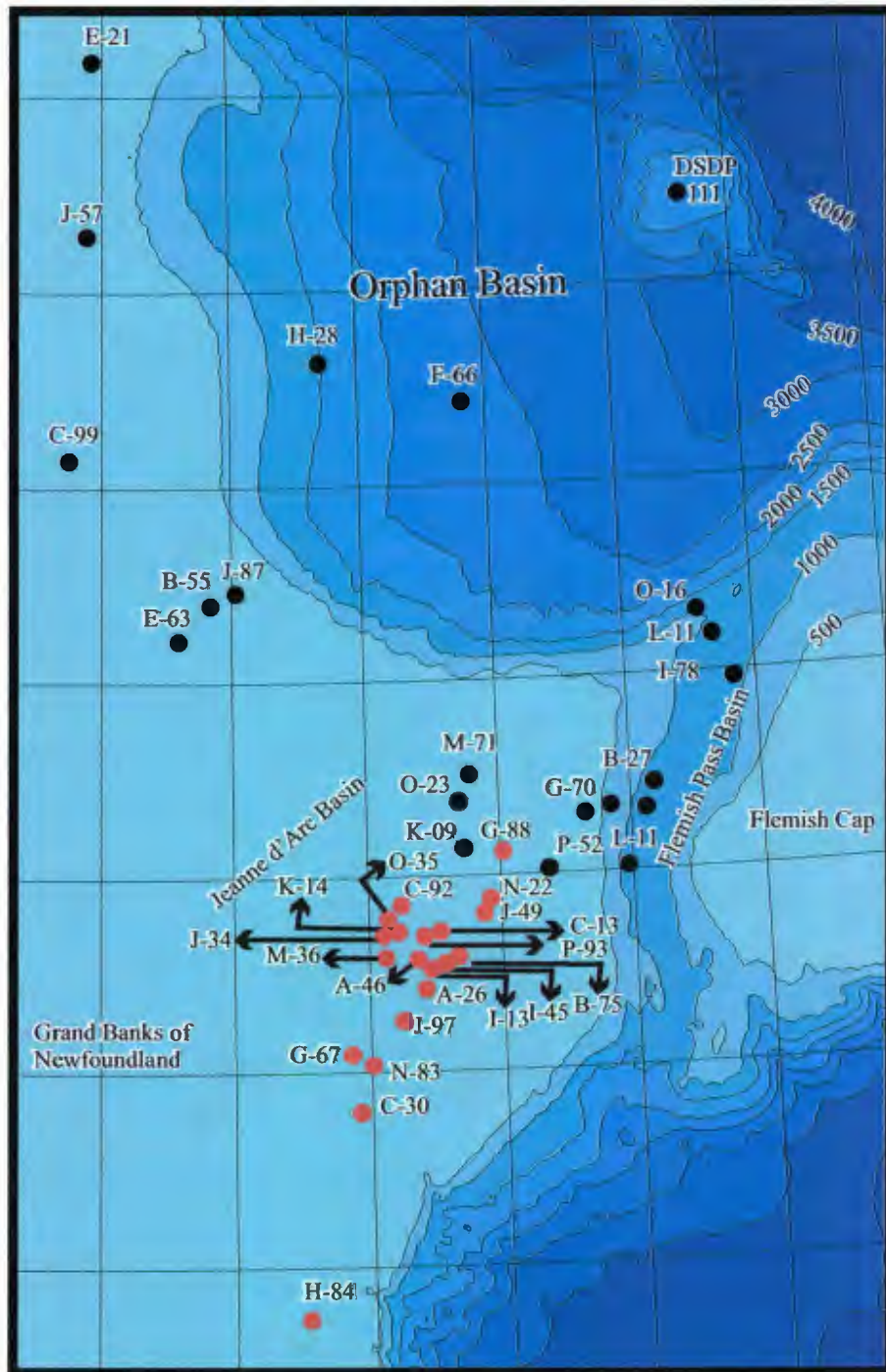


Figure 1.7. Bathymetry map of Northern Grand Banks of Newfoundland, showing the key well locations of the study area (black dots) and also some type section wells of the Jeanne d'Arc Basin (red dots). Water depth is in meters.

Osprey Formation, displaying a conformable upper boundary. In addition, the Osprey Formation shows an intercalated contact with a tongue of the Eurydice Formation. At the type section (i.e., Osprey H-84; Fig. 1.6, 1.7), the boundary between the Argo and Osprey formations is unconformable (McAlpine, 1990). Well data show that the Argo Formation is more widespread than the Osprey Formation, extending from the southern Scotian Shelf to the Northern Grand Banks of Newfoundland.

The Argo Formation represents mostly colourless to light pink massive salt, but comprises minor thin intercalations of grey, green, and red shale and anhydritic dolomite in the south-western portion of the Jeanne d'Arc Basin (i.e., Spoonbill C-30 and Cormorant N-83 wells; Fig. 1.6, 1.7; McAlpine, 1990). The gradually overlying Iroquois Formation is ubiquitous above the Argo Formation on the Grand Banks of Newfoundland (McAlpine, 1990).

At the type section (i.e., Murre G-67 well; Fig. 1.7) the Iroquois Formation has a 113 m thick lower dolomite-halite-anhydrite unit, a 123 m thick middle dolomite-anhydrite unit and finally a 110 m thick upper limestone unit (Jansa et al., 1976; McAlpine, 1990). The upper boundary with the Downing Formation is gradational and conformable (e.g., Murre G-67 and Cormorant N-83 wells; Fig. 1.7), but is also unconformable as a result of early salt displacement.

The Downing Formation consists of a thick unit characterized by silty and marly grey shales with interbedded limestones and minor fine-grained sandstones (Fig. 1.6; McAlpine, 1990). This formation is subdivided into three units: a) the lower, grey,

variably calcareous and marly and locally silty shale unit, b) the middle limestone unit (i.e., Whale Member) consisting of skeletal-pelletoidal grainstones and wackestones with thinner oolitic grainstones and intraclast-bioclast packstones and c) the upper siltstone and fine grained sandstone beds (Fig. 1.6; Jansa and Wade, 1975; Jansa et al., 1976; Grant and McAlpine, 1990). The Whale Member has gradational and conformable contacts with the lower and upper shale units. Overall, the Downing Formation was deposited during a prolonged marine transgression over the Grand Banks of Newfoundland (Jansa and Wade, 1975; Jansa et al., 1976).

The Voyager Formation gradually and conformably overlies the Downing Formation. It consists of two units. In the type section (i.e., Rankin M-36 well; Fig. 1.7), the lower unit is composed of a 447 m-thick interbedded sandstone, siltstone and shale succession containing a few thin limestone beds and coal seams (Fig. 1.6; McAlpine, 1990). Here, the upper unit is 161 m thick and includes shales containing minor limestone and siltstone beds (McAlpine, 1990). The Voyager Formation occurs throughout the Jeanne d'Arc Basin and the Outer Ridge Complex. The shale-dominated upper contact between the Voyager and overlying Rankin formations is conformable but lithologically abrupt.

The Rankin Formation is subdivided into three units. The lower massive limestone unit (288 m thick in the type section; Rankin M-36 well; Fig. 1.7) is composed of oolitic and skeletal wackestones, packstones and grainstones. The middle unit consists of fine siliciclastics with minor lime mudstones and oolitic and skeletal wackestones. The upper

unit consists of thinly-interbedded limestones, marls and shales, and includes an organic-rich shale referred to as the Egret Member by Bujak et al. (1977a, b), Swift and Williams (1980), Boudreau et al. (1986), Tankard and Welsink (1987) and McAlpine (1990). The Egret Member is an oil source rock in the Jeanne d'Arc Basin; containing sparsely interbedded and laminated brown marls, calcareous shales, claystones, and brown and grey lime mudstones in the southern portion of the basin (Rankin M-36 well; Fig. 1.6; McAlpine, 1990). It becomes slightly calcareous and coarser toward the northeast (i.e., South Tempest G-88, Rankin M-36 wells; Fig. 1.7). Here, argillaceous and very fine-to fine-grained sandstones are dominant lithologies. The upper and lower boundaries of the Egret Member are sharp but conformable with either limestones in the south or fine siliciclastics in the north (Fig. 1.6; McAlpine, 1990).

The Jeanne d'Arc Formation is divided into three units; a lower shale, a middle sandstone and an upper shale. The lower unit is composed of grey to grey-brown, fissile, calcareous, and silty shale with a few thin interbeds of brown argillaceous lime mudstones (McAlpine, 1990). The middle unit consists mainly of sandstones grading to conglomerates with minor interbedded shales and siltstones. The upper unit contains mainly shales and siltstones with several thin sandstone interbeds and rare thin limestones (McAlpine, 1990). The sandstones include horizontal lamination, erosion surface, low-angle cross bedding, slump structures, current ripples and intraformational mudclasts (McKenzie, 1980; McAlpine, 1990). In the southern portion of the basin, the sediments of the Jeanne d'Arc Formation were deposited as northward-thickening stacked siliciclastic wedges (Sinclair et al., 1992). The Jeanne d'Arc Formation unconformably

overlies the limestones of the Rankin Formation, and is in turn, conformably overlain by the Fortune Bay Formation.

The Fortune Bay Formation is composed of grey, fissile to blocky, slightly calcareous, fossiliferous shales. In addition to the upward-grading siltstone to shale succession, the formation locally includes thin interbedded sandstones (Fig. 1.6; McAlpine, 1990). The formation occurs ubiquitously north of the Egret Fault in the Jeanne d'Arc Basin (McAlpine, 1990). The lower boundary of the Fortune Bay Formation is sharp.

The Hibernia Formation gradually and conformably overlies the Fortune Bay Formation (Fig. 1.6; McAlpine, 1990). It is composed of two units; the lower unit and upper unit (i.e., the Hebron Well Member; McAlpine, 1990). The lower unit consists of white to light grey, fine-to coarse-grained, carbonaceous, sandstones with thin shale, siltstone, sandstone, and rare coal interbeds (McAlpine, 1990; Sinclair et al., 1992). The sandstones of this unit are grey to buff color and have sharp erosive bases, current ripples, cross bedding and planar horizontal laminations (McAlpine, 1990). The upper unit mainly contains thick, massive sandstones at the base and thinner sandstones containing shale and siltstone interbeds at the top of the succession (i.e., Hebron I-13 well; Fig. 1.7). The sandstones of the upper unit are pale grey-brownish grey and exhibit planar horizontal laminations and wavy discontinuous bedding, abundant burrows (McAlpine, 1990). The overlying B Marker limestone seals the formation with a sharp, but generally conformable boundary (Fig. 1.6).

The B Marker Member consists of a light grey, oolitic/skeletal limestone succession. At the base of the unit, in the type section (i.e., Ben Nevis I-45; Fig. 1.7), the limestone is intercalated with grey, calcareous, fine-grained sandstones and dark grey calcareous siltstones and shales (McAlpine, 1990). The upper contact with the Catalina Formation is conformable and sharp with the Catalina Formation. Where the Catalina Formation is missing, the upper boundary with the White Rose Formation is gradational (McAlpine, 1990).

The Catalina Formation consists of thin sandstones, siltstones, shales and minor limestones (Fig. 1.6). The sandstones are very fine-grained, calcite-cemented, shaly, and bioturbated and exhibit current ripples, horizontal laminations, erosive bases and abundant burrows (e.g., Hibernia P-15 and Hibernia O-35; McAlpine, 1990; Fig. 1.7). The Catalina Formation thins to the northeastern of the Jeanne d'Arc Basin and it passes laterally and vertically in to the White Rose Formation (Fig. 1.6; McAlpine, 1990; Sinclair, 1992). The boundary between the Catalina Formation and its laterally equivalent Eastern Shoal Formation is gradational and conformable. This boundary is not detected in the logs or borehole samples (McAlpine, 1990).

The Eastern Shoal Formation, in the type section (i.e., Ben Nevis I-45; Fig. 1.7), is divided into two lithofacies: (i) Massive calcareous sandstones and oolitic limestones consisting of light grey to brown fossiliferous chalky limestones, oolitic and sandy wackestones and packstones. The thinly bedded shales are grey, green and red coloured and waxy and pyritic and silty (McAlpine, 1990). (ii) Very fine-to fine-grained,

argillaceous sandstones with dark grey thin siltstones and shales. The sandstones exhibit horizontal laminations and low angle cross-bedding containing occasional mudclasts, pebbles and shell fossils. The siltstones include rippled and burrowed sand lenses. The Eastern Shoal Formation is thickest at the western portion of the Jeanne d'Arc Basin. It thins toward the south and along the basin axis. The upper contact with the Avalon Formation is sharp and changes from unconformable to disconformable. The boundary between the underlying Whiterose and Catalina formations and the Eastern Shoal Formation is conformable and gradational at the western portion of the basin.

The Whiterose Formation in the well type section (i.e., Whiterose N-22; Fig. 1.7), is separated into an upper and a lower tongue by a thin limestone (B Marker Member). Both the upper and the lower tongues are mostly composed of medium to dark grey blocky, silty and calcareous shales, containing thin siltstone and limestone beds. The uppermost portion of the Whiterose Formation includes A Marker Member stray oolitic limestones which occur across the basin. The Whiterose Formation is ubiquitous in the Jeanne d'Arc Basin. The upper boundary with the Eastern Shoal Formation is abrupt. Where the Eastern Shoal Formation is absent, the contact is an unconformity at the base of the Avalon Formation (McAlpine, 1990).

The A Marker Member of the Avalon Formation is a thin (< 25 m) light grey, oolitic/skeletal lime grainstones and packstones unit and includes intercalated thin, calcareous sandstone, siltstone and shale beds (McAlpine, 1990). The member occurs only in the west-central portion of the Jeanne d'Arc Basin (i.e., Hibernia Field to the

South Mara C-13; Fig. 1.7). The lower contact of the A Marker Member with the Whiterose Formation is gradational, but its upper contact with the Eastern Shoal Formation is sharp, and both contacts are conformable.

The Avalon Formation contains a coarsening-upward mudstone and sandstone succession (Fig. 1.6). In the type section (Ben Nevis I-45; Fig. 1.7), the formation is divided into three units: (i) a red mudstone sequence consisting of various coloured, locally calcareous, fissile, fossiliferous shales and a few thin, very fine-to fine-grained, grey to light brown, calcareous and fossiliferous sandstone beds, (ii) a thick unit consisting of white to light grey, very fine-to fine-grained, silica- and calcite-cemented sandstone beds and grey shale interfingers, and (iii) a ubiquitous, very fine to fine grained, white to light brown, poorly calcite- and silica-cemented, coarsening upward sandstone unit, containing thin grey fossiliferous, fissile shales and laminated coal fragments. Basinward, the formation passes laterally into the Nautilus Shale Formation (McAlpine, 1990). The upper boundary with the Ben Nevis Formation is abrupt and unconformable at the basin margins and over major structures. This boundary becomes disconformable to conformable toward the basin axis.

The Ben Nevis Formation is a fining-upward, coal-bearing sandstone succession (Fig. 1.6). In the type section (Ben Nevis I-45; Fig. 1.7), this succession comprises of two units: a thinly-interbedded shale and sandstone unit and a minor coal-bearing sandstone sequence. The lower unit (i.e., the Gambo Member) comprises medium-to dark grey, fissile, silty, pyritic, and carbonaceous shales, and white, fine-to medium-grained, partly

silica-and calcite-cemented sandstones with black, vitreous, coal beds (Fig. 1.6; McAlpine, 1990, Sinclair, 1993). The upper unit contains light grey, quartzose, carbonaceous sandstones which become argillaceous toward the top of the succession. The formation occurs mostly in the eastern-central portion of the Jeanne d'Arc Basin (i.e., from the Port au Port J-97 to Whiterose J-49). The base of the Ben Nevis Formation is defined by the regional mid-Aptian Unconformity which overlies the Avalon Formation and older units (Sinclair, 1993). The upper part of the Ben Nevis Formation is also defined by an unconformity (McAlpine, 1990).

The Nautilus Shale Formation consists of grey calcareous shales and/or mudstones (Fig. 1.6). In the type section (i.e., Nautilus C-92; Fig. 1.7), the formation is divided into three units: (i) a brown, very fine-grained, silty sandstone unit which gradually fines upward into a grey to brown, calcareous sandy siltstone unit (e.g., the Ben Nevis Formation equivalent), (ii) a mainly sandstone unit consisting of rare siltstone stringers, and (iii) a very calcareous, grey, argillaceous siltstones containing argillaceous, white to grey, microcrystalline to chalky, silty limestone unit (e.g., the Eider Formation equivalent; McAlpine, 1990). The formation is ubiquitous in the Jeanne d'Arc Basin. The boundary with the overlying Petrel Member of the Dawson Canyon Formation is sharp, but assumed to be conformable (McAlpine, 1990). Where the underlying Ben Nevis Formation is present, the lower contact is abrupt and is defined by the Albian Unconformity (McAlpine, 1990).

The Dawson Canyon Formation is mainly composed of fine-to coarse-grained siliciclastic rocks to chalky carbonates (Fig. 1.8; McIver, 1972). The formation is divided into three members: the Petrel, Otter Bay and Fox Harbour members (Boudreau et al., 1986; Sinclair, 1992; de Silva 1993 and Deptuck 2003). However, Deptuck (2003) defined two additional new members: the Red Island and Bay Bulls members. The Petrel Member of the Dawson Canyon Formation consists of a coccolith-rich, microcrystalline limestone and marlstone succession with glauconite-rich sandstone stringers (Fig. 1.8; Shimeld et al., 2000; Deptuck et al., 2003). The upper boundary of the Petrel Member with the Red Island Member is sharp to gradational. The Red Island Member is composed mainly of gray mudstones and siltstones containing minor sandstone stringers and also abundant microfossils, detrital plant fragments, and large shell fragments (Fig. 1.8). The upper boundary of the unit with the Otter Bay Member is sharp to gradational. Where the overlying Otter Bay Member is absent, the upper contact with the Bay Bulls Member is not detectable at the well logs (Deptuck et al., 2003). In the type section (i.e., Hibernia J-34; Sinclair, 1988) the Bay Bulls Member is a medium-to coarse-grained sandstone succession, containing chert and quartz pebbles, shell debris and glauconite-rich sandstones. The member occurs along the western margin of the Jeanne d'Arc Basin, but pinches out abruptly to the east, where, it interfingers with the shales of the Red Island Member (Fig. 1.8; Deptuck et al., 2003). The upper contact of the unit with the Bay Bulls Member is commonly abrupt. The overlying Bay Bulls Member consists of gray glauconite-rich shales and siltstones with rare sandstone stringers (Deptuck et al., 2003). The member occurs in the western portion of the Jeanne

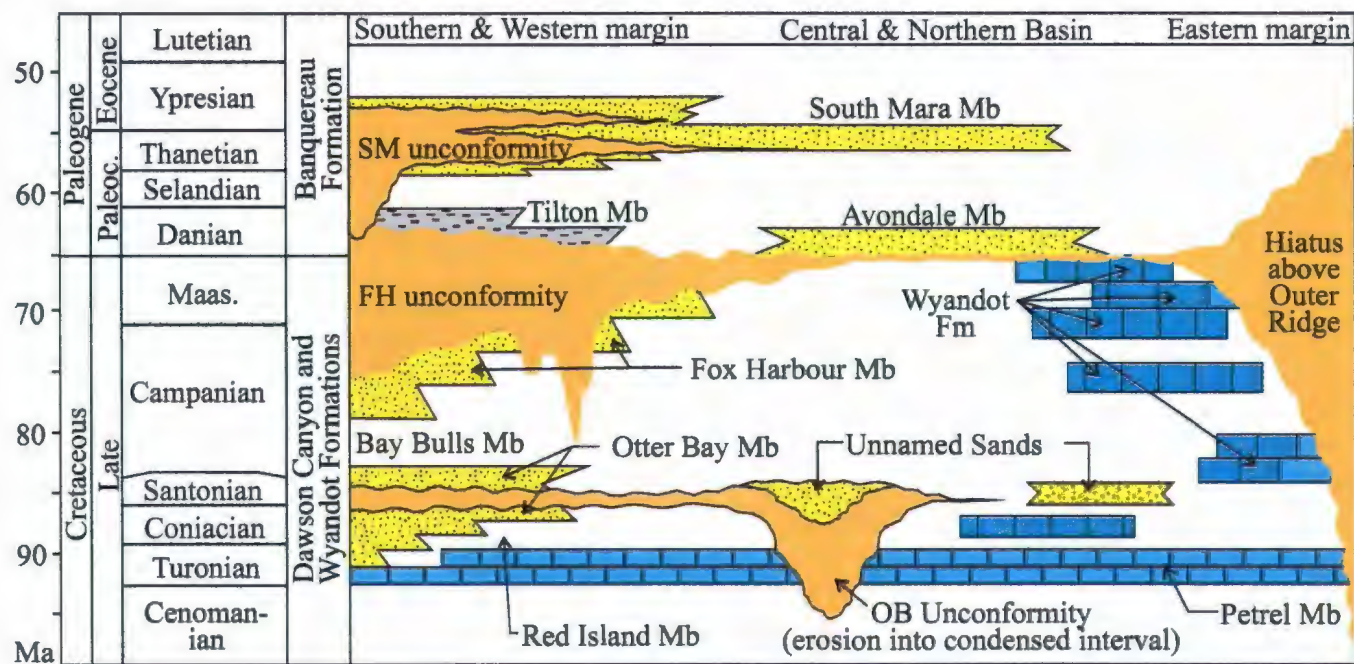


Figure 1.8. Generalized lithostratigraphic chart for the Upper Cretaceous and the lower part of the Paleogene stratigraphic succession in the Jeanne d'Arc Basin (modified from Sinclair, 1987 and Deptuck, 2003). Absolute ages on the timescale are from Gradstein et al. (1995) and Berggren et al. (1995). OB = Otter Bay; FH = Fox Harbour; SM = South Mara; Mb = Member; Fm = Formation.

d'Arc Basin and thickens to the east of the basin (e.g., from 122 m in the Hibernia J-34 to 225 m in the Hibernia K-14; Deptuck et al., 2003; Fig. 1.7). The Fox Harbour Member gradually overlies this formation in the Hibernia Field (e.g., Hibernia J-34; Fig. 1.7). However, further south, in the regions where the fine-to very coarse-grained succession of this formation is overlain by the pebble conglomerates of the Fox Harbour Formation, the boundary becomes sharp. The Fox Harbour Member contains an upward-coarsening succession, consisting of 50% coarse sandstones and granule-to pebble-conglomerates. The sandstones are primarily composed of quartz grains, with minor glauconite, chert, sparse feldspar grains, and sporadic limestone stringers (Deptuck et al., 2003). This member is thickest in the eastern portion of the Jeanne d'Arc Basin.

The Wyandot Formation is composed of pelagic coccolithic-foraminiferal chalks and marlstones. The formation is thickest in the northern portion of the Jeanne d'Arc Basin (e.g., Conquest K-09), but progressively thins toward the south (e.g., North Ben Nevis P-93; Fig. 1.7), becoming absent in the southern portion of the basin (e.g., West Ben Nevis B-75; Fig. 1.7).

The Banquereau Formation is composed of shales containing minor chalks, siliceous mudstones and sandstones (McIver, 1972; McAlpine, 1990). The formation is divided into three members: the Avondale Member, the Tilton Member and the South Mara Member (Sinclair, 1988, McAlpine, 1990; Deptuck, 2003). In the type section (i.e., Avondale A-46; Fig. 1.7), the Avondale Member is composed of very fine- to coarse-grained, loosely consolidated sandstones with traces of glauconite. The member is

laterally discontinuous and exhibits thick sandstone pinch-outs or shaling-outs over short distances. The lower boundary of the Avondale Member with the Dawson Canyon Formation is abrupt and unconformable, whereas the upper contact may be gradational (e.g., Avondale A-46; Fig. 1.7) or abrupt (e.g., North Ben Nevis P-93; Fig. 1.7). The Tilton Member is composed of a grey to brown, glauconitic, siliceous, slightly dolomitic siltstone and shale succession (e.g., King's Cove A-26; Deptuck et al., 2003; Fig. 1.7). This member is commonly developed both along the western margin and farther south near the Terra Nova Field of the Jeanne d'Arc Basin. The Tilton Member sharply overlies the Dawson Canyon Formation. The upper boundary of the Tilton Member is commonly gradational, but it is sharp and unconformable in the western portion of the basin (e.g., Rankin M-36; Fig. 1.7). The South Mara Member is mainly composed of fine- to very coarse-grained sandstones. In the type section (South Mara C-13), this unit consists predominantly of sandstones (Deptuck et al., 2003). South Mara Member conformably overlies the Tilton and Avondale Members (North Ben Nevis P-93; Fig. 1.7).

1.6. Thesis Objectives

The main objectives of this thesis are:

(1) to construct a reliable stratigraphic framework between existing boreholes that will allow the determination of temporal and spatial variations of lithofacies, and seismofacies in the study area;

(2) to establish a tectonic framework that will allow the determination of the depositional environment in time and space,

(3) to correlate major unconformities between the Orphan, Jeanne d'Arc and Flemish Pass basins.

These objectives will be achieved through an integrated comprehensive study which will use the available seismic reflection profiles, the well logs from 9 exploration boreholes, and the lithological data, including chips and cores. The regional seismic reflection profiles will allow depiction of the basin-wide three-dimensional geological setting. The borehole data (both lithological and electrical logs) will permit the ground-truthing of the seismic reflection data. Below, the specific topics associated with each primary objective are described in detail.

Objective 1: to erect a reliable chronostratigraphic framework between existing boreholes that will allow the determination of temporal and spatial variations of lithofacies, and seismofacies in the study area. The above objective will be achieved as indicated below:

- to compile a lithological column for each exploration well in the Orphan Basin, using the well-site lithological information obtained through chips coming to shaker via the circulation mud, the cored intervals, as well as the various well logs acquired during the final phase of the drilling process. The well logs will be carefully correlated with the lithological column to ensure that the exact

boundaries between various lithological units are accurately delineated in each exploration well.

- to establish a regional seismic stratigraphic framework for the Orphan Basin, using several cross-basin seismic reflection profiles, and applying the sequence stratigraphic method. Seismic profiles will be divided into discrete packages, bounded by regional unconformities at their tops and bases (i.e., depositional sequence of Posamentier et al., 1988; Myers and Milton, 1996; Coe and Church, 2003).
- to determine the seismic facies in seismic reflection profiles using the amplitude and azimuth information, and to extend the spatial variation of seismic facies across the Orphan Basin (i.e., seismic facies analysis).
- to compile synthetic seismograms for each exploration well using the sonic and density well logs; the synthetic seismograms are readily correlated with the lithological column of a given well, as well as the seismic reflection profiles that cross the well site, allowing transposition of the lithological information onto the seismic reflection profiles.
- to extend the lithological information obtained in wells regionally across the Orphan Basin using the newly constructed seismic stratigraphic framework, within the confines of the seismic facies analysis.

Objective 2: to establish a sedimentological framework that will allow the definition of the depositional environment in time and space, and a better understanding between

source and reservoir rocks and also to identify and correlate major unconformities between the three basins involved in this study (Orphan, Jeanne d'Arc and Flemish Pass basins). The above objective will be achieved following the specific topics listed below:

- to carry out detailed sedimentological description of cores recovered from each exploration well from the Orphan Basin. The data will be used to delineate the lithofacies (and sub-facies if necessary) in the cores, so that a general depositional environmental interpretation for each major lithological unit can be ascertained.
- to use detailed correlations between the well logs and the detailed lithofacies descriptions, as well as basic principles of log interpretation so that the lithological signature of the well logs can be extended into un-cored successions with a clear sedimentological interpretation.
- to compare/contrast and correlate the lithofacies interpretation obtained using the well logs (including cored intervals) with the seismic facies (i.e. seismic facies analysis), which will allow a basin-wide evaluation of lithofacies and/or seismic facies variations, thus the definition of the depositional environment in time and space.
- to evaluate the relationship between the timing of deposition of the potential source rock(s) and that of the reservoir rock(s).

Objective 3: to determine a reliable tectonic framework that will allow the delineation of the events responsible for basin development, specifically the relationships between the

development of structures and sedimentation. The above objective will be achieved following the specific topics listed below:

- to built a tectonic framework using the existing 2-D multichannel seismic reflection profiles, so that a holistic evaluation of the geological evolution of the Orphan Basin can be made, including the development of large-scale structures in the region.
- to evaluate the evolution of Orphan Basin within a regional plate tectonics context, particularly the understanding of the evolution of the Orphan Basin in relation to the perceived rotation and southward migration of Flemish Cap.
- to propose a holistic regional model for the evolution of Orphan basin and environs.

These objectives will assist in the understanding of the relationships between the development of structures, the timing of entry of source rock into the oil generation window, the timing of migration of hydrocarbons into the reservoir(s), and finally the presence and integrity of the seal rock .

CHAPTER 2. DATA SET AND METHODOLOGY

2.1. Data Set

The data used in this thesis consist of 25,000 km of multichannel seismic reflection profiles and the lithological and borehole data from 13 exploration wells (Fig. 2.1).

2.1.1. Borehole Data

Borehole data for this project have been made available by the Geological Survey of Canada-Atlantic Basin Database (www.gasca.nrcan.gc.ca/BASIN) and the Canada-Newfoundland and Labrador Offshore Petroleum Board (<http://www.cnlopb.nl.ca>). Seven wells from the Orphan Basin, three wells from the Flemish Pass Basin and three wells from the Jeanne d'Arc Basin are used in this thesis (Fig. 2.1, Table 2.1). Time-depth data for several wells were made available by the Canada-Newfoundland and Labrador Offshore Petroleum Board. Digital logs for several wells (Gamma-Ray, Sonic, Density and SP logs) used in this project were donated by IHS and lithostratigraphic logs were donated by Stratalog, both of Calgary, Alberta.

2.1.2. Seismic Data

The Orphan Basin 2-D seismic dataset was provided by Geophysical Service Incorporated (GSI). The data were acquired using a 480-channel 6 km-long streamer with 12.5 m hydrophone interval, and a 3000 cubic inch tunned airgun array. The

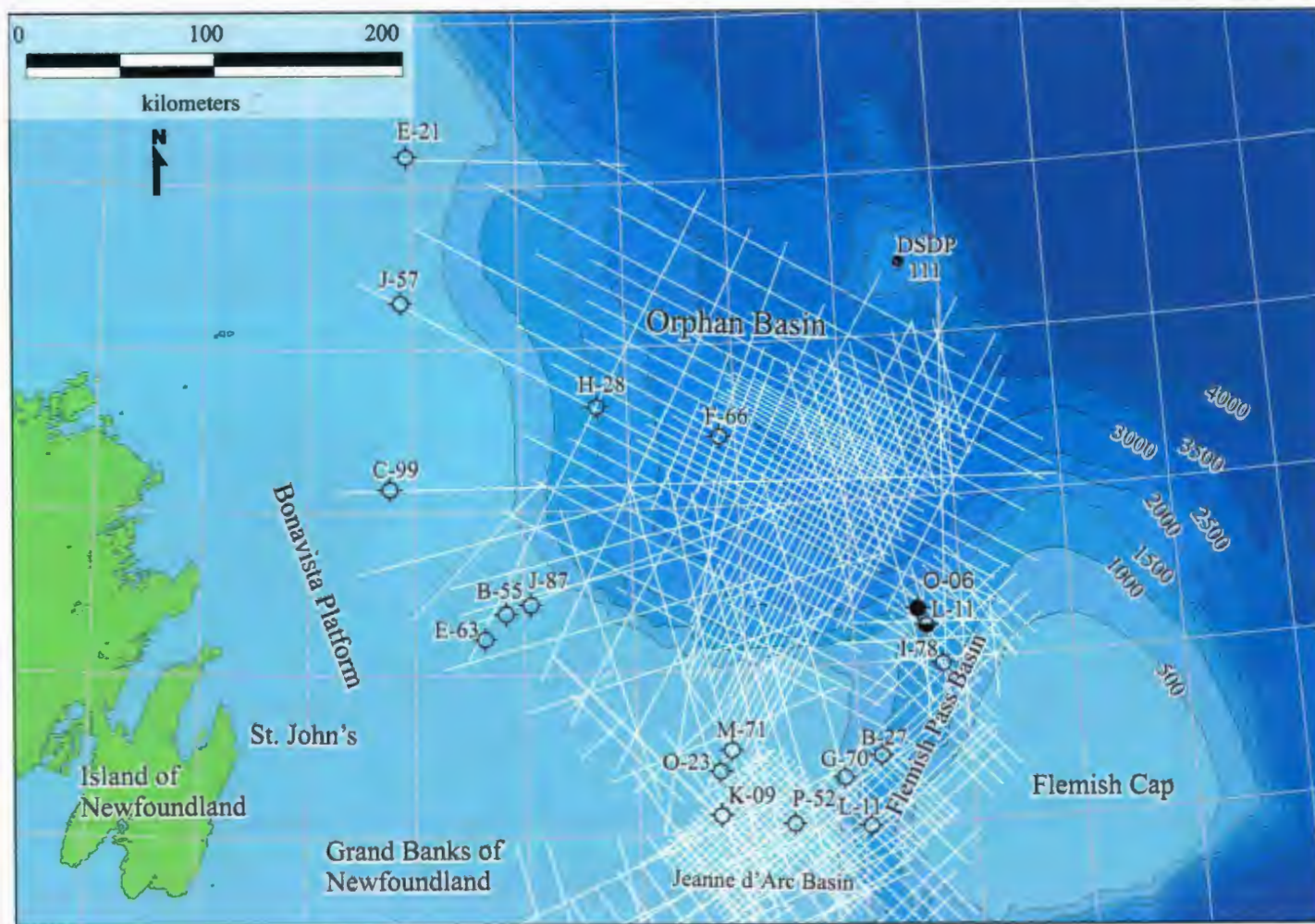


Figure 2.1. Basemap of the study area, showing the location of modern regional 2D seismic grid and exploration wells.

Well Name	Year Drilled	Type	Latitude (NAD83)	Longitude (NAD83)	Datum (KB) (m)	Total Depth (m)
<u>Key Wells Used in the Study Area</u>						
Blue H-28 (Texaco et al.,)	1979	Exploration	49° 37' 26.49" N	49° 17' 58.18" W	14.7	6103
Hare Bay E-21 (BP et al.,)	1979	Exploration	51° 10' 21.80" N	51° 04' 23.30" W	24.2	4874
Baie Verte J-57 (BP et al.,)	1985	Exploration	50° 16' 43.58" N	51° 07' 49.77" W	25	4911
Bonavista C-99 (BP et al.,)	1974	Exploration	49° 08' 06.16" N	51° 14' 24.21" W	12.2	3779
Mizzen L-11 (Petro-Canada et al.,)	2003	Exploration	48° 10' 31.75" N	46° 17' 35.55" W	23.8	3820
Kyle-11 (Esso et al.,)	1986	Exploration	47° 00' 36.50" N	47° 02' 45.03" W	24.1	4200
Baccalieu I-78 (Esso et al.,)	1985	Exploration	47° 57' 41.49" N	46° 10' 46.76" W	23.7	5135
Bonanza M-71 (Mobil et al.,)	1982	Exploration	47° 30' 47.19" N	48° 11' 51.35" W	26.8	4492.8
Linnet E-63 (Mobil et al.,)	1982	Exploration	48° 12' 29.27" N	50° 25' 22.28" W	27.1	4520.2
<u>Other Relevant Wells</u>						
Panther P-52 (Husky et al.,)	1985	Exploration	47° 01' 53.01" N	47° 37' 39.81" W	22	4203.2
Sheridan J-87 (Mobil et al.,)	1981	Exploration	48° 26' 39.56" N	49° 57' 35.30" W	29.7	5486.4
Cumberland B-55 (Mobil et al.,)	1975	Exploration	48° 24' 12.21" N	50° 07' 54.49" W	29.9	4136.5

Table 2.1. Summary table of the wells showing the location, datum and total depth information gathered from the C-NLOPB, 2007. See Figure 2.1. for well locations.

resultant 96-fold data were recorded digitally for 12 seconds at 2 ms intervals. The multi channel data were processed at Precision Seismic, with the following steps: FK filter for swell, deconvolution and data sampled to 4 ms, normal moveout and mute, parabolic radon transform for multiple attenuation, prestack velocity analysis, prestack time migration (Kirchhoff) and scaling. The seismic data form a tight NE-SW and NW-SE oriented grid with an approximately 3 km line spacing, with the exception of regional lines which are variably oriented (Figs. 2.1, 2.2). The Lithoprobe and older regional GSI data in the Orphan Basin were also used to tie seismic horizons from the Orphan, Flemish Pass and the Jeanne d'Arc basins.

2.2. Methods

Detailed interpretation of faults and structural architecture of the basin is a necessary step prior to any stratigraphic interpretations. Thus, the first step involved seismic structural interpretation and mapping of major faults, elongated ridges and depressions (i.e., basins) throughout the study area and environs, using the available 2-D seismic data.

The second step was the seismic sequence interpretation and the construction of a seismic stratigraphic framework. On the basis of acoustic character and reflector continuity, the seismic profiles were divided into discrete seismic units. The unit boundaries were defined by strong reflectors representing unconformities or drastic change in lithologies which were correlated with well-log data using time-depth conversions and synthetic seismograms.

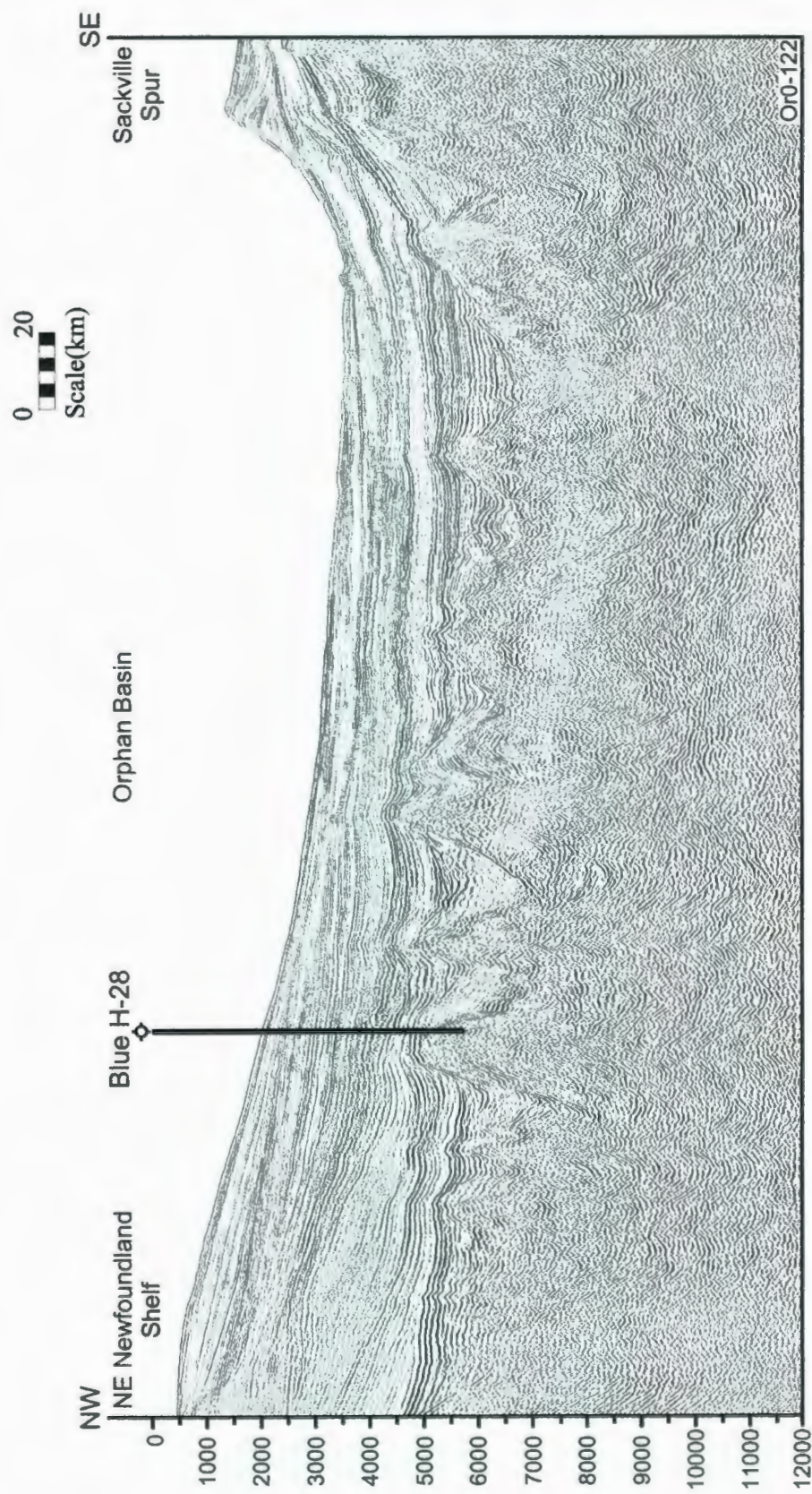


Figure 2.2. Example of GSI 2000-2003 2D seismic dip line. Vertical scale is two way travel time (ms).

The third step was mapping of seismic unit boundaries. In order to use the mapping modules (e.g., SeisWorksTM), the horizons and faults were exported to the Landmark® software. The following interpretation steps: gridding, contouring and depth conversions were carried out using the SeisWorksTM program. Time-structure and time-thickness (isochron) maps were generated for all major seismic unit boundaries. The methodologies and practical application of software used to achieve the project objectives are described in the following sections.

2.2.1. Seismic Stratigraphy

The main purpose of seismic stratigraphy is to erect a framework on which the interpretation of the basin's geological history can be described. The technique allows the identification of sedimentary sequences based on reflection configurations and the discrimination of the causative factors that resulted in this particular geometry, including eustasy, subsidence, sediment flux and regional and local tectonics. A seismic stratigraphic framework was established for the study area using the biostratigraphic and lithostratigraphic information from existing exploration wells. Synthetic seismograms were used to correlate major lithological boundaries and unconformities. Sequence boundaries were recognized and associated in both exploration wells and seismic reflection profiles. It was noted that nearly all boundaries and unconformities correspond to strong, regionally extensive reflections in seismic profiles. These strong reflections were selected as seismic unit boundaries. Seismic profiles were also examined to

delineate the geometric relationship between the reflectors that define the unit boundaries and the underlying and overlying reflectors.

Reflection stratal terminations beneath seismic unit boundaries are truncation and toplap. Reflection terminations above the boundaries consist of onlap and downlap (Mitchum et al., 1977; Fig. 2.3). In order to describe reflection configurations, various seismic stratigraphic terms are explained below.

Lapout is the lateral termination of a reflector at its original depositional limit, whereas *truncation* signifies that the reflector originally extended further but was cut off against either an overlying erosional surface (*erosional truncation*) or a syn- or post-depositional fault, slump, glide or intrusion plane (*fault truncation*; Fig. 2.3; Mitchum et al., 1977). *Baselap* marks the lower boundary of a seismic package. Baselap can be divided into *downlap*, where the dip of the inclined seismic reflector is less than the overlying strata, or *onlap*, where the dip of underlying strata is greater than the inclined reflectors (Fig. 2.3). *Toplap* is the updip termination of an inclined reflector against an overlying lower angle surface (Mitchum et al., 1977; (Fig. 2.3)

The internal reflection configuration of seismic packages is the first parameter that can be described on a seismic profile. These internal patterns can be further defined as parallel, subparallel, divergent, prograded and chaotic due to geometric relationships between reflections (Fig. 2.4, Mitchum et al., 1977). Prograded reflection configurations can be classified as sigmoid, oblique, shingled and hummocky (Fig. 2.4, Mitchum et al., 1977).

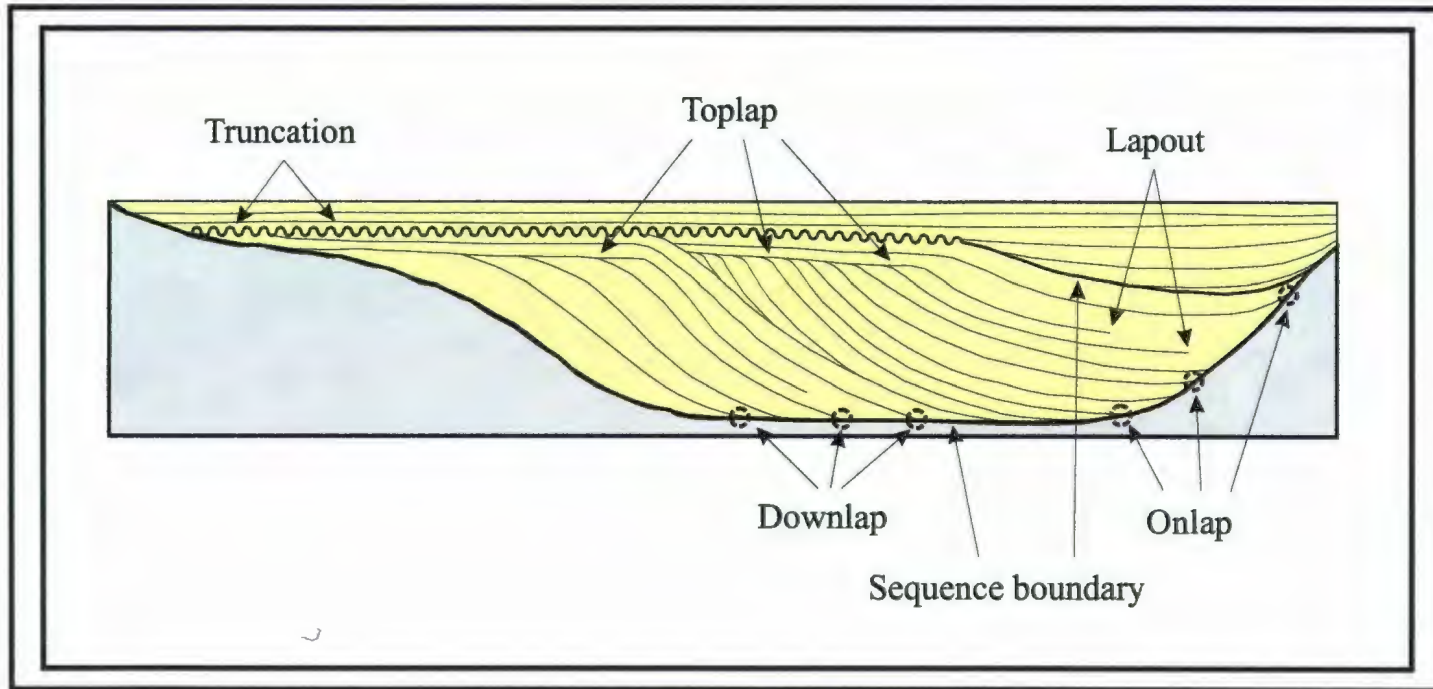


Figure 2.3. Schematic cross-section showing depositional sequences, sequence boundaries and typical internal reflection termination patterns (modified from Mitchum et al., 1977b).

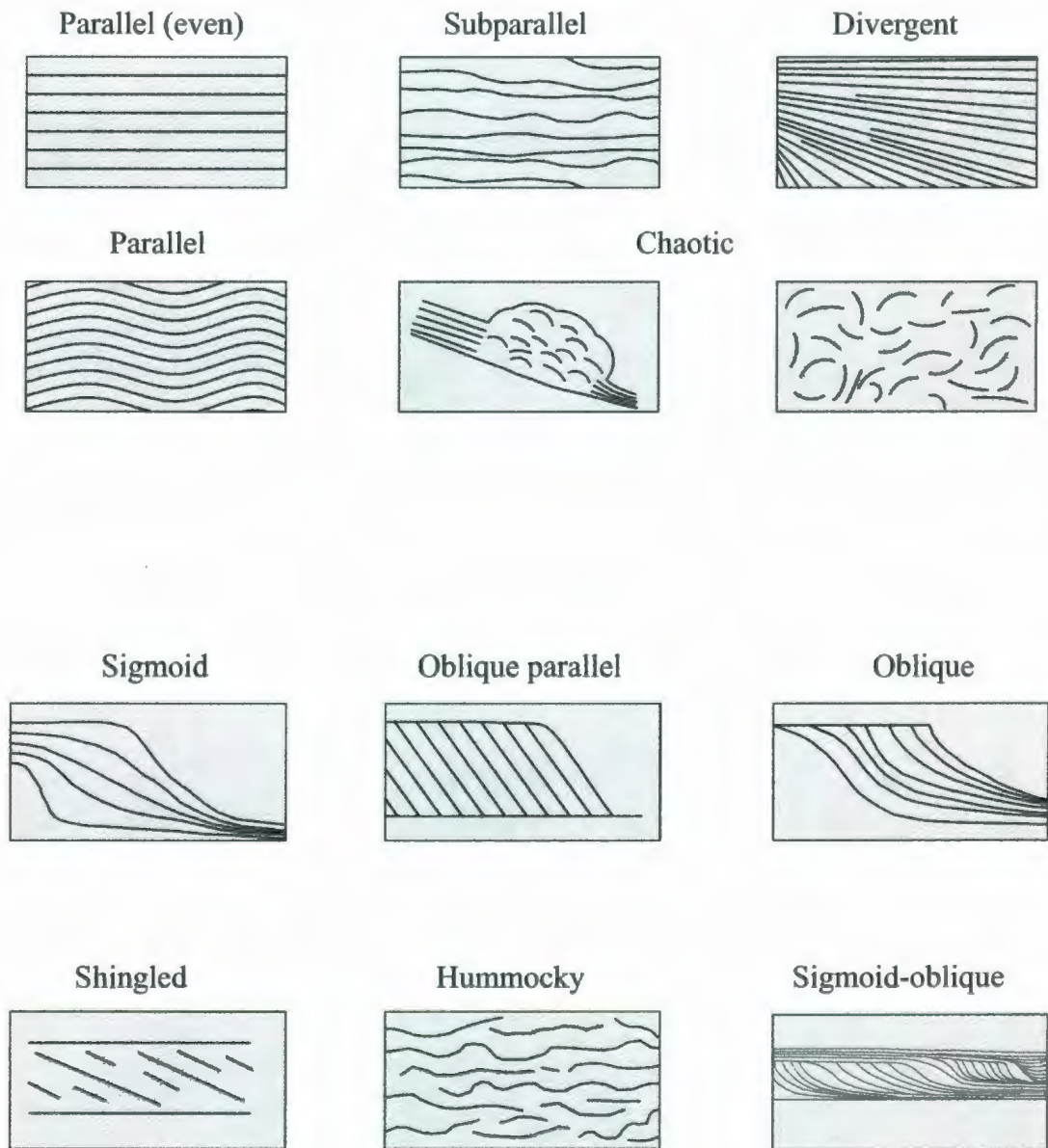


Figure 2.4. Types of reflection configurations and seismic reflection patterns of prograding clinoforms (modified after Mitchum et al., 1977).

2.2.2. Fault Mapping

Major fault planes were identified based on abrupt changes in the dip amount and offset of reflectors in seismic reflection profiles across the study area. The faults were then correlated between adjacent seismic lines based on similarities in the geometries of the sedimentary successions on the footwall and hanging wall of the faults. Correlation of faults resulted in a fault map constructed both manually on paper copies and in the workstation using the SeisWorks™ software module. In order to compare and triangulate major fault orientations in the study area with the regional direction of extension, the OpenWorks™ data base was used.

2.2.3. Mapping Techniques

Unconformities and lithostratigraphic tops identified in exploration wells were converted to two-way travel time and using the velocity survey (or check-shot survey) for each well tied to the corresponding strong reflectors on seismic profiles. These key geological markers are traced from the well locations into the seismic grid and as far in the basin as possible. The accuracy of the correlations was checked by closing a loop formed by several seismic lines (Fig. 2.5). In regions where the above technique failed to provide a good correlation, the key reflectors were transferred to the adjacent profile using jump correlation. Seismic reflection characteristics are used as a guide to perform jump correlation.

Preliminary horizon and fault interpretations were carried with a Landmark® software program using mapping modules (i.e. SeisWorks™). The “Auto Dip, Auto

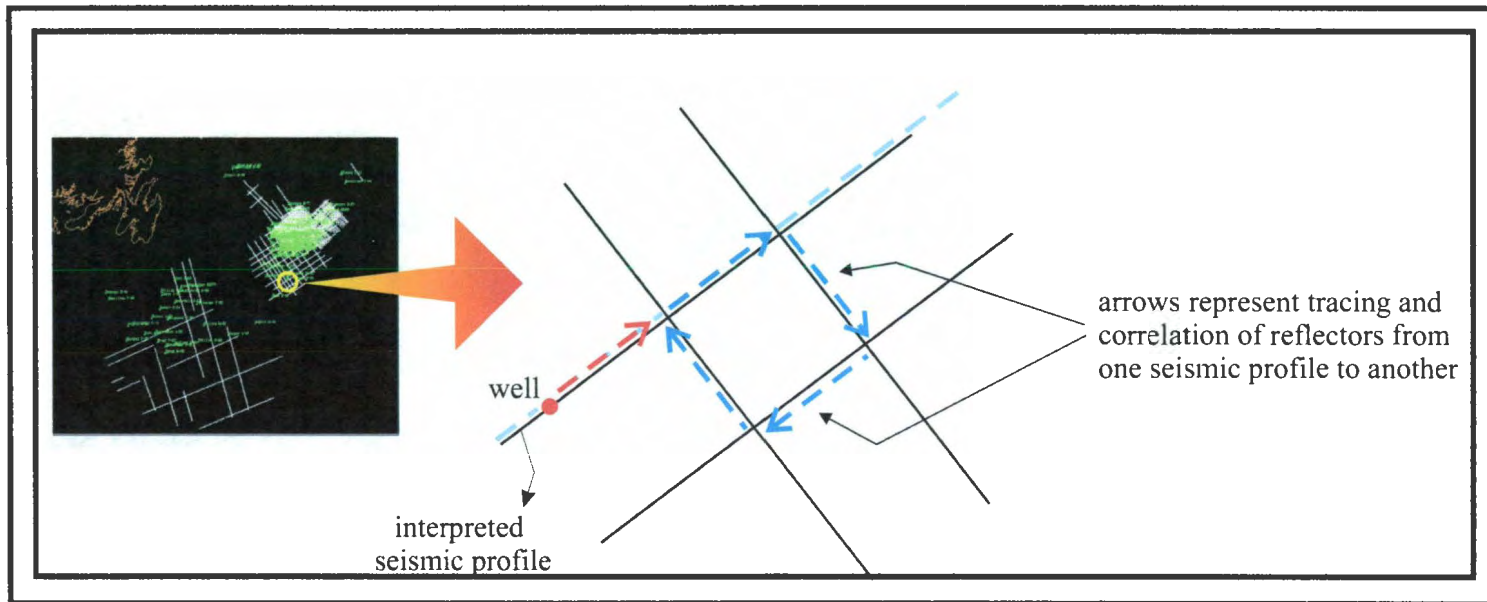


Figure 2.5. Schematic profiles and a well showing the technique used in seismic stratigraphy (arrows represent tracing and correlation of reflectors from one seismic profile to another)

Tracking and Correlation” options for horizon picking were used, depending on the quality and continuity of reflectors and the presence of fault zones.

Subsequently, the interpreted key horizons were used to create the TWT time-structure and time thickness (isochron) maps. The gridding and contouring of interpreted horizons is automatically done using SeisworksTM mapping algorithms. Time structure maps define the general shape of the basin at different levels, local and regional structural lows and highs, major fault zones and minor faults and help clarify structural controls on sediment accumulation. They also identify possible structural traps, stratigraphic and combination traps, which are important in the hydrocarbon exploration of the basin. Time thickness maps present the variations of sediment thickness and indicate possible areas of sediment entry in the basin, differential compaction, local tectonic subsidence, etc. They also can provide indications where the sand prone sequences and source rock intervals are thicker and therefore indicate areas where the chance of finding hydrocarbons is higher. These maps are further described in chapter 3.

2.2.4. Synthetic Seismograms

In order to develop the most accurate interpretation, seismic reflection data are correlated with well-log information using synthetic seismograms. To create a synthetic seismogram, well-log velocity data (from sonic logs and check-shot surveys) and density information (density logs) are first converted into acoustic impedance logs. The next step is the calculation of a reflection coefficient series which is subsequently convolved with a

wavelet (input wavelet approximating the shape of the airgun source used to record the field data). This convolution produces a synthetic trace starting from the subsea depth at which sonic and density logs were recorded to the total depth of log recorded. Then the trace is repeated and a synthetic seismogram is constructed which can be inserted in the processed seismic data displayed either as a hardcopy or screen image. The synthetic seismogram data is displayed on the seismic section in two-way-time and can be adjusted until major reflectors from the synthetic seismogram line up with the same reflectors from the seismic lines.

2.2.5. Time-Depth Conversion

Time-depth conversions were made using 12 key wells for the study area. From north to south, these wells are Hare Bay E-21, Baie Verte J-57, Blue H-28, Bonavista C-99, Linnet E-63, Cumberland B-55, Sheridan J-57, Dominion O-23, Bonanza M-71, Kyle-11, Baccalieu I-78 and Mizzen L-11. Time depth data have been made available for the some of these wells by the C-NLOPB (<http://www.cnlopb.nl.ca>) and the GSC Atlantic BASIN (www.gsc.nrcan.gc.ca/BASIN). For those wells which did not have time-depth data, sonic and density logs (from IHS Energy) were used to create the necessary time depth tables using the *SynTool*TM module of the Landmark software. A velocity model was constructed using the time-depth tables and the TDQTM depth conversion module. The velocity model was used to interpolate the data points between the wells and to obtain deeper depth conversions. Finally, seismic time trace files were converted to depth using the velocity model created with time-depth tables.

2.3. Software Used

2.3.1. *SeisWorks*TM

*SeisWorks*TM is a proficient software that offers comprehensive geological and geophysical data interpretation and display. It supports seismic and fault interpretation, generation and annotation of maps and contours both in time and depth. This module uses also the *OpenWorks*TM database which allows the integration and sharing with other software packages (i.e. *SynTool*TM and *StratWorks*TM).

2.3.2. *StratWorks*TM

*StratWorks*TM is an efficient 2-D software module for correlating well logs, creating cross-sections, modeling faults and surfaces and generating maps. This module can be integrated and associated with other geological and geophysical softwares under the *OpenWorks*TM project data management environment such as *SeisWorks*TM and/or *SynTool*TM leading to more accurate data displays and interpretation. For instance, by using *SynTool*TM, it is possible to build time-depth curves for well data and then to display in the time scale on seismic sections using *StratWorks*TM.

2.3.3. *SynTool*TM

*SynTool*TM is an advanced synthetic seismogram software program used to create synthetic seismograms and velocity models and/or calculate time/depth relationships. It

allows the accurate correlation of seismic data with well results such as lithostratigraphic tops and lithologies. Most important for hydrocarbon exploration is allowing identification in seismic data of reservoir and source rock intervals.

CHAPTER 3. STRATIGRAPHY

3.1. Exploration Well Data

There are several exploration wells drilled in the Orphan Basin, Flemish Pass and the northern portion of the Jeanne d'Arc Basin (Fig. 3.1). Nine wells are selected as key for the lithostratigraphic and biostratigraphic investigation of the Orphan Basin: these are Blue H-28, Hare Bay E-21, Baie Verte J-57, Bonavista C-99, Mizzen L-11, Kyle L-11, Baccalieu I-78, Bonanza I-27 and Linnet E-63 (Fig. 3.1). Except for the Great Barasway F-66 well, which was drilled in 2006-2007 over a large roll-over structure within a eastern basinal setting, all other wells are drilled over structural basement highs, where the Mesozoic successions are very attenuated. The data from the Great Barasway F-66 are still classified as "confidential", thus not available for this study. The lithological and biostratigraphic data from the remaining nine key wells assist in the delineations used to provide a chronostratigraphic framework for the seismic units in the Orphan Basin. The well data show that the chronology of the successions which constitute the core of the structural highs is much better delineated than the successions observed within the deep depocentres in Orphan Basin. In this study, the chronological information obtained from the exploration wells are correlated into the deep basins using the existing recently acquired seismic data and basic seismic stratigraphic methods. Tentative ages for the markers and successions observed in the deepwater basinal settings, which are not intersected in the exploration wells, are assigned using long-distance seismic correlations of key unconformity surfaces, primarily the top of Paleozoic/Precambrian pre-rift

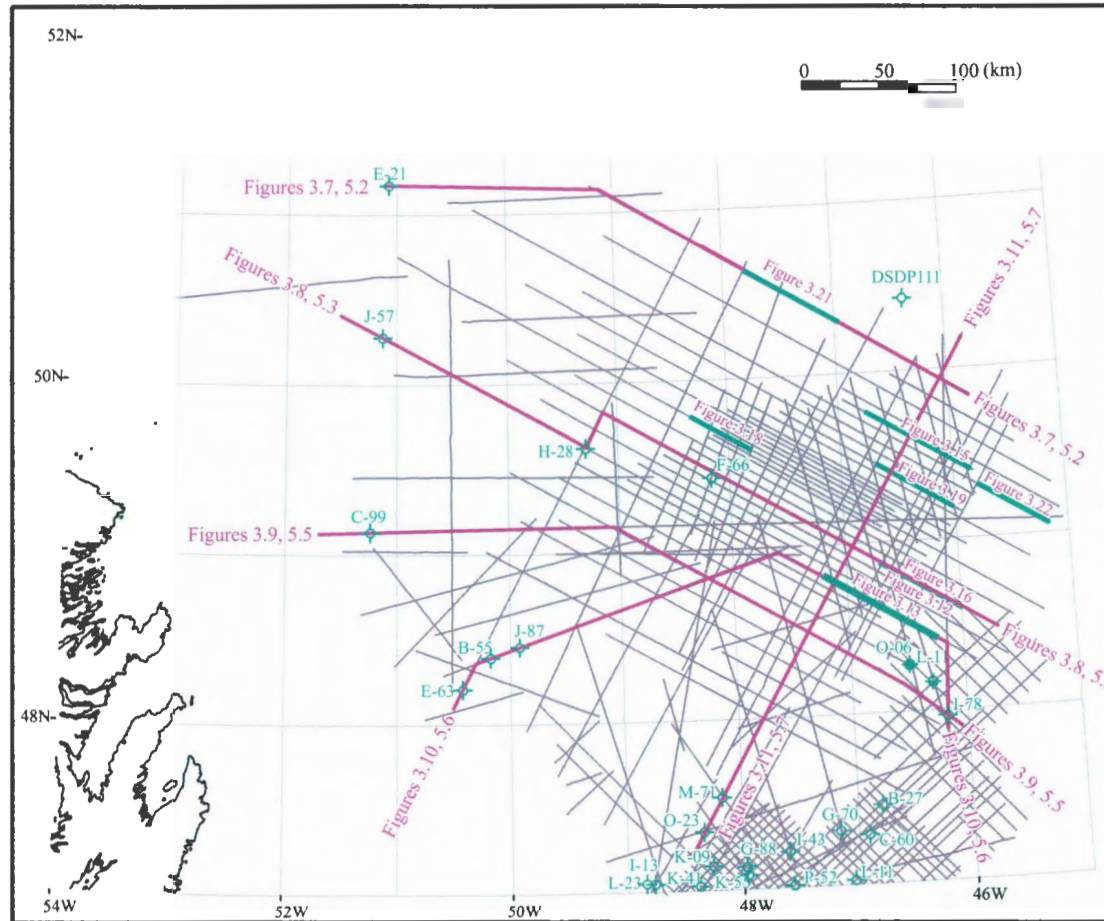


Figure 3.1. Index map showing 2D seismic profiles, locations of exploration wells drilled in Orphan Basin and environs, portions of various seismic reflection profiles shown in figures in this chapter (green lines), and five regional cross-sections (purple lines) across the Orphan Basin.

basement, top of Jurassic (Tithonian) and Mid-Cretaceous (Cenomanian) unconformities (discussed below). These tentative correlations are anchored on results of several industrial exploration key wells and achieved using deductive reasoning based on the style of tectonism and the regional architecture of the seismic sequences.

Below, detailed lithostratigraphy and biostratigraphy of the key wells are summarized, which are based on published information in open literature (e.g., McIver, 1972; Jansa and Wade, 1975; Davies, 1979; Koning et al., 1988; Smee, 2003), as well as those that are made public through the Canadian - Newfoundland and Labrador Offshore Petroleum Board (C-NLOPB), and data obtained through the Canadian Stratigraphic Service Limited.

3.1.1. Hare Bay E-21

The Hare Bay E-21 well is located at 51E10N23.1ON – 51E04N30.2OW, in ~ 239 m water depth, in the northwestern portion of the Orphan Basin (Fig. 3.1). The well was drilled by British Petroleum et al., in 1979 (see Appendix A). The main objective for drilling this well was to test an interpreted Mesozoic subcrop edge prospect. Two cores were recovered in the well. A core between 3414.0 - 3423.0 m below sea floor (mbsf) recovered mostly an upper Palaeozoic red bed succession. The second core was obtained from 4516.5 to 4525.9 mbsf, and recovered a fine-grained siliciclastic succession with few coal stringers of Late Palaeozoic age. Based on well logs, well cuttings, occasional sidewall cores and two conventional cores; the succession drilled in well is divided into three broad lithostratigraphic units, separated by two major unconformities (Fig. 3.2;

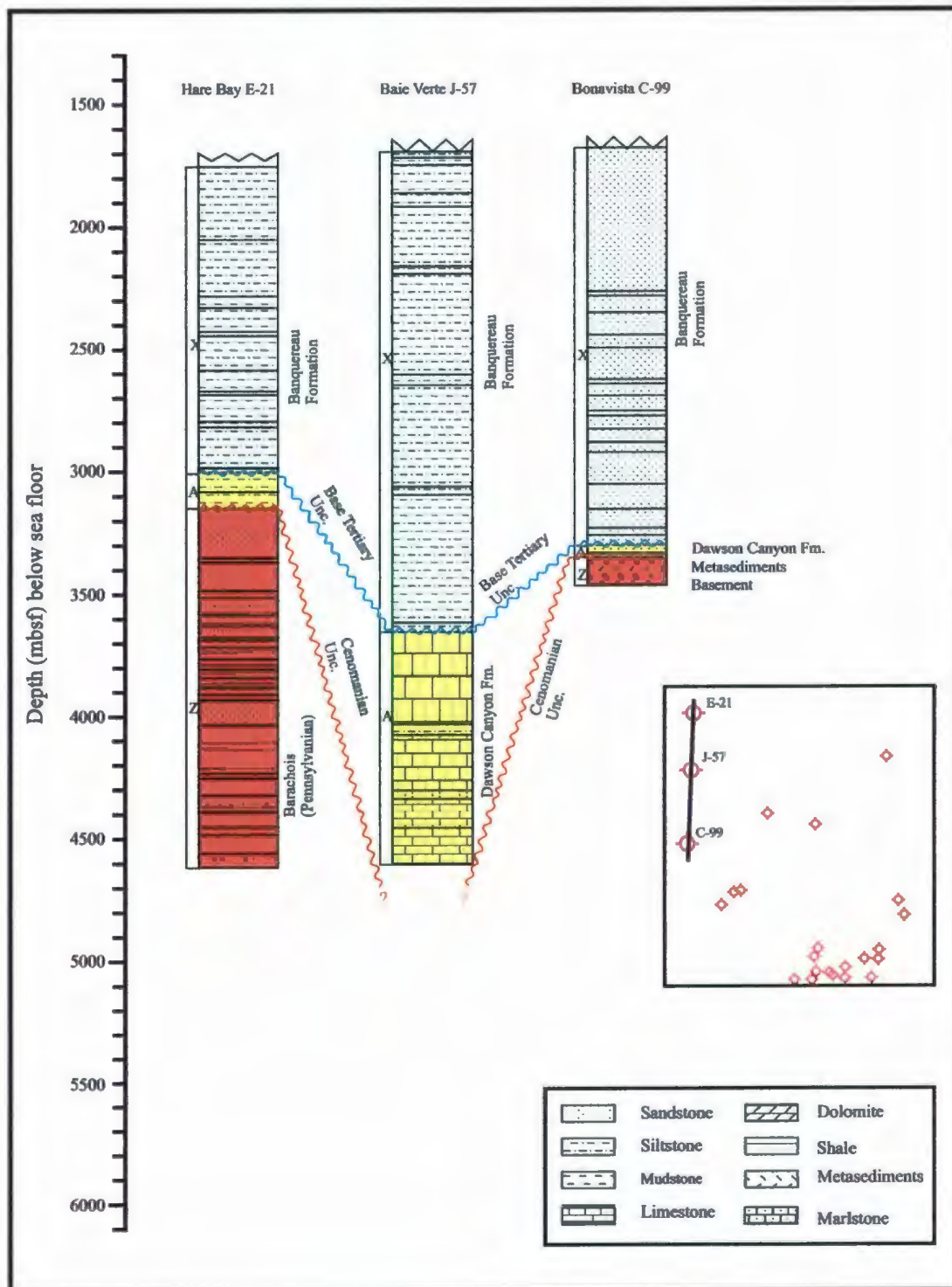


Figure 3.2. Summary lithostratigraphic logs of exploration wells Hare Bay E-21, Baie Verte J-57 and Bonavista C-99 (See figure 3.1. for well locations).

Appendix B). These unconformities are delineated by biostratigraphic and palynologic data (e.g., Davies, 1979). Age identification of these sequences was mainly based on planktonic and benthonic foraminifera. The upper 3001.7 m of sediments drilled in this well consist of dark gray, silty shales, mudstones and siltstones with very thin limestone interbeds. On the basis of diagnostic planktonic and agglutinating benthic foraminifera, these sediments are assigned to the Banquereau Formation (Figs. 3.2, 3.3; C-NLOPB Basin Database at http://basin.gsc.nrcan.gc.ca/index_e.php; Davies, 1979). The base of this succession is delineated by the regional Base Tertiary Unconformity. An approximately 157 m-thick tightly cemented sandstone succession with thinner siltstone and shale intervals occurs below the Base Tertiary Unconformity between 3001.7 mbsf and 3158.7 mbsf (Fig. 3.2). Planktonic and benthic foraminifera suggest that the unit is Cretaceous in age (i.e., Late Campanian to Early Maastrichtian; e.g., Davies, 1979). This succession is assigned to the Dawson Canyon Formation. It is separated from the underlying undifferentiated basement by the regional Cenomanian Unconformity (see below). The basement rocks are encountered from 3158.7 mbsf to 4634.7 mbsf. They are composed of interbedded sequence of tight, well-cemented, red-brown sandstones, indurated shales and siltstones, overlying a thick grey limestone, sandstone sequence with coaly intervals (Fig. 3.2). Lack of diagnostic microfossils precludes a firm age assignment. However, regional correlations between the Hare Bay E-21 well and the successions mapped in northwestern Newfoundland, suggest that this section may be correlative with the continental Barachois Formation of Lower Pennsylvanian age (BP et al., 1979). In this well, the regional unconformity between the Dawson Canyon

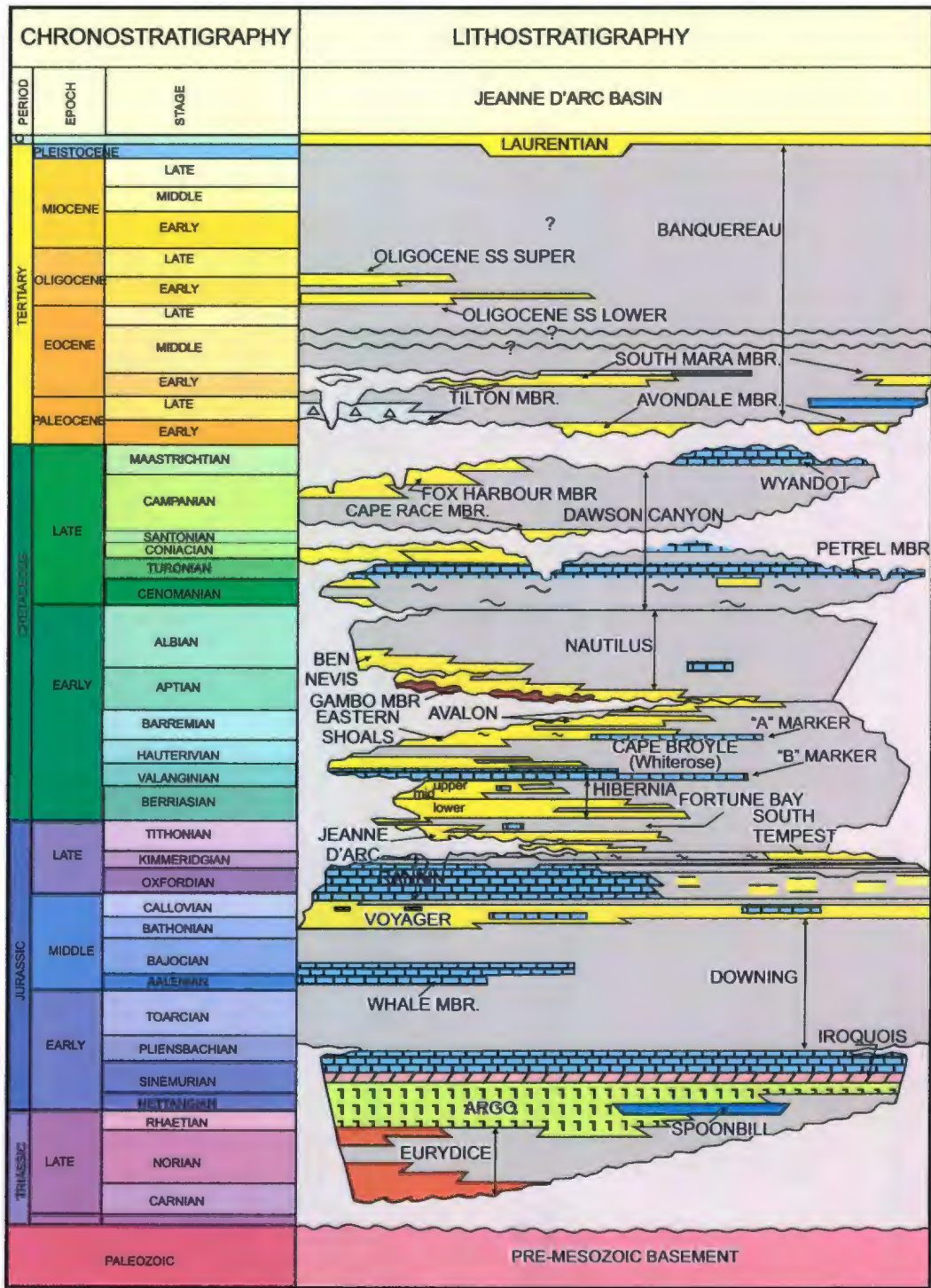


Figure 3.3. Lithostratigraphic chart of the Jeanne d'Arc and Orphan Basins modified after Sinclair (1988) and C-NLOPB (2003).

Formation and the underlying Paleozoic basement rocks must represent a major composite unconformity, which includes the unconformity that defines the top of the Paleozoic successions, the top Jurassic Unconformity as well as the Mid-Cretaceous (Cenomanian) Unconformity commonly observed elsewhere in the Jeanne d'Arc and Orphan basins (Grant and McAlpine, 1990), with the Mid-Cretaceous (Cenomanian) Unconformity being the last major erosional episode that decapitated the structural high over which the Hare Bay E-21 was drilled.

No significant oil or gas shows were encountered while drilling the Hare Bay E-21 well. However, the lower part of the Banquereau Formation has thermally immature organic rich shales with 1.7 - 3.5% total organic carbon, which could become an effective source rock, if buried into the oil-generative window elsewhere in the Orphan Basin (Smee, 2003).

3.1.2. The Baie Verte J-57

The Baie Verte J-57 well was drilled by British Petroleum et al. in 1985 (see Appendix A). The well is located at 50E16N43.95ON – 51E07N53.52O W, in 303 m water depth in the Orphan Basin (Fig. 3.1). It was drilled to test a four way anticlinal closure identified using seismic data. The reservoir target was the Lower Cretaceous succession, draped over an underlying basement high.

Based on well logs, well cuttings, and occasional sidewall cores, the succession drilled in the Baie Verte J-57 well is divided into two units, separated by a major

unconformity (Fig. 3.2; Appendix B). Age identifications of these sequences and the unconformity were based on the biostratigraphy of planktonic and benthic foraminifera and coccoliths (Robertson Research, 1985). The sediments in the upper 3660.8 mbsf are composed of grey to brown mudstone grading upward into an interbedded sandstone/siltstone succession (Figs. 3.2, 3.3). These sediments are correlated with the Banquereau Formation. Deep water agglutinated and calcareous benthic foraminiferal assemblages in sediments from 916.8 mbsf and 3964.0 mbsf suggest an outer shelf to bathyal environment and a Paleocene to Oligocene age (Robertson Research, 1985). The Base Tertiary Unconformity marks the base of the Banquereau Formation. The underlying sediments extend from the Base Tertiary Unconformity to the total depth of 4607.8 mbsf, and include an upper unit consisting mainly of a sandstone succession with siltstone interval and a lower unit characterized by grey to brown, mudstone in the lower unit which grades upward into a silica-cemented sandstone and grey siltstones succession (Figs. 3.2, 3.3). These sediments are assigned to the Late Cretaceous Dawson Canyon Formation. Sandstones in the upper unit are fine to medium grained, argillaceous and include tight silica cement. Micropaleontological data reveal a Coniacian to Turonian age for the upper unit (BP et al., 1989) and an Albian to Cenomanian age for the lower unit (Robertson Research, 1985).

In the Baie Verte J-57 well the Tertiary sediments contained 1.5% - 6.0% total organic carbon, but they are thermally immature (Smee, 2003).

3.1.3. Bonavista C-99

The Bonavista C-99 well is located at 49E08N05ON - 51E14N25OW, in ~ 329 m water depth in the western portion of the Orphan Basin (Fig. 3.1). The well was drilled by British Petroleum and Columbia Gas in 1974 and re-drilled in 1975 to a depth of 3769 mbsf (see Appendix A). The primary objective was to test a structural closure that had been interpreted on seismic sections and to test the potential of Early Cretaceous and Tertiary reservoirs.

Based on well logs, well cuttings, occasional sidewall cores; the succession drilled in Bonavista C-99 well is divided into three broad sequences, separated by two major unconformities (Fig. 3.2; Appendix B). Age identifications were made using the biostratigraphy of planktonic and benthic foraminifera. The upper 3299.3 m of sediments drilled in this well consist of a fine grained sandstone, mudstone, limestone, siltstone and shale succession at the base, grading upward into a predominantly coarse-grained sandstone sequence (BP et al., 1981; Figs. 3.2, 3.3). Planktonic foraminiferan and dinoflagellate assemblages suggest a Tertiary age for this sequence (Williams, 1975). These sediments are correlated with the Banquereau Formation. The base of this sequence is assigned to the Base Tertiary Unconformity. An approximately 50 m-thick, predominantly coarse grained, porous sandstone succession with limestone and shale intervals occurs between 3299.3 mbsf and 3349.8 mbsf (Figs., 3.2, 3.3). Dinoflagellate, planktonic foraminifera and ostracod assemblages indicate a Late Cretaceous age (Late Campanian to Early Maastichtian) for these sediments (Williams, 1975). This succession

is correlated with the Dawson Canyon Formation. The regional Cenomanian Unconformity delineates the base of the Dawson Canyon Formation. From 3349.8 mbsf and 3355.8 mbsf the well encountered an igneous succession, including granite and pegmatite of possibly Paleozoic age. These rocks are interpreted as the part of pre-rift granitic basement sequence (Figs., 3.2, 3.3).

The Late Cretaceous sandstones of the Dawson Canyon Formation are good reservoir rocks. Early Cretaceous shales are organic rich, but they are immature at the well location.

3.1.4. Blue H-28

The Blue H-28 well is located at 49E37N26.49ON – 49E17N58.18OW in the Orphan Basin, ~ 340 km northeast of St. John's (Fig. 3.1; Koning et al., 1988; Robertson Research, 1985). It was drilled in ~1486 m water depth by Texaco et al. in 1979 (see Appendix A). Routine cuttings and sidewall cores were collected, but no cores were retrieved. The Blue H-28 well was drilled slightly off the crest of the Paleozoic Gander structure (see Chapter 4) to test the up-dip truncation edge of the Lower Cretaceous succession and to evaluate the source potential of the Paleozoic successions (Koning et al., 1988).

Based on well logs, well cuttings, and occasional sidewall cores, the succession drilled in Blue H-28 well is divided into four broad lithostratigraphic units, separated by three unconformities which are delineated by biostratigraphic and palynologic data (Figs.

3.3, 3.4; Appendix B; Koning et al., 1988; McAlpine, 1988). Age identification of these units was mainly based on the biostratigraphy of planktonic foraminifera and pollen and spores. These units are briefly described below:

The upper 3350.8 m of sediments in the Blue H-28 well consists of grey shales and thin indurated mudstones (Figs. 3.3, 3.4). This succession is assigned to the Banquereau Formation; the uppermost un-sampled portion must also include the unconsolidated Pleistocene – to Recent Laurentian Formation. Rare foraminifera and palynomorph taxa in sediments between 1403.8 mbsf and 3350.8 mbsf suggest an open marine deep water environment and a Paleocene to Oligocene age for the succession (Koning et al., 1988). The base of this unit is marked by the regional Base Tertiary Unconformity. The underlying unit extends from 3350.8 mbsf to 3461.8 mbsf. It is divided into two subunits. The upper subunit is composed of mainly dark grey shale and thin limestone interbeds which become more arenaceous toward its base (Fig. 3.4). Planktonic foraminifera suggest that it is Late Cretaceous (Maastrichtian) in age and that it was deposited in an open shelf and/or deeper slope environment (Koning et al., 1988). The lower subunit is mainly composed of grey shales, siltstones and thin mudstones (Fig. 3.4). The sandstones are predominantly mature, medium- to coarse-grained orthoquartzites with observable porosity (Koning et al., 1988). The sediments between 3433.8 mbsf-3463.8 mbsf is assigned to Cenomanian -? Campanian (Robertson Research, 1979). The succession that occurs between 3350.8 mbsf to 3461.8 mbsf is correlated with the Dawson Canyon Formation (Figs. 3.3, 3.4). A predominantly shale unit between 3461.8 to 3794.8 mbsf in this well revealed distinct microfaunal assemblages which

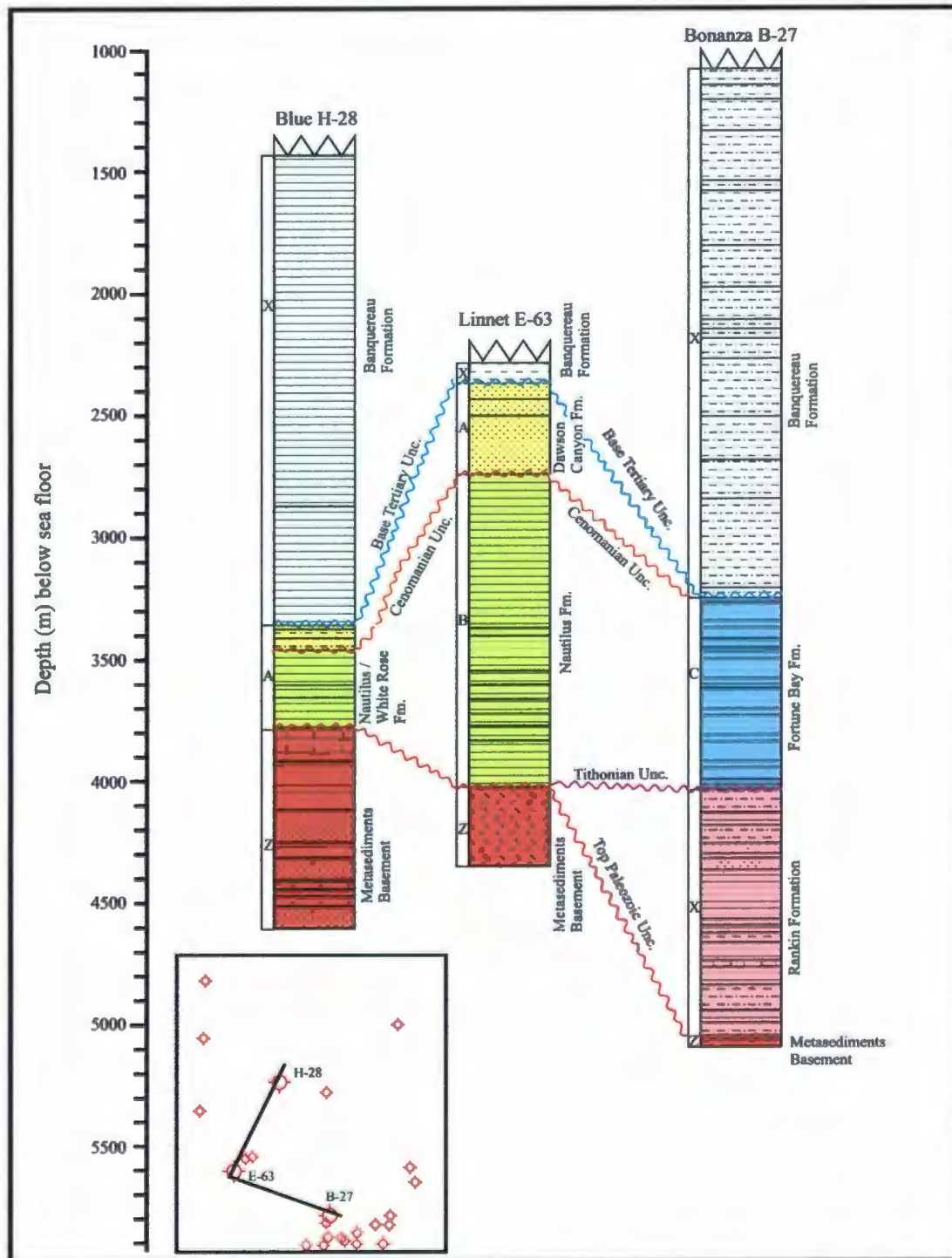


Figure 3.4. Summary lithostratigraphic logs of exploration wells Blue H-28, Linnet E-63 and Bonanza B-27. Lithological symbols are given in Figure 3.2.

suggest a shallow marine environment and an Early Cretaceous (Neocomian) to Late Jurassic (Oxfordian) age (McAlpine, 1988) for the ~333 m-thick succession that occurs below the lower subunit (Robertson Research 1979). McAlpine (1988) correlated this succession with the Early Cretaceous Nautilus Formation. However, the Late Jurassic (i.e., Oxfordian, as referenced in Robertson Research, 1979) to Early Cretaceous (i.e., Albian to Aptian, as referenced in Gradstein and Thomas, 1983 cited in the C-NLOPB Basin Database at http://basin.gasca.nrcan.gc.ca/index_e.php) age of this succession clearly suggest that the shale-dominated unit must therefore correlate with the Late Jurassic to Early Cretaceous White Rose Formation, extending into the Nautilus Formation. The Cenomanian Unconformity separates the lower subunit of the Dawson Canyon Formation from the shale-dominated White Rose and/or Nautilus formations. Several coarsening-upward successions suggest periods of regression. The Dawson Canyon Formation is separated from the underlying metasediment basement sequence by the nonconformity (Fig. 3.3). The pre-rift basement rocks are divided into two subunits; the upper subunit is ~ 90 m thick, and is composed of micritic limestones. Age-diagnostic fauna are rare in this unit, but a Carboniferous age is proposed by Koning et al. (1988). The lower subunit is composed of ~ 720 m-thick sandstones, shales, minor micritic limestones with minor dolomites. The spores and vascular tissues suggest a post-late Silurian age. It was deposited in a shallow marine environment.

The regional unconformity between the Dawson Canyon Formation and the underlying Paleozoic basement rocks must include the nonconformity that defines the top of the Paleozoic successions, as well as the top Jurassic Unconformity observed

elsewhere in the Jeanne d'Arc and Orphan basins (Grant and McAlpine, 1990), with the top Jurassic Unconformity being the last major erosional episode over the structural high where the Blue H-28 was drilled.

The Blue H-28 well did not encounter any significant oil or gas shows. The sandstones intersected in the pre-rift basement succession are angular to subrounded, medium – to coarse-grained with ~ 19% porosity (Koning et al., 1988) and may constitute a reservoir rock elsewhere in the Orphan Basin. Although the organic matter within the Dawson Canyon Formation was largely oxidized in the Blue H-28 well, the relatively high percentage of amorphous, oil generating kerogen, suggests that this succession could be a potential oil source rock in the Orphan Basin (Dow, 1979). Banquereau Formation has 0.80% to 3.44% total organic carbon which is defined as good to very good potential source rock, if buried into the oil-generative window elsewhere in the Orphan Basin.

3.1.5. Linnet E-63

The Linnet E-63 well was drilled in 1982 by the consortium led by Mobil Oil et al. (see Appendix A). The well is located at 48E12N30ON - 50E25N27OW in ~ 160 m water depth in the southwestern portion of the Orphan Basin (Fig. 3.1). The well was drilled to evaluate the presence of hydrocarbons in a structural closure formed by a tilted fault block on the flank of the Bonavista Platform (Smee, 2003). A seven metre core was cut into the Paleozoic metasedimentary succession. Based on well logs, well cuttings, occasional sidewall cores and one conventional core, the succession drilled in Linnet E-63 well is divided into four lithostratigraphic units, separated by three major

unconformities (Fig. 3.4; Appendix B). Age identifications of these sequences and unconformities were based mainly on the biostratigraphy of foraminifera, and pollen and spores (Mobil et al., 1983).

The uppermost ~ 2385 m are predominantly composed of a shale succession, with thin sandstones beds (Fig. 3.4). This formation is assigned a Tertiary age (Mobil et al., 1983), and thus correlated with the Banquereau Formation (Figs. 3.3, 3.4). The underlying Dawson Canyon Formation is separated from the Banquereau Formation by the Base Tertiary Unconformity, which occurs at 2385.0 mbsf (Figs. 3.3, 3.4; Appendix B). The Dawson Canyon Formation extends from 2385.0 mbsf to 2756.0 mbsf and is comprised of a medium- to coarse-grained sandstone succession, overlain by a shale and marl succession. Foraminifera and spores suggest a Late Cretaceous (i.e., Cenomanian to Maastrichtian) age for the sequence (Mobil et al., 1983; Bujak Davies Group, 1988). The base of the Dawson Canyon Formation is marked by the prominent Cenomanian Unconformity (Figs. 3.3, 3.4). A shale-dominated succession lies beneath the Cenomanian Unconformity extending from 2756.0 mbsf to 4018.0 mbsf (Appendix B). This succession is divided into two units: an upper ~1025 m-thick shale unit with minor sandstone stringers near the base and a lower ~237 m-thick shale unit (Fig. 3.4). On the basis of dinoflagellate assemblages the upper unit is assigned to the Early Cretaceous age (i.e., Barremian to Albian; Mobil et al., 1983), whereas the lower unit is assigned to the Late Jurassic age (i.e., Oxfordian; Mobil et al., 1983). However, Bujak Davis Group (1988) suggests that the sediments between 2993.0 mbsf and 3963.0 mbsf only contain palynological evidence for an Albian - Aptian age. If the former age is correct, the lower

unit can be correlated with the White Rose Formation and its distal equivalent, the Fortune Bay Formation. However, if the latter age is correct, the lower unit can be correlated with the Nautilus Formation. The boundary between the White Rose Formation or the Nautilus Formation and the underlying metasedimentary basement sequence is marked by a nonconformity (Fig. 3.4). The lowermost sequence of this well is composed of slightly metamorphosed undifferentiated Palaeozoic-aged basement rocks (Chaplin et al., 1982; Mobil et al., 1983).

The Linnet E-63 well was drilled to a total depth of 4363.0 mbsf without encountering any hydrocarbon bearing zones. However, the total organic carbon of shales in the Dawson Canyon Formation and the lower part of the Banquereau Formation ranges from 1% - 7% which is defined as excellent potential source rock if buried to sufficient depths. The sandstones of the Dawson Canyon Formation could be excellent reservoir in other prospects in the Orphan Basin (Smee, 2003).

3.1.6. Bonanza M-71

The Bonanza M-71 well is located at 47E30N47.34ON – 48E11N55.15OW in the northern Jeanne d'Arc Basin (Fig. 3.1). It was drilled in ~193.5 m water depth by Mobil et al. in 1982 (see Appendix A). Routine cuttings, sidewall cores and one conventional core were collected. The Bonanza M-71 well was drilled to test the hydrocarbon potential of the Late Jurassic sandstones and shales in this region of the Orphan Basin.

Based on well logs, well cuttings, occasional sidewall cores and one conventional core, the successions drilled in the Bonanza M-71 well are divided into four major lithostratigraphic units, separated by three prominent unconformities (Figs. 3.3, 3.4; Appendix B; Mobil et al, 1983; McAlpine, 1988). Age identification of these units was mainly based on palynomorph and planktonic foraminiferal assemblages. These units are briefly described below:

The uppermost ~ 3266.5 m in the well is predominantly composed of a siltstone-dominated succession with mudstone and limestone stringers (Fig. 3.4). This succession grades down-section into a mainly shale succession with thin limestone beds. These sediments are Tertiary in age (Mobil et al., 1983), and thus, are correlated with the Banquereau Formation (Figs. 3.3, 3.4). The underlying Fortune Bay Formation is separated from the Banquereau Formation by the Base Tertiary Unconformity, which occurs at 3266.5 mbsf (Figs. 3.3, 3.4; Appendix B). The Fortune Bay Formation extends from 3265.5 mbsf to 4046.5 mbsf and is comprised of a shale-dominated succession with siltstone, sandstone and limestone stringers. In the lower portion, this succession includes sandstone and siltstone stringers (Fig. 3.4). Diagnostic foraminiferal assemblages suggest a Cretaceous (i.e., Valangian to Upper Campanian) age for the succession (Mobil et al., 1983). The base of the Fortune Bay Formation is marked by the prominent top Jurassic (Tithonian) Unconformity occurring at 4046.5 mbsf (Figs. 3.3, 3.4). A shale-dominated succession lies beneath the Tithonian Unconformity and extends from 4046.5 mbsf to 5088.5 mbsf (Appendix B). It consists of numerous sandstone beds and siltstone stringers which traced down section grade into frequent sandstone interbeds, minor siltstone

stringers and limestone beds (Fig. 3.4). On the basis of foraminiferal assemblages this succession is assigned to the Early Portlandian to Kimmeridgian age (C-NLOPB, 2007). It is correlated with the Rankin Formation (C-NLOPB, 2007; Basin Database at http://basin.gsc.nrcan.gc.ca/index_e.php). The boundary between the Rankin Formation and the underlying metasedimentary basement sequence is marked by a nonconformity (Fig. 3.4). The lowermost ~12 m-thick sequence of this well is composed of slightly metamorphosed undifferentiated basement rocks (CNLOPB, 2007).

3.1.7. Kyle L-11

The Kyle L-11 well is located at 47E00N36.897ON – 47E02N48.910OW, in the Flemish Pass Basin in 1118.7 m water depth (Fig. 3.1). It was drilled by ESSO Resources Canada Limited in 1986.

Based on well logs, well cuttings, occasional sidewall cores the succession drilled in the Kyle L-11 well is divided into three broad lithostratigraphic units, separated by two major unconformities (Figs. 3.3, 3.5; Appendix B). Age identification of these units was based on the dinoflagellate, pollen, spore and foraminiferal assemblages (Esso Parex et al., 1986). The upper 827 m in the well is characterized by a predominantly shale succession with sandstone, siltstone and limestone intervals (Fig. 3.5). This succession is correlated with the Banquereau Formation (Fig. 3.5). The base of this sequence is marked by the Base Tertiary Unconformity (Esso Parex et al., 1986). The sediments underlying the Base Tertiary Unconformity consist of mudstones, shales with limestones

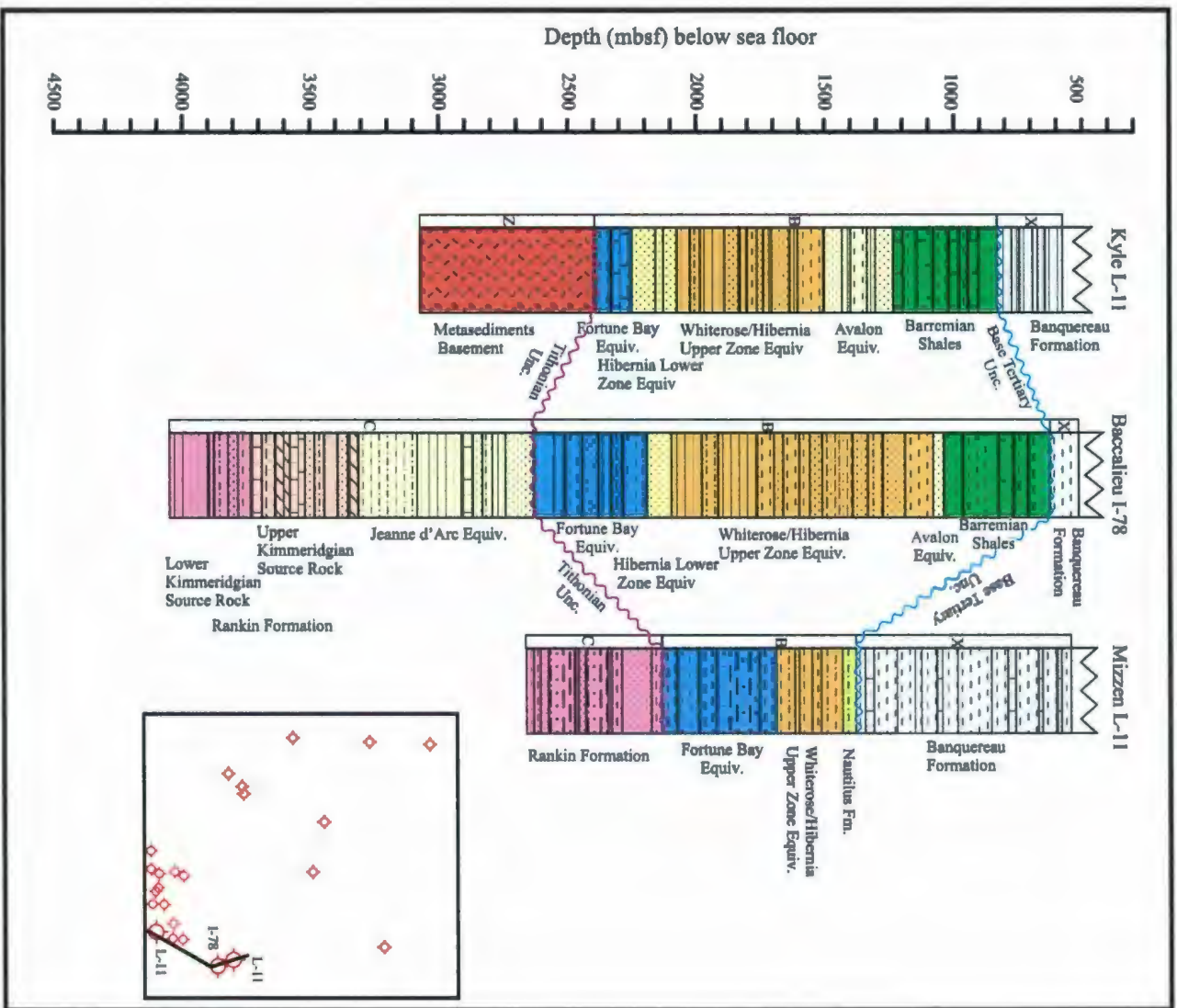


Figure 3.5. Summary lithostratigraphic logs of exploration wells Kyle L-11, Baccalieu I-78 and Mizzen L-11. Lithological symbols are given in Figure 3.2.

and thin sandstone stringers. The unit extends from 827.3 mbsf to 2398.3 mbsf, and it is divided into three subunits. The upper subunit consists of interbedded limestone and mudstone (827.3 mbsf to 1249.3 mbsf). The middle subunit occurs between 1249.3 mbsf and 2088.3 mbsf and is composed of interbedded sandstones mudstone and shale, which down-section becomes a mainly shale-dominated succession with siltstone stringers (Fig. 3.5). The lower subunit occurs from 2088.3 mbsf to 2398.3 mbsf, and is composed predominantly of sandstones and siltstones with trace amount of shale interbeds, with a prominent 75-80 m-thick limestone interval occurring within this unit (Fig. 3.5). Palynological data show that the successions from 843.8 mbsf to 1022.3 mbsf and from 1058.9 mbsf to 1560.8 mbsf are of Barremian and Late Hauterivian-Barremian age, respectively (BP Exploration, 1991, see http://basin.gasca.nrcan.gc.ca/index_e.php). Thus the upper unit is correlated with the Barremian Shales (Figs. 3.3, 3.5). Similarly, the palynological data show that the succession from 1571.3 mbsf to 1856.3 mbsf and 1885.3 mbsf to 1956.3 mbsf are Early Hauterivian and Valanginian in age, respectively. Therefore, the middle subunit is correlated with the Avalon and Hibernia formations, and their lateral (basinal) equivalent, the White Rose Formation (Fig. 3.3). The palynological data further suggest that the lower subunit must correlate with the lower portion of the Hibernia Formation and its distal lateral equivalent, the Fortune Bay Formation (Fig. 3.3).

There are two prominent limestone-dominated successions within the sediments between the Base Tertiary Unconformity and the unconformity that separates the metasedimentary basement succession. The interbedded limestones and mudstones that occur between ~971.3 mbsf and 1166.3 mbsf within the upper subunit are correlated with

the regional A Marker Member of the White Rose Formation (Figs. 3.3, 3.5). Similarly, the prominent limestone succession that occurs within the lower subunit from 2261.3 mbsf to 2381.3 mbsf is correlated with the regional B Marker Member of the White Rose Formation (Figs. 3.3, 3.5).

The base of the lower subunit (i.e., the Hibernia Formation and its distal lateral equivalent, the Fortune Bay Formation) is defined by the prominent top Jurassic (Tithonian) Unconformity (C-NLOPB Basin Database, electronic source is at http://basin.gsc.nrcan.gc.ca/index_e.php). The underlying sequence is ~700 m thick and is dominated by metamorphosed sandstone and siltstone and is correlated with the undifferentiated metasedimentary basement succession (Figs. 3.3, 3.5). No *in-situ* microfossils were found within this unit (Esso Parex, et al., 1986).

The Tertiary sequence includes 1-3% organic matter (Esso Parex et al., 1988) and is interpreted to be a potentially gas-prone Type III source rock. No oil source rocks were encountered in the drilled section.

3.1.8. Baccalieu I-78

The Baccalieu I-78 well was drilled by Esso et al. in 1985 (Fig. 3.1; Appendix A). It is spudded at 47E57N41.49ON – 46E10N46.76OW, in ~1092.8 m water depth, within the Flemish Pass Basin.

Based on well logs, well cuttings, occasional sidewall cores and four conventional cores, the succession in the Baccalieu I-78 well is divided into three lithostratigraphic

units, which are separated by two major unconformities (Figs. 3.3, 3.5; Appendix B). Age identification of these units was mainly based on the biostratigraphy of nannofossils, dinoflagellates, foraminiferal and ostracode assemblages. The upper ~613.2 m of sediments drilled in this well are composed of grey, blocky mudstones (Fig. 3.5). It is assigned to the Banquereau Formation (Figs. 3.3, 3.5). The base of this formation is delineated by the regional Base Tertiary Unconformity. A predominantly siliciclastic succession underlies the Base Tertiary Unconformity and extends from 613.2 mbsf to 2767.2 mbsf (Fig. 3.5). It is divided into a mudstone-dominated upper unit (i.e., 613.2 mbsf - 2097.2 mbsf) and a shale-dominated lower unit (i.e., 2097.2 mbsf - 2677.2 mbsf). The upper unit grades downward into siltstones with sandstone, mudstone and shale interbeds. Foraminifera and nannofossil assemblages suggest an early Cretaceous age (i.e., Aptian to Barremian) for the upper unit (Pocock, 1986). The lower unit includes siltstone, sandstone and shale stringers. On the basis of nannofossil, foraminifera and dinoflagellate assemblages the lower unit is assigned an Early Cretaceous age (i.e., Aptian to Portlandian; Pocock, 1986). Similar to that described in the Kyle L-11 well, this sequence in the Baccalieu I-78 well also includes several formations and members: (i) the upper unit is correlated with the Barremian Shales, their lateral equivalents the White Rose Formation, and (ii) the lower unit is correlated with the Jeanne d'Arc Formation and its lateral equivalent, the Fortune Bay Formation (Figs. 3.3, 3.5).

The contact between the lower unit (i.e., Jeanne d'Arc Formation and its lateral equivalent, the Fortune Bay Formation) and underlying sediments is characterized by the regional Tithonian Unconformity (Figs. 3.3, 3.5; C-NLOPB Basin Database at

http://basin.gsc.nrcan.gc.ca/index_e.php) or top Jurassic Unconformity (Smee, 2003, Enachescu et al., 2005). The lowermost sequence in this well (i.e., 2677.2 mbsf - 4042.2 mbsf) is composed of shales with minor siltstone, sandstone, limestone and dolomite stringers (Fig. 3.5). Based on the presence of distinct ostracode and foraminiferal assemblages this sequence is assigned a Kimmeridgian to Bathonian age and a middle/inner neritic to lagoonal environment (Pocock, 1986), and it is correlated with the Rankin Formation (Figs. 3.3, 3.5).

3.1.9. Mizzen L-11

The Mizzen L-11 well was drilled by Petro Canada et al. in 2003 (Appendix A). It is located in the Flemish Pass Basin at 48E10N31.76ON – 46E17N35.59OW, ~ 484 km east-northeast of St. John's, Newfoundland (Fig. 3.1). The water depth at the well site is 1153 m. The primary objectives were to evaluate the hydrocarbon potential of (i) the Early Cretaceous (Berriasian) "Baccalieu Sandstone", which was initially encountered in the Baccalieu I-78 well, 25.5 km to the south-southeast of the Mizzen L-11 well (Petro Canada Oil and Gas Report, 2003) and (ii) the Late Jurassic sandstone succession which was encountered within the source rock interval in Baccalieu I-78. Based on well logs, well cuttings, and occasional sidewall cores, the succession drilled in Mizzen L-11 well is divided into three lithostratigraphic units, separated by two major unconformities (Figs. 3.3, 3.5; Appendix B). Age identification of these sequences was mainly based on the biostratigraphy of foraminifera, and pollen and spores.

The upper 827 m is composed of gray claystones and shales (Fig. 3.5). This succession is assigned to Late Paleocene to Pleistocene age (Robertson, 2008) and thus, it is correlated with the Banquereau Formation (Figs. 3.3, 3.5; CNLOPB, 2007). The base of this sequence is marked by the Base Tertiary Unconformity occurring at 1369.0 mbsf. The sediments underlying the Base Tertiary Unconformity consist of approximately 782 m thick siliciclastic succession, including interbedded sandstones, siltstones and shales with stringers of argillaceous white lime mudstone and siltstone laminations (Fig. 3.5). This unit can be divided into three subunits; the upper subunit extends from 1369.0 mbsf to 1428.0 mbsf. It contains a mainly siltstone succession with minor mudstone interbeds. The upper subunit is assigned to Late Albian age and it is correlated with the Nautilus Formation (Figs. 3.3, 3.5; Robertson, 2008; CNLOPB, 2008). The middle subunit ranges from 1428.0 mbsf to 1699.0 mbsf and consists of a siltstone-dominated succession with mudstone intervals and minor limestone interbeds. According to Robertson (2008), this middle subunit spans from Early Hauterivian to Early Barremian. Thus, it is correlated with the White Rose Formation (Figs. 3.3, 3.5). The lower subunit is ~452 m thick and extends from 1699.0 mbsf to 2151.0 mbsf. It consists of a succession composed of alternating siltstones and mudstones. It is assigned to latest Berriasian - Early Valanginian age and it is correlated with the Fortune Bay Formation (Figs., 3.3, 3.5; Robertson, 2008; CNLOPB 2008). The base of this succession is marked by a prominent unconformity, which occurs at 2151.0 mbsf. This unconformity is correlated with the Tithonian Unconformity. The underlying succession is ~519 m-thick and extends from 2151.0 mbsf to 2670.0 mbsf. This succession consists of mainly a siltstone and sandstone

alternations with minor limestone interbeds and two massive, clean sandstone beds occurring at the lower portion of the succession (Fig. 3.5). This succession is assigned to Late Jurassic age (i.e., from the earliest Tithonian to Late Tithonian; Robertson, 2008). It is correlated with the Rankin Formation (Fig. 3.3). Deon and Timmons (2003) further correlate the massive sandstone packages with the Jurassic Sandstones 1 and 2.

The upper sandstone succession of the Rankin Formation contains significant oil shows with 15% inter-granular porosity. However, the Jurassic Sandstone 1 and 2 show only residual oil stains, and based on low LWD (logging while drilling) resistivities, this sequence is suggested to be wet. These two massive sandstones within the lower portion of the Rankin Formation have very-good porosities, but lack any hydrocarbon shows.

3.1.10. Great Barasway F-66

The Great Barasway F-66 well is located at 49E25N25.25O - 48E09N52.36O, in the Orphan Basin, ~ 400 km northeast of St. John's (Fig. 3.1). The well was drilled in ~ 2350 m water depth, by Chevron, Shell, Exxon Mobil and Imperial Oil in 2006. The primary objective for this well was to test the very large Mesozoic structural closure. The well is still classified as "confidential", thus no other information is available.

3.2. Summary Stratigraphy Across the Study Area

Figure 3.6 shows the summary stratigraphic correlation between key wells used in this study. The figure shows that the Banquereau Formation is ubiquitous in the Orphan Basin. The Base Tertiary Unconformity is a prominent surface which is identified in all key wells examined. The Cretaceous successions were rarely encountered in the drilled wells: the Late Cretaceous Dawson Canyon Formation occurs in wells from the western and northern portion of Orphan and Flemish basins (e.g., Hare Bay E-21, Baie Verte J-57, Bonavista C-99 and Blue H-28), whereas the Lower Cretaceous Fortune Bay and White Rose, Nautilus formations (e.g., Linnet E-63, Mizzen L-11), as well as the Jurassic successions were drilled only in the neighbouring Jeanne d'Arc and Flemish Pass basins (e.g., Bonanza B-27, Kyle L-11, Baccalieu I-78 and Mizzen L-11). Across nearly the entire Orphan Basin, the synrift Mesozoic succession is floored by a low – to slightly – metamorphosed Paleozoic basement succession (Fig. 3.6).

3.3 Seismic Stratigraphy

Five regional composite seismic reflection profiles are constructed to illustrate the seismic stratigraphic architecture and structural development (discussed in Chapter 4) of the Orphan Basin (Figs. 3.7-3.11). These profiles are deliberately selected crossing the existing key exploration wells, so that the chronology of the successions drilled in these wells can be convincingly retrieved and correlated with the seismic reflection profiles. These regional composite profiles will further allow the evaluation of the occurrence and distribution of seismic stratigraphic units across Orphan Basin.

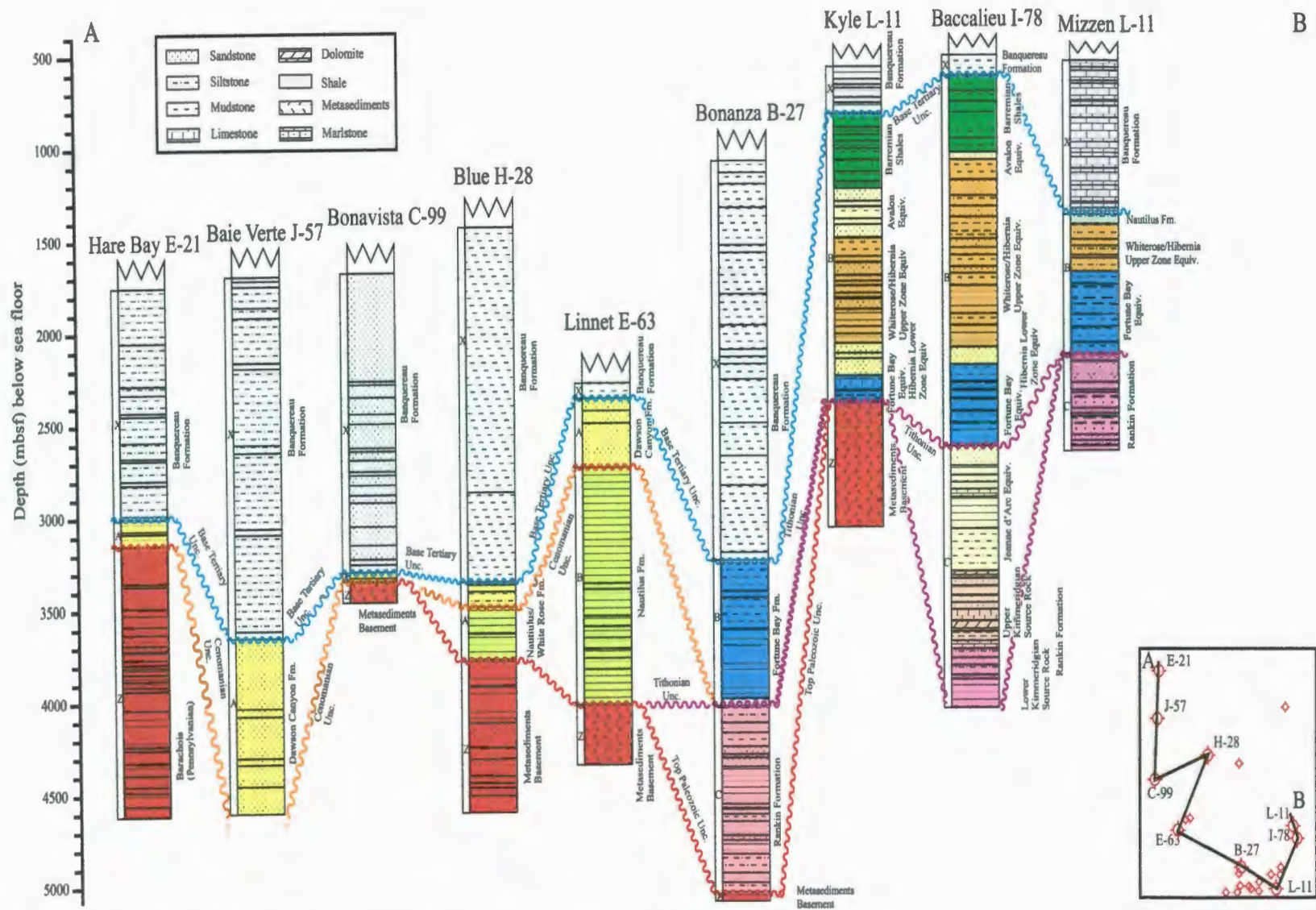


Figure 3. 6. North to south summary lithostratigraphic correlation between nine key exploration wells in study area.

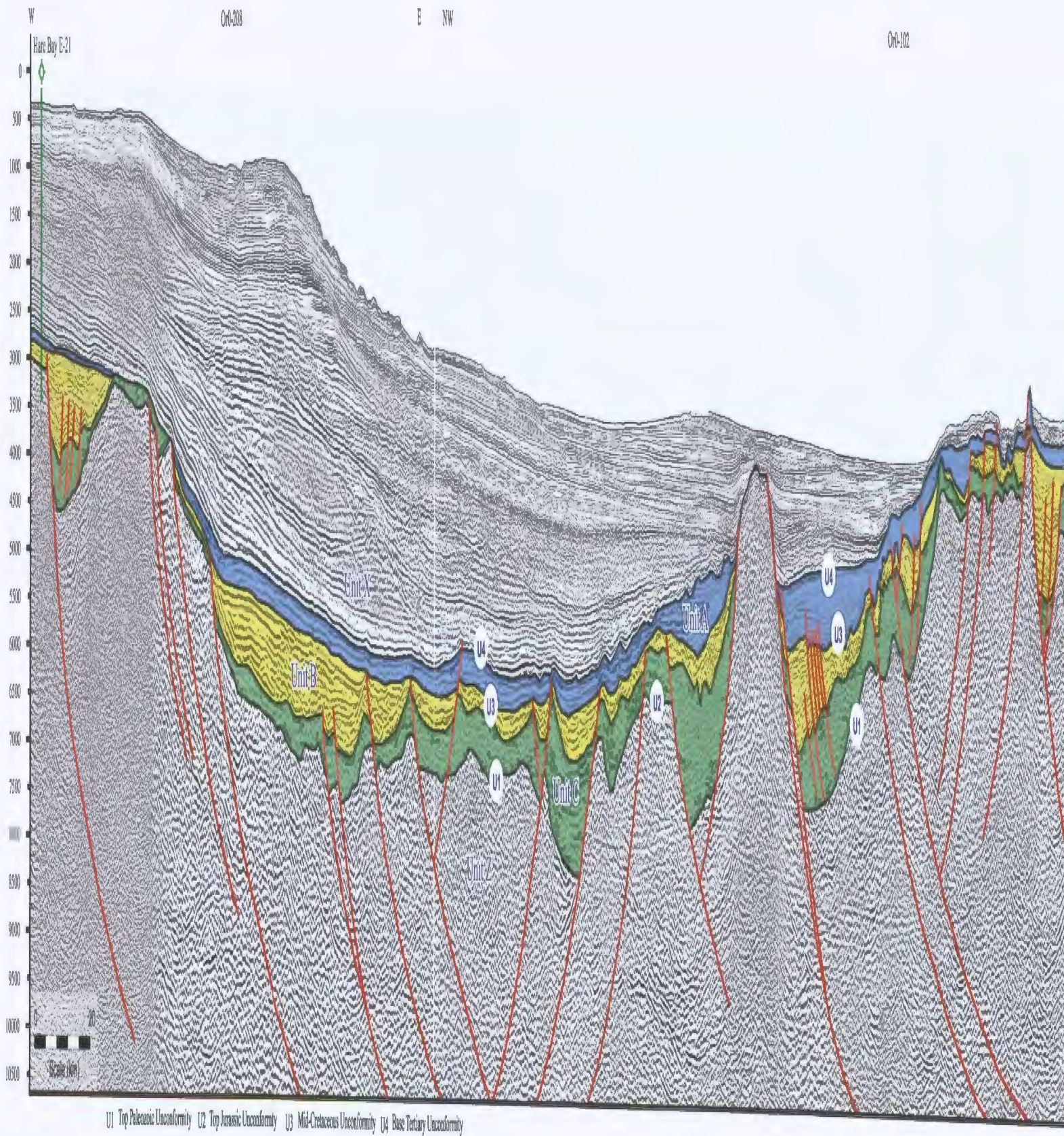
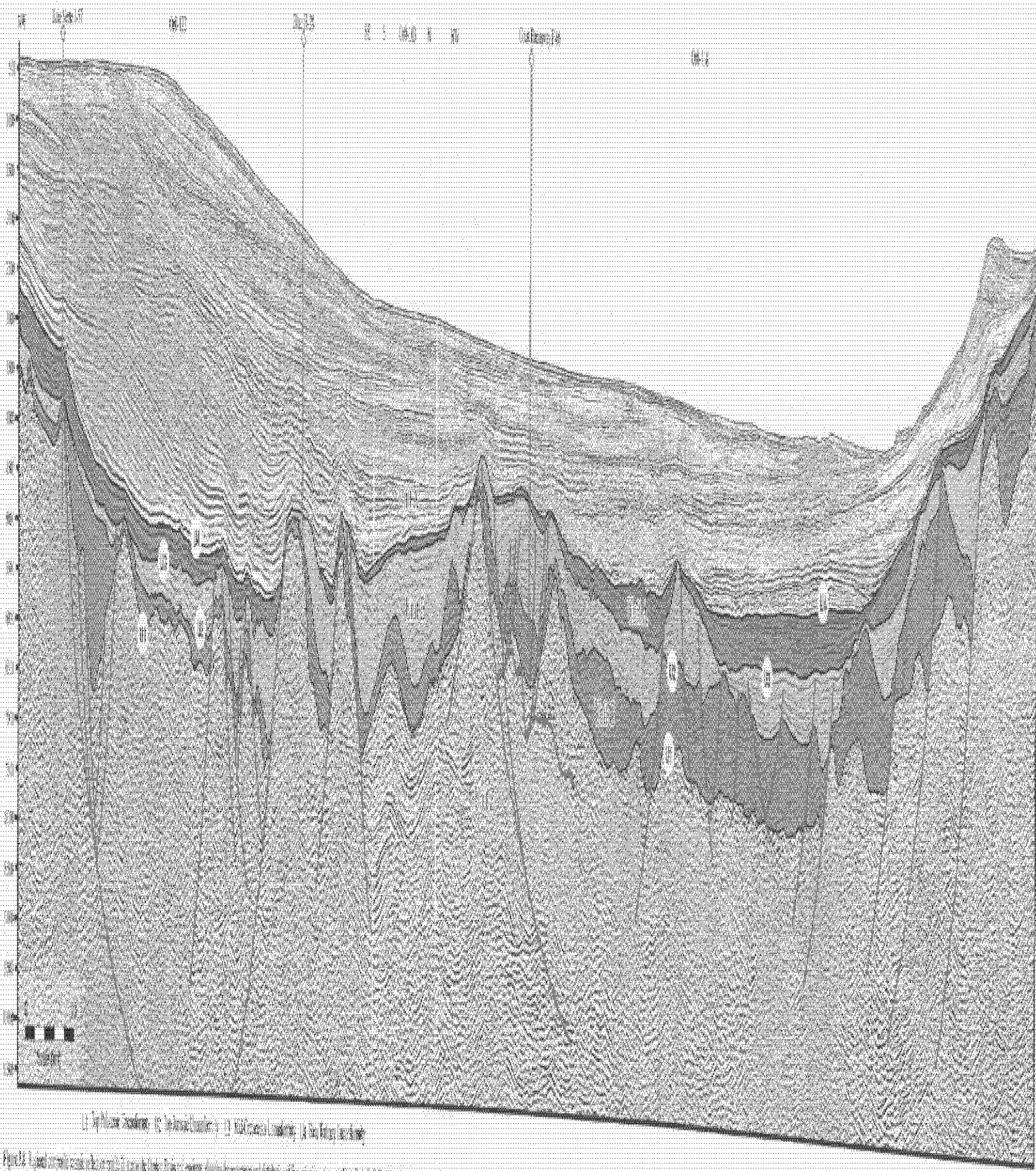
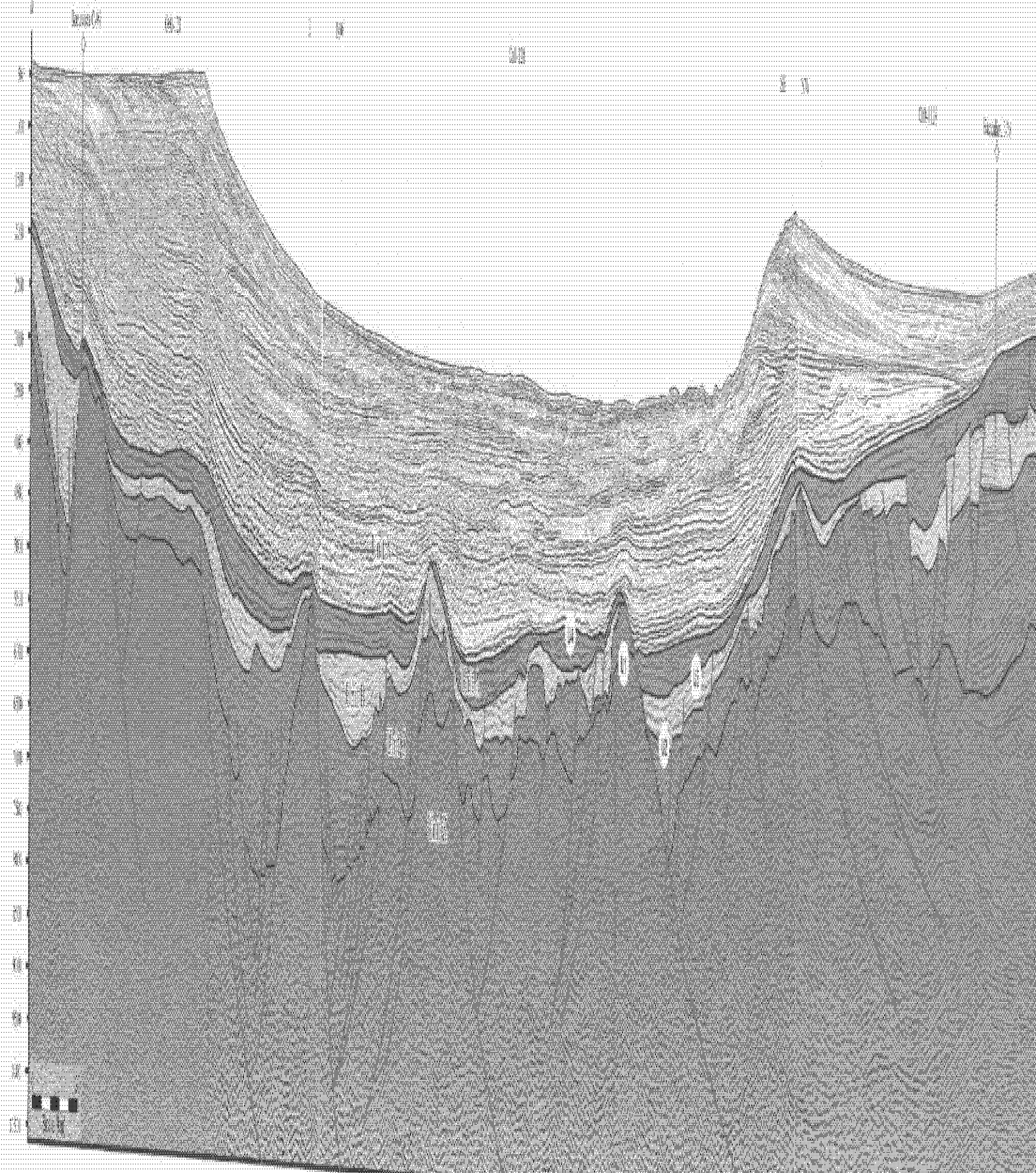


Figure 3.7. Regional composite seismic reflection profile A across the Orphan Basin, showing the occurrence and distribution of five seismic stratigraphic Units X, A, B, C, Z, prominent regional unconformities U1-U4, faults delineating basement-sored ridges and intervening basins (discussed in Chapter 4), and the location of exploration well Hare Bay E-21. Location is shown in Figure 3.1. Vertical scale given in TWT (ms).



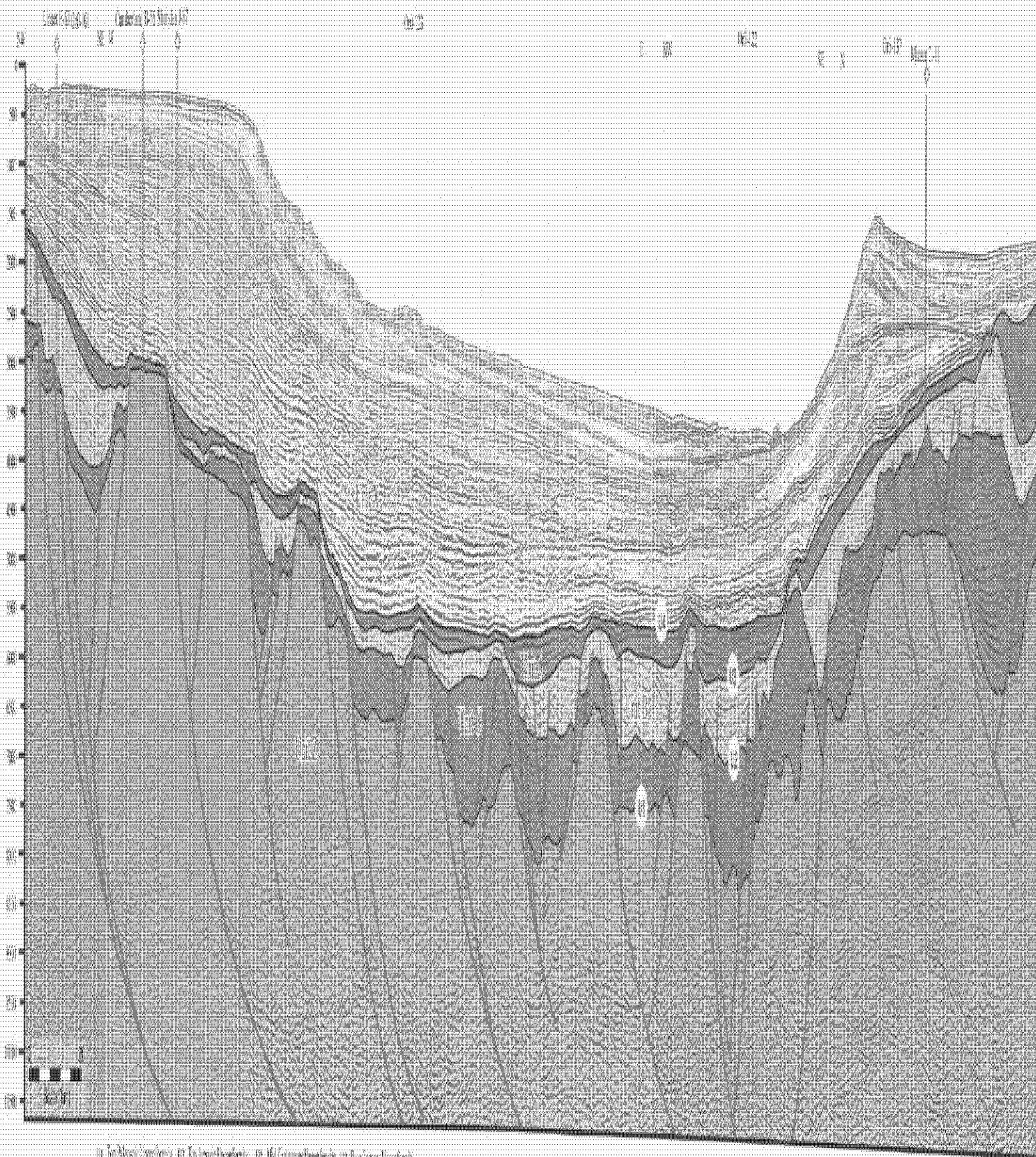
(1) Quaternary deposits; (2) Pleistocene sands and silts; (3) Pleistocene clays; (4) Pliocene clays.

Figure 2.6. A geological cross-section of the coastal plain of Cape Town, showing the sequence and distribution of the various deposits of the Quaternary, Pleistocene and Pliocene. The section is based on data from the Cape Town Geological Survey, and is a simplified version of the section shown in Figure 2.5. Vertical scale is in meters.



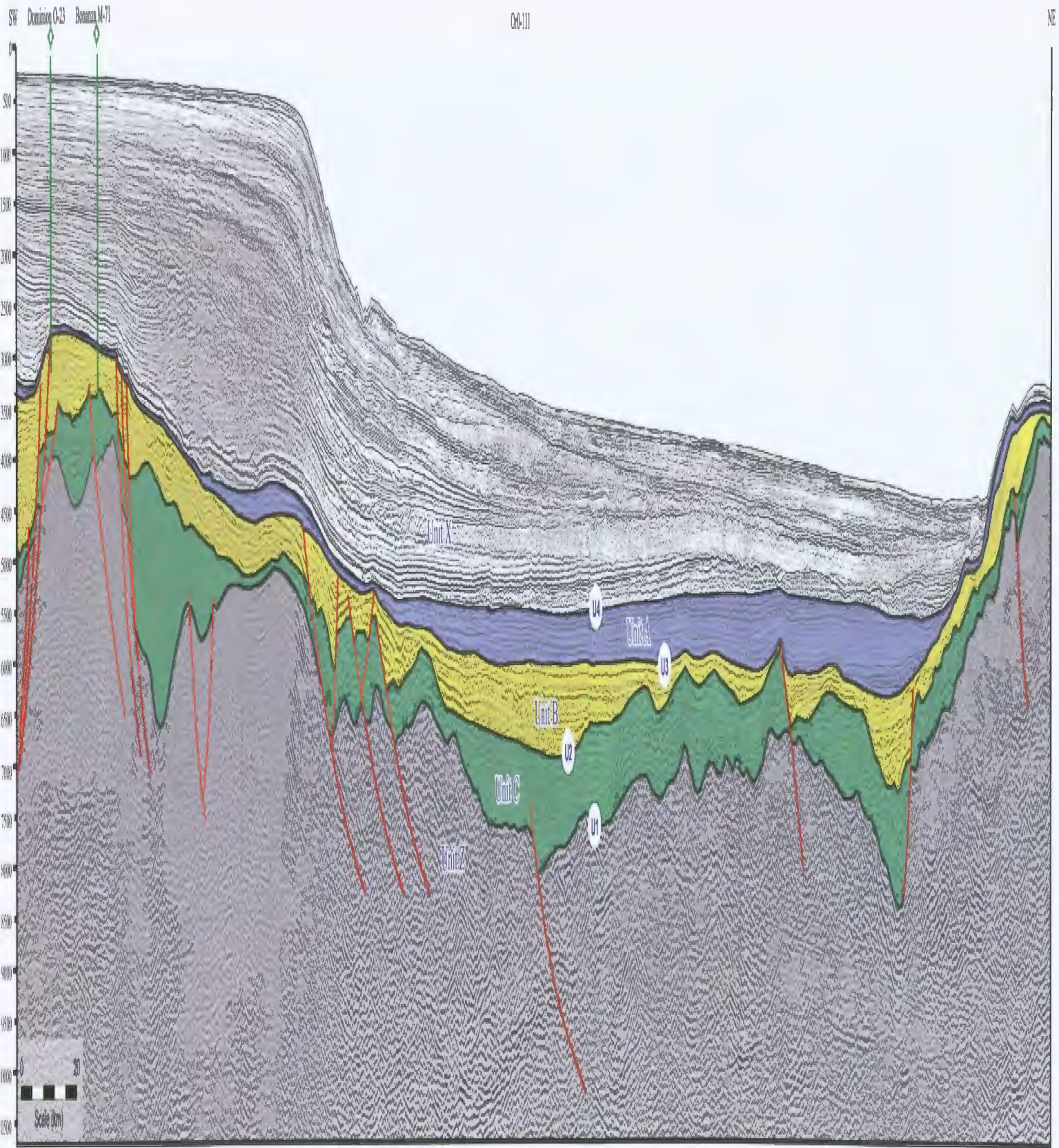
1) Top Plateau (sandstone) 2) Red sandstone 3) Mid Plateau (sandstone) 4) Basal Plateau (sandstone)

Figure 1. A geological cross-section of the study area showing the relationship between the various geological units and the structural features. The scale bar represents 100 m. The units are: 1) Top Plateau (sandstone), 2) Red sandstone, 3) Mid Plateau (sandstone), and 4) Basal Plateau (sandstone). The structural features include: 1) Fault, 2) Thrust, 3) Syncline, and 4) Anticline.



(1) Top Marine Sandstone (2) Top Marine Sandstone (3) Mid-Cretaceous Sandstone (4) Blue Shales (Unconformity)

Figure 118. Regional cross-section showing the distribution of the various stratigraphic units A, B, C, Z, primary regional unconformity (U-1), and the location of the major faults and structural features. The location of the major faults and structural features is shown in Figure 1. Vertical scale in feet (1000 ft).



U1 Top Paleozoic Unconformity U2 Top Jurassic Unconformity U3 Mid-Cretaceous Unconformity U4 Base Tertiary Unconformity

Figure 3.11. Regional composite seismic reflection profile E, across the Cribban Basin, showing the occurrence and distribution of five seismic stratigraphic Units X, A, B, C, Z, prominent regional unconsformities U1-U4, faults delineating basement-cored ridges and intervening basins (discussed in Chapter 4), and the locations of exploration wells Dominion O-23 and Bonanza M-71. Location is shown in Figure 3.1. Vertical scale given in TWT (ms)

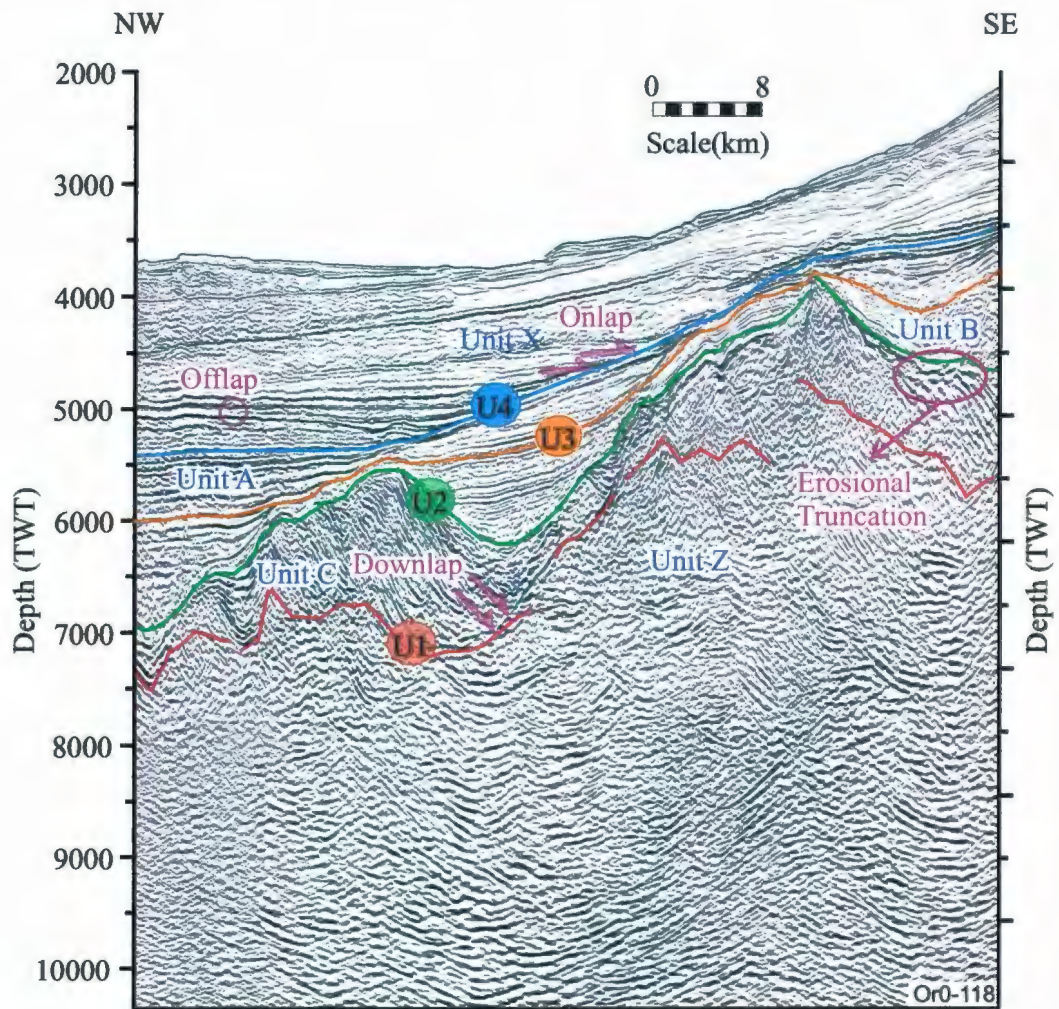
On the basis of the acoustic character, reflectivity, and reflector strength and continuity, the seismic profiles examined during this study are divided into five major seismic stratigraphic units, labeled as Units X, A, B, C and Z (Figs. 3.7-3.11). These units are separated from one another by prominent and widespread regional seismic markers U1-U4, representing major unconformities in seismic profiles. The separating unconformity surface markers are described in section 3.3.1 and the seismic units are described in section 3.3.2.

3.3.1 Regional Seismic Markers Representing Unconformity Surfaces

There are a number of prominent reflectors in seismic reflection profiles that are present in the entire Orphan Basin seismic database. These surface markers labelled U1-U4 clearly represent major discontinuities between the overlying and underlying seismic sequences. These discontinuities are marked by distinctive reflection terminations, including onlap, offlap, downlap and erosional truncation and therefore constitute major erosional and depositional unconformities (Fig. 3.12). The technique associated with the delineation of the unconformities using reflection terminations is described in Chapter 2.

3.3.1.1 Unconformity - U1: surface capping Unit Z

Regional marker U1 is a prominent surface that lies deep in all seismic reflection profiles (Fig. 3.13). U1 unconformity separates a thick package of variably reflective, often low amplitude, discontinuous and reverberatory reflections (i.e., Unit Z described



- U1 Top Paleozoic Unconformity
- U2 Top Jurassic Unconformity
- U3 Mid-Cretaceous Unconformity
- U4 Base Tertiary Unconformity

Figure 3.12. Multichannel seismic reflection profile Or0-118 showing examples of onlap, offlap, downlap and erosional truncation. Location is shown in Figure 3.1.

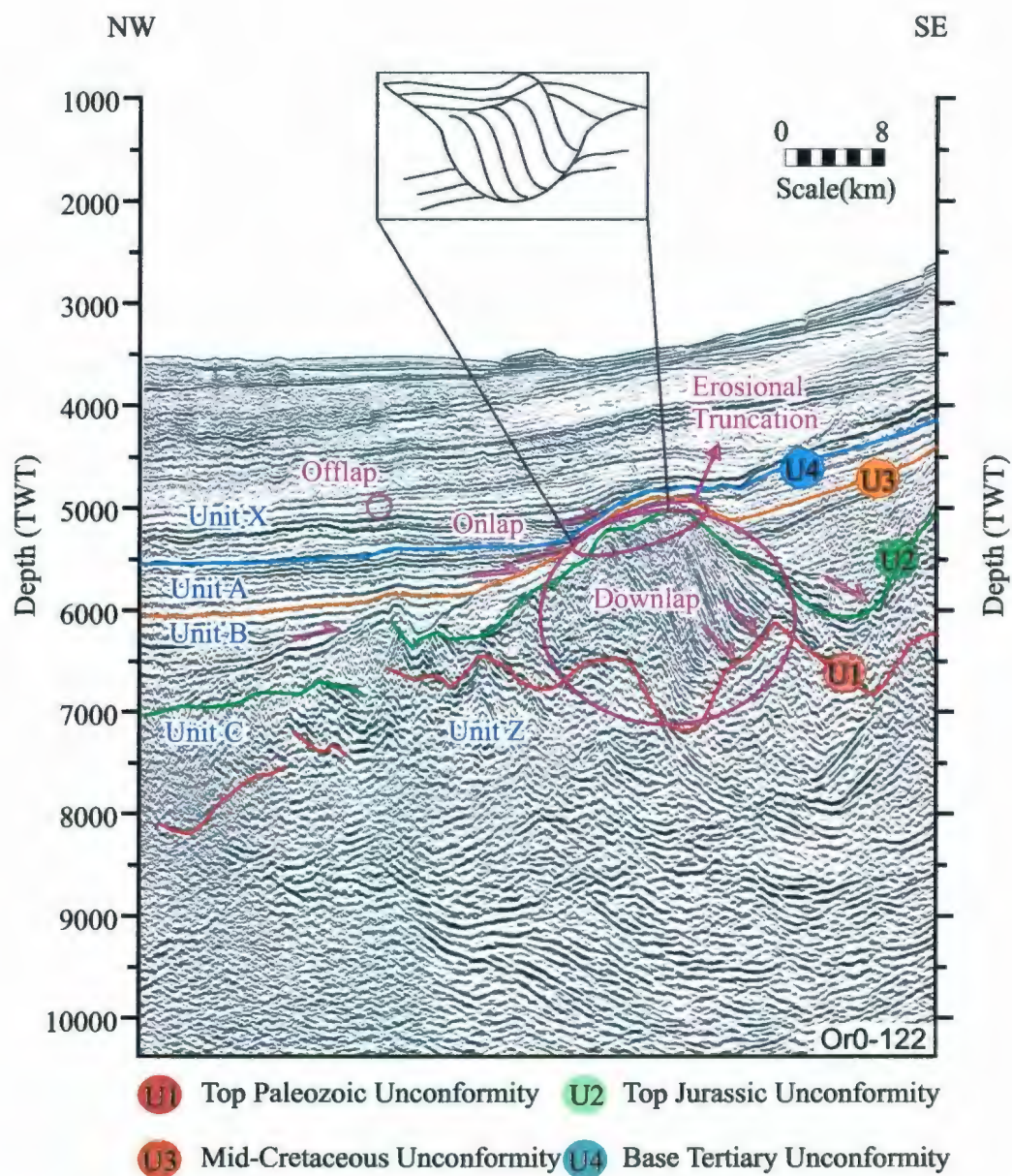


Figure 3.13. Multichannel seismic reflection profile showing examples of onlap, offlap, downlap and erosional truncation. Location is shown in Figure 3.1.

below) from a package characterized by high amplitude, strong and continuous reflections (i.e., Unit C). The prominent apparent downlap and onlap of reflections of the overlying Unit C over the regional marker U1, and the mild to moderate erosional truncation of reflections of the underlying Unit Z, collectively indicate that marker U1 is an unconformity surface (Fig. 3.13).

The overall morphology and the structural fabric of the Orphan Basin are clearly depicted by the attitude of this regional unconformity U1 (Fig. 3.14). For example, the time-structure map shows that the western, southwestern and eastern margins of the basin are defined by the shallow occurrence of the U1 surface, whereas the basinal setting is depicted by the generally deep occurrence of the surface. Away from the margins, and across the Orphan Basin the regional unconformity U1 defines a hugely corrugated surface rising and falling 1 to 3 seconds (Fig. 3.14). This morphology is best developed within the northwestern portion of the Orphan Basin, where the unconformity U1 creates a series of northeast-southwest oriented high blocks defined by shoaling of the unconformity surface, separated by depressions defined by deepening of the unconformity surface. Thus, the U1 unconformity delineates a number of ridges and their intervening basins: these are further described in Chapter 4 (Fig. 3.14). Within the study area, the unconformity surface U1 is also offset by the large synrift faults that dominate the structure in this region: these faults are also described in Chapter 4. Correlations with exploration wells show that the U1 unconformity represents the prominent erosional surface which marks the top of the Paleozoic and/or Pre-Cambrian

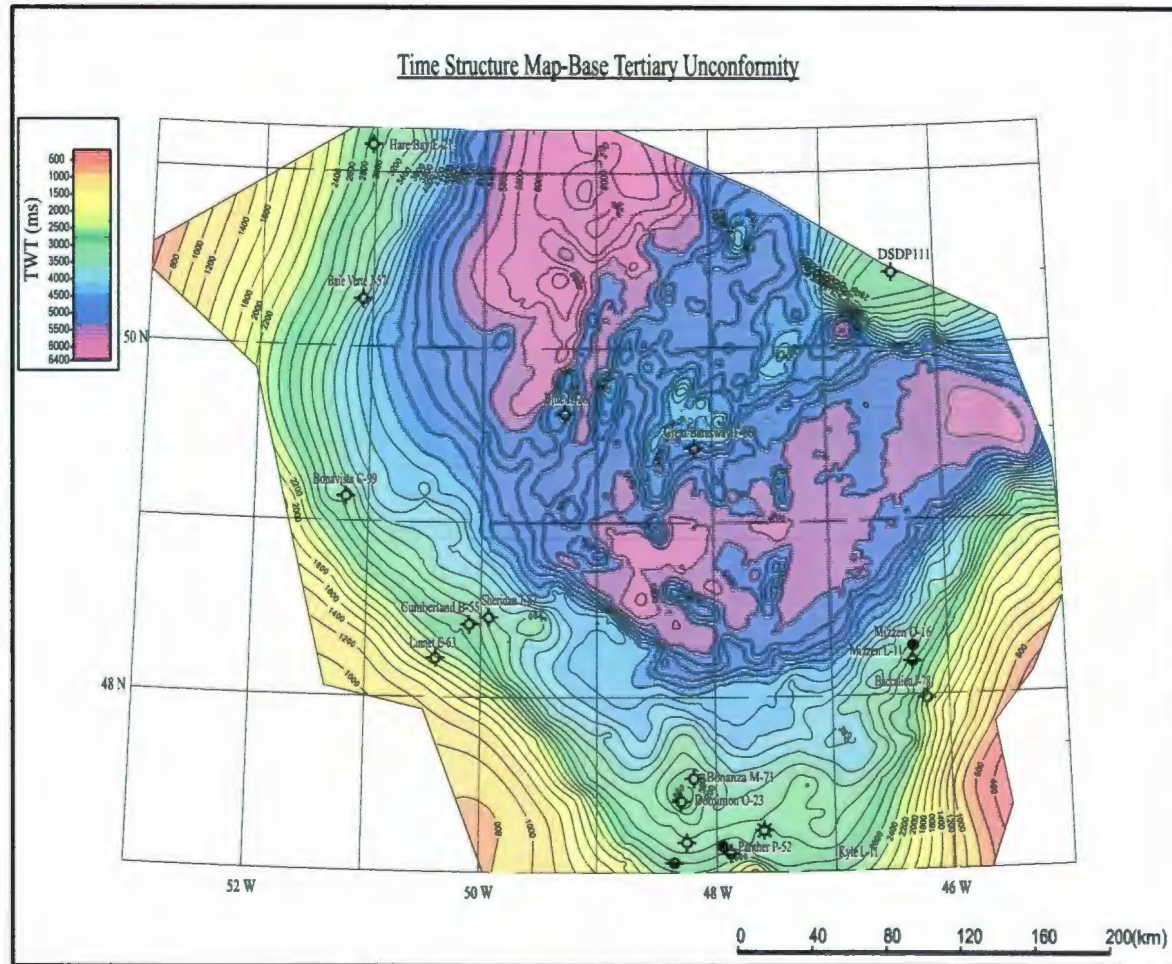


Figure 3.14. Time-structure map of the regional marker (unconformity) U1. Isochrons are in milliseconds twt. Also shown are the exploration wells in the region.

successions in the region. This unconformity further marks the base of the pre-rift successions in the study area.

3.3.1.2 Unconformity - U2: Surface Capping Unit C

Seismic marker U2 is a moderate to variably high amplitude reflector, which separates Unit C from Unit B (Fig. 3.13). It defines a laterally traceable and broadly undulating surface ranging in depth from 7500 ms in the basin axis and up to 2500 ms at the crests of the ridges. The high amplitude reflections of the underlying Unit C show pronounced truncations along the seismic marker U2 (Fig. 3.13), whereas, the overlying Unit B displays strongly stratified packages consisting of alternating low and high amplitude continuous reflections of a protracted progressive onlap over the marker U2 (Fig. 3.12). These geometric relationships suggest that seismic marker U2 is also a widespread regional angular unconformity surface.

Seismic reflection profiles show that the regional marker U2 can be readily traced into the deeper basins, where the unconformable relationship is still visible by the mild truncation of the underlying high amplitude reflection of Unit C, as well as a very gentle downlap relationship of the overlying lower amplitude reflections (Fig. 3.15). In the central portion of the study area, particularly in regions proximal to the eastern basin margin, the unconformity U2 is invariably cut by major extensional faults (Fig. 3.16; further discussed in Chapter 4).

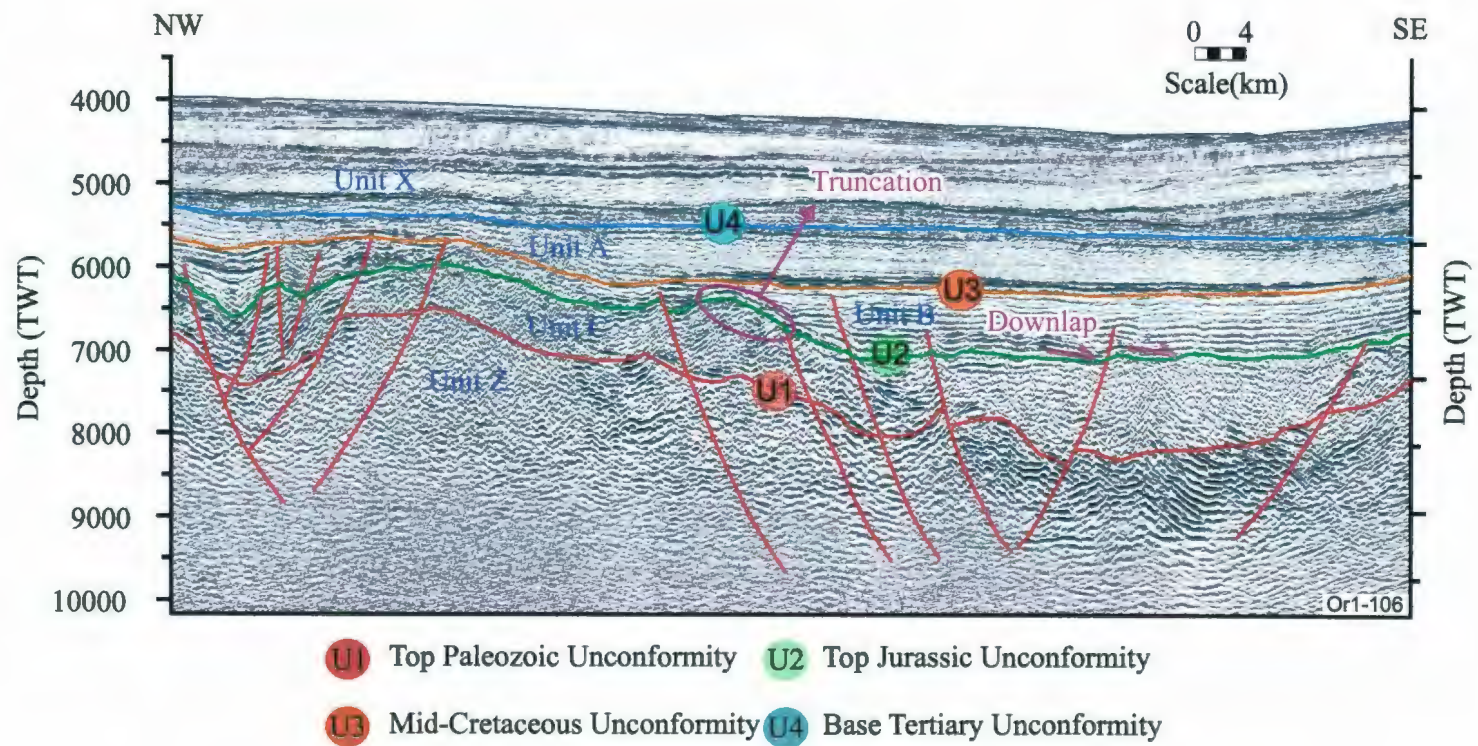


Figure 3.15. Multichannel seismic reflection profile Or1- 106 showing the mild truncation of the Unit C (? Triassic-Jurassic) and the gentle downlap of the overlying Unit B (Early Cretaceous) at the regional marker U2 (Cenomanian Unconformity). Location is shown in Figure 3.1.

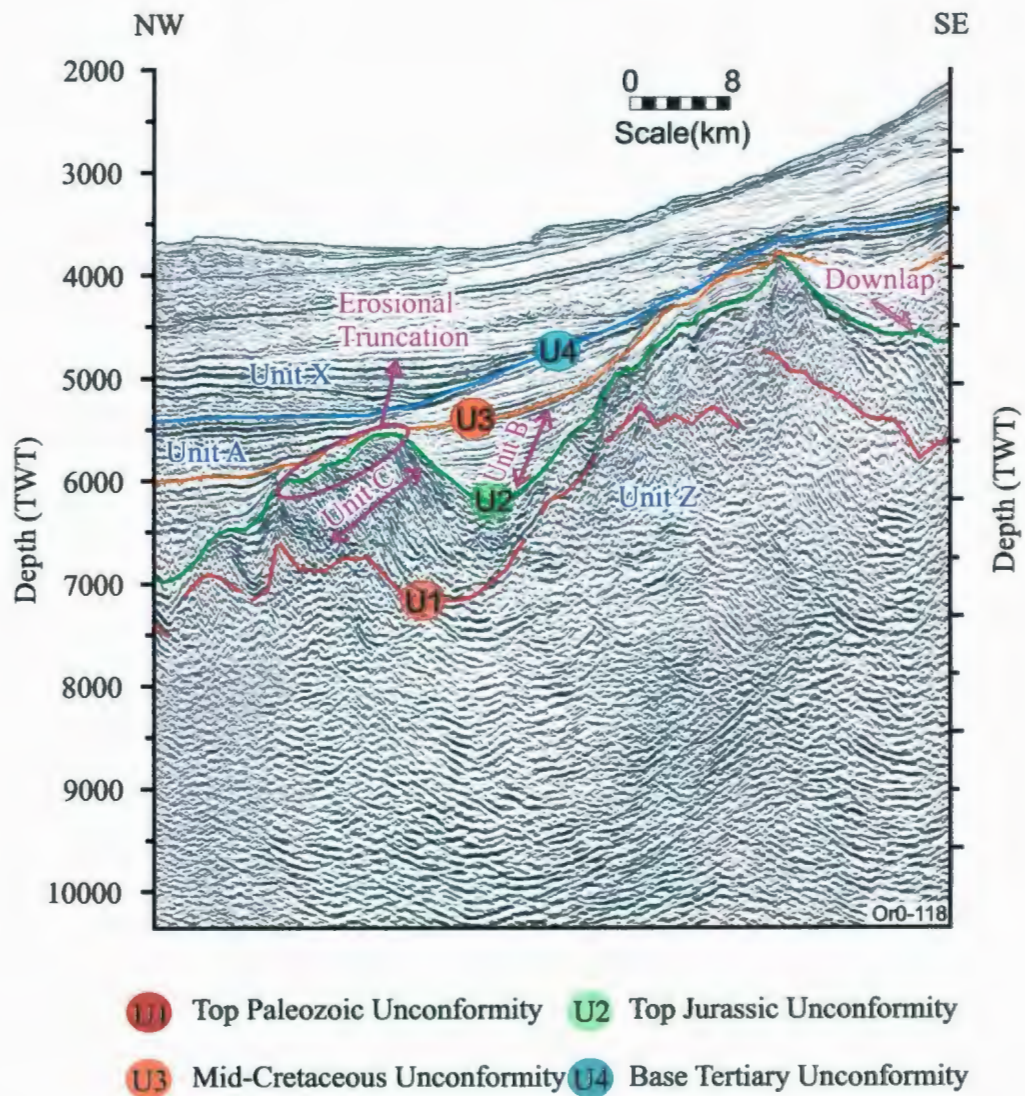


Figure 3.16. Multichannel seismic reflection profile Or0- 118 showing the truncation of the Unit C (?Triassic-Jurassic) and the gentle downlap of the overlying Unit B (Early Cretaceous) at the regional marker U2(Mid-Cretaceous Unconfomity). Location is shown in Figure 3.1.

The morphology of the U2 unconformity at the top of Unit C delineates a broad depocentre in the northeastern portion of the study area (Fig. 3.17). This broad basin is best depicted by the 4500 to 5000 ms isochrons. When examined in detail, two smaller and mainly northeast-southwest trending basins emerge: one of these basins is situated in the northwestern portion of the Orphan Basin, and the other is nestled along the eastern basin margin. A broad and southward tapering high, defines the separation between these two depocentres (Fig. 3.17). These two subdivisions of the Orphan Basin and the intervening high are further described in Chapter 4.

Over the crests of the high blocks (i.e., ridges described in Chapter 4), regional unconformity U2 seismically merges with the underlying regional unconformity U1 (e.g., Fig. 3.18). Correlations with the exploration wells suggest that the U2 unconformity separates predominantly Jurassic successions from either Kimmeridgian / Oxfordian from Tithonian or Late Jurassic from Early Cretaceous. Thus, the U2 surface is broadly correlated with the regional top Jurassic (Tithonian) Unconformity.

3.3.1.3 Unconformity - U3: Surface Capping Unit B

Regional marker U3 is a high to moderate amplitude, laterally continuous reflection that separates Unit B from Unit A (Figs. 3.12, 3.13, 3.15). The overlying weak to high amplitude continuous reflectors of Unit A show apparent onlap terminations along the seismic marker U3. These geometric relationships collectively suggest that the regional seismic marker is a major unconformity surface.

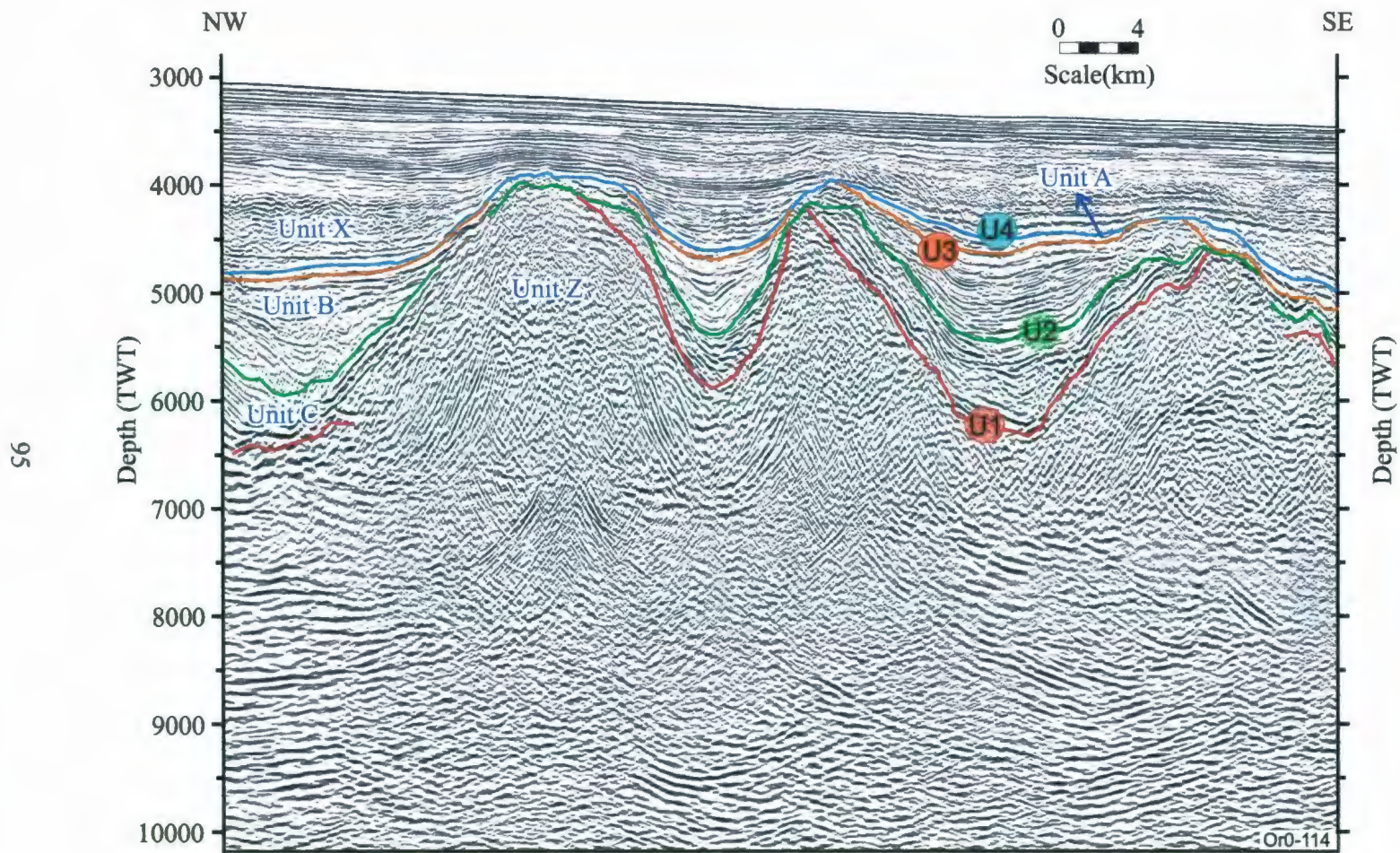


Figure 3.18. Multichannel seismic reflection profile OR0-114 showing the convergence of regional unconformities U1 (Top Paleozoic Unconformity) and U2 (Top Jurassic-Tithonian Unconformity) over the crests of large ridges in West Orphan Basin. Location is shown in Figure 3.1.

Over the crestal regions of local highs, the regional marker U3 is clearly an erosional unconformity. However, traced toward the central portion of basins, the marker becomes conformable with the overlying and underlying reflections (Fig. 3.19). Whether there is a significant time gap across this apparent conformity in such settings is conjectural.

The time structure map of the regional marker U3 shows the morphological elements of the study area, where the Orphan Basin emerges as a very broad near circular depocenter surrounded by high terrain (Fig. 3.20). A wide and shallow zone is centrally located within the near-circular basin, and it broadly partitions the basin into a broadly northeast-southwest trending eastern basin (i.e., basin α 10, see Chapter 4), a similarly trending western basin (i.e., combined basins α 1 and α 2) and a predominantly northwest-southeast trending southern basin. These three basins appear interconnected at the level of the regional marker U3, creating the near-circular appearance (Fig. 3.20).

Over the high blocks cored by basement, (also see Chapter 4) the unconformity U3 truncates the underlying unconformities U2 and U1, creating a strong composite erosional unconformity (Fig. 3.21). Well ties show that the U3 unconformity separates Upper Cretaceous from Lower Cretaceous strata. Thus, it is correlated with the regional Mid-Cretaceous (Cenomanian) Unconformity in the study area.

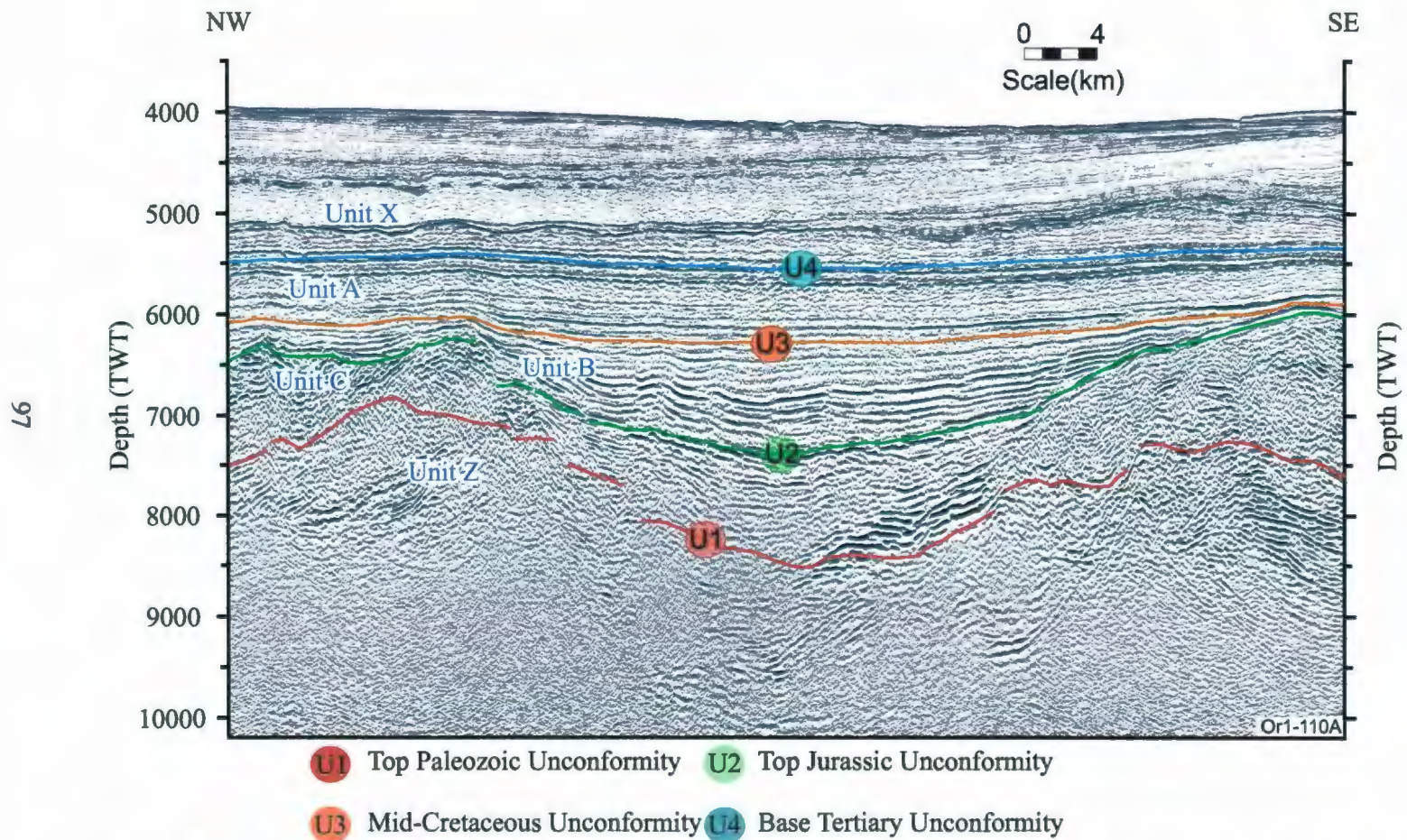


Figure 3.19. Multichannel seismic reflection profile OR0-114 showing the apparent conformable character of the regional marker U3 (Mid-Cretaceous Unconformity) in the central portion of a basin within the eastern portion of the study area. Location is shown in Figure 3.1.

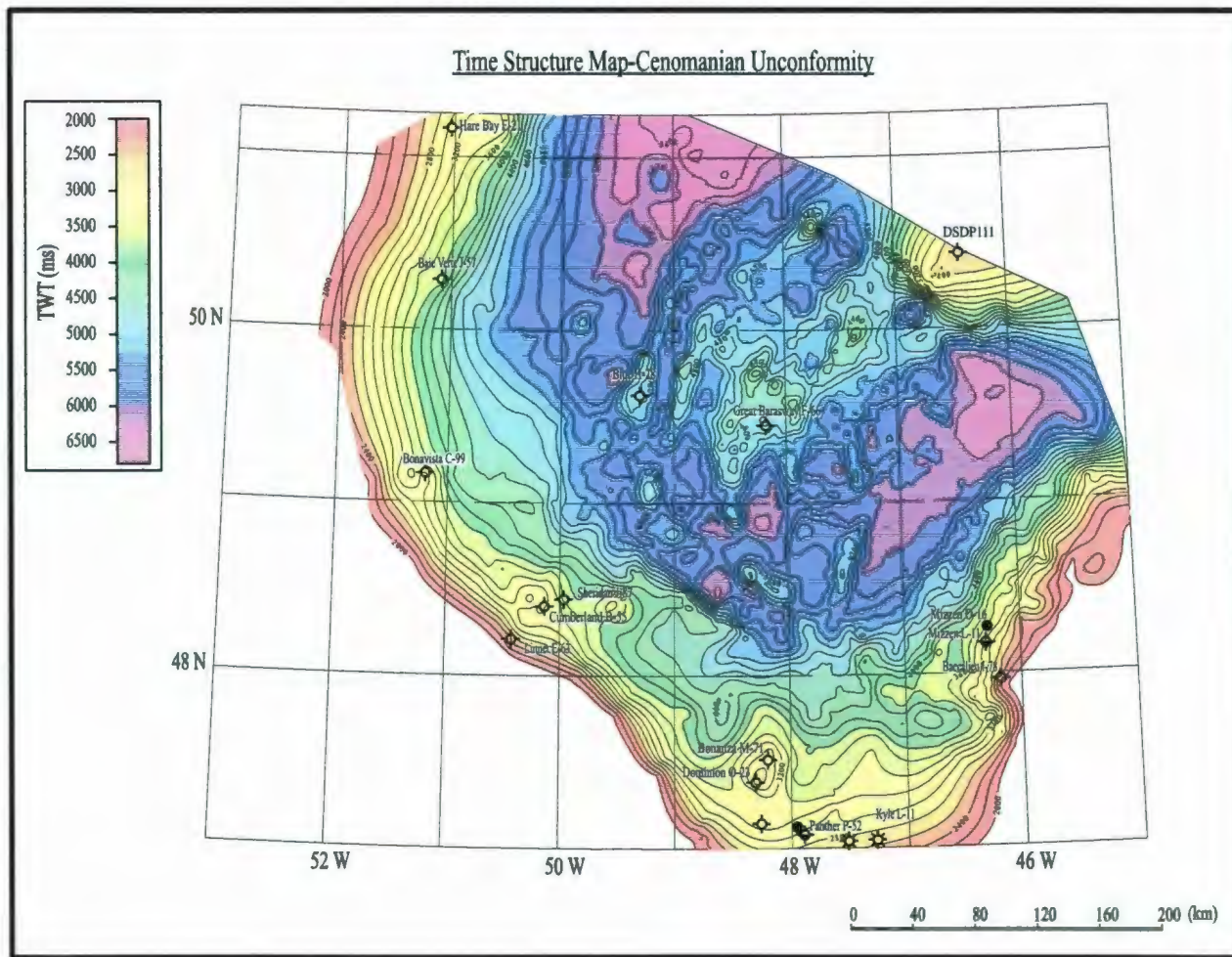


Figure 3.20. Time-structure map of the regional marker (unconformity) U3. Isochrons are in milliseconds twt. Also shown are the exploration wells in the study area.

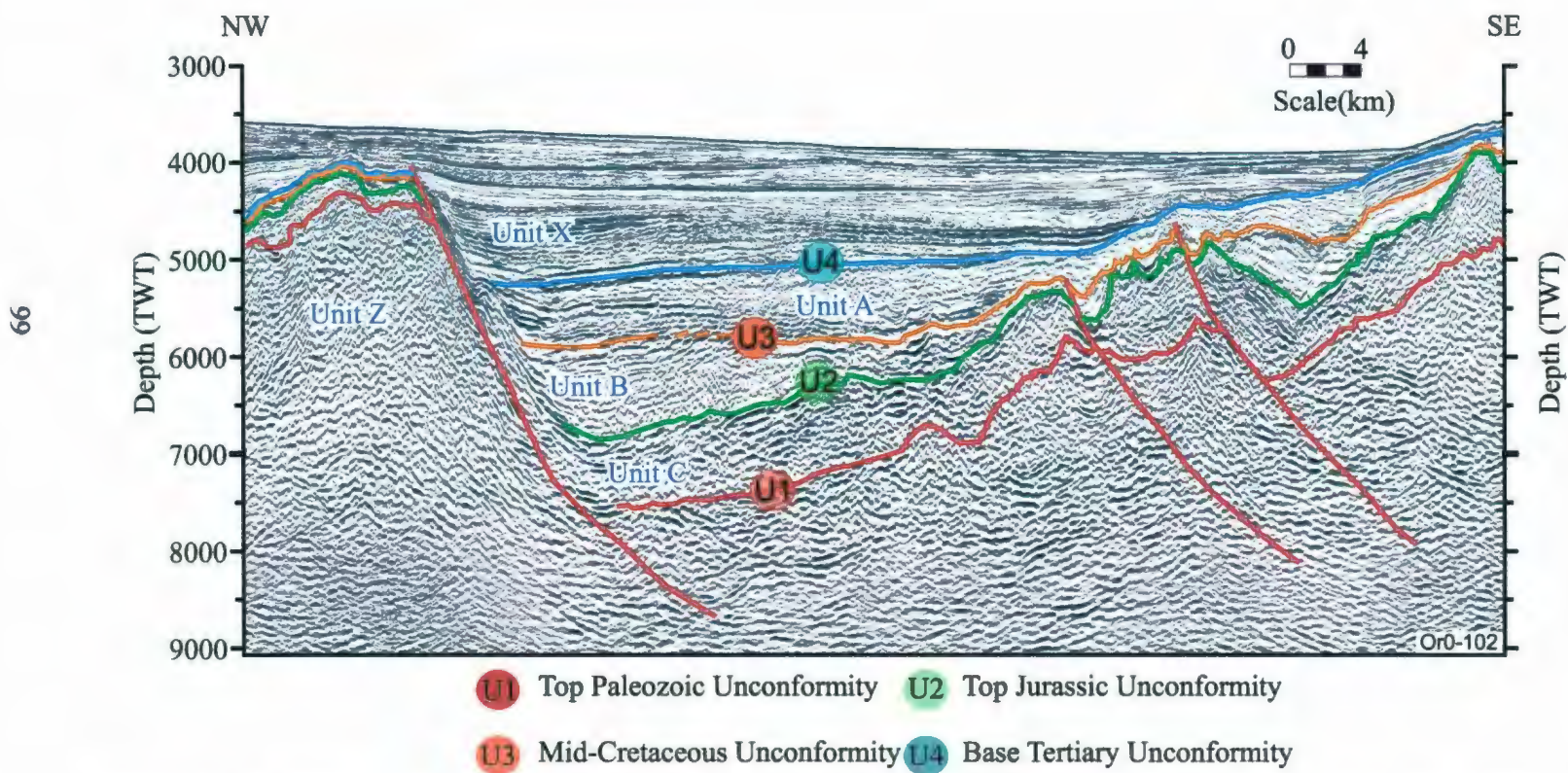


Figure 3.21. Multichannel seismic reflection profile Or0- 102 showing the convergence of regional unconformities U1(Top Paleozoic), U2(Top Jurassic) and U3(Mid-Cretaceous) over the crests of large ridges in western Orphan Basin. Location is shown in Figure 3.1.

3.3.1.4 Unconformity - U4: Surface Capping Unit A

Seismic marker U4 is a high amplitude, laterally continuous, regional reflection that separates Unit A from Unit X (Fig. 3.22). The strongly stratified high amplitude and continuous reflections of the overlying Unit X show onlap and downlap terminations over the marker U4, whereas the moderate to high amplitude reflections of the underlying Unit A display erosional truncation at the marker, collectively indicating that this is a major regional unconformity. In places along the margin of the Orphan Basin, or over the crests of high blocks, the unconformity U4 truncates the underlying unconformity U3 to form a composite erosional unconformity (e.g., Fig. 3.18).

The time structure map of the U4 unconformity resembles, in its broad morphology, the time structure map of the U3 unconformity (Figs. 3.20, 3.23). The north-northeast - south-southwest trending western basin and the northeast-southwest trending eastern basin are clearly depicted in Figure 3.23. Away from the margins, within the shallower central portion of the Orphan Basin, unconformity U4 exhibits a relatively undisturbed, smooth topography (Fig. 3.23). The U4 Unconformity marks the base of the thick Tertiary strata. In the exploration wells, it invariably separates the underlying Upper Cretaceous from the Tertiary strata. Thus, it is correlated with the Base Tertiary Unconformity.

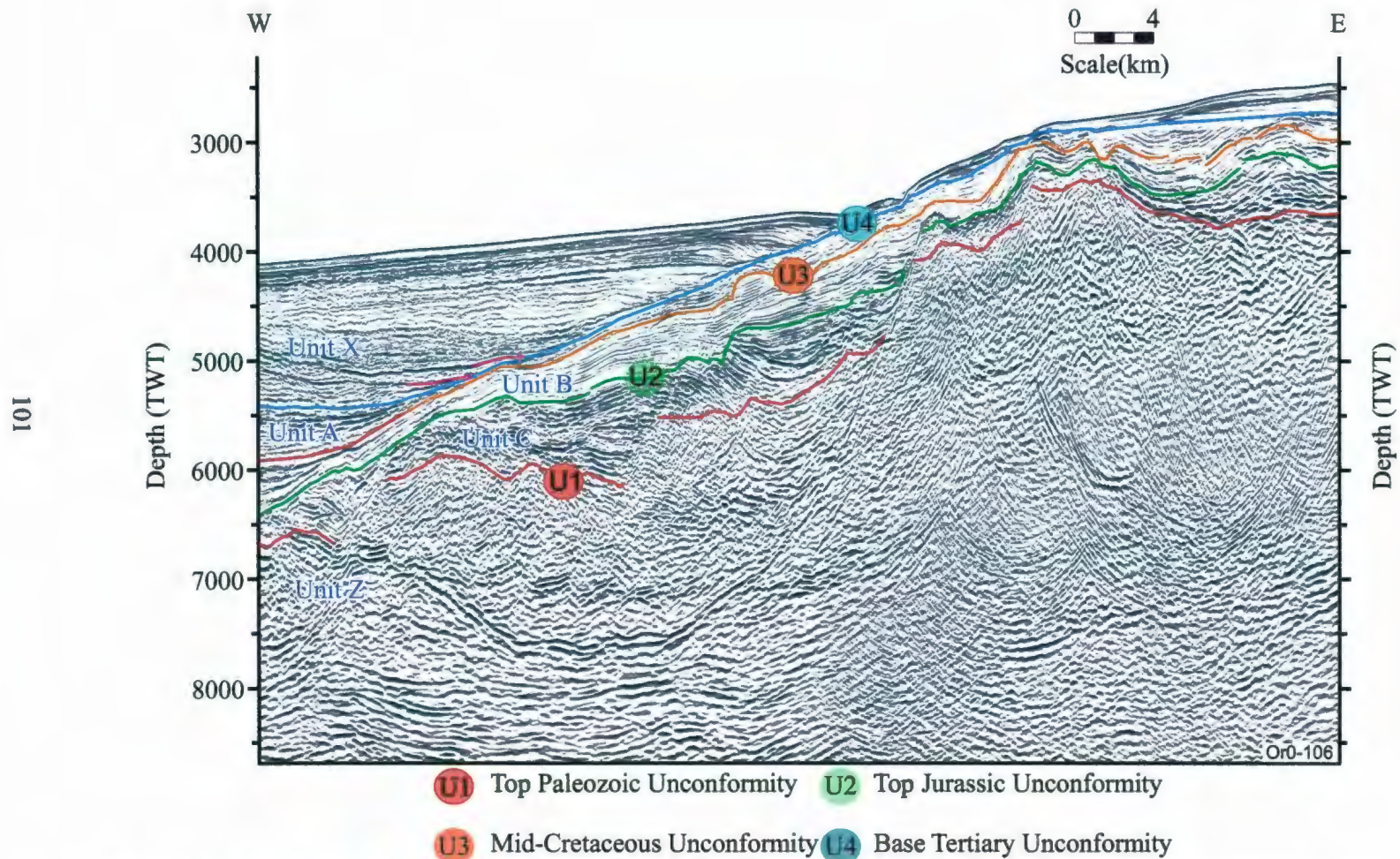


Figure 3.22. Multichannel seismic reflection profile Or0-106 showing the character of the regional unconformity U4 (Base Tertiary) along the eastern margin of the Orphan Basin. Location is shown in Figure 3.1.

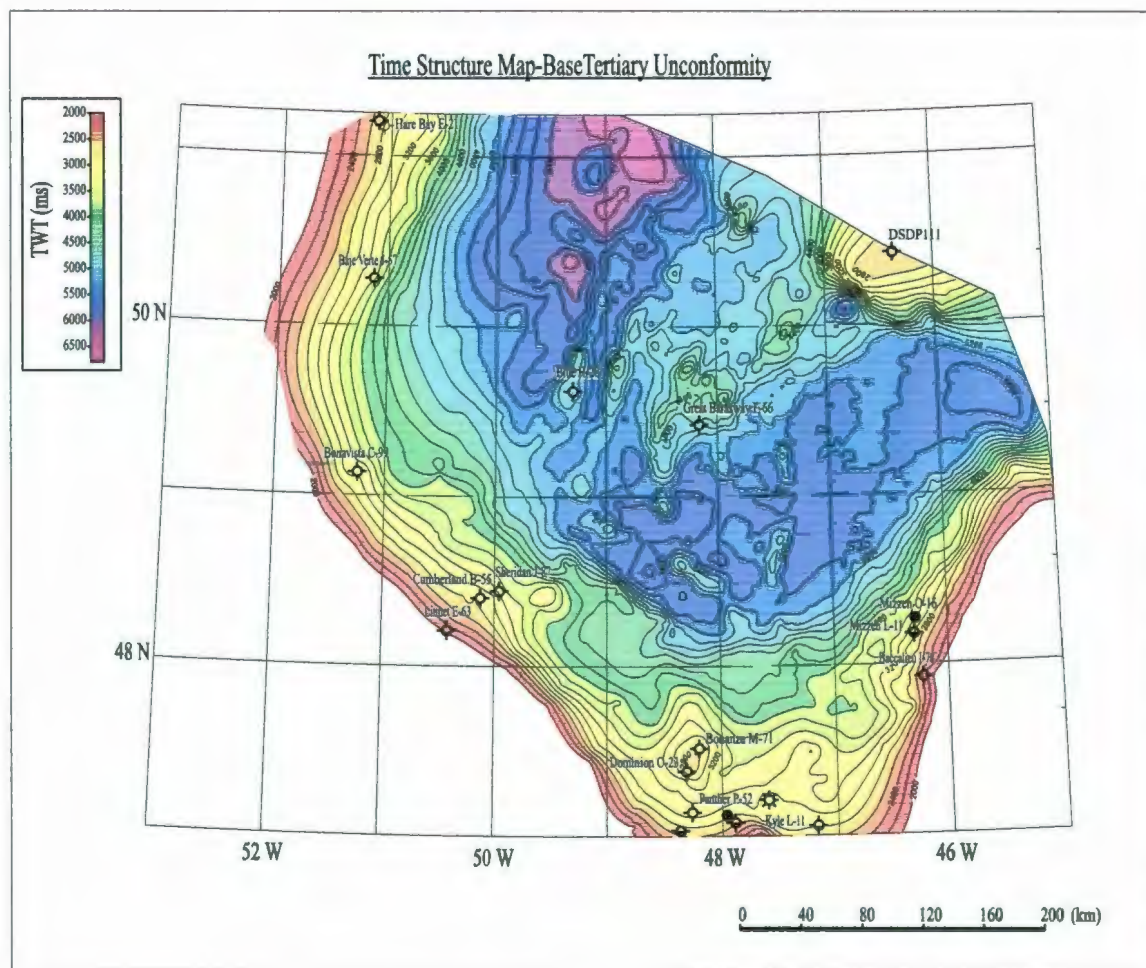


Figure 3.23. Time-structure map of the regional marker (unconformity) U4. Isochrons are in milliseconds twt. Also shown are the exploration wells in the region.

3.3.2 Seismic Units

3.3.2.1 Unit Z (Paleozoic and Precambrian Basement)

Unit Z constitutes the pre-rift basement throughout the Orphan Basin. It is defined by a regionally variable acoustic character, ranging from (i) weak to moderate amplitude, quasi-continuous reflections, to (ii) moderate to high amplitude reverberatory reflections that show considerable lateral continuity, to (iii) low amplitude discontinuous reflection segments that display a chaotic appearance. This variable acoustic character is indicative of the presence of diverse lithologies with varying degrees of stratification and intrusive rocks. The recovery of Paleozoic or Precambrian basement rocks in several exploration wells, confirms this lithological variability. For example, the Bonavista C-99 well is drilled over a basement high, where Unit Z is characterized by low amplitude discontinuous and chaotic reflections. Here, the well recovered granitic basement rocks below the U1 unconformity. Similarly, the Hare Bay E-21, Blue H-28 and Linnet E-63 wells are also drilled over basement highs, where Unit Z is characterized by high amplitude and near-continuous reflections. The wells recovered thick Paleozoic sedimentary and meta-sedimentary successions.

3.3.2.2 Unit C (Jurassic / ? Late Triassic)

Unit C is characterized by generally strong, moderate to high amplitude reflections. The unit is bounded at its base and top by the U1 and U2 unconformities, respectively. It displays two distinctly different internal geometries: (i) a geometry

defined by parallel to sub-parallel reflections, such as seen in the easternmost portion of Figure 3.10 and (ii) a geometry marked by steeply dipping (25° - 35°) reflections bounded by major extensional faults that create prominent rotated and tilted blocks (see Chapter 4).

In the key exploration wells in the Orphan Basin and its environs, Unit C is encountered in five wells: Blue H-28, Linnet E-63, Bonanza M-71, Mizzen L-11 and Baccalieu I-78 (Figs. 3.9, 3.10). According to McAlpine (1988), in the Blue H-28 well, the shale succession from 3461.8 mbsf to 3794.8 mbsf might contain Oxfordian to Albian-Aptian age sediments. In the Baccalieu I-78 well the lowermost succession dominated by shales with minor siltstone, sandstone, limestone and dolomite stringers (i.e., from 2677.2 mbsf to 4042.2 mbsf) is assigned to a Bathonian to Kimmeridgian age (Pocock, 1986). In the Linnet E-63 well the lower unit (i.e., 2756.0 mbsf to 4018.0 mbsf) is either Oxfordian (Mobil et al., 1983) or Albian - Aptian age (Bujak Davis Group, 1988). Seismic stratigraphy suggests that a very thin succession of Unit C may be present in the Linnet E-63 well, underlying an approximately 700 ms of Unit B. In the Bonanza M-71 well, the shale-dominated succession from 4046.5 mbsf to 5088.5 mbsf is assigned to the Early Portlandian to Kimmeridgian age (Associated Biostratigraphic Consultants, 1991). In the Mizzen L-11 well, the lowermost ~ 519 m-thick siliciclastic (extending from 2152 mbsf to 2670 mbsf) succession is assigned to Late Jurassic age (from earliest Tithonian to late Tithonian; Robertson, 2008).

The total thickness map shows that Unit C is thick (>1500 ms) along basinal areas, but thins toward the flank of the ridges, becoming very thin or absent over the

ridges (Fig. 3.24). Unit C is thickest near in the southeastern most part of the Orphan Basin and Flemish Pass Basin (i.e., the Baccalieu and Mizzen wells area; Fig. 3.24). Thus, the overall distribution of this unit roughly mimics the northeast-southwest structural trend of the study area (further discussed in Chapter 4).

The well chronologies suggest that Unit C is predominantly Jurassic in age, and that the unconformity between Units C and B separates a predominantly Early Cretaceous succession from a Late Jurassic succession. Thus, this unconformity (i.e., the U2 surface) is most likely correlated with the regional Kimmeridgian-Tithonian Unconformity, which is often informally referred to as the top Jurassic unconformity (Enachescu et al., 2005).

One of the most important questions regarding the sedimentary and/or geologic evolution of the Orphan Basin is whether or not there are Triassic and Early Jurassic sediments preserved within the deeper parts of the basins. No exploration well has ever drilled Triassic or Early Jurassic sediments in the Orphan Basin. However, nearly all wells were spudded over structural highs, where Triassic or Early Jurassic sediments are expected to be eroded by the younger unconformities. No diapiric salt and associated structures are recognized during the interpretation of seismic reflection profiles. However, Triassic-aged stratified evaporites were postulated to occur in the eastern portion of the Orphan Basin by Enachescu et al., (2005). Similar evaporite sequences were drilled in the conjugate Porcupine Basin in the Irish offshore. There is a possible candidate for an example of stratified evaporates in the central portion of the Orphan

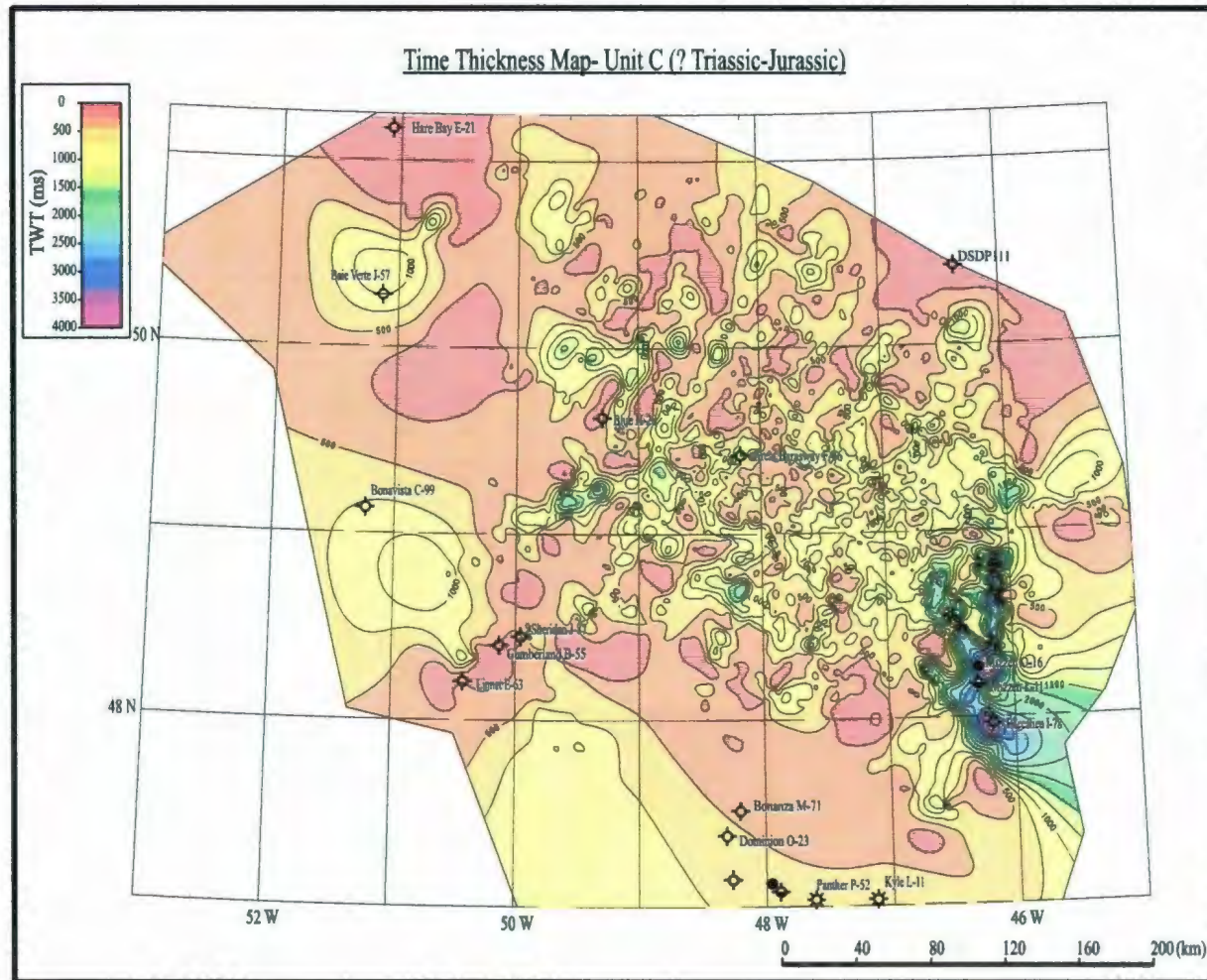


Figure 3.24. Isopach map of Unit C (?Triassic-Jurassic) showing the thickness variations in ms twt. Also shown are the locations of the exploration wells in the study area.

Basin. A discrete interval of very strong, reverberatory, continuous reflections occurs at ~7500 ms depth between R4 and R6 (Fig. 3.8). Careful examination of the seismic data shows that the lenticular unit immediately below the strong reflector at the base of Unit C exhibiting a stratified internal architecture with high-amplitude reflections. This lenticular unit might be interpreted as a stratified evaporate succession of Late Triassic - Early Jurassic age. However, detailed interpretation of seismic reflection profiles, shows that the strong reflector at the base of Unit C is better correlated with the top of the Paleozoic basement Unit Z. The nature and age of this stratified package can only be determined through deep exploration drilling in such a setting.

3.3.2.3 Unit B (Early Cretaceous)

Unit B is generally characterized by high amplitude, strong and continuous reflections. In places, this unit contains parallel to sub parallel, continuous and often corrugated reflections. Over the structural highs, the unit becomes notably corrugated and wavy. The top of this unit is generally delineated by the Mid-Cretaceous Unconformity, whereas its base is defined by the top Jurassic Unconformity. However, in places where Unit C is absent, Unit B lies directly over the pre-rift basement Unit Z.

The thickness of Unit B is highly variable across the study area (Fig. 3.25), ranging from 1400 ms along the axes of basins to <100 ms over the crest of ridges and rotated fault blocks (see Chapter 4). The overall thickness distribution of Unit B defines prominent northeast-southwest oriented lineations within the central portion of the Orphan Basin (Fig. 3.25). Later in Chapter 4, it will be shown that thickest occurrences

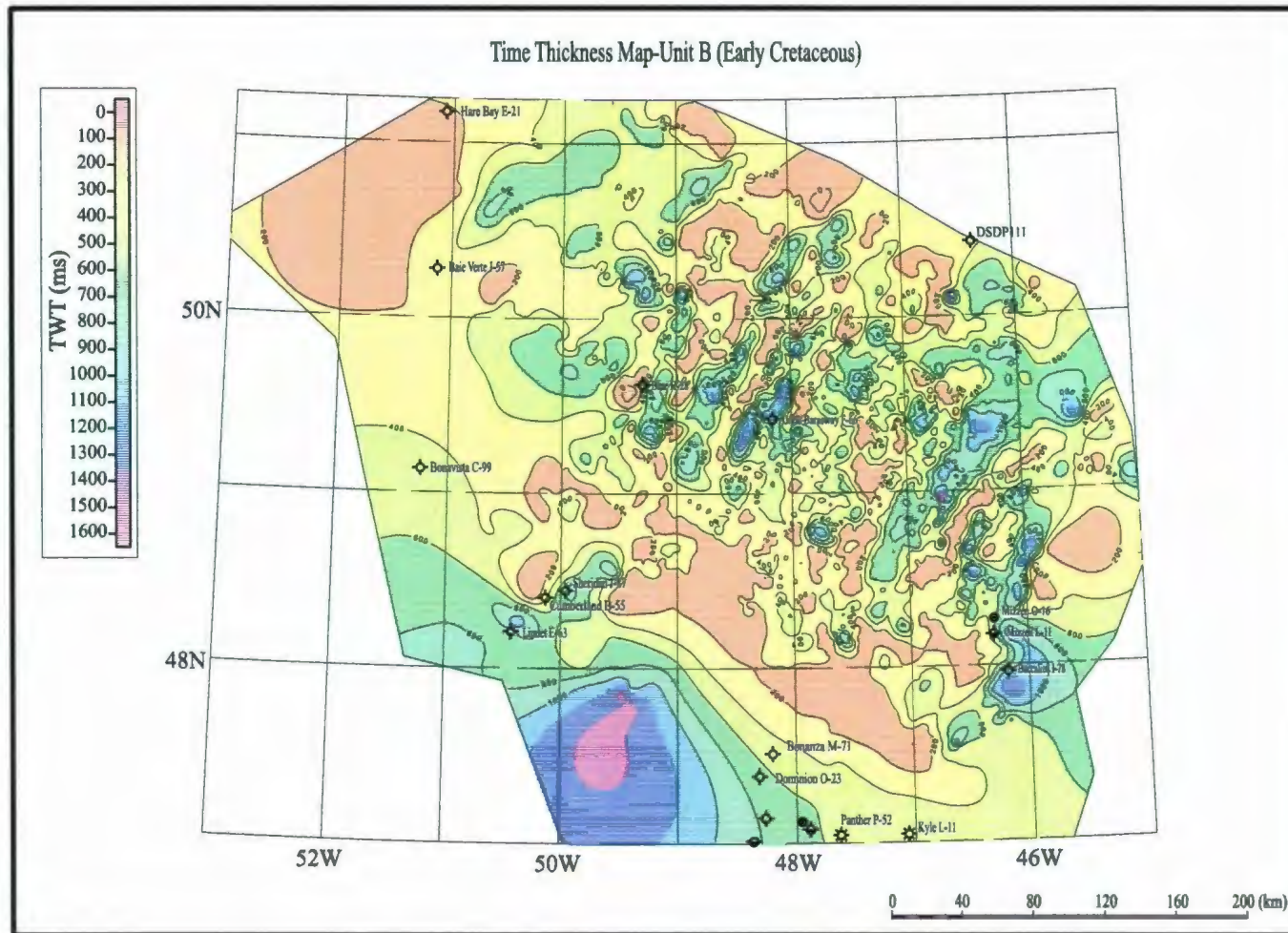


Figure 3.25. Isopach map of Unit B (Early Cretaceous) showing the thickness variations in ms twt. Also shown are the locations of the exploration wells in study area.

of Unit B (and Unit A) correlate with the development of large troughs within the basin during rifting. The unit is notably thin along the northwest-southeast trending structural high that defines the southern boundary of the Orphan Basin, and its linkage with the northernmost Jeanne d'Arc Basin (Fig. 3.25). Unit B is also noticeably thin along the western margin of the Orphan Basin.

The unit is widespread in Orphan Basin, as also observed in six of the key exploration wells used in this study: Blue H-28, Linnet E-63, Kyle L-11, Bonanza M-71, Mizzen L-11 and Baccalieu I-78 (Fig. 3.6). As indicated in section 3.2.2.2 above, the shale succession from 3461.8 mbsf to 3794.8 mbsf in the Blue H-28 well contains microfossils that indicate an Oxfordian to Albian-Aptian age for these sediments (McAlpine, 1990). Similarly, in the Linnet E-63 well the lower unit (i.e., 2756.0 mbsf to 4018.0 mbsf) is either Oxfordian (Mobil et al., 1983) or Albian - Aptian age (Bujak Davis Group, 1988). Seismic stratigraphy shows that there is an approximately 700 ms-thick succession at the well site, which defines Unit B, and broadly correlates with the lower unit occurring between 2756.0 mbsf to 4018.0 mbsf depth in the well. In the Kyle L-11 well, the sediments underlying the Base Tertiary Unconformity consisting of mudstones, shales with limestones and thin sandstone stringers and extending from 827.3 mbsf to 2398.3 mbsf reveal a Barremian to Valanginian age. Seismic correlation shows that there is a thick package of Unit B at the well site, which correlates with the successions encountered between 827.3 mbsf to 2398.3 mbsf (Figs. 3.3, 3.5). In the Baccalieu I-78, a mainly siliciclastic succession below the Base Tertiary ranges between 613.2 mbsf and 2677.2 mbsf (Figs. 3.3, 3.5). Microfossil data show that the succession is

Aptian to Portlandian in age (Pocock, 1986). The seismic data at the well site clearly depict that there is a 1300 ms-thick seismic package, situated between the Base Tertiary and Mid-Cretaceous unconformities (i.e., Unit B; Fig. 3.9). This package correlates with the Aptian to Portlandian age siliciclastic succession described above.

The well chronologies suggest that Unit B is mainly Early Cretaceous in age, and that the unconformity between Units B and A separates a predominantly Early Cretaceous succession from a Late Cretaceous succession. Thus, this unconformity (i.e., the U3 surface) is most likely correlated with the regional Mid-Cretaceous Unconformity, which is also informally referred to as the Mid-Aptian (Smee, 2003, Avalon Unconformity, Enachescu et al., 2005 and Cenomanian Unconformity (Sinclair, 1988 and 1993).

3.3.2.4 Unit A (Late Cretaceous)

Unit A is characterized by strong high amplitude reflections, which show notable lateral continuity across the study area (Figs. 3.7-3.11). This unit is better developed in the eastern portion of the Orphan Basin. Here, the unit exhibits mostly continuous and parallel to sub-parallel reflections. Toward the west, the unit thins and loses its character and becomes non discrete, nearly indistinguishable from the underlying and overlying units.

Unit A is thickest (800-1000 ms) along the eastern segment of the study area, where it defines a broad northeast-southwest trending depocentre (Fig. 3.26). It

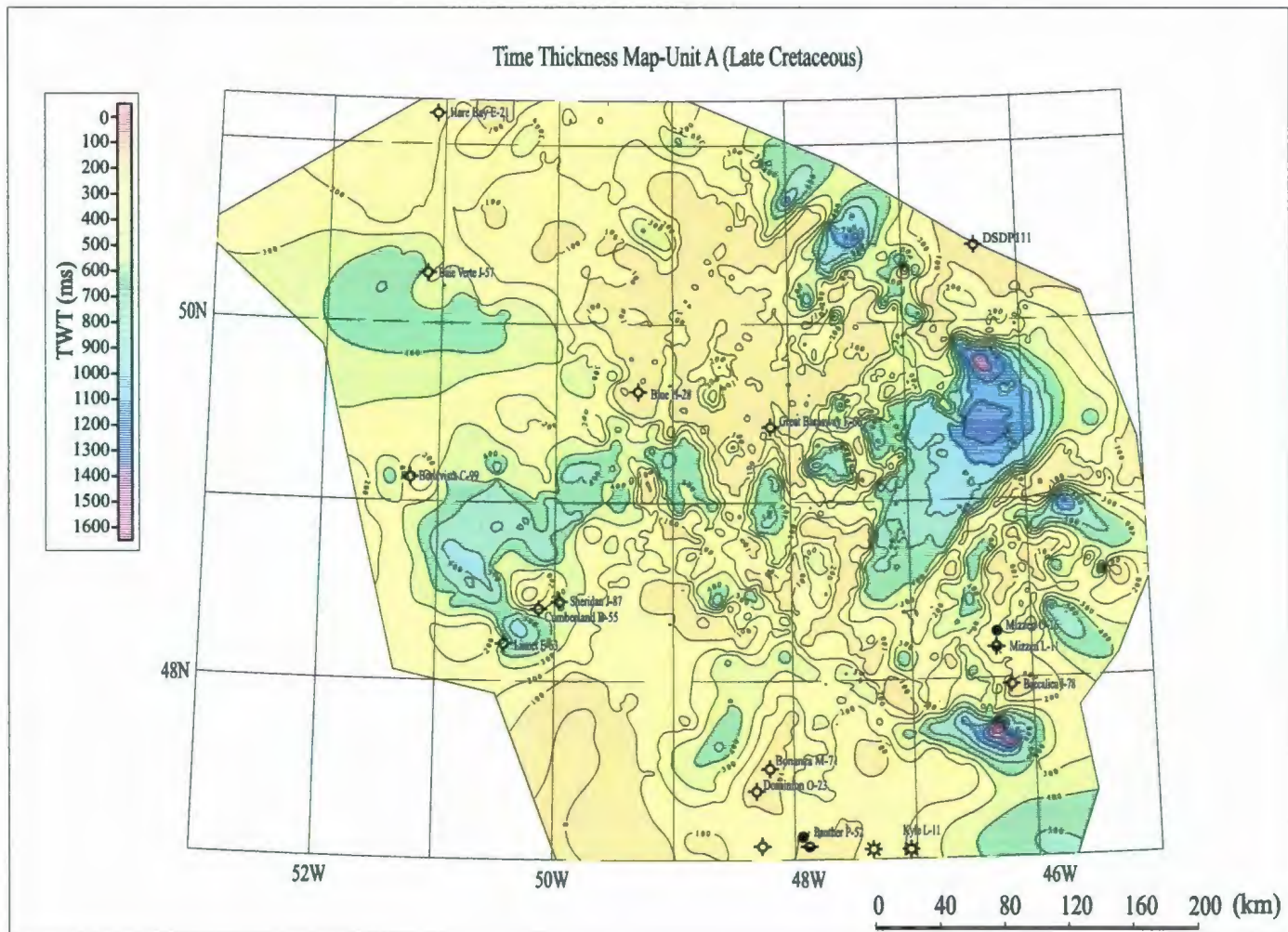


Figure 3.26. Isopach map of Unit A (Late Cretaceous) showing the thickness variations in ms twt. Also shown are the locations of the exploration wells in study area.

drastically thins (to <100 ms) toward the west, but is also very thin over the basement highs. In the western portion of Orphan Basin, Unit A shows modest thickening within the northeast-southwest trending troughs (Fig. 3.26). It is important to note that Unit A abuts the flanks of the ridges, but rarely oversteps their crests. Thus, this unit is absent on some of the ridges and horst blocks. In this case, the underlying Unit B is directly overlain by the Base Tertiary Unconformity and Tertiary Unit, X.

The unit is observed in five of the key exploration wells used in this study, including Blue H-28, Hare Bay E-21, Baie Verte J-57, Bonavista C-99, and Linnet E-63 (Fig. 3.6). Planktonic foraminifera suggest that the succession between 3350.8 mbsf and 3461.8 mbsf in the Blue H-28 well contains a near continuous record ranging from Cenomanian - ?Campanian to Maastrichtian (Robertson Research, 1979; Koning et al., 1988). Seismic correlation shows that there is a 100 ms-thick package of Unit A at the well site, which correlates with the successions encountered between 3350.8 mbsf and 3461.8 mbsf (Figs. 3.3, 3.5). In the Hare Bay E-21 well, the succession which occurs from 3001.7 mbsf to 3158.7 mbsf contains planktonic and benthic foraminifera which suggest that the unit is Late Campanian to Early Maastrichtian in age (Davies, 1979). Seismic data show that the ~70 ms-thick package of Unit A at the well site correlates well with the successions encountered between 3001.7 mbsf to 3158.7 mbsf (Fig. 3.7). In the Baie Verte J-57 well the sediments below the Base Tertiary Unconformity extending from 3964.0 mbsf to 4607.8 mbsf contain microfossils which reveal an Albian to Coniacian age for this succession (Robertson Research, 1985; BP et al., 1989). This succession correlates well with a ~500 ms-thick package of Unit A at the well site (Fig. 3.8). In the

Bonavista C-99 well the sediments between 3299.3 mbsf and 3349.8 mbsf show microfossil assemblages indicating Late Campanian to Early Maastrichtian age for these sediments (BP, 1975 as cited in the http://basin.gsca.nrcan.gc.ca/index_e.php). This 50 m thick package correlates with the ~50 ms thick seismic unit A at the well site (Fig. 3.9). Finally, in the Linnet E-63 well the sediments between 2385.0 mbsf to 2756.0 mbsf contain palynomorphs which reveal Cenomanian to Maastrichtian (Bujak Davies Group, 1988). This succession correlates with the 150 ms thick seismic Unit A in this well.

The well chronologies suggest that Unit A is mainly Late Cretaceous in age, and that the unconformity between Units A and X separates a predominantly Late Cretaceous succession from the Tertiary succession. The unconformity U4 is correlated at many wells with the regional Base Tertiary Unconformity.

3.3.2.5 Unit X (Tertiary)

Seismic unit X is the uppermost package within Orphan Basin and environs. It is characterized by strong to very strong high amplitude reflections (Figs. 3.7-3.11). The reflections within the unit are notably continuous, and can be traced throughout the study area. The base of Unit X is marked by the Base Tertiary Unconformity (Smee et al., 2003; Enachescu et al., 2004 a, b), whereas the top of the unit is marked by the seafloor. The stratigraphy and architecture of this unit is beyond the scope of this thesis, thus it is only briefly described in this section.

The thickness of the Unit X varies drastically through the Orphan Basin (Fig. 3.27). It is generally thickest on the shelf where it reaches 4000-4500 ms, but it progressively thins to ~600 ms toward the east. Within this general trend, the unit also shows notable thinning over the basement-cored ridges and other structural highs that are revealed in the morphology of the Base Tertiary Unconformity. Micropaleontological studies clearly document that seismic Unit X is Tertiary in age.

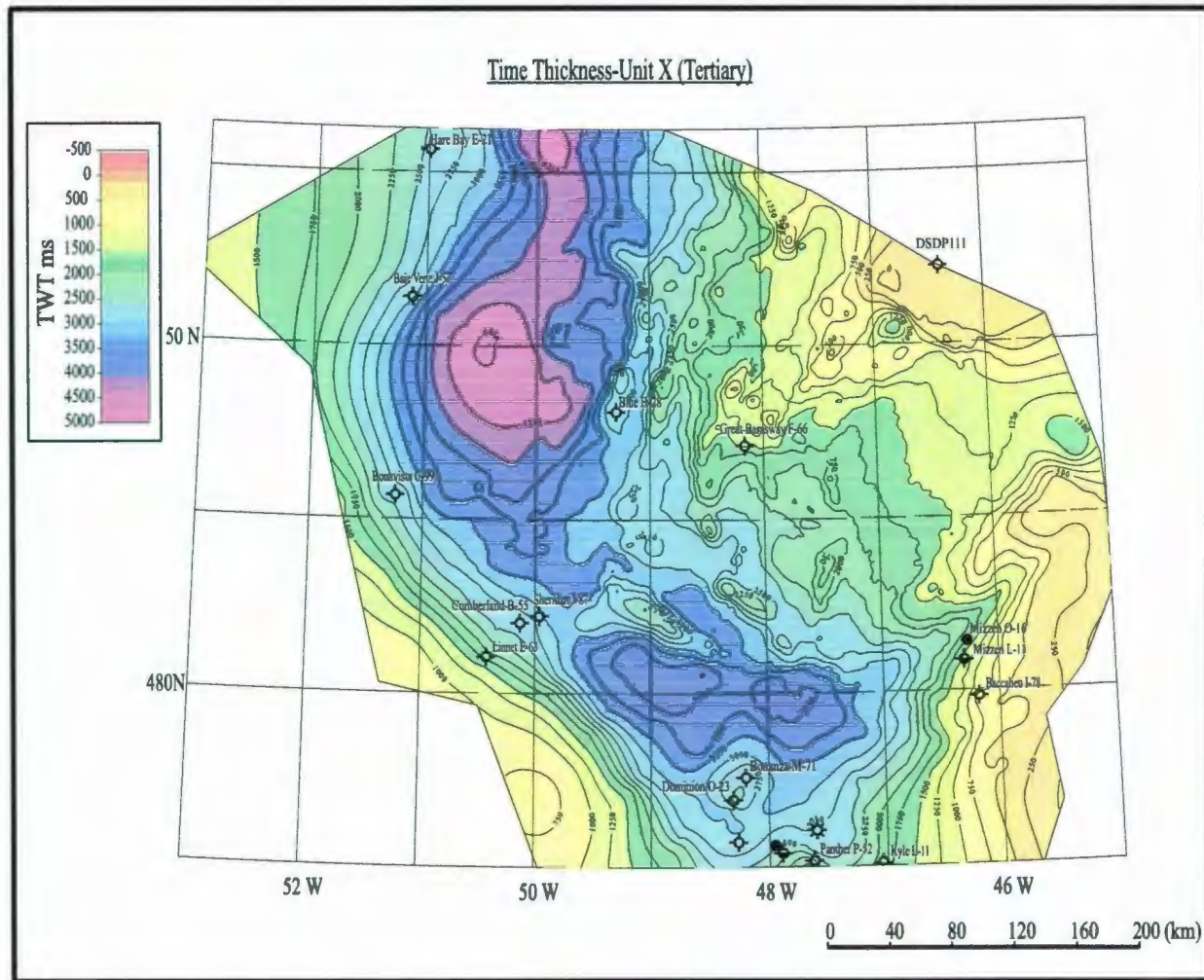


Figure 3.27. Isopach map of Unit X -Tertiary (water bottom to Base Tertiary Unconformity) showing the thickness variations in ms twt. Also shown are the locations of the exploration wells in study area.

CHAPTER 4. TECTONIC ARCHITECTURE OF THE STUDY AREA

4.1. Introduction

The western and southwestern margins of the Orphan Basin are delineated by the Bonavista Platform, whereas the northeastern and southeastern margins of the study area are marked by the Orphan Knoll and Flemish Cap, respectively (Fig. 4.1). The northern margin of the Orphan Basin is not readily discernible in the available seismic reflection profiles, and the Orphan Basin gradually merges with the Northeast Newfoundland Basin toward the north and northeast.

On the basis of stratigraphic architecture and structural style, the successions below the Base Tertiary Unconformity in the Orphan Basin are broadly divided into five tectonic provinces (Smee *et al.*, 2003; Enachescu *et al.*, 2004 a and b; Fig. 4.2): (i) Western and Southwestern Basin Margin, (ii) the Eastern Basin Margin, (iii) the White Sail Fault Zone, (iv) West Basin and Ridge Province and (v) the East Basin.

4.2. Western and Southwestern Basin Margin

The western and southern margins of the study area are defined by a 3-5 km wide conspicuous fault zone (Figs. 4.2 and 4.3). This zone displays an arcuate, convex to the west map view, where its northern segment has a northeast-southwest trend (030°N), whereas its southern segment exhibits a northwest-southeast trend (120-150°N). The fault zone is composed of two larger master faults and several minor faults, showing

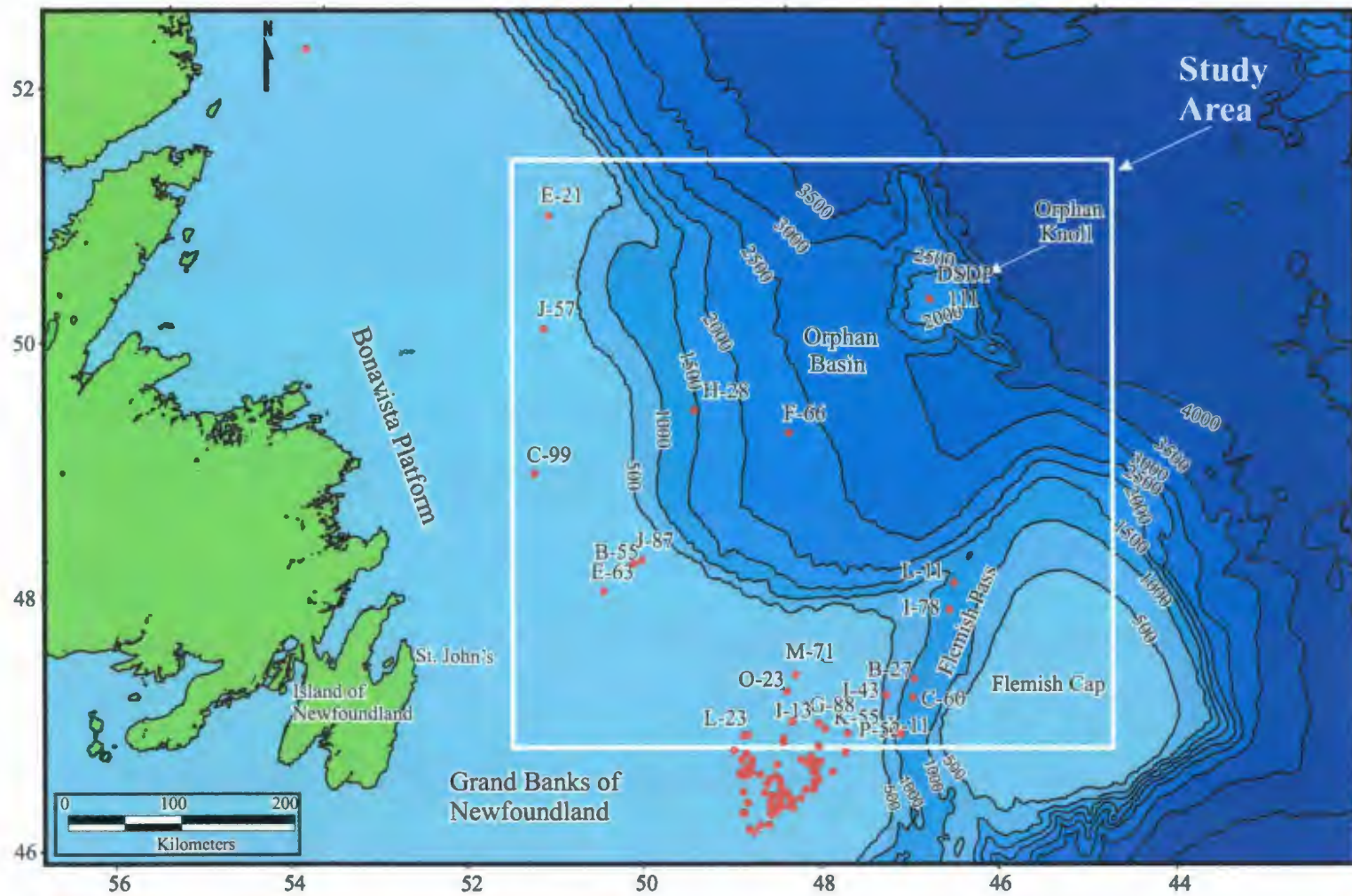


Figure 4.1. Location map of the study area showing major bathymetric elements in the north-central portion of the Grand Banks of Newfoundland. Isobaths are at 500 m. intervals. Inset shows the study area.

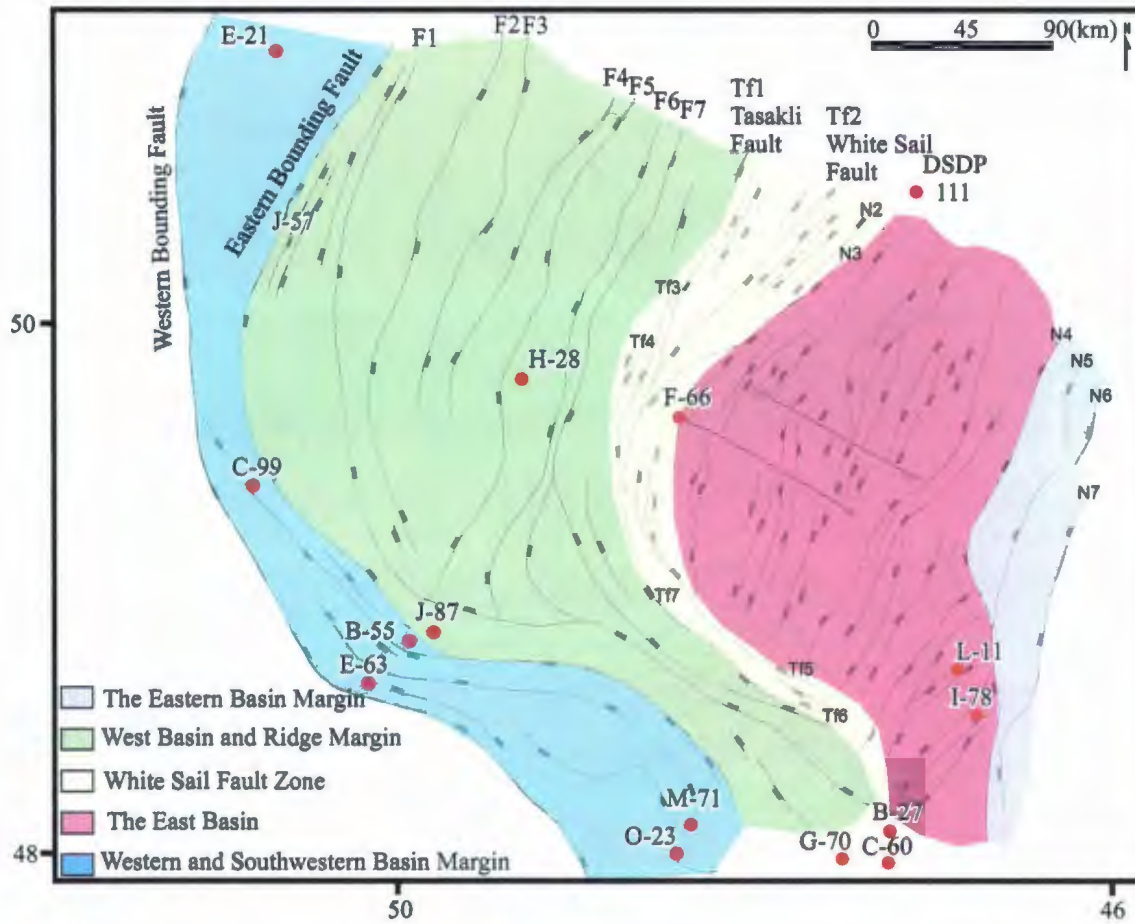


Figure 4.2. Map of the study area, showing the distribution of five tectonic provinces identified on the basis of stratigraphic and structural interpretation of the seismic reflection profiles, including (i) the Western and Southwestern Basin Margin, (ii) the Eastern Basin Margin, (iii) the White Sail Fault Zone, (iv) West Basin and Ridge Province and (v) the East Basin.

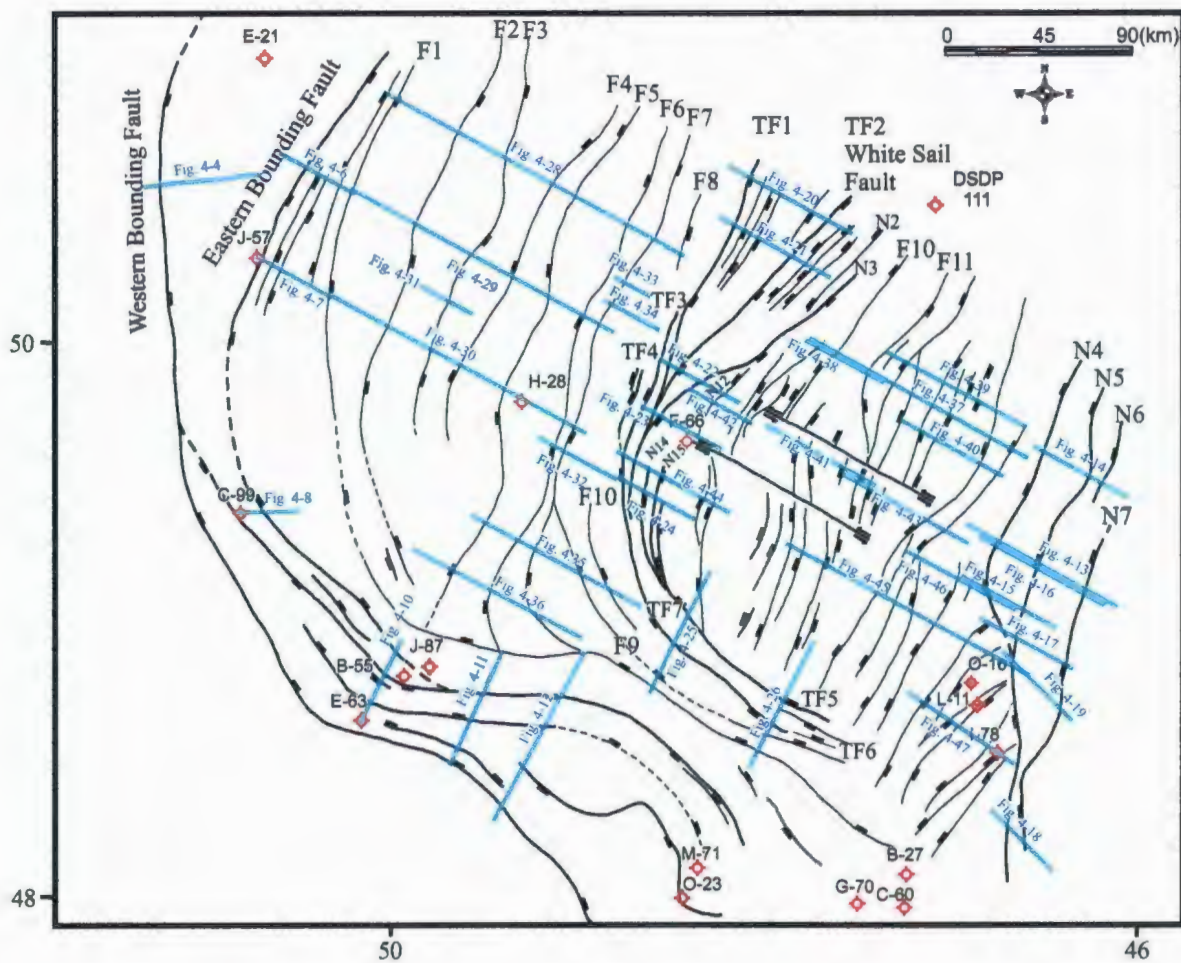


Figure 4.3. Map of the study area showing the distribution of major faults that cuts the top of the Jurassic successions in seismic reflection profiles. The position of the faults on the map is drawn as the mid-point between the footwall cutoff and the hanging wall cutoff. Also shown are the location of seismic lines used in this chapter.

normal-sense vertical stratigraphic separations (Figs. 4.4, 4.5): (i) the Western Bounding Fault and (ii) the Eastern Bounding Fault. Both the Eastern and the Western Bounding Faults further include 2-3 smaller synthetic faults which also show normal-sense stratigraphic separations, soling into the master faults at depth. Because of its position and the structural and stratigraphic architecture as a basin-bounding fault zone at the eastern fringes of the Bonavista Peninsula (e.g., de Voogd et al., 1990), this fault zone is broadly correlated with the Bonavista Fault of Enachescu et al. (2005), and herein referred to as the “Bonavista Fault Zone”.

In the northwestern portion of the study area, the Bonavista Fault Zone is only tentatively mapped, because the seismic coverage in this region is very sparse (Fig. 4.3). A single seismic reflection profile extends westward and images the Western Bounding Fault of this zone (Fig. 4.4). Here, the basin margin is delineated by three parallel well-developed east-dipping normal faults, which up dip invariably cut the Base Tertiary Unconformity, tipping within the lowermost portion of the Cenozoic successions and affecting pre-rift basement. Footwall and hanging wall cutoffs of marker horizons illustrate that these faults show between 200 and 500 ms vertical stratigraphic separations. The faults clearly extend downward to 4.6 seconds, showing well delineated listric trajectories (Fig. 4.4). In this seismic profile, the synthetic faults appear to sole at depth into the master fault (i.e., the Western Bounding Fault). In this area, the Eastern Bounding Fault of the Bonavista Fault Zone is composed of three prominent east-dipping normal faults (e.g., Figs. 4.3, 4.6, 4.7). These three faults can be correlated across the northwestern segment of the study area with some degree of confidence using the limited

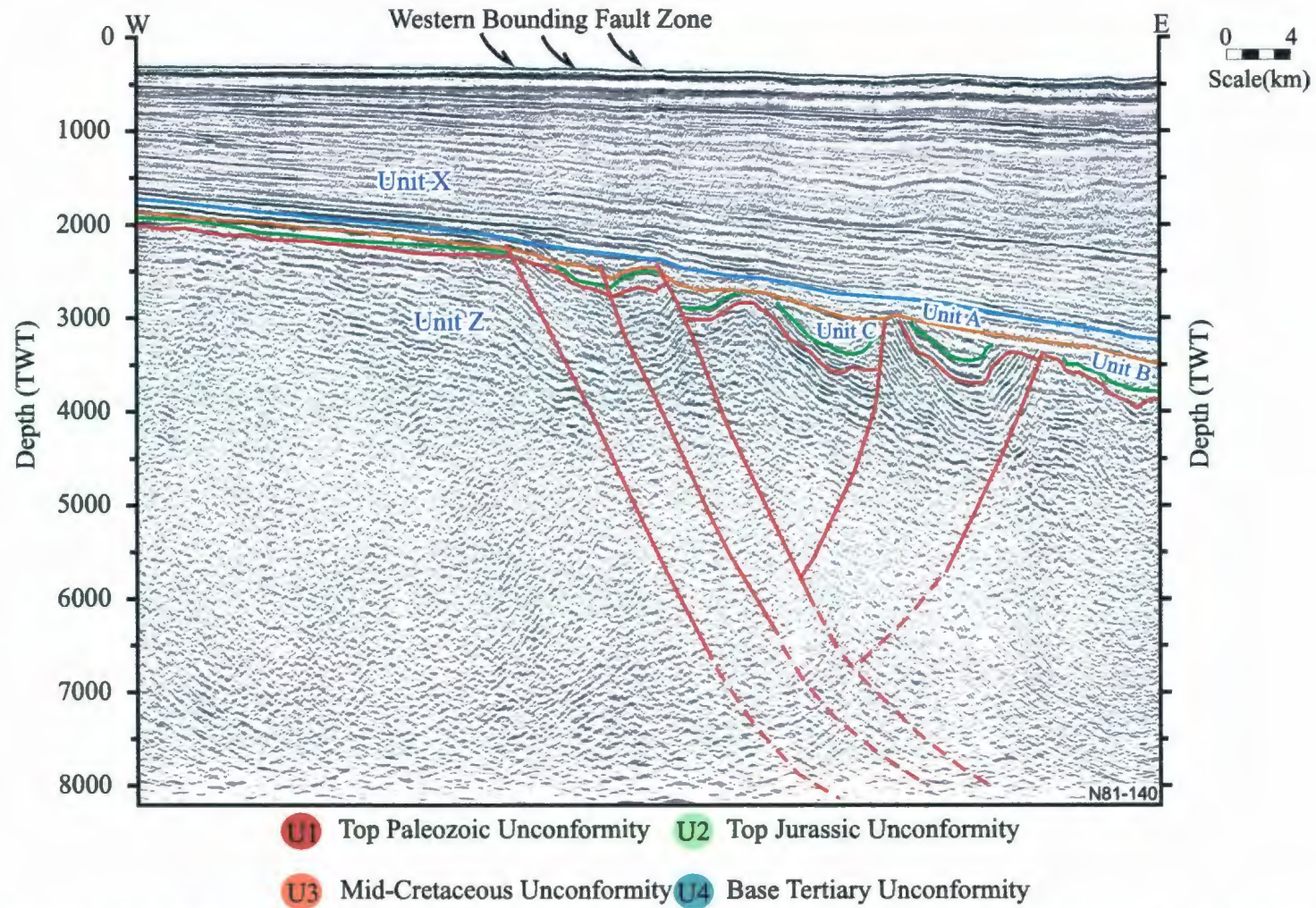


Figure 4.4. Multichannel seismic reflection profile N81-140 showing the western margin of the study area. Note the three east-dipping normal faults defining the basin margin and also two minor antithetic splays. Location shown in Figure 4.5.

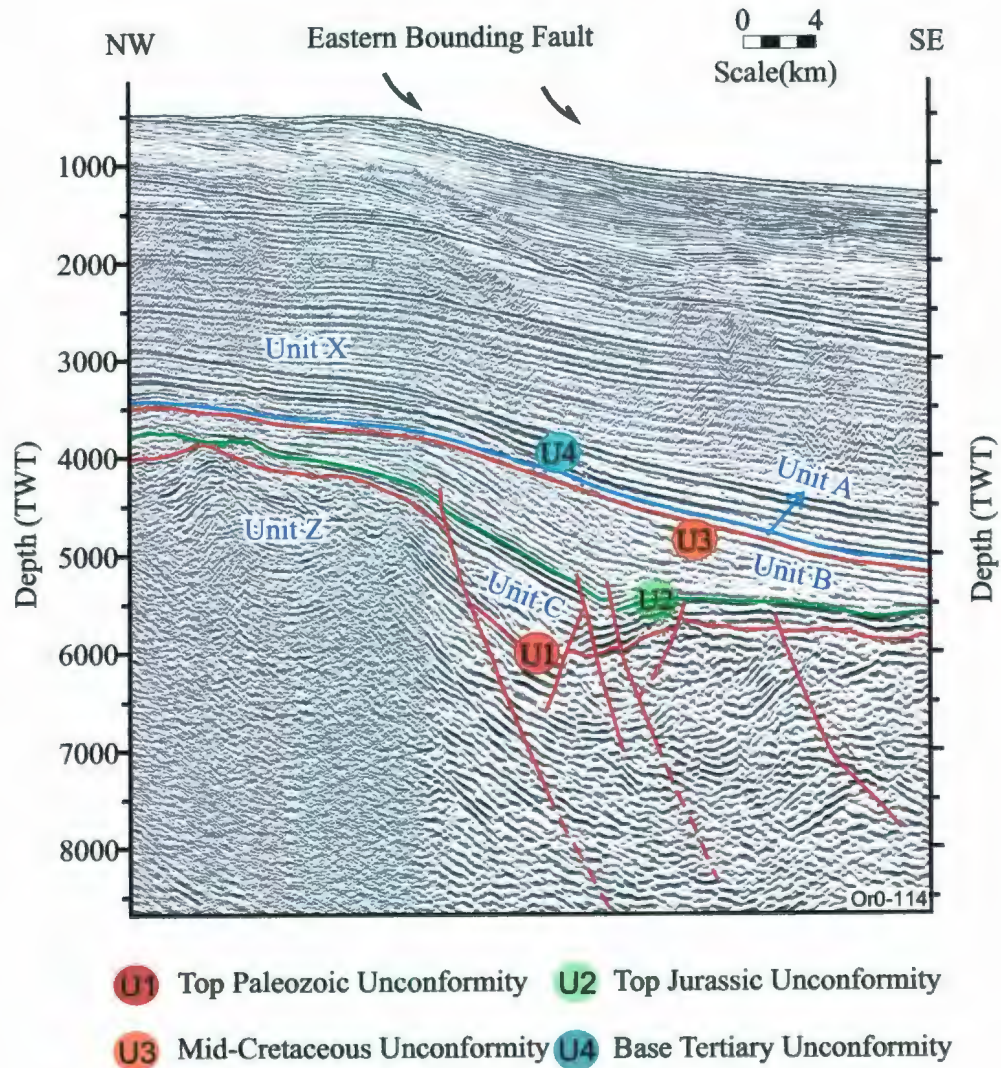


Figure 4.6. Multichannel seismic reflection (ORO-114) profile showing the Eastern Bounding Fault of the Bonavista Fault Zone and its splays.

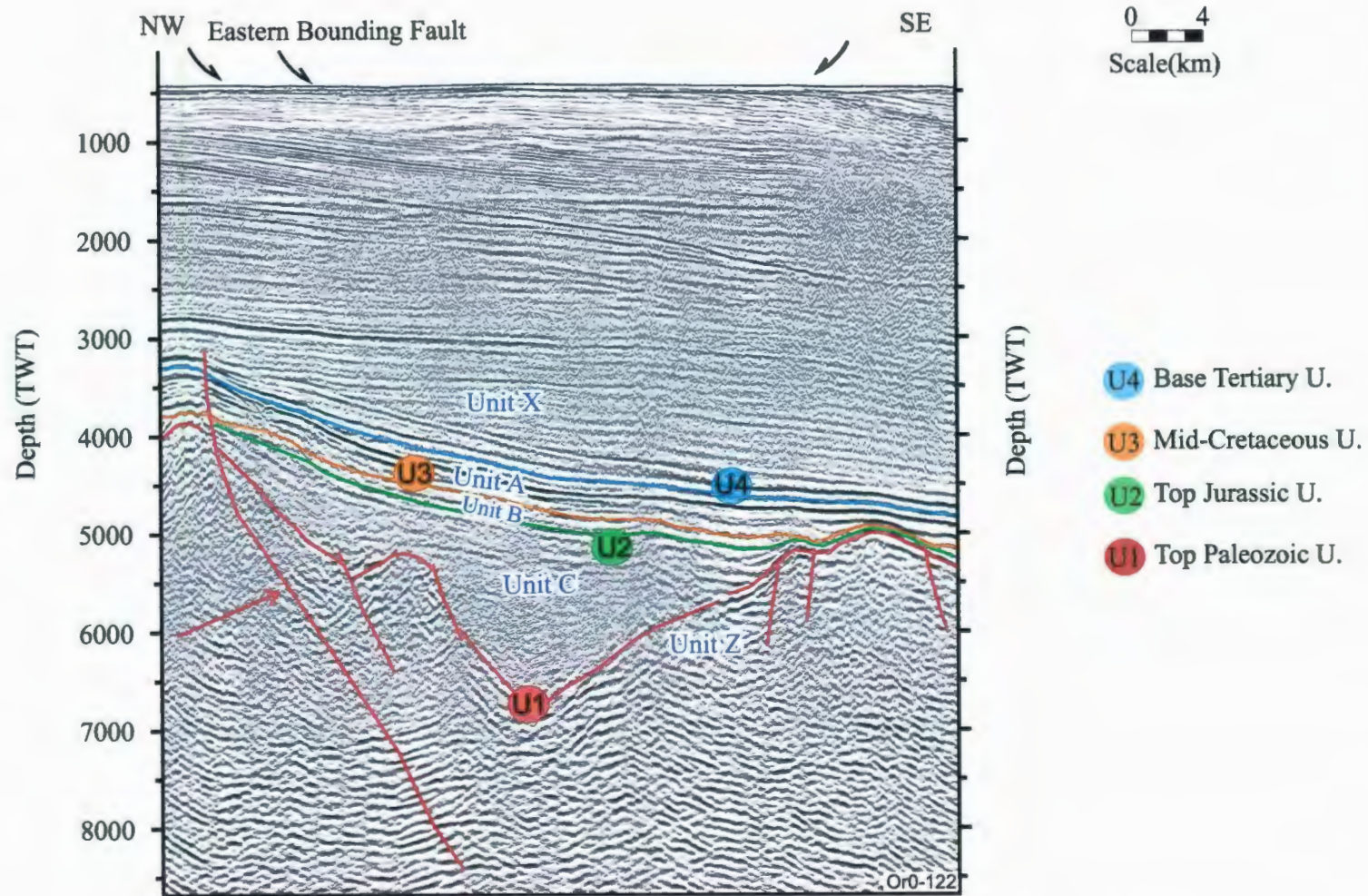


Figure 4.7. Multichannel seismic reflection (ORO-122) profile showing the Eastern Bounding Fault and its splays of the Bonavista Fault Zone. Location shown in Figure 4.5.

number of seismic reflection profiles. This mapping exercise illustrates that the Eastern Bounding Fault displays a 030°N trend. Further south, the Eastern Bounding Fault of the Bonavista Fault Zone is well expressed in seismic reflection profiles (e.g., Fig. 4.8). Here the fault defines a northwest-southeast trending map trace, with a northeast-dipping fault plane that displays ~400 ms vertical stratigraphic separation. Two equally well-developed synthetic faults run parallel to the western basin-bounding fault, and similarly show northeast-dipping fault trajectories and 200-300 ms offsets (Fig. 4.8). The Eastern Bounding Fault and its two synthetic faults delineate the western fringes of a narrow, but > 2.5 seconds deep basin situated west of the Bonavista Fault Zone (Figs. 4.3, 4.8). This small basin is informally referred to as α0 (Fig. 4.8). Several seismic reflection profiles in this area suggest that this basin primarily trends in a northwest-southeast direction, paralleling the overall trend of the master fault (Fig. 4.9). The northeastern margin of this narrow basin is depicted by a prominent northwest-southeast trending and southwest-dipping normal fault, and its 2-3 synthetic splays. Further to the northeast of this fault system, a 1.5 km wide platform is developed. The northeastern margin of this platform is delineated by 2-3 well-developed northwest-southeast trending and northeast-dipping faults that display normal-sense stratigraphic separation (Fig. 4.8). Careful examination of seismic profiles and the footwall and hanging wall cutoffs show that these faults display 200-300 ms offsets. These faults further define the Eastern Bounding Fault of the Bonavista Fault Zone. Thus, the northeast-dipping Western and Eastern Bounding Faults of the Bonavista Fault Zone, together with southwest-dipping antithetic faults that developed between the bounding faults collectively delineate the prominent set of the

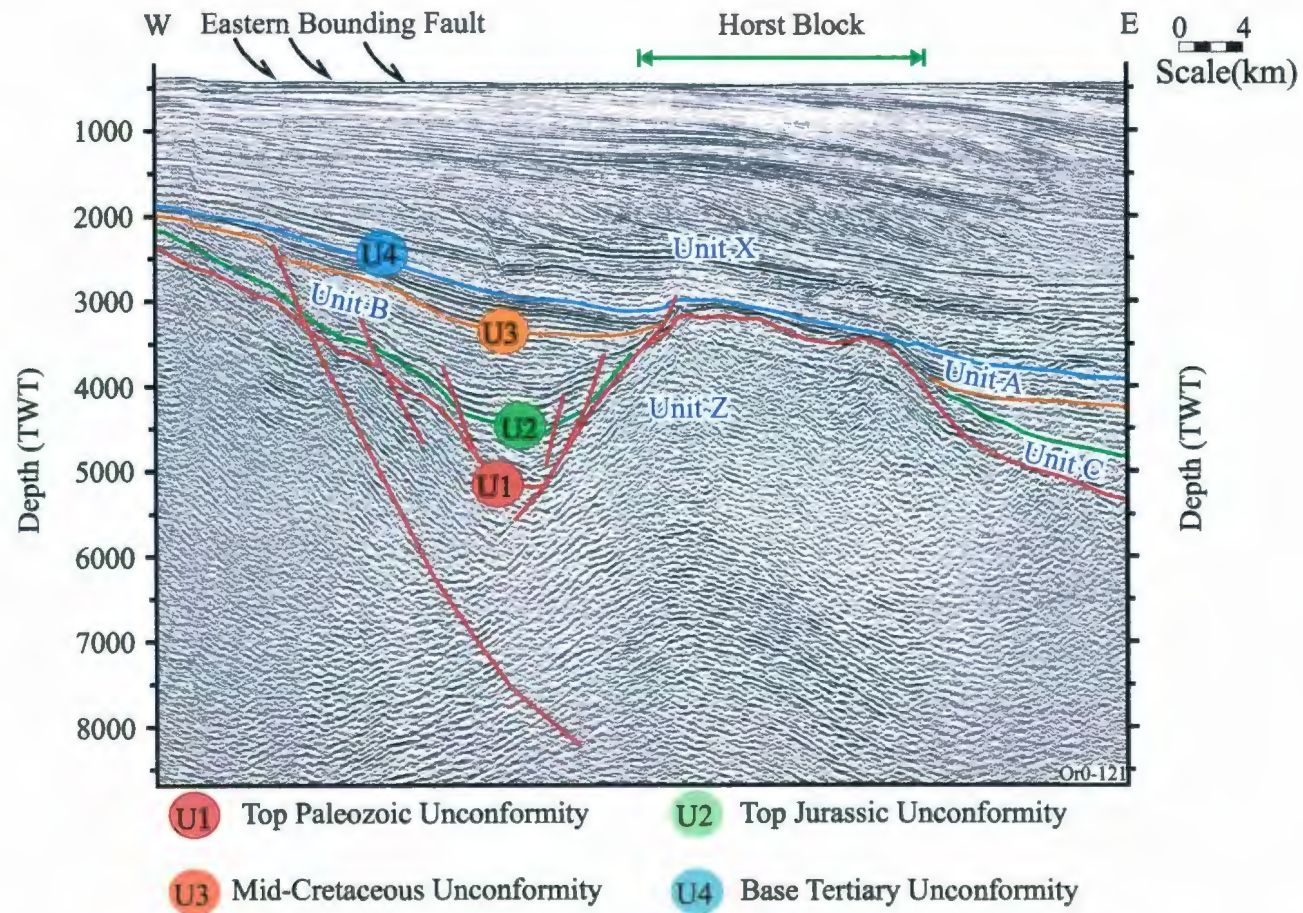


Figure 4.8. Multichannel seismic reflection (ORO-121) profile showing the western margin of the study area. A well delineated horst block is situated immediately east of the basin-bounding listric normal faults that define the western margin of the basin. Location shown in Figure 4.5

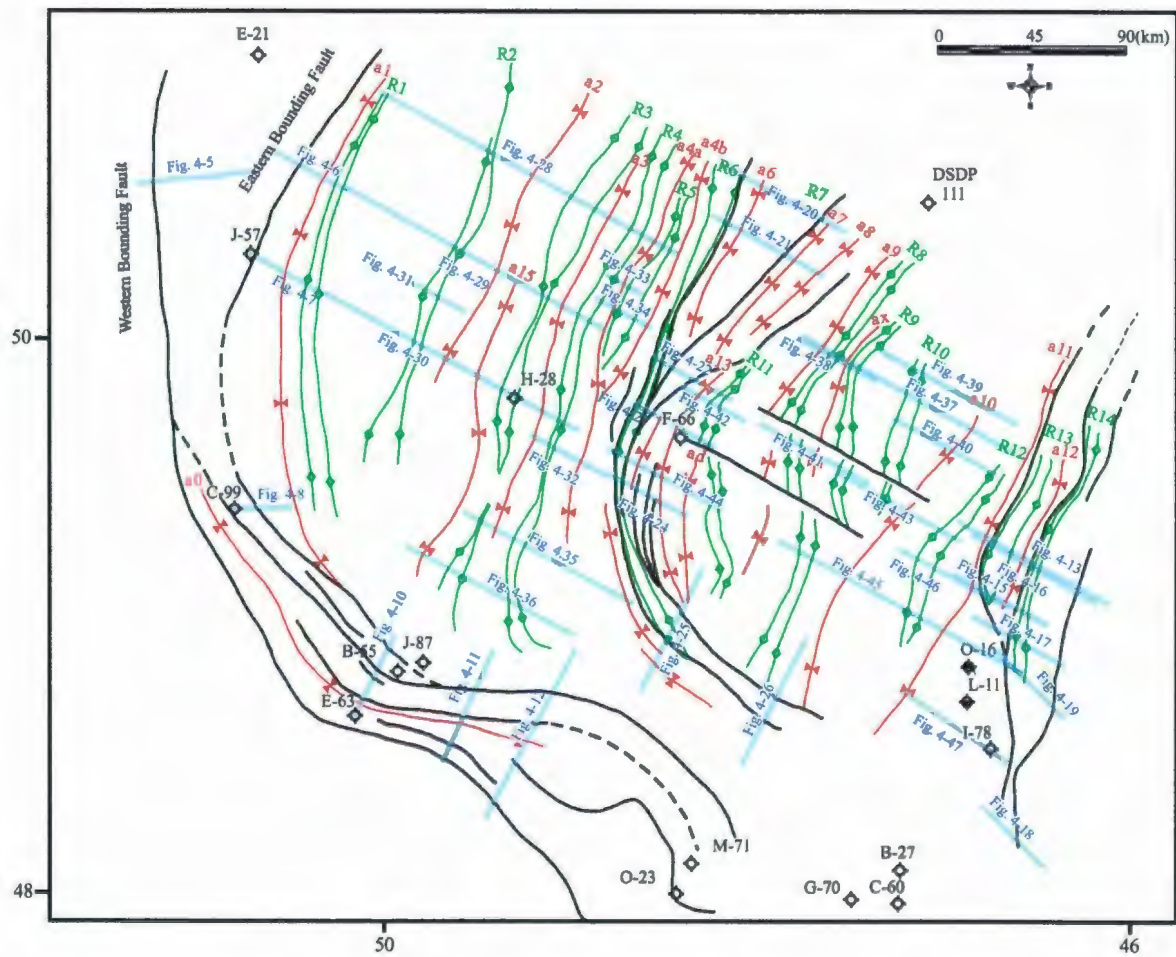


Figure 4.9. Map of the study area showing the distribution of major basin and ridge structures. The hinge line of anticlines and the trough of the syncline structures defines the basin and ridges. Also shown are the location of seismic reflection profiles used in this chapter.

horst and graben structures observed in this region (Figs., 4.3, 4.9). These structures are mainly developed in the pre-rift basement successions, but have affected the deposition of the entire Mesozoic succession.

The Bonavista Fault Zone can be readily traced toward the southeast, where it widens from ~3 km at the apex of the convex to the west structure, to ~10 km at the southern fringes of the Orphan Basin (Fig. 4.3). This broadening is accomplished by the divergence in the trends of the master faults of the zone: the Eastern Bounding Fault shows a progressive counterclockwise swing towards the south from a northwest-southeast trend to a west-northwest – east-southeast trend (i.e., 150°N to 110°N), while the Western Bounding Fault shows a reciprocal but clockwise swing from a northwest-southeast trend to a north-northwest – south-southeast trend. The fault map shows that this broadening is further accompanied by the development of a number of new faults between the Western and Eastern Bounding Faults of the Bonavista Fault Zone (Fig. 4.3). Comparison of seismic reflection profiles OR0-101 (Fig. 4.10), OR0-103 (Fig. 4.11) and OR0-117 (Fig. 4.12) shows that the broadening between the Western and Eastern Bounding Faults is largely accommodated by the widening of the basin α 0 toward the south and southeast.

In the southwestern portion of the study area, the Western Bounding Fault is well imaged as a northwest-southeast to east-northeast – west-southwest trending prominent listric normal fault. It includes two similar-trending synthetic splays southwest of basin α 0 (Fig. 4.10). Footwall and hanging wall cutoffs of several prominent marker horizons

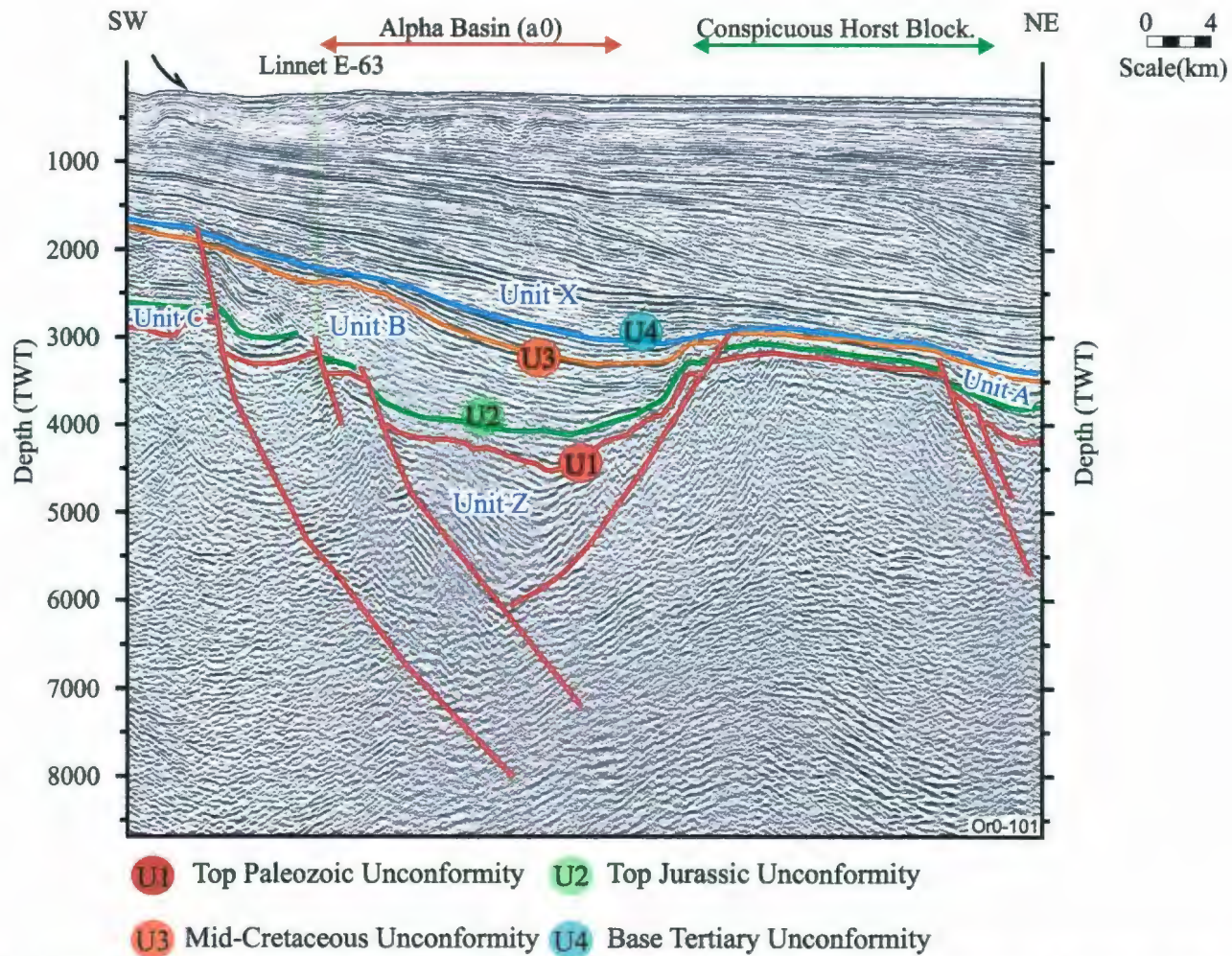


Figure 4.10. Multichannel seismic reflection (ORO-101) profile showing the southwestern margin of the study area. Note the presence of several prominent listric normal faults, a narrow but deep basin (Alpha Basin - $\alpha 0$) and a conspicuous horst block. Location shown in Figure 4.5

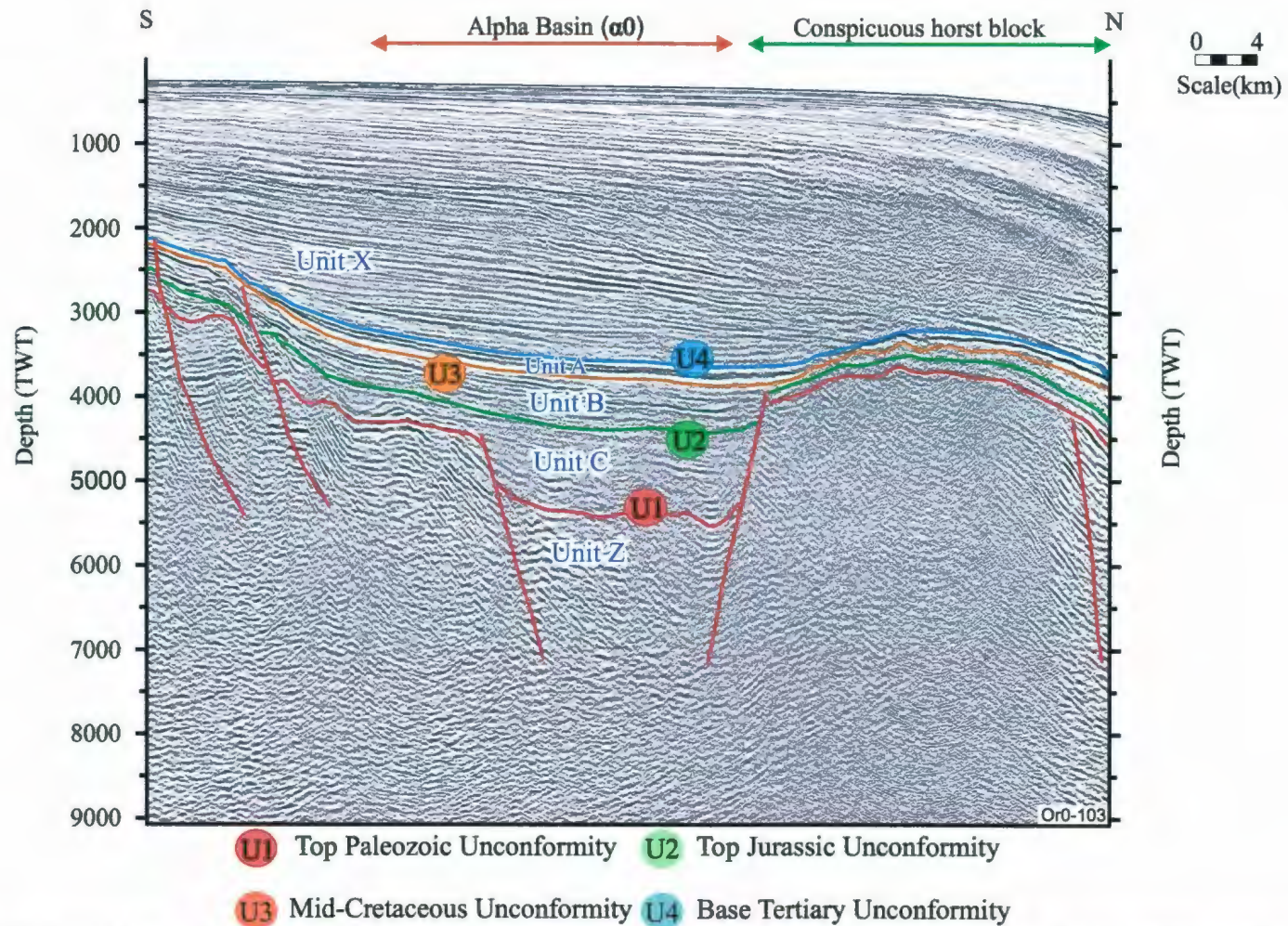


Figure 4.11. Multichannel seismic reflection (ORO-103) profile showing the southwestern margin of the study area. Note the presence of several listric normal faults, a deep basin (Alpha Basin) and a conspicuous horst block. Location shown in Figure 4.5.

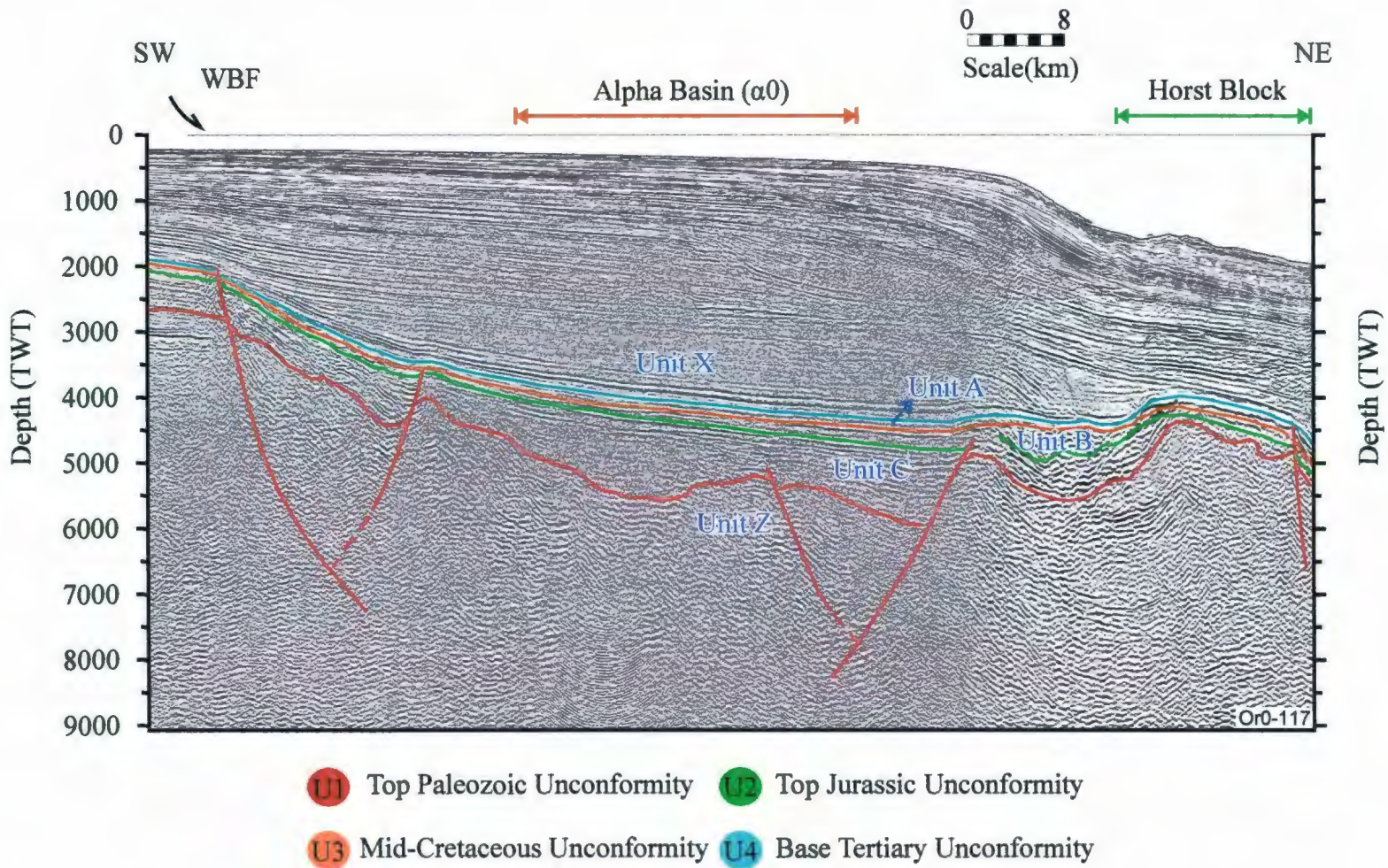


Figure 4.12. Multichannel seismic reflection (ORO-117) profile showing the southwestern margin of the study area. Note the presence of the Western Bounding Fault (WBF), several subsidiary listric normal faults, a wide and deep basin (Alpha Basin- $\alpha 0$) southwest of the prominent horst block. Location shown in Figure 4.5.

well below the Base Tertiary Unconformity within the Mesozoic successions show 300-600 ms vertical stratigraphic separation across these faults. Careful examination of the seismic profiles shows that reflections within the hanging wall of the master fault as well as the subsidiary faults are acutely tilted toward the fault planes, creating a series of rotated and back-tilted blocks. The east-northeast – west-southwest trending, southwest-dipping fault that delineates the northeastern margin of the basin α_0 and the southwestern margin of the horst block is clearly imaged in this seismic profile. Here, a series of similar-trending and dipping smaller synthetic fault splays are also observed. These faults merge with the main fault plane at various depths (Fig. 4.10). The fault that delineates the northeastern margin of basin α_0 can be traced with confidence to depths >7 seconds, where it appears to abut the northeast-dipping Western Boundary Fault. This geometric architecture suggests that the fault delineating the northeastern margin of basin α_0 and the Western Boundary Fault may define a crustal-scale synthetic – antithetic fault pair.

Further to the south, at the northern regions of the Jeanne d'Arc Basin the Western Boundary Fault assumes a nearly north-south trend, but retains its structural character as a basin-bounding fault (Fig. 4.3). Whereas, in this area, the Eastern Bounding Fault loses its expression as a basin bounding fault and becomes indistinguishable from the numerous east-northeast – west-southwest trending faults that bound the southern margin of the Orphan Basin (Fig. 4.3).

4.3. Eastern Basin Margin

The structural framework of the eastern margin of the study area is delimited by 4-5 northeast-southwest trending northwest-dipping major faults and several similar trending and northwest-dipping and southeast-dipping minor faults (Figs. 4.3, 4.9). All these faults display normal-sense stratigraphic separations, with listric fault trajectories that sole into the pre-rift basement units (Fig. 4.13). The tip points of these faults invariably lie beneath the Base Tertiary Unconformity. The seismic stratigraphic character of the hanging wall of many of these faults shows the development of prominent growth stratal wedges within the Cretaceous successions. These wedges clearly thicken toward the fault plane showing growth ranging from 400 ms to >900 ms (Fig. 4.13). However, it is noteworthy that the Unit X successions (i.e., the Jurassic strata) do not show similar growth strata development. In several hanging walls, the prominent marker that defines the unconformity at the top of the Jurassic succession dips to the southeast (i.e., toward the fault plane), accentuating the growth strata development in the overlying successions within the northwest-dipping fault blocks. The footwalls of these major faults delineate 2-3 basement-cored structural highs which are referred to as ridges R13 and R14, and their intervening basin α 12 (Figs. 4.3, 4.9).

The northern segment of the eastern basin margin is marked by three northeast-southwest striking and northwest-dipping major faults which display normal-sense stratigraphic separations (Figs. 4.3, 4.14). From west to east in this area, the faults are labeled as N4, N5, and N6 (Fig. 4.3). A few similar-trending and northwest-dipping

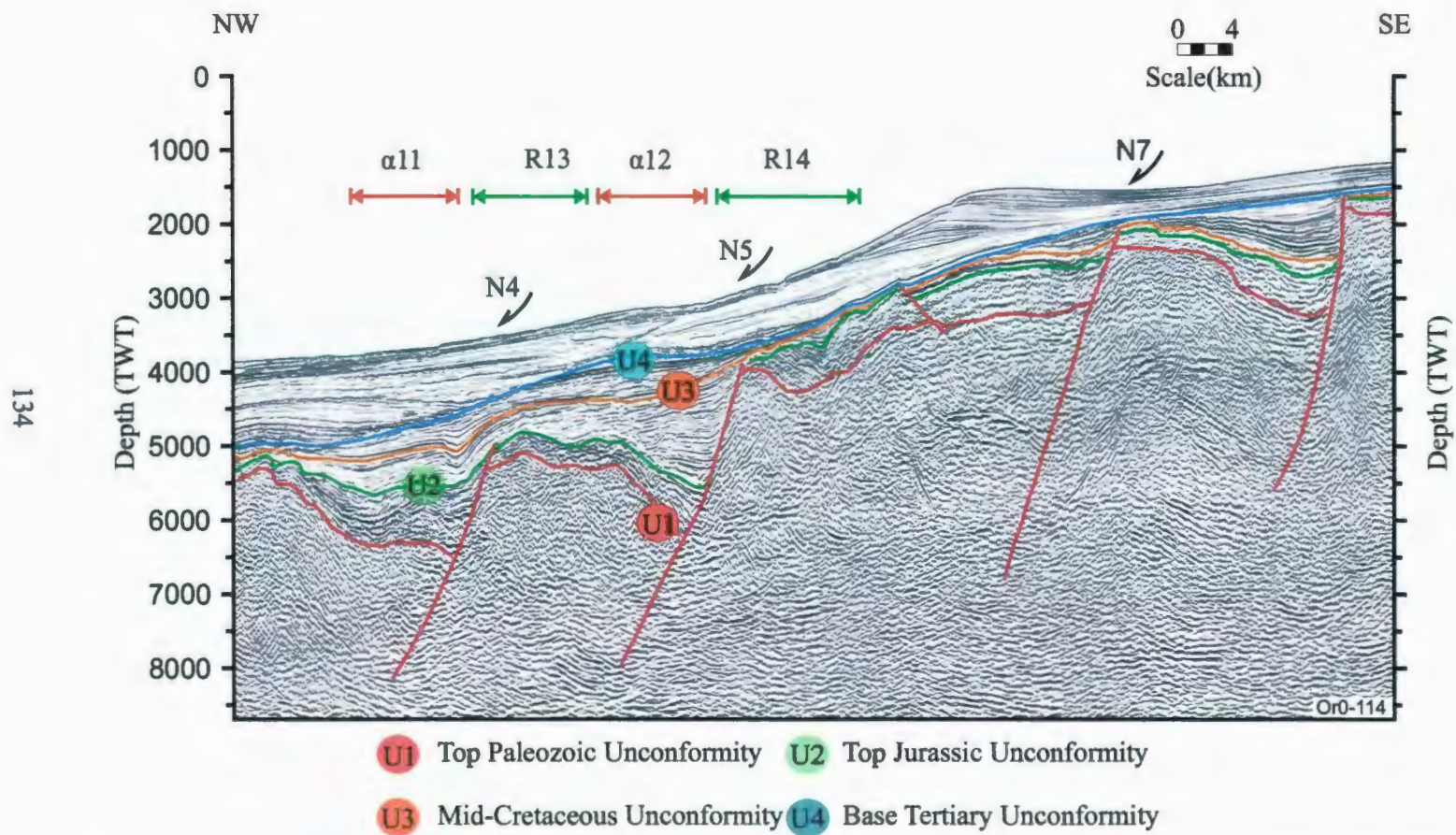


Figure 4.13. Multichannel seismic reflection (OR0-114) profile showing the eastern margin of the study area. Note the presence of the several listric normal faults (N4, N5 and N7) creating rotated and tilted fault blocks with distinctive growth staratal wedges. Location shown in Figure 4.5.

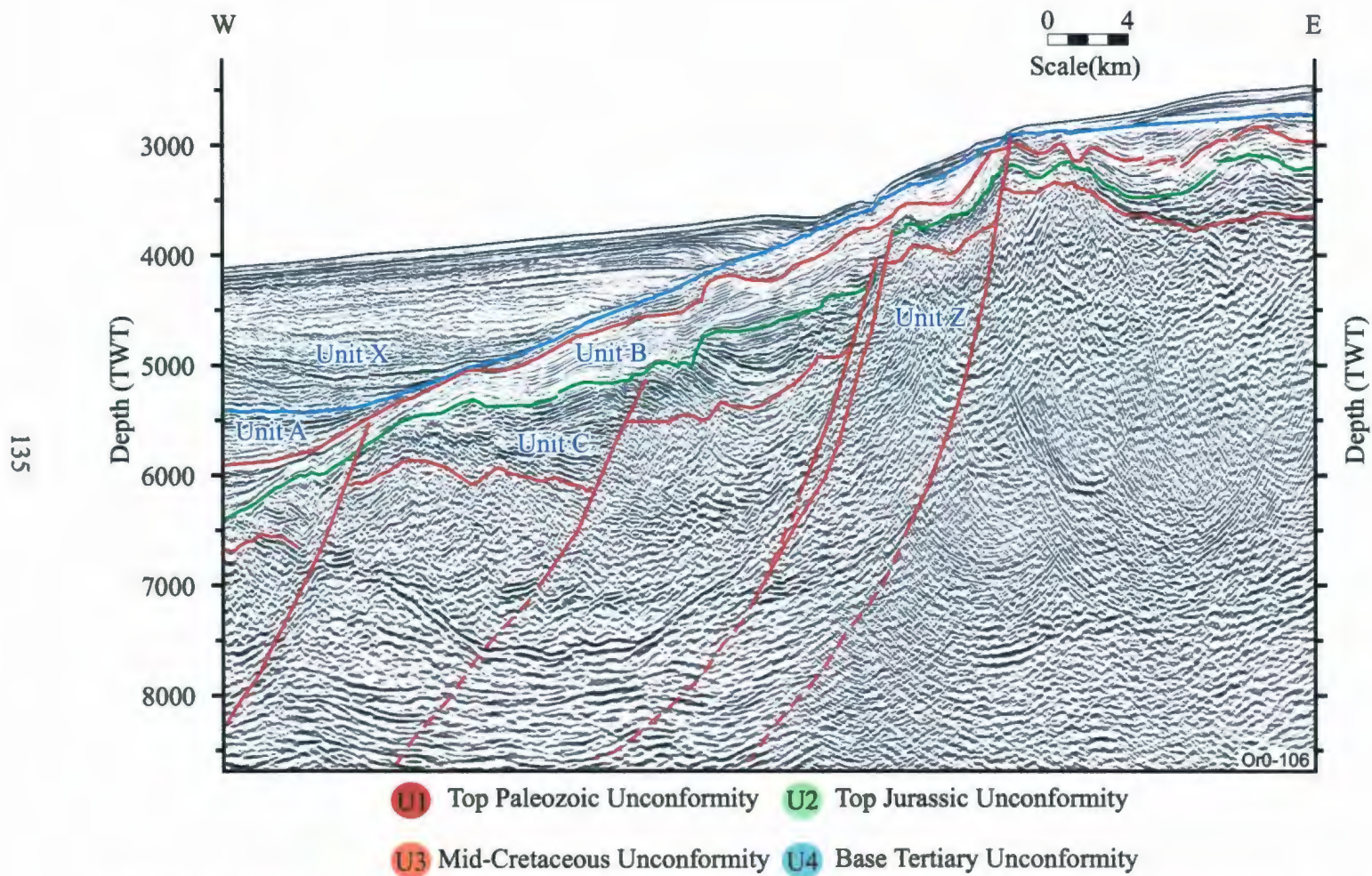


Figure 4.14. Multichannel seismic reflection (OR0-106) profile showing the northeastern margin of study area. Note the presence of the major normal faults creating a step-wise pattern and rotated and tilted fault blocks with distinctive growth staratal wedges. Location shown in Figure 4.5.

synthetic and southeast-dipping antithetic faults are associated with this major fault system. Across the fault zone, these major faults (i.e., N4-N6) display a progressively westward-increasing extensional separation on the Top Jurassic Unconformity, creating a staircase morphology along the easternmost boundary of the Orphan Basin (Figs. 4.14, 4.15). Faults N4, N5 and N6 are morphologically similar: they display listric fault trajectories with angles of $\sim 45^\circ$ in the uppermost fault segments, progressively decreasing down section to $\sim 23^\circ$, soling into the pre-rift basement rocks of Unit Z. They exhibit 200-500 ms offsets between footwall and hanging wall cutoffs at the Top Jurassic Unconformity. Thus, faults N4-N6 create a prominent fault fan with rotated and tilted blocks displaying prominent growth stratal wedges within the Lower Cretaceous successions of Unit B (Fig. 4.3). In these tilted blocks, the hanging wall of a fault block also represents the footwall of the adjacent fault block (Figs. 4.15, 4.16). For example, the hanging wall of fault N5 includes an approximately 900 ms-thick growth strata onlapping onto the fault plane (e.g., Fig. 4.16). These strata dramatically thin westward to ~ 300 ms over the footwall of adjacent fault block associated with fault N4.

The easternmost fault of the three major fault (i.e., fault N6) can be easily identified in seismic reflection profiles across the northeastern portion of the Eastern Basin Margin. However, it is difficult to confidently map and trace this fault further to the south. For example, there is a prominent fault (i.e., N7) in the southernmost segment of the Eastern Basin Margin (see below), which shows a similar orientation, trend and dip direction to fault N6. This fault is also situated at approximately similar geographical setting, 3-4 km south of fault N6. However, the sparse seismic grid in this region also

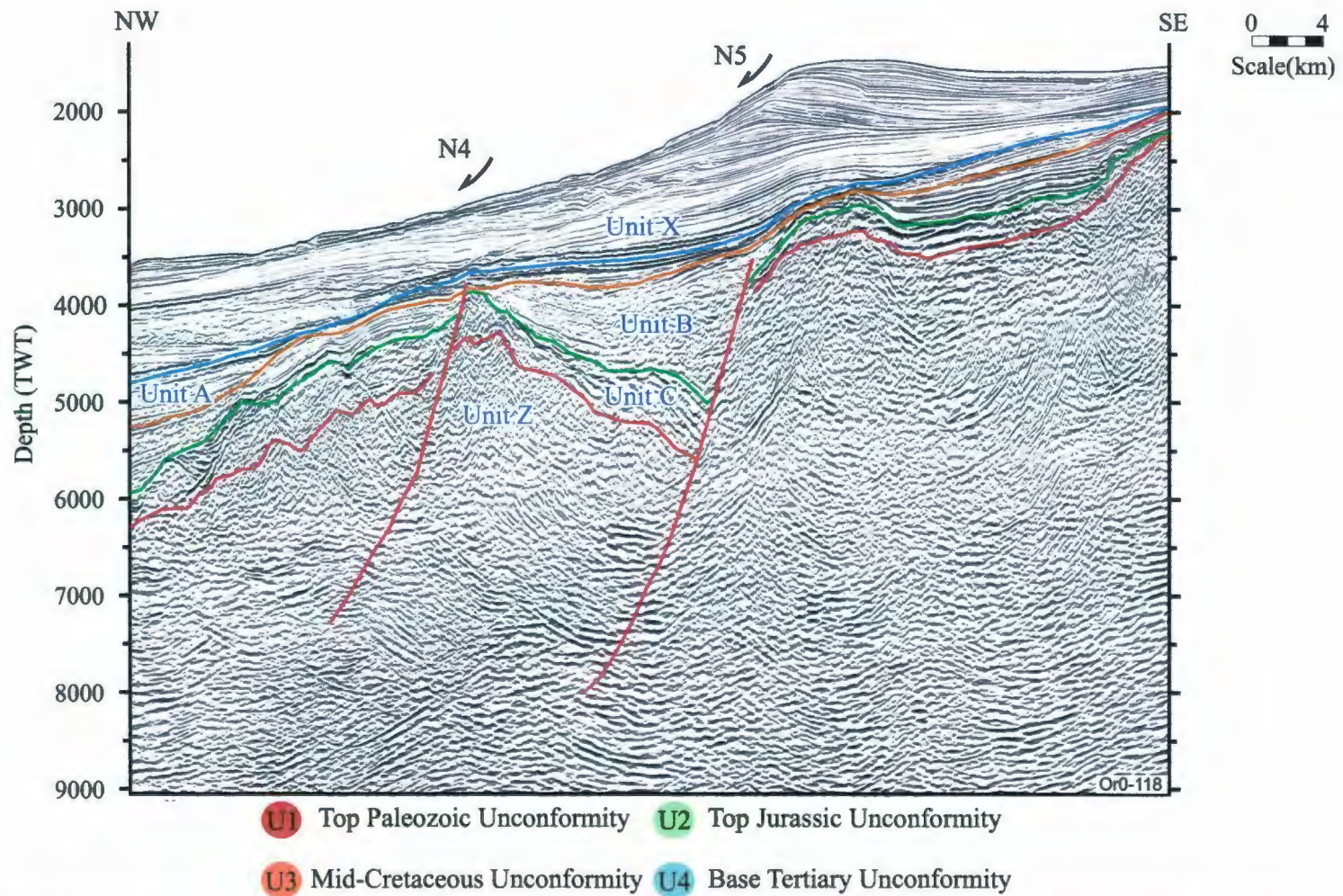


Figure 4.15. Multichannel seismic reflection (OR0-118) profile showing the northeastern margin of study area. Note the presence of the major normal faults (N4, N5) creating a step-wise pattern and rotated and tilted fault blocks with distinctive growth stratal wedges. Location shown in Figure 4.5.

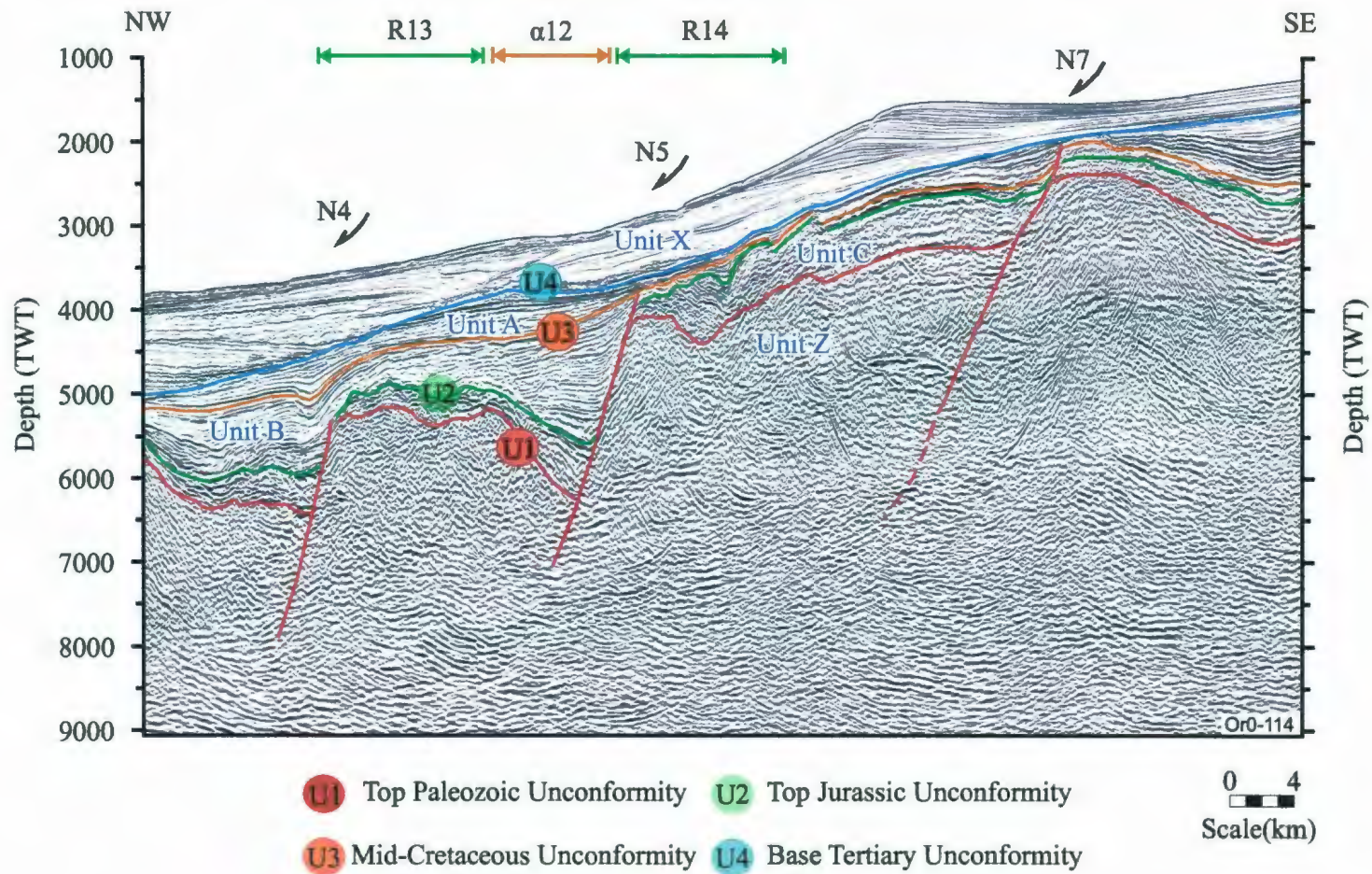


Figure 4.16. Multichannel seismic reflection (OR0-114) profile showing the northeastern margin of study area. Note the presence of the major normal faults creating a step-wise pattern and rotated and tilted fault blocks with distinctive growth strata, where the reflectors show downlap against the fault trajectory. Location shown in Figure 4.5.

precludes the southward mapping of fault N6, and its relationship and linkage with fault N7 (Fig. 4.3).

The hanging wall of faults N4 and N5 define two major ridges: R13 and R15 and the intervening basin $\alpha 12$ is nested over the footwall of fault N5 (Figs. 4.3, 4.9). Ridge R13 is a ~10 km wide, double crested, northeast-southwest trending structure which can be easily traced southwards paralleling fault N4 into the central portion of the province. Ridge R13 has a gently southeast-dipping eastern flank and a steeply northwest-dipping, fault controlled western flank. Internally, it is cored by high amplitude and continuous reflections and the chaotic reflections of the basement Unit Z (Fig. 4.16). In general, the high amplitude continuous reflectors (assigned to the Jurassic succession) defines the ~5° east-tilted crest of ridge R13. In this area, the upper portion of the Lower Cretaceous succession progressively onlap and eventually overstep the tilted fault block defined by ridge R13 in the west.

Basin $\alpha 12$ is situated between ridges R13 and R14 (Figs. 4.3, 4.9). It is a ~10 km wide depocenter which contains ~1300 ms thick lower Cretaceous and ~700 ms Jurassic successions. The reflector packages within these successions delineate a tilted wedge-shaped body with a ~1000 ms growth strata, which show remarkable thickening towards fault N5 that controls the western flank of ridge R14 (Fig. 4.16). The reflectors that are assigned to the Jurassic succession clearly abut fault N5 in the east, whereas they thin towards the west, where the uppermost portion of the succession oversteps ridge R13. This thinning is mainly accomplished by a west-directed onlap and convergence of

reflectors. The reflectors within the lower Cretaceous succession appear to abut the western flank of the ridge R14 (Fig. 4.16).

Ridge R14 is a 5-7 km wide, northeast-southwest-trending structural high, that shows a parallel trend to fault N5 (Figs. 4.3, 4.9). It stands as a huge wall with its steep, fault-controlled western flank rising ~2200 ms from the adjacent floor of basin α 12 (Fig 4.16). The internal architecture of the ridge is characterized by a mainly pre-rift basement succession and a ~300 ms-thick veneer of Jurassic succession. On the crest of the ridge the reflectors that are assigned to the Jurassic succession display approximately 7° dip towards the southeast, with the lower Cretaceous succession defining a half graben structure (Fig. 4.16).

The structure of the southeastern segment of the Eastern Basin Margin is characterized by 2-3 major listric extensional faults, two of which further extend southwards to the Flemish Cap (Fig. 4.3). In this region, the westernmost fault (i.e. N4) initially displays a counterclockwise swing and assumes a northwest-southeast trend, heading towards fault N5, eventually merging with it (Figs. 4.3, 4.17, 4.18). Comparison between seismic reflection profiles OR0-114 (Fig. 4.16) and FP99-1060 (Fig. 4.19) shows the dramatic southward narrowing of the fault block between faults N5 and N7 from 17 km to 5.5 km (Fig. 4.3). The merged faults N4 and N5, (referred to as fault N5) then exhibit a mainly north-south trend, and west-directed dip direction. Similar to the northern segment of the Eastern Basin Margin, fault blocks display prominent growth strata within the Cretaceous successions, ranging between 200-400 ms. The growth

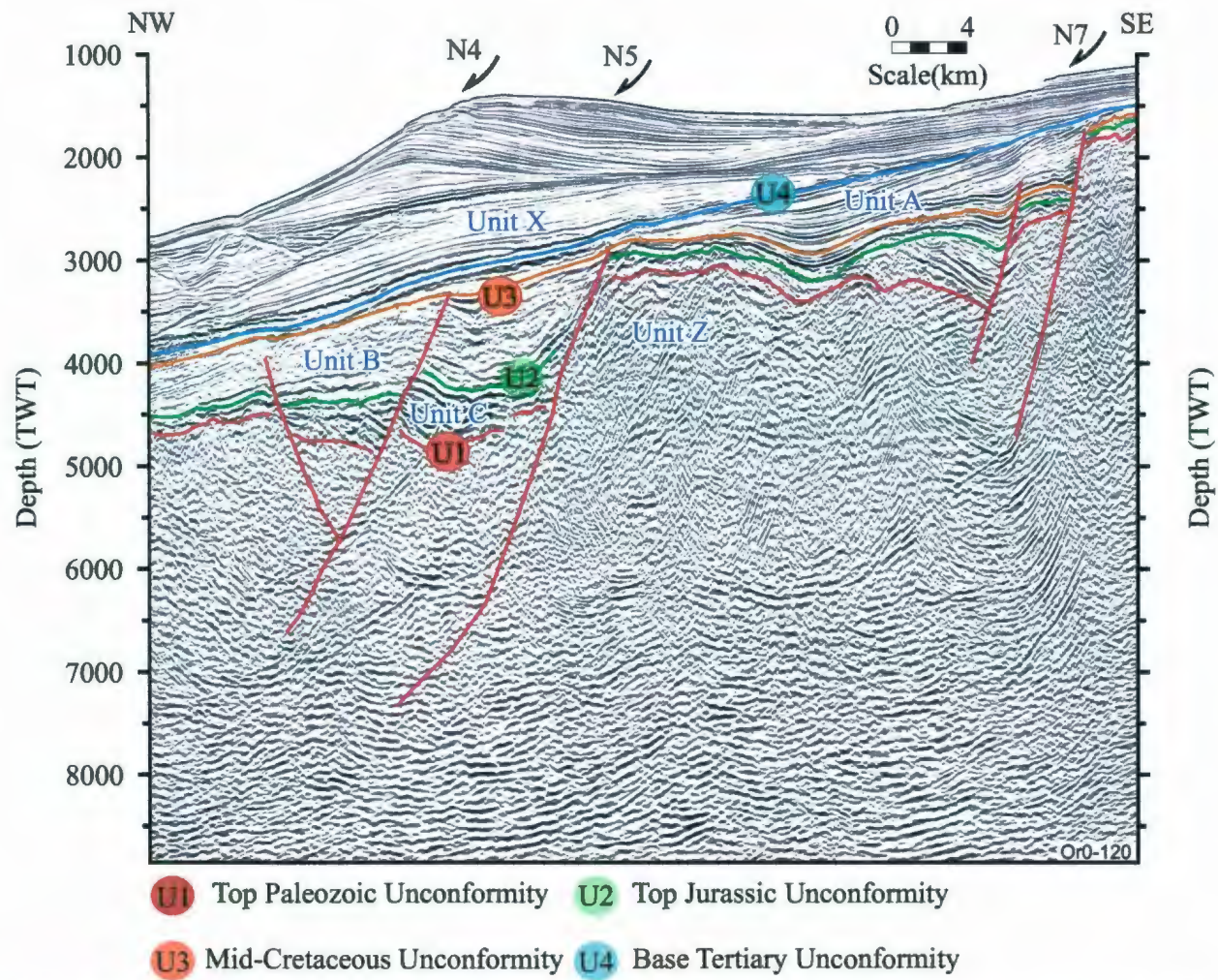


Figure 4.17. Multichannel seismic reflection (OR0-120) profile showing the northeastern margin of study area. Note the dramatic narrowing of the block between faults N4 and N5. Location shown in Figure 4.5.

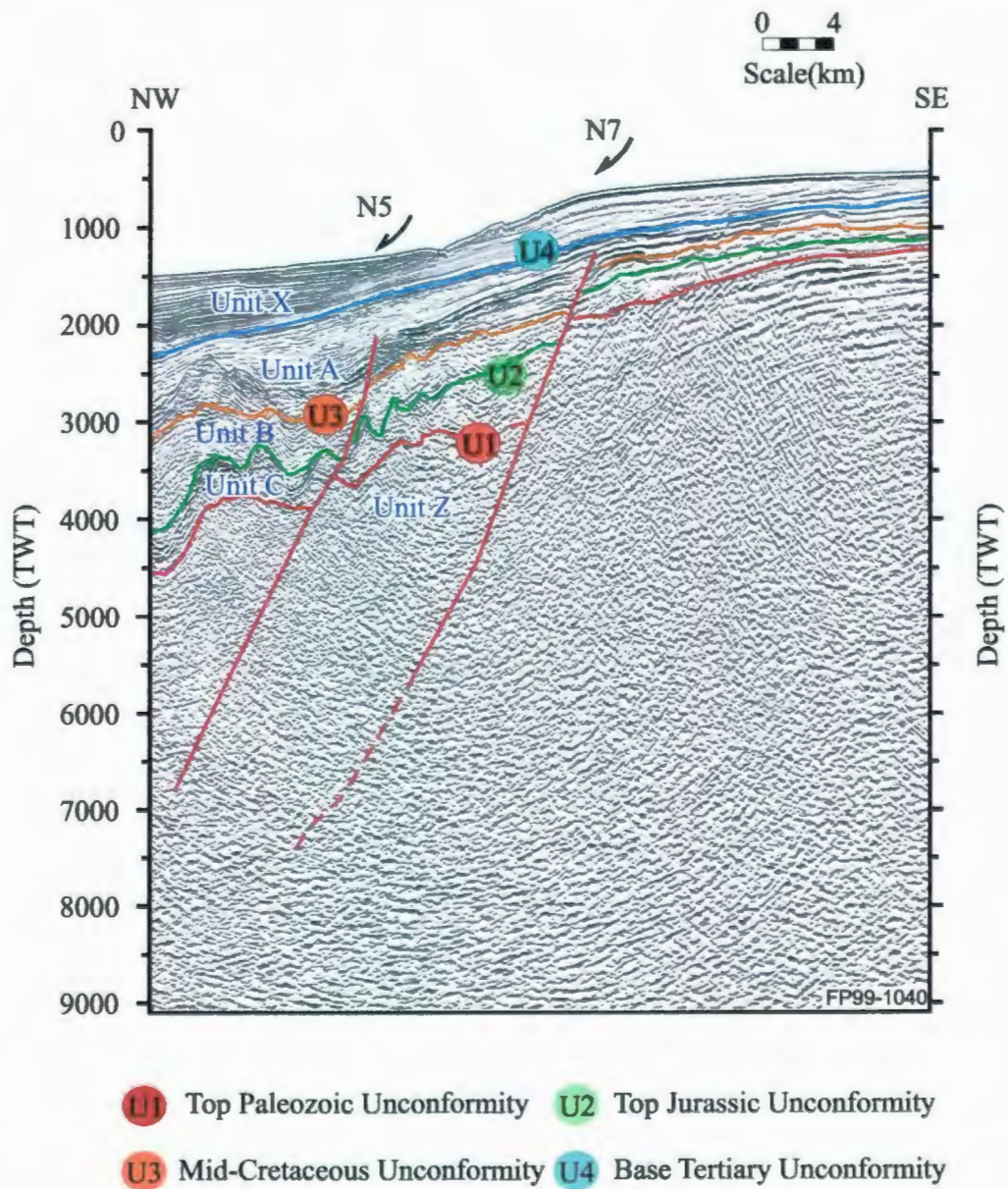


Figure 4.18. Multichannel seismic reflection (FP99-1040) profile showing the northeastern margin of study area. Note that fault N4 is not visible in this profile. Mapping shows that it merged with fault N5 immediately north of this seismic profile. (see Figure 4.3). Location shown in Figure 4.5.

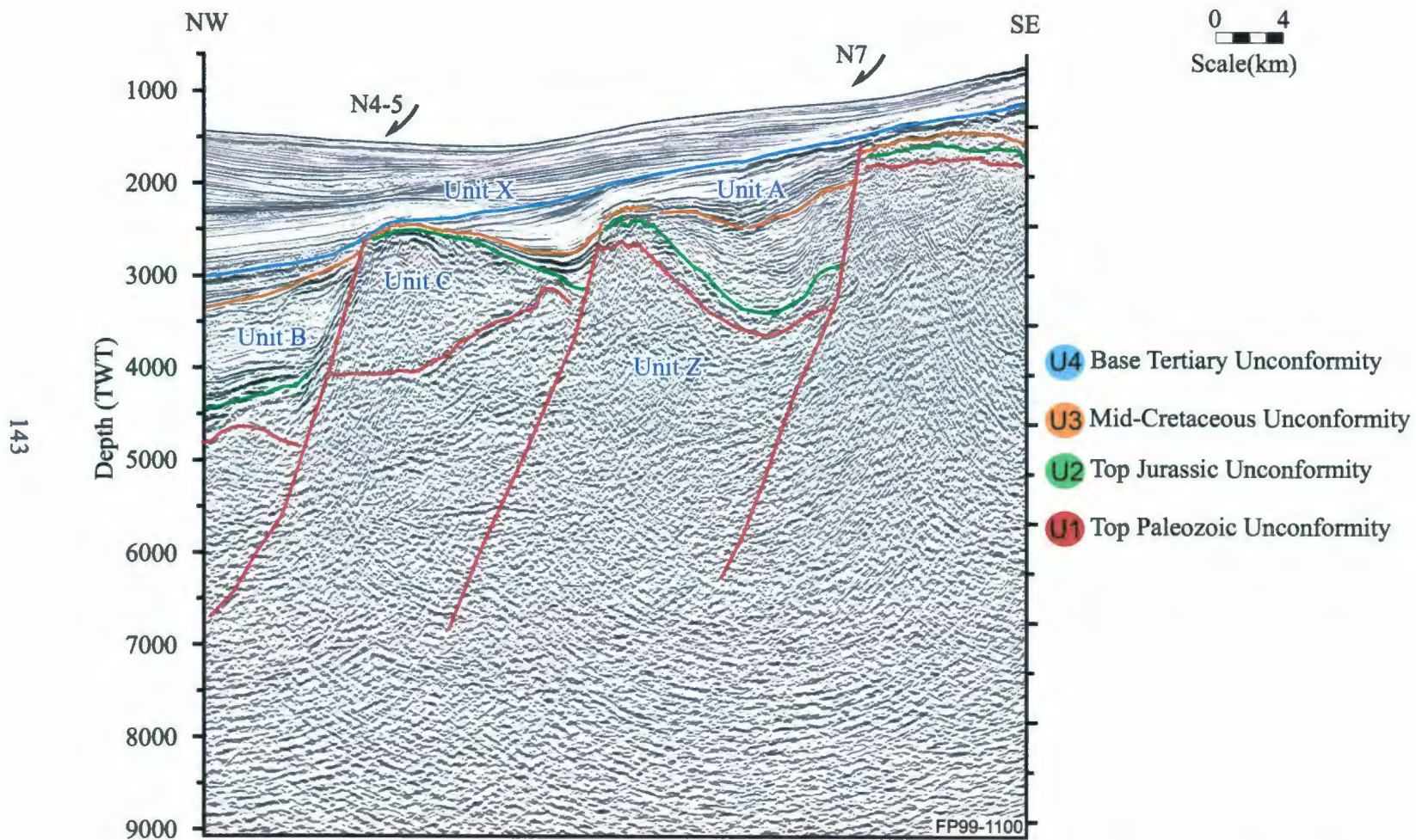


Figure 4.19. Multichannel seismic reflection (FP99-1100) profile showing the well-developed tilted and rotated fault blocks bounded by major faults N4 and N5. Location shown in Figure 4.5.

stratal package on the hanging wall of the fault N7 is comparably less than that in the northern segment of the eastern basin margin. The Top Jurassic Unconformity is also visible as a prominent marker (Figs. 4.17, 4.18), showing a clear east-directed dip, creating distinctly-tilted and rotated fault blocks associated with listric normal faults (Fig. 4.19).

4.4. White Sail Fault Zone

A prominent fault zone partitions the central regions of Orphan Basin into two distinct morpho-tectonic provinces, namely the West Basin and Ridge Province and the East Basin (Fig. 4.3). The fault zone is characterized by 2-3 major fault blocks, which define a 4.5 km wide zone bounded in the west and east by two major faults: TF1 and TF2, respectively (Figs. 4.20, 4.21). The eastern fault TF2 is correlated with the White Sail Fault of Enachescu et al. (2005), and herein is informally referred to as the "White Sail Fault". The fault TF1 is not previously identified as a major fault, but it is considered in this study as part of the western bounding fault of the White Sail Fault Zone (Fig. 4.3).

In the northernmost study area, fault TF1 is a huge northeast-southwest trending and southeast-dipping structure, with numerous similar trending smaller synthetic splays. The fault displays normal-sense vertical stratigraphic separations ranging from 0 - 1100 ms at the Base Tertiary Unconformity to >3000 ms at the Top Jurassic Unconformity (e.g., Figs. 4.20, 4.21). However, the lack of good stratigraphic control on the successions that core the major ridge bounding the northwestern margin of fault TF1

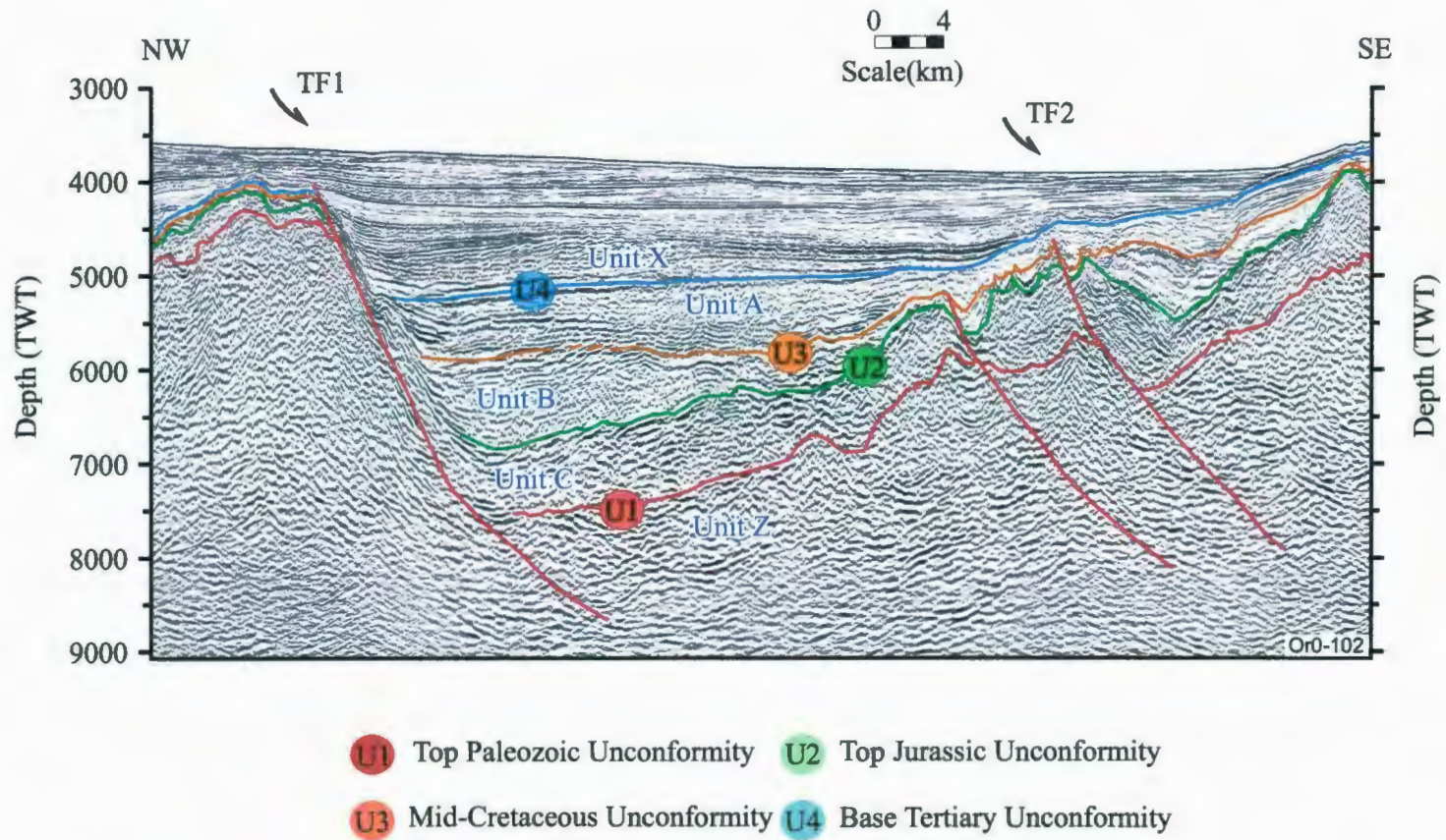


Figure 4.20. Multichannel seismic reflection (OR0-102) profile showing a significant growth at the Mid-Cretaceous Marker and the Top Jurassic Unconformity on the major rotated and tilted fault block which is bounded two major fault TF1 and TF2. Location shown in Figure 4.5.

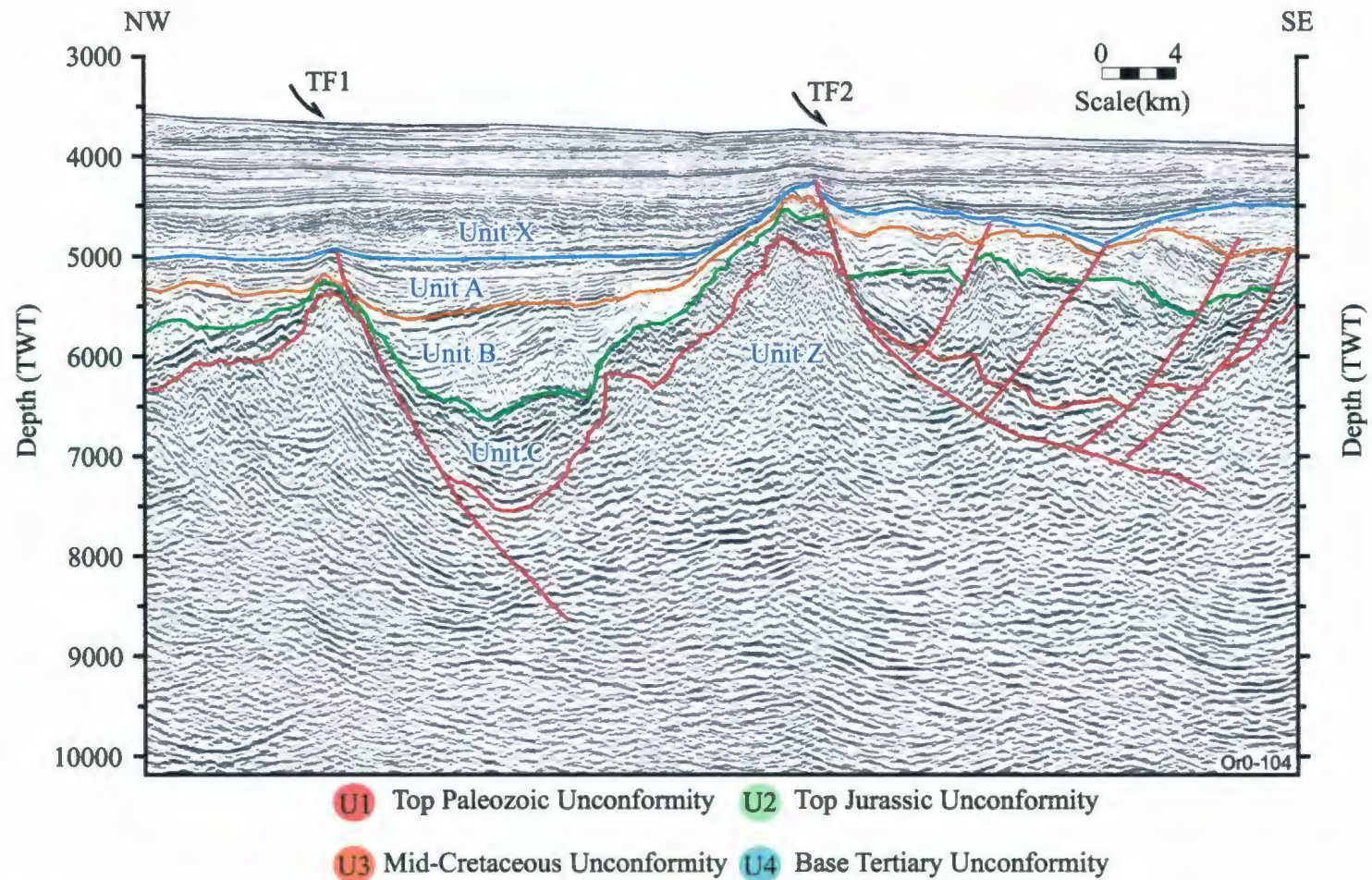


Figure 4.21. Multichannel seismic reflection (OR0-104) profile showing two major listric faults; TF1 and TF2 and their synthetic and antithetic splays. Note the presence of curved fault trajectories of the antithetic faults, which intersect the TF2 lower segment of the fault plane and Base Tertiary and Mid-Cretaceous Markers appear to abut the upper segment of this fault plane. Location shown in Figure 4.5.

precludes a firmer determination of the vertical stratigraphic separations observed on this fault. In the northern portion of the study area, this fault appears to tip within the middle-upper Cenozoic successions (Fig. 4.20). However, a seismic profile, ~3 km south shows fault TF1 tipping below the Base Tertiary Unconformity, and creates a noticeable inflection at this level (Fig. 4.21). In seismic reflection profiles, the fault extends to depths exceeding 9 seconds with a clearly listric fault trajectory displaying 30° in the upper, to 17° in the middle, to 7° in the lower fault segments, soling into the pre-rift basement (e.g., Fig. 4.20). The synthetic splays can be traced extending to depths also with listric trajectories, where they merge with fault TF1 (Figs. 4.20, 4.21). Numerous Cenozoic, as well as Cretaceous reflectors abut the fault surface, and show acutely upwardly-curved reflection segments immediately adjacent to the fault plane, possibly suggesting drag along the hanging wall and/or the footwall (Figs. 4.20, 4.21). A few of the upper-middle Cenozoic packages show growth stratal wedges on the hanging wall of the fault (Fig. 4.20 on TF1). However, the seismic succession situated between the Base Tertiary Unconformity and the Mid-Cretaceous Unconformity shows little to no growth as reflections delineate a nearly isopachous unit (Koning et al., 1988), whereas significant growth of ~800-900 ms is observed between the Mid-Cretaceous Unconformity and the Top Jurassic Unconformity (e.g., Fig. 4.20). Distinctive marker horizons below the Top Jurassic Unconformity clearly show that there is little to no growth within the Jurassic successions. This stratigraphic architecture suggests that fault TF1 became reactivated numerous times since the Jurassic, with tectonically quiet intervals in between. The prominent marker that defines the Top Jurassic Unconformity displays ~6° dip towards

the northwest, with the lower Cretaceous defining a thick wedge. Thus, the observed morpho-tectonic architecture delineates a major rotated and tilted fault block over the pre-rift basement successions (Figs. 4.3, 4.20, 4.21).

In the northernmost study area, fault TF2 is another very large northeast-southwest trending and southeast-dipping fault (Figs. 4.3, 4.20, 4.21). It exhibits 2-4 similar trending, northwest-dipping antithetic faults. In the northern portion of the study area, fault TF2 tips within the lower Cenozoic successions (Fig. 4.21). A distinct reflector bundle representing the fault trace is observed in many seismic reflection profiles, and dips with listric trajectories to depths between 8 and 9 seconds (e.g., Fig. 4.20). Reflections between the Base Tertiary and Mid-Cretaceous Unconformity appear to abut the fault surface (e.g., Fig. 4.21). The antithetic faults are well-developed and also display curved fault trajectories that intersect the TF2 fault trace (Figs. 4.20, 4.21). The successions between the Base Tertiary Unconformity and the Top Jurassic Unconformity show prominent growth on the hanging walls of the antithetic faults (Figs. 4.20, 4.21). However, there is no growth either on the Cenozoic or the Jurassic sequences within the fault blocks created by the TF2 or its antithetic splays.

The bounding faults TF1 and TF2 of the White Sail Fault Zone can be traced toward the south, where fault TF2 progressively merges with fault TF1 at around 49°57'N latitude (Fig. 4.3). Approximately 2 km further to the south, a major fault of the East Basin (i.e., fault N3) also merges with fault TF1, creating a very narrow single fault strand. This single fault strand extends southward for a very short distance and abuts the

major fault TF3, discussed below (Fig. 4.3). Whether fault N3 is part of the White Sail Fault Zone or a member of the faults observed within the East Basin remains conjectural, and requires further data and careful mapping. In the region where TF1 and N3 merges with the White Sail Fault Zone, a northeast-southwest trending, northwest dipping fault pair appears in seismic reflection profiles, west of the merged single fault strand (e.g., Figs. 4.3, 4.22, 4.23). These faults are labeled as TF3 and TF4 (Figs. 4.3). Fault TF4 is clearly traced toward the south and southeast, where it becomes a prominent fault that defines the western and southwestern boundary of the White Sail Fault Zone. Here, the fault zone assumes a nearly parallel trend with the faults that define the southeastern segment of the Western and Southwestern Basin Margin, becoming indistinguishable in structural and stratigraphic character from one another.

Around 49°50'N latitude, major fault TF2 merges at depth with fault TF1 (i.e., Fig. 4.23). A notable, high amplitude reflector bundle observed in seismic reflection profiles represents the fault plane of fault TF1, which clearly dips with listric trajectory to depths between 7 and 8 seconds. Here, the fault plane has ~30° dip in the vicinity of its tip point (i.e. within the upper Cretaceous succession), but becomes gentler ~15° as traced down-section into the pre-rift basement succession (i.e., Unit Z; Fig. 4.23). Footwall and hanging wall cutoffs of several prominent markers display between 400-500 ms vertical stratigraphic separations. Reflectors on the hanging wall of fault TF2 form a northwest-thinning wedge in the lower Cretaceous and possibly the upper Jurassic succession, and altogether display a roll-over against the TF2 fault surface (Fig. 4.23). This wedge is transected by 5-6 northeast-southwest trending, northwest dipping

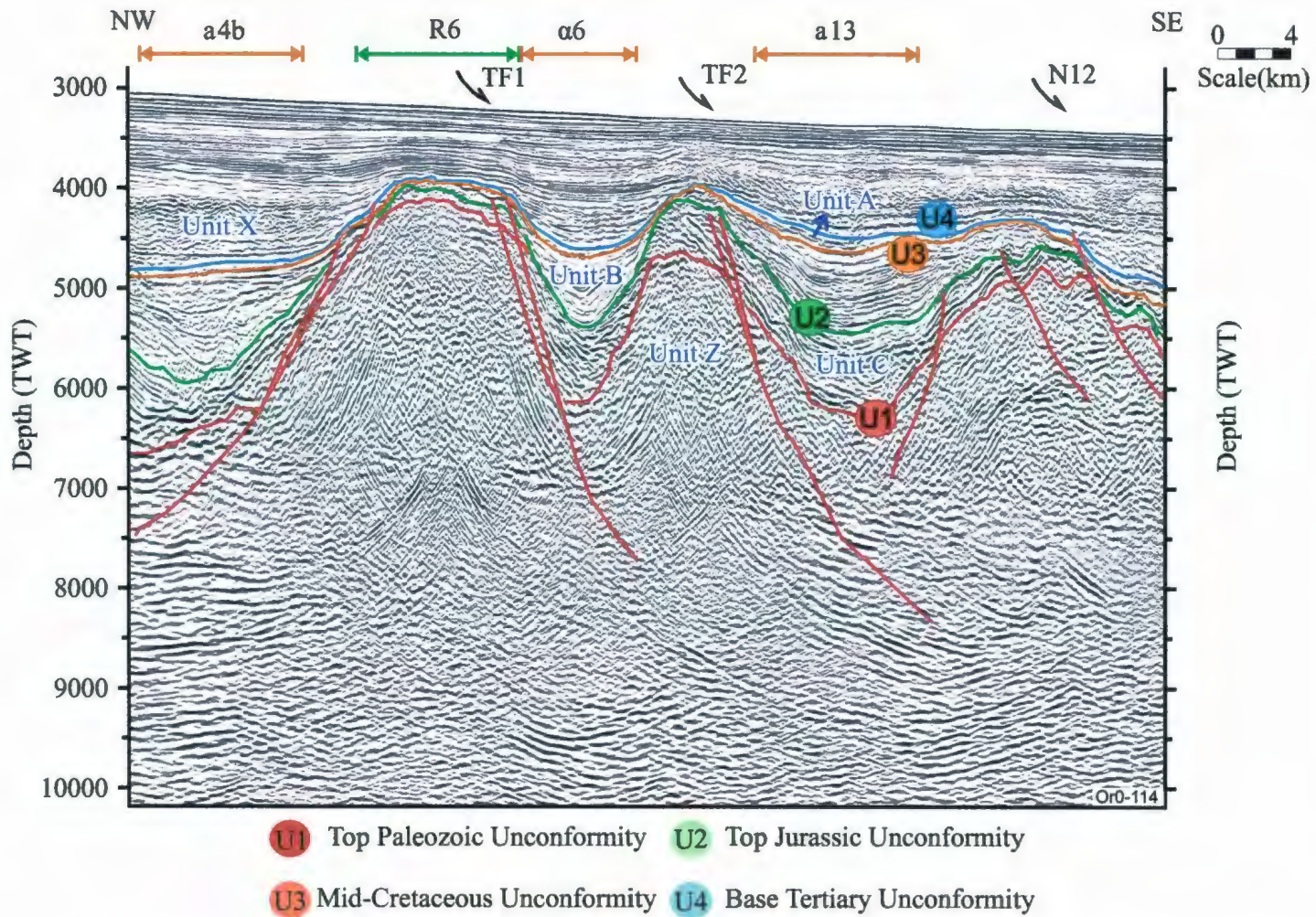
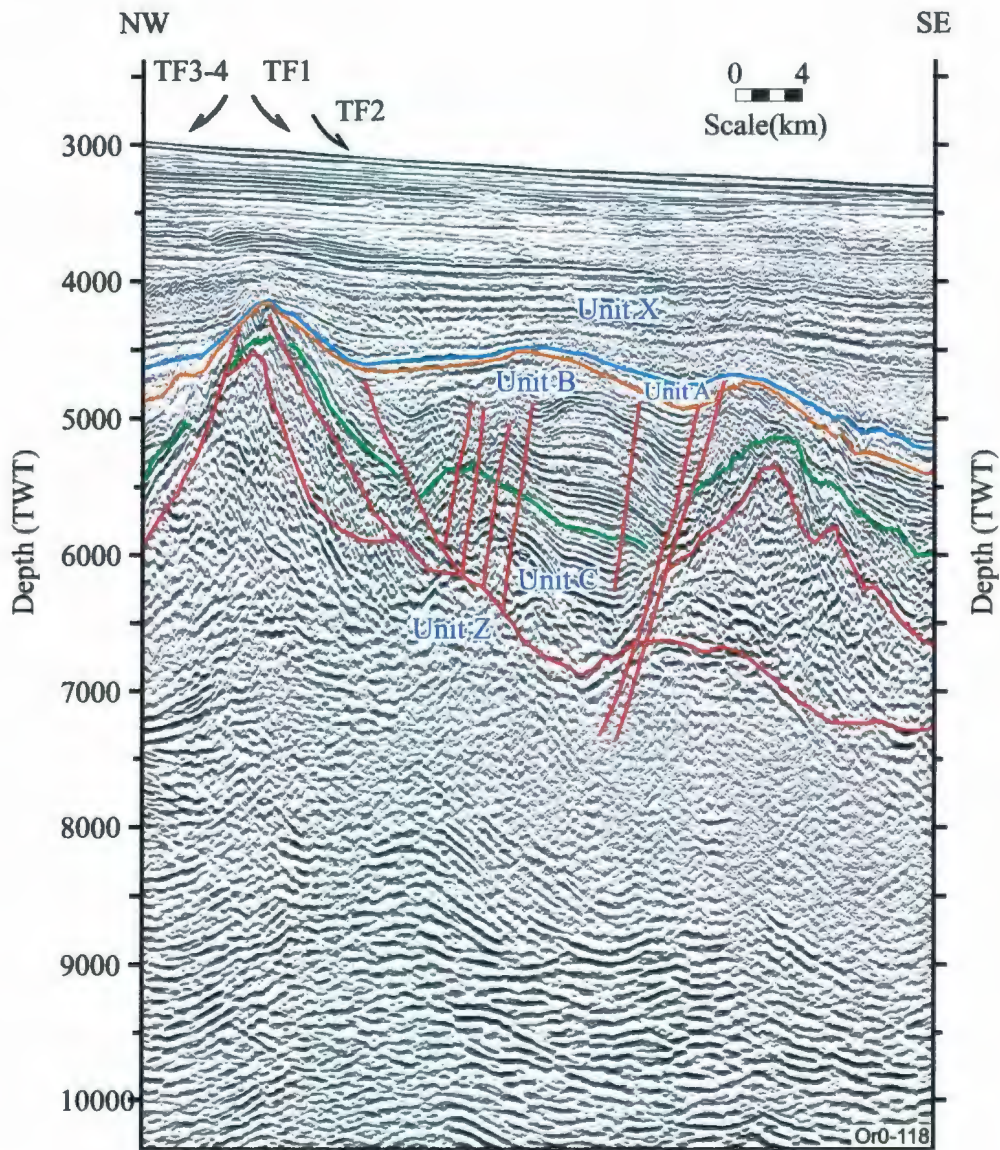


Figure 4.22. Multichannel seismic reflection (OR0-114) profile defining a prominent ridge morphology/structure is delineated by two fault pairs/groups with opposite sense of dip. Location shown in Figure 4.5.



- U1 Top Paleozoic Unconformity
- U2 Top Jurassic Unconformity
- U3 Mid-Cretaceous Unconformity
- U4 Base Tertiary Unconformity

Figure 4.23. Multichannel seismic reflection (OR0-118) profile showing the well imaged fault zone which shows the TF1 fault appearing sole into the TF2 fault at depth. Location is shown in Figure 4.5.

antithetic faults (discussed in detail in the East Basin Province). The southeastern most boundary of this wedge is defined by one of the northwest dipping antithetic faults where the Mid-Cretaceous Unconformity as well as several lower Cretaceous reflections abut this fault plane (also discussed later).

In seismic reflection profiles, fault TF3 soles into the fault TF4 fault at ~7 seconds depth (Fig. 4.23). Here, a strong reflector bundle representing the fault trace(s), dips with listric trajectories to depths between 7 and 8 seconds. A couple of small synthetic and antithetic faults occur between TF3 and TF4 faults. The tip point of fault TF3 lies within the lower Cenozoic succession, whereas fault T4 tips at or below the Mid-Cretaceous Unconformity. The prominent Base Tertiary Unconformity and Mid-Cretaceous Unconformity abut the TF3 fault surface (e.g., Figs. 4.22, 4.23). In fault TF3, vertical stratigraphic separations of the Mid-Cretaceous Unconformity as well as the pre-rift basement reflectors range between 400 - 500 ms and 600 - 700 ms, respectively. The lower Cretaceous and possibly the Jurassic successions show minor growth within the hanging wall of fault TF3, but there appears to be no growth of these successions within the hanging wall of fault TF4.

South of 49°10'N latitude, the White Sail Fault Zone displays a dramatic swing from a northeast-southwest trend to northwest-southeast trend, creating a very tight convex- to- the- west map trace, associated with a dramatic decrease in the width of the fault zone from 4.5 km to <1 km (Fig. 4.3). This swing is accomplished by the development of several prominent fault splays and subsidiary faults that are formed east

of the single strand that was created by the merger of the faults TF1 and TF2 (Fig. 4.3). Fault TF5 is one of these faults, which becomes the major fault that defines the eastern and northeastern bounding fault of the White Sail Fault Zone (Figs. 4.3, 4.24). In this region, the White Sail; Fault Zone is delineated by a prominent horst block, created by the southwest-dipping fault TF4 and the northeast-dipping fault TF5, discussed below (Figs. 4.3, 4.22, 4.23, 4.24, 4.25).

Toward the southeast, the White Sail Fault Zone is delineated by fault TF4 in the west and a new major fault TF5 in the east (Figs. 4.3, 4.24). In this area, TF1 is still visible in seismic profiles, but it has lost its character as a major basin-bounding fault. The foot wall block of TF4 includes a tear-drop shaped package bounded at its base by a prominent unconformity at the top of the pre-rift basement. The western margin of this package is sharply cut by TF4, whereas the package itself is dissected by a prominent imbricate fault fan (Fig. 4.24). The imbricate fault fan is characterized by 3-4 southeast-dipping normal faults which create 3-4 southeast-facing tilted blocks. No discernible growth is observed on the hanging walls of these faults. Vertical separations on the Top Jurassic Unconformity range between 100-200 ms along the strike of the fault fan. These faults have tip points that lie within the lower Cretaceous succession, and sole onto a common detachment surface coincident with the prominent unconformity at the top of the pre-rift basement (Fig. 4.24). This detachment surface can be readily traced eastward/southeastward over the pre-rift basement Unit Z, where it connects with fault TF5 (Figs. 4.3, 4.24). Fault TF5 extends downward to 7-8 seconds with a relatively high

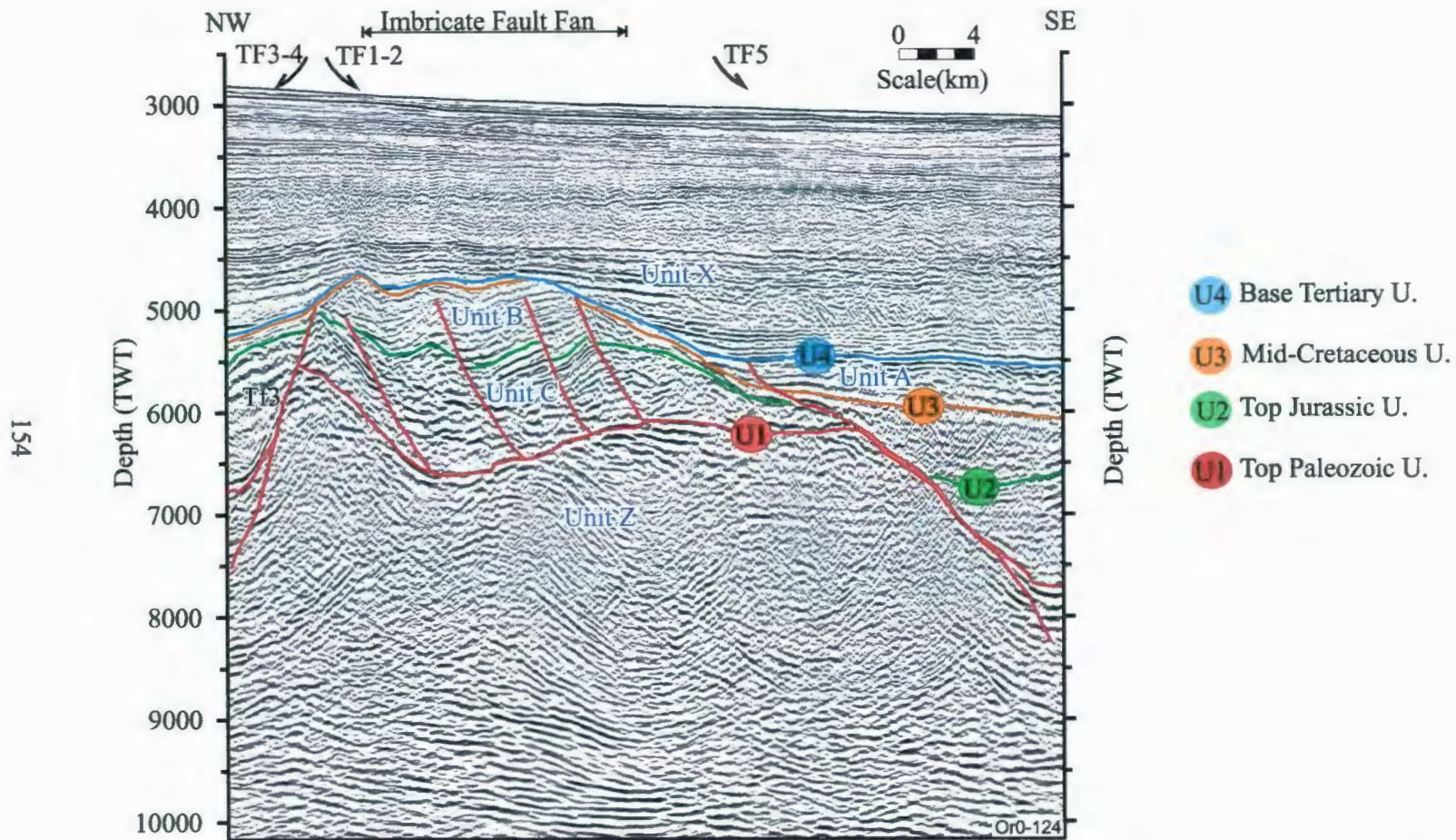


Figure 4.24. Multichannel seismic reflection (OR0-124) profile demonstrates key components in the central portion of the White Sail Fault Zone; TF1, TF2, TF3, TF4 and a normal-sense slip imbricate fault fan. Location is shown in Figure 4.5. (See also, Fig 4.3.).

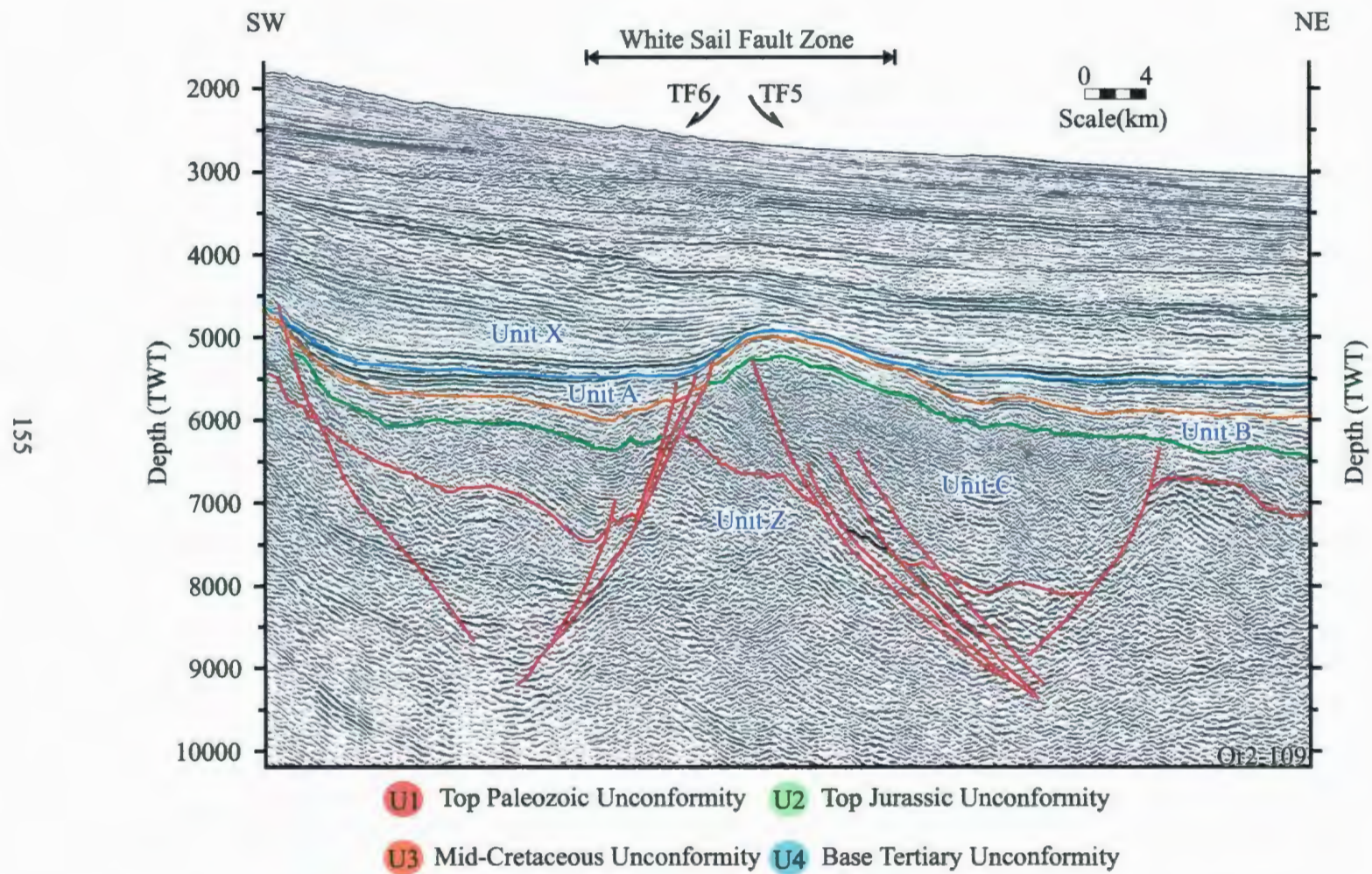


Figure 4.25. Multichannel seismic reflection (OR2-109) profile showing the major faults of the White Sail Fault Zone and their synthetic and antithetic minor faults. Location shown in Figure 4.5.

angle trajectory. The fault TF4 is confined to the lower Cretaceous succession with its tip point lying near the mid-Cretaceous Unconformity. The Top Jurassic Unconformity and Jurassic succession reflectors abut the fault TF4 fault and show no or little growth on the hanging wall block.

In the southernmost portion of the study area, the White Sail Fault Zone assumes a parallel trend with the Western and Southwestern Basin Margin Province. The region is characterized by a series of northwest-southeast trending and northeast- and southwest-dipping normal faults that display varying amounts of vertical stratigraphic separations (Figs. 4.3, 4.24, 4.25, 4.26). On map view, these faults trend toward the southeast where they form a complicated and unresolved intersection between the southwest-trending fault that define the southernmost segment of the Eastern Basin Province (Fig. 4.3). Comparison between seismic reflection profiles OR0-124, OR2-109 and OR0-111 shows that the faults of the imbricate fan continue toward the southeast and merge with fault TF5 (e.g., Figs. 4.24, 4.25, 4.26). In the southeastern most regions of the White Sail Fault Zone there are a few prominent faults, such as faults TF6 and TF7 (Fig. 4.3), however, the relationship between TF5 and these faults is not clear. The tip points of faults TF6 and TF7 invariably lie beneath the Mid-Cretaceous Unconformity (Fig. 4.26). The hanging walls of these faults display ~400-500 ms growth within the Jurassic successions, but the Cretaceous and prerift successions do not show any growth strata development (Fig. 4.26). The high amplitude reflectors of the Jurassic and/or prerift successions are clearly tilted toward the southwest, creating rotated fault blocks associated with listric normal faults (Fig. 4.26).

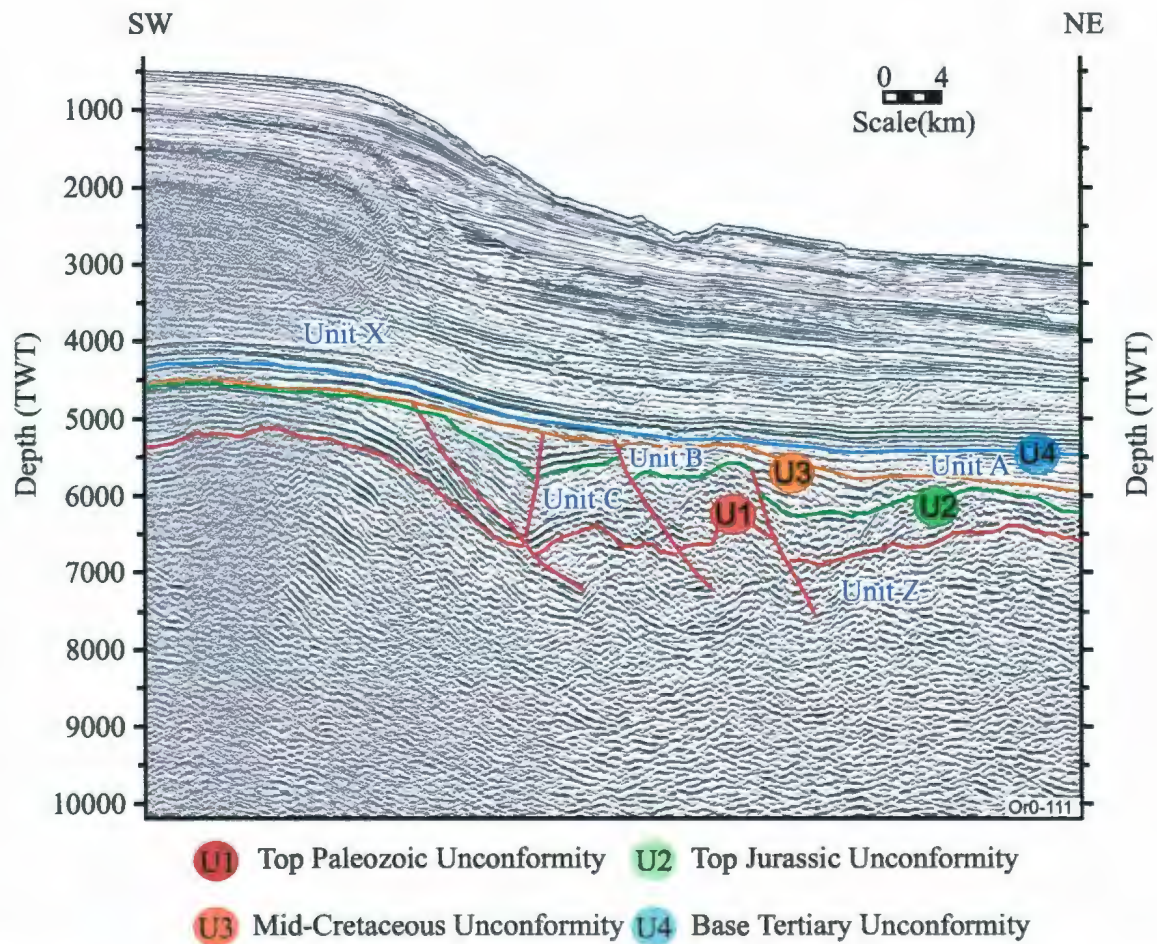


Figure 4.26. Multichannel seismic reflection (OR0-111) profile showing the solitary continuation of the imbricate fault fan as a normal-sense extensional fault. Note the presence of strong reflectors, tilting toward the fault plane, defining distinctly tilted and rotated fault blocks. Location shown in Figure 4.5.

4.5. West Basin and Ridge Province

The West Basin and Ridge Province is positioned between the Western and Southwestern Basin Margin and the White Sail Fault Zone (Fig. 4.3). It covers a comparably wider area than its bounding provinces. The West Basin and Ridge Province is characterized by several prominent basement-cored ridges (R1–R5) and their intervening basins ($\alpha 1$ – $\alpha 4$), which can be readily correlated in seismic reflection profiles and can be regionally mapped (Figs. 4.3, 4.9). The mapping of the hinge lines of the large-scale folds created by the basins and ridges (Fig. 4.9) and the isopach map of the total Mesozoic strata (Fig. 4.27) collectively show that basins and ridges delineate northeast-southwest trending prominent structures.

Detailed interpretation of the seismic reflection profiles show that the ridges are bounded on their northwestern and southeastern margins by prominent faults, which from west to east, are labeled as F1 to F8 (Fig 4.3). In this province the seismic data is rather sparse, however the structures are so large and noticeable that they can be easily mapped. The faults that bound the ridges show northeast-southwest trends, and northwest and southeast dips (Fig. 4.3). They exhibit broadly curvilinear map traces (Figs. 4.3, 4.9). These faults display curved trajectories that extend deep into the pre-rift basement successions (Unit Z), with the tip points generally lying between lower and/or upper sections of the Cretaceous successions.

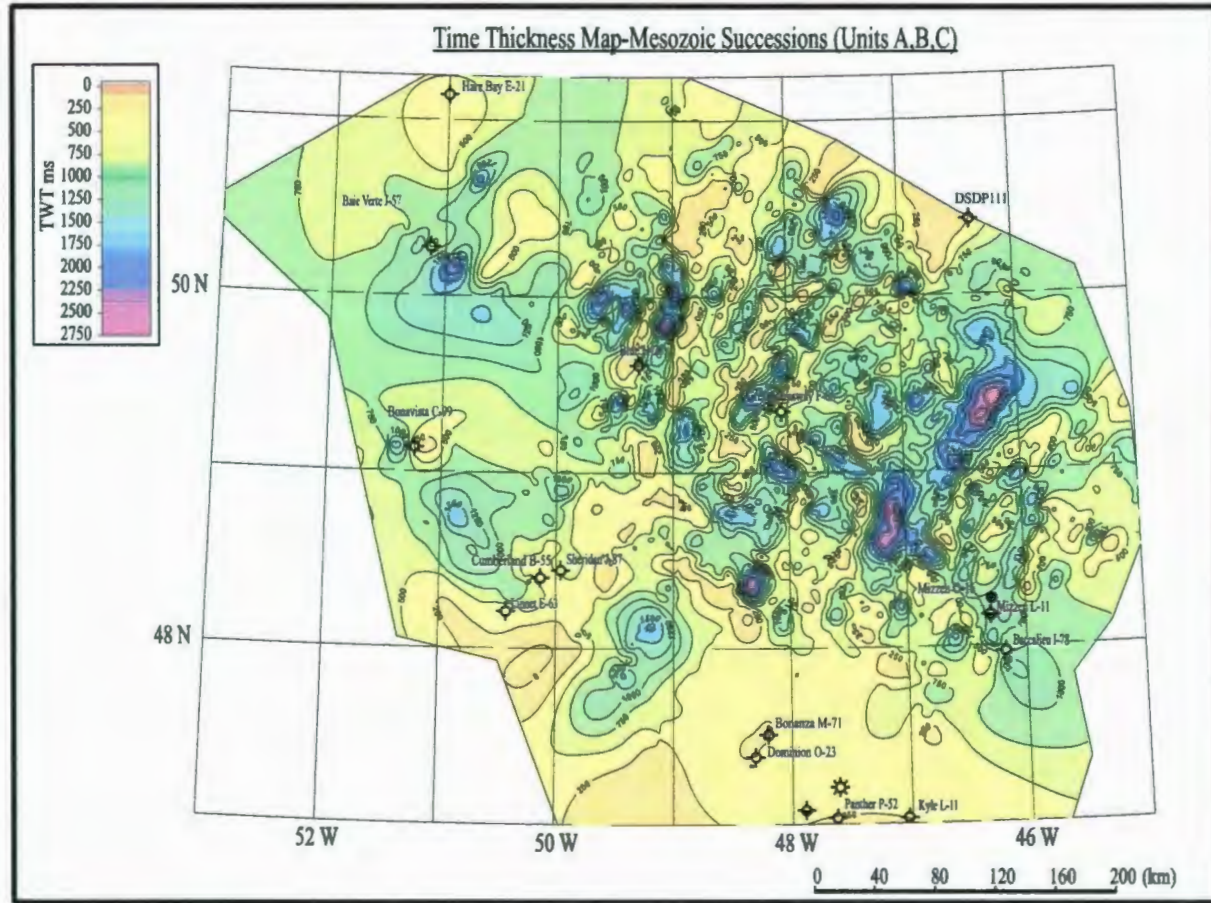
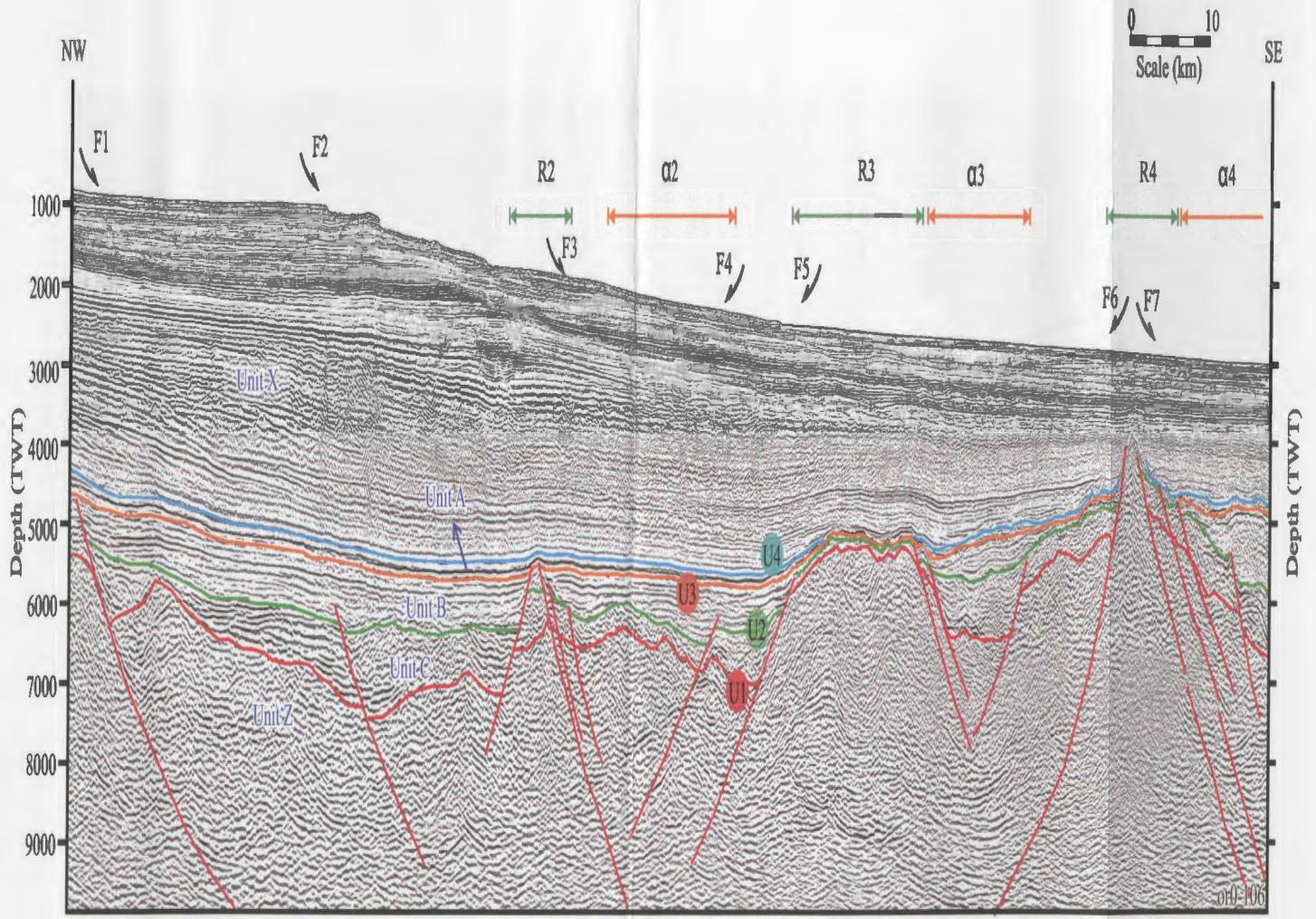


Figure 4.27. The isopach map (in milliseconds twt) of the total Mesozoic strata, defined as the package situated between the unconformity that depicts the top of Unit Z (i.e., the Paleozoic basement) and the Base Tertiary Unconformity.

4.5.1. Northern Portion of the West Basin and Ridge Province

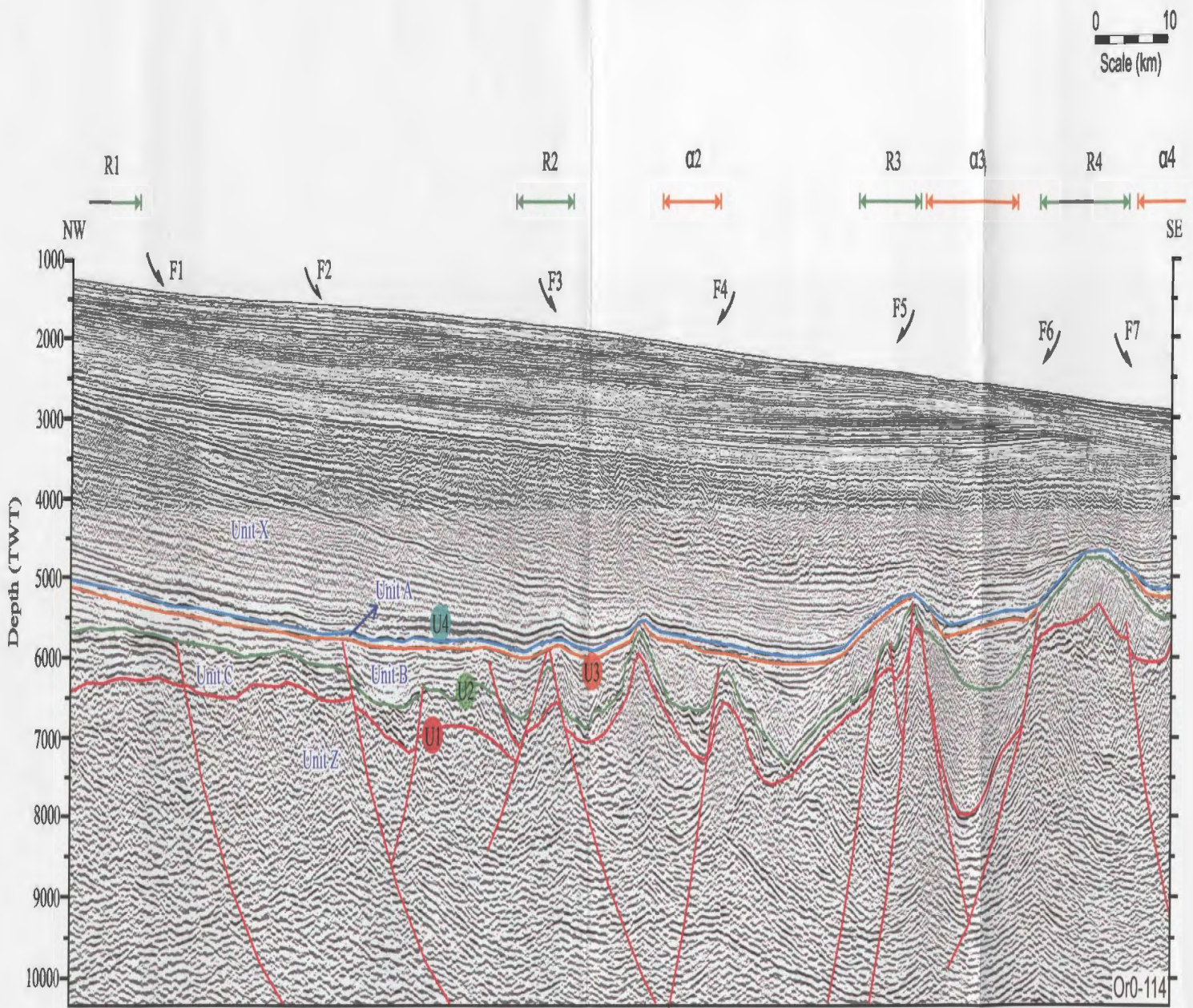
In the northern part of the West Basin and Ridge Province, the structural framework is characterized by a series of northeast-southwest-trending major extensional faults (i.e., F1 to F7; Figs. 4.3, 4.28, 4.29, 4.30). Some of these faults delineate the boundary of the prominent basement-cored ridges and their intervening basins (Fig. 4.9).

Fault F1 is well imaged in the northwestern portion of the study area, but becomes less evident in the seismic reflection profiles towards the south (Fig. 4.3). This fault has an overall northeast-southwest trend, which assumes a north-south trend towards the south (Fig. 4.3). Fault F1 creates a vertical stratigraphic separation on the Top Jurassic Unconformity ranging between 150 – 200 ms (Fig. 4.28). It has a high angle ($\sim 35^\circ$) fault plane in the vicinity of its tip point (i.e. lower Cretaceous succession), but becomes gentler ($\sim 23^\circ$) as it is traced down-section into the pre-rift basement successions of Unit Z, assuming an overall listric trajectory (Figs. 4.29, 4.30). Seismic reflection profile OR0-106 shows that fault F1 creates a small inflection at the Base Tertiary Unconformity. Here, the pre-rift basement successions abut the fault plane with up-curved reflection segments (Fig. 4.28). Fault F2 is another northeast-southwest trending structure, which is situated ~ 3.5 km east of fault F1 (Fig. 4.3). This fault dips towards the southeast at an average angle of $\sim 26^\circ$ and displays extensional separations ranging between 50 – 300 ms on the Top Jurassic Unconformity (Figs. 4.28, 4.29). The tip point of this fault lies in the lower portion of the Cretaceous successions (Fig. 4.29). Seismic reflection profile OR0-114 reveals that this fault has a high angle trajectory ranging from



- U1 Top Paleozoic Unconformity
- U2 Top Jurassic Unconformity
- U3 Mid-Cretaceous Unconformity
- U4 Base Tertiary Unconformity

Figure 4.28. Multichannel seismic reflection (OR0-106) profile showing northern part of the West Basin and Ridge Province. Note the presence of the major normal faults and the prominent basement-cored ridges and their intervening basins. Location is shown in Figure 4.5.



- U1 Top Paleozoic Unconformity ● U2 Top Jurassic Unconformity
- U3 Mid-Cretaceous Unconformity ● U4 Base Tertiary Unconformity

Figure 4.29. Multichannel seismic reflection (OR0-114) profile showing the major structures of the northern part of the West Basin and Ridge Province including a series of northeast-southwest trending major normal-sense faults. Note that some of these faults delineate the boundary of the prominent ridges and their intervening basins. Location is shown in Figure 4.5.

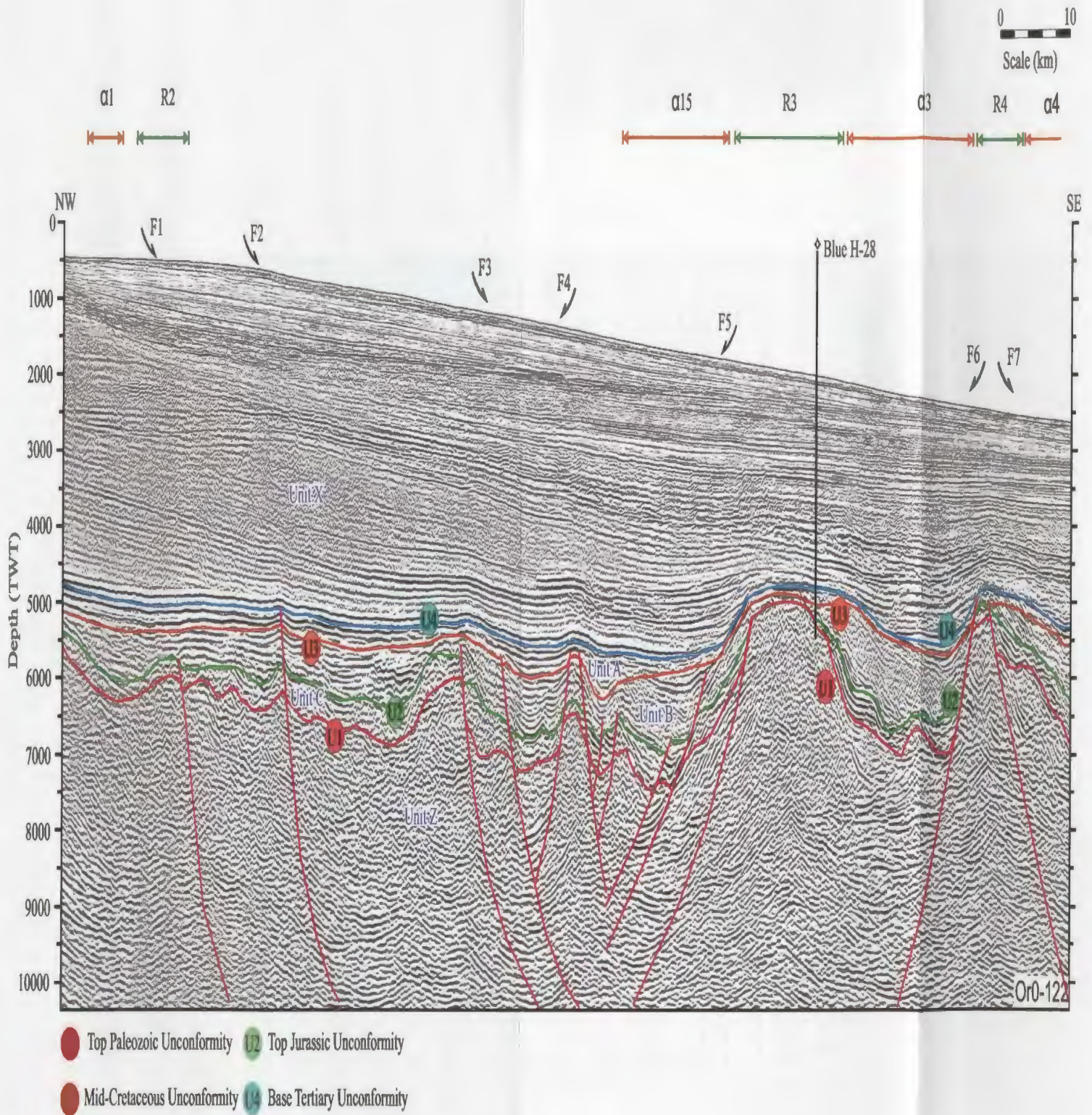


Figure 4.30. Multichannel seismic reflection (OR0-122) profile showing the structures of the central part of the West Basin and Ridge Province. Note the presence of the one of the exploration well (Blue H-28) delineating the Jurassic and lower Cretaceous successions over the ridge R3 crest. Location is shown in Figure 4.5.

~35° at its upper section to ~17° at its lower section (Fig. 4.29). The footwall of the fault F1 defines a major ridge, referred to as R1 (Fig. 4.9). The western flank of ridge R1 is delimited by a set of small northeast-southwest-trending and northwest-dipping normal faults, with together with the ridge, determine the eastern margin of a large elongated depocentre, basin α_1 , which extends westward to the foothills of the Western and Southwestern Basin Margin (Fig. 4.9).

Basin α_1 is a northeast-southwest trending, elongate depocenter (Figs. 4.9, 4.27). It is only traced from the northern portion to the central portion of this province through a strike length of ~100 km. The basin displays an asymmetrical cross-sectional geometry with a steeper western flank dipping southeast and a gentler eastern flank dipping northwest (Fig. 4.30). The thickest basin fill of ~1400 ms occurs within the central part of the province. Detail correlations of reflections with borehole data (see Chapter 3) reveal that the basin α_1 has a thick lower Cretaceous succession (~1000 ms) and a comparably thin (~400 ms) upper Cretaceous succession. Lack of a tight seismic grid seismic reflection profiles in this portion of the province precludes an accurate correlation of the borehole data and seismic data to the east and south. The lower part of the upper Cretaceous succession gradually onlaps the northwestern margin of ridge R1, whereas the uppermost reflections overstep the crest of ridge R1 (Fig. 4.29). Whereas the lower Cretaceous succession appear to abut the major fault(s) of the Western and Southwestern Basin Margin to the west and ridge the fault(s) that define the western margin of ridge R1 to the east (Fig. 4.29).

Seismic reflection profiles and structure maps show that ridge R1 define a broadly northeast-southwest trending, mildly convex-to-the west map trace (Figs. 4.3, 4.9). It stands as a ~5-7 km wide structure with a nearly symmetrical cross-sectional geometry. The upper Cretaceous succession extends with a uniform thickness (~350 ms) across ridge R1 into basin α 1, with a minor inflection at the Mid-Cretaceous Unconformity (Fig. 4.29). The lower Cretaceous succession displays a notable east and west-directed onlap against a high amplitude reflector bundle defining the pre-rift basement successions along the both sides of the ridge. At the crest of ridge R1, the lower Cretaceous succession is notably absent. The internal architecture of the core of the ridge R1 is defined by high-amplitude, chaotic pre-rift basement reflections. Ridge R1 plunges toward the southwest; however, absence of a tight grid of seismic profiles does not allow a detailed mapping of this structure further south (Figs. 4.3, 4.9).

Ridge R2 appears as a symmetrical cylindrical-shaped structure in the northern portion of the province: however, towards the south, it widens and displays a west-slanted asymmetric cross-sectional geometry (Figs. 4.9, 4.28, 4.31). In the northern portion of the province, it creates a minor inflection at the Base Tertiary Unconformity. Here, the lower Cretaceous succession shows a nearly uniform thickness of ~200 ms, which drapes over the pre-rift basement coring of the ridge (Fig. 4.28). Lower Cretaceous succession displays gradual thinning towards the flanks of the ridge, where thinning is accomplished by progressive convergence of reflections and onlap terminations. Further south, where the ridge becomes wider and steeper, the ridge creates

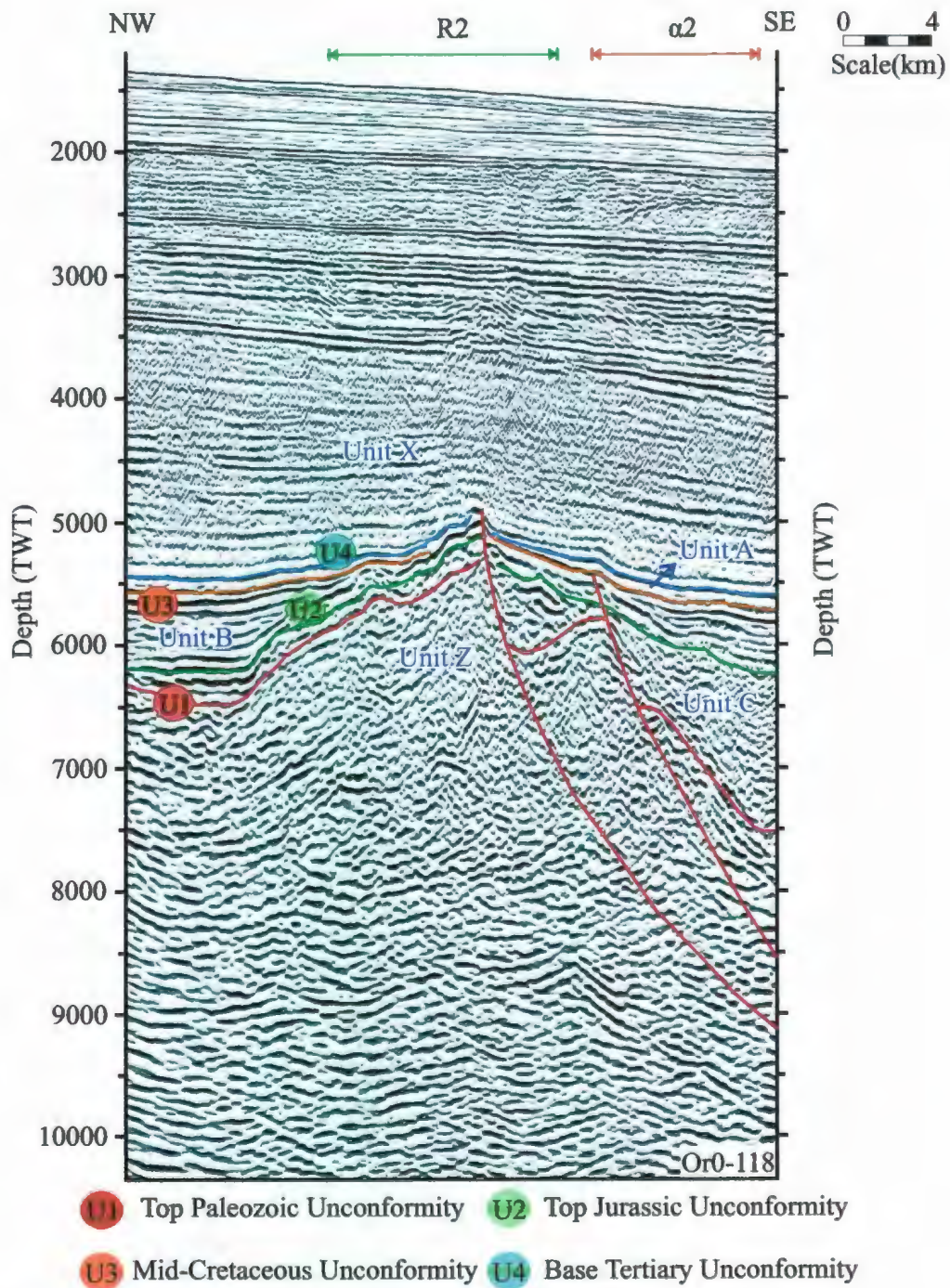


Figure 4.31. Multichannel seismic reflection (OR0-118) profile showing Ridge R2 and its intervening basin $\alpha 2$. Note the major inflection in the Base Tertiary Unconformity, where the ridge becomes wider and steeper. Location shown in Figure 4.5.

a major inflection in the Tertiary succession (Fig. 4.31). Here, both the lower Cretaceous and upper Cretaceous successions gradually thin towards the ridge.

Fault F3 is another northeast-southwest trending, southeast-dipping structure (Fig. 4.3). It displays between 200 ms and 500 ms vertical separations on the Top Jurassic Unconformity, and tips below or at the Mid-Cretaceous Unconformity (Figs. 4.28, 4.29). The reflectors within the lower Cretaceous and Upper Jurassic successions display well-defined hanging wall and footwall cutoffs (e.g., Fig. 4.29). The footwall block of fault F3 defines the eastern margin of ridge R2. Further to the east, fault F5 is a northeast-southwest trending, southwest-dipping structure (Fig. 4.3). It delineates the western margin of ridge R3. Both faults F3 and F5 have prominent synthetic splays: Fx is a splay of fault F3 and F4 is a splay of F5 (Figs. 4.3, 4.28). The master faults (i.e., F3 and F5) and their splays (i.e., F4) create a basin labeled as α_2 , which is situated between ridges R2 and R3.

Basin α_2 is a northeast-southwest trending elongate depocenter situated between ridges R2 and R3 (Fig. 4.9). The basin is widest (~50 km) at its northeastern extremity and progressively narrows down to ~15 km at its central region, broadly maintaining its constant width toward the southwest. It exhibits an asymmetrical cross-sectional geometry with a gentler (~3°) western flank dipping southeast and a steeper (~10°) eastern flank dipping northwest. Basin α_2 contains ~1000 ms of Mesozoic successions deposited above the pre-rift basement (e.g., Figs. 4.28, 4.30). Seismic stratigraphy and long-distance correlations of reflections with borehole data (see Chapter 3) suggest that

the sediments accumulated within the basin are primarily composed of Cretaceous and upper Jurassic successions. Broadly east-west oriented seismic reflection profiles across the basin show that, the Top Jurassic Unconformity defines a gently southeast-dipping (i.e., $\sim 4^\circ$) erosional surface (e.g., Fig. 4.28). In the northern portion of the province, the lower Cretaceous succession (i.e., Unit B) defines a wedge-shaped, northwest-thinning succession, which clearly shows ~ 500 ms growth towards the axis of the basin and dramatically thins to ~ 300 ms toward the northwest. Whereas, the upper Cretaceous succession (i.e., Unit A) forms a nearly uniform thickness (e.g., 150-200 ms) across the basin, dramatically thinning over the ridge R3 (e.g., Fig. 4.28). The sediment is thickest along the axis of basin α_2 , with ~ 800 ms of lower Cretaceous and ~ 150 -200 ms upper Cretaceous successions. The eastern flank of the basin α_2 is defined by the northeast-southwest trending fault F5 (Figs. 4.3, 4.9).

In seismic reflection profiles, the plane of fault F5 can be traced to depth where it appears to abut the plane of fault F3 (Fig. 4.28). This geometry gives the impression that fault F5 is an antithetic to fault F3. The notable southeast-dip of the Top Jurassic Unconformity within the hanging walls of faults F4 and F5, and the presence of the southeast-thickening wedge within the Cretaceous successions (i.e., between the Top Jurassic Unconformity and the Mid Cretaceous Unconformity) collectively point to the development of a half graben between faults F3 and F5 (Figs. 4.3, 4.28). The fault plane of F5 has a low angle trajectory (i.e., $\sim 20^\circ$) in the north, while it becomes progressively steeper (i.e., $\sim 35^\circ$) southwards (i.e., Figs. 4.28, 4.30). The tip points of the faults F4 and

F5 lie within the lower Cretaceous successions in the northern portion of the province; however towards the south the fault appears to cut into younger successions (i.e., into the upper Cretaceous; Figs. 4.28, 4.30). Vertical separations on the Top Jurassic Unconformity range between 200-700 ms along the strike of this fault (Figs. 4.28, 4.29).

Fault F5 defines the northwest flank of the prominent ridge R3, which is one of the well-known basement-cored ridges in the Orphan Basin (Fig. 4.3). The exploration well Blue H-28 was drilled over this ridge (Fig. 4.3). In the northern portion of the West Basin and Ridge Province, ridge R3 stands as a ~12 km wide, flat-crested structure with a nearly symmetrical cross-sectional geometry (Fig. 4.28). Towards the south, the structure becomes narrower, but remains as a remarkably steeper ridge that created a major inflection of reflections within the Tertiary successions (Fig. 4.30). Correlation with the exploration well Blue H-28 confirms the presence of Jurassic and lower Cretaceous successions over the ridge crest (see Chapter 3). Detailed examination of seismic reflection profiles further shows that the strong reflectors of the Jurassic and lower Cretaceous successions observed within basins α_2 and α_3 (discussed below) exhibit dramatic thinning towards the crest of the ridge (Fig. 4.28). This thinning is largely accomplished by progressive convergence of individual reflections, as well as internal onlap and offlap terminations toward the ridge. Seismic data show that there is a major angular unconformity over the crest of ridge R3. The internal architecture of the core of the ridge is characterized by highly disturbed, high-amplitude reflections of pre-rift basement successions that give the core its corrugated and chaotic appearance, which

are truncated at the unconformity. The borehole data show that this major unconformity separates the upper Mesozoic from the pre-rift basement strata.

Basin $\alpha 3$ is a northeast-southwest-trending elongate depocenter that is situated between ridges R3 in the west and R4 in the east (Fig. 4.9). In the northern portion of the West Basin and Ridge Province basin $\alpha 3$ has a relatively constant width of ~ 10 km, but it widens to ~ 20 km toward the south. Basin $\alpha 3$ shows an asymmetrical cross-sectional geometry with a steeper eastern flank dipping northwest and a gentler western flank dipping southeast (Fig. 4.28). The Cretaceous and Jurassic successions show gradual thinning from ~ 600 ms along the axis of the basin to 50 ms toward ridges R3 and R4. This thinning is accomplished by the progressive convergence, onlap (and offlap) of the Mesozoic successions over the flanks of the ridge, as well as the over-step of the uppermost Cretaceous strata on the crest of the ridge R3. These strata are eventually truncated by the Base Tertiary Unconformity (Fig. 4.28). The 2-3 synthetic splays of fault F6 control the geometry of the eastern flank of the basin. Towards the central portion of this province, basin $\alpha 3$ becomes deeper and contains ~ 900 - 1000 ms of Mesozoic successions over the pre-rift basement Unit Z (Fig. 4.30). Seismic correlations across the ridge R3 with the chronological data from the Blue H-28 well suggest that the sediments contained within the basin $\alpha 3$ must include a thick Jurassic succession (~ 500 - 600 ms) and a comparably thin Cretaceous succession (~ 150 - 200 ms). The presence of Triassic successions cannot be excluded; however, there is no concrete evidence for this (Fig. 4.30). In the central portion of the province, the Base Tertiary and Mid-Cretaceous

Unconformities and the stratigraphic package between these surfaces (i.e., unit A), collectively display a convergent pattern along the flanks of the ridges R3 and R4. The lower Cretaceous and Jurassic successions progressively thin via multiple phases of interstratal onlap along the western flank of basin α 3. Whereas, along the eastern flank, these successions appear to abut the major fault F6 (Fig. 4.30). Careful examination of seismic reflection profiles as well as borehole data suggest that the Base Tertiary Unconformity is locally erosional over the crests of the ridges R3 and R4.

Further to the east this province is characterized by two prominent northeast-southwest trending major faults: F6 and F7 (Fig. 4.3). In the northern portion of this province, the tip points of these faults lie within the Tertiary succession, whereas further south they lie within the older successions (i.e., upper Cretaceous; Figs. 4.28, 4.30). Little or no growth is observed on the hanging walls of these faults. The northwest-dipping fault F6 and the southeast-dipping fault F7 define the ridge R4 (Figs. 4.3, 4.9, 4.28). These faults show dip amounts ranging between $\sim 40^\circ$ and $\sim 20^\circ$ (Fig. 4.28). Fault F7 has 2-3 synthetic splays running parallel to the master fault, and dipping to the southeast. Toward the south, the crest of ridge R4 plunges to the southwest, and its bounding faults lose their character associated with this plunge (compare Fig. 4.28 with Fig. 4.30).

Ridge R4 appears as a prominent, relatively high structure that has a cone-shaped symmetrical cross sectional geometry with a notably narrow crestral region, which penetrates the Base Tertiary Unconformity defining a prominent high of ~ 800 - 900 ms

within the lower Tertiary successions. Towards the central part of the province, the ridge loses its expression and widens, yet it still creates a moderate inflection in the lower Tertiary successions (Fig. 4.30). Tracing southward, the ridge becomes progressively wider, and swings to the southeast merging with the west-northwest – east-southeast trending high-standing fault blocks of the southern segment of the Western and Southwestern Basin Margin (Figs. 4.3, 4.9). Moreover, the crestal portion of the ridge at the Mid-Cretaceous Unconformity becomes noticeably flat, where the underlying successions are profoundly decapitated at the surface of the unconformity: this intense phase of erosion is further discussed in the next section (Fig. 4.32). Careful correlations of seismic reflection profiles show that the Jurassic and lower Cretaceous successions are the thickest (~1600 ms) beneath the axial trough of basin α_4 , but show a strong thinning of ~1300 ms toward the ridge R4 (Fig. 4.30). Seismic data show that most of the Jurassic succession can be traced over the eastern margin of ridge R4, while nearly all of the Cretaceous successions are eroded at the Mid-Cretaceous Unconformity (Fig. 4.30). A ~200 ms thin isopachous upper Cretaceous succession (i.e., the package between the Mid-Cretaceous and Base Tertiary Unconformities) is present in basins α_3 and α_4 (Figs. 4.9, 4.30). This package gradually thins to ~50-100 ms across the ridge R4 and is eventually truncated at Base Tertiary Unconformity. This thinning is mainly attained by east- and west-directed convergence of the upper Cretaceous successions, as well as the onlap and offlap terminations of reflections toward the ridge. The internal architecture of ridge R4 is characterized by weak and discontinuous reflections that give a chaotic

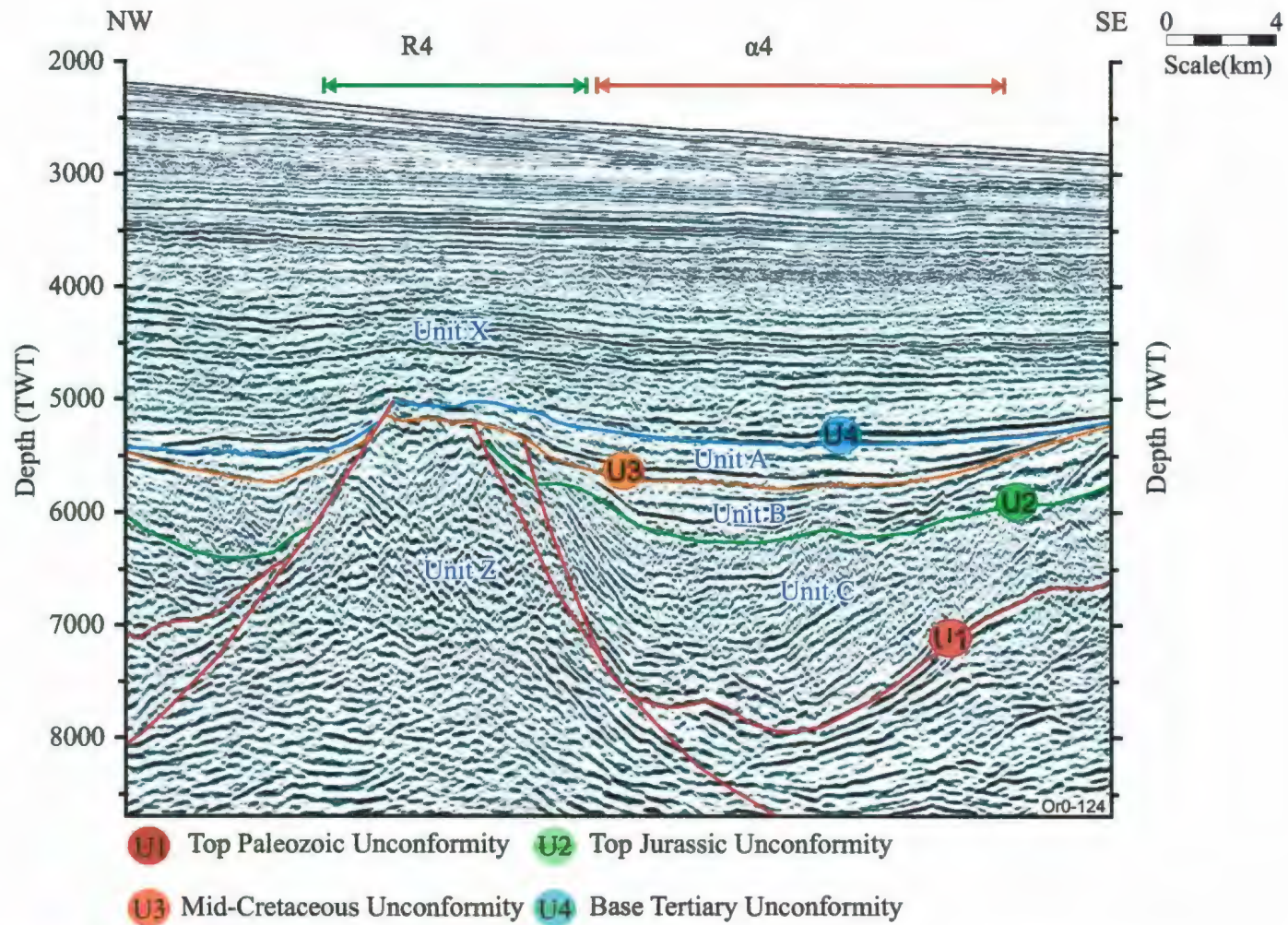


Figure 4.32. Multichannel seismic reflection (OR0-124) profile showing the prominent ridge R4 and major depocenter basin $\alpha 4$. Note that the crest of the ridge becomes wider and flat (compare with Figure 4.25.). Location shown in figure 4.5.

appearance (Figs. 4.28, 4.29, 4.30). The eastern flank of ridge R4 delimits the prominent basin $\alpha 4$ (Fig. 4.9).

Basin $\alpha 4$ is a large northeast-southwest trending elongate depocenter situated between ridges R4 and R6 (Figs. 4.3, 4.9). As traced southward, the development of ridge R5 partitions the basin $\alpha 4$ into two subbasins: $\alpha 4a$, and $\alpha 4b$ (Fig. 4.9). The axial trough of subbasin $\alpha 4a$ progressively swings towards the southeast associated with the plunge of the ridge R5: ultimately subbasin $\alpha 4a$ merges with subbasin $\alpha 4b$ and is traced southward as a single prominent basin $\alpha 4$ (Fig. 4.9). In the northern part of the West Basin and Ridge Province, subbasin $\alpha 4a$ displays an asymmetrical cross sectional geometry with a steeper eastern flank dipping northwest and a gentler western flank dipping southeast (Fig. 4.33). Here, the lower Cretaceous and Jurassic successions are ~900 ms thick along the axial trough of the subbasin $\alpha 4a$ and show thinning to <200 ms towards ridge R4. The upper part of these successions are characterized by high amplitude, southeast dipping, and southeast thickening reflectors within the subbasin, which show 50-100 ms growth towards ridge R5 (Fig. 4.33). However, the upper Cretaceous successions show uniform thickness in the subbasin with a mild thinning towards the surrounding ridges R4 and R5 (Figs. 4.9, 4.33). Subbasin $\alpha 4b$ is a northeast-southwest oriented wider and deeper depocenter with ~10-15 km width across the basin (Fig. 4.9). It has an asymmetrical cross-sectional geometry with a relatively gentle dipping western flank and a mildly steeper eastern flank (Fig. 4.34). In the northern portion of the province subbasin $\alpha 4b$ contains ~1000 ms of Mesozoic successions along

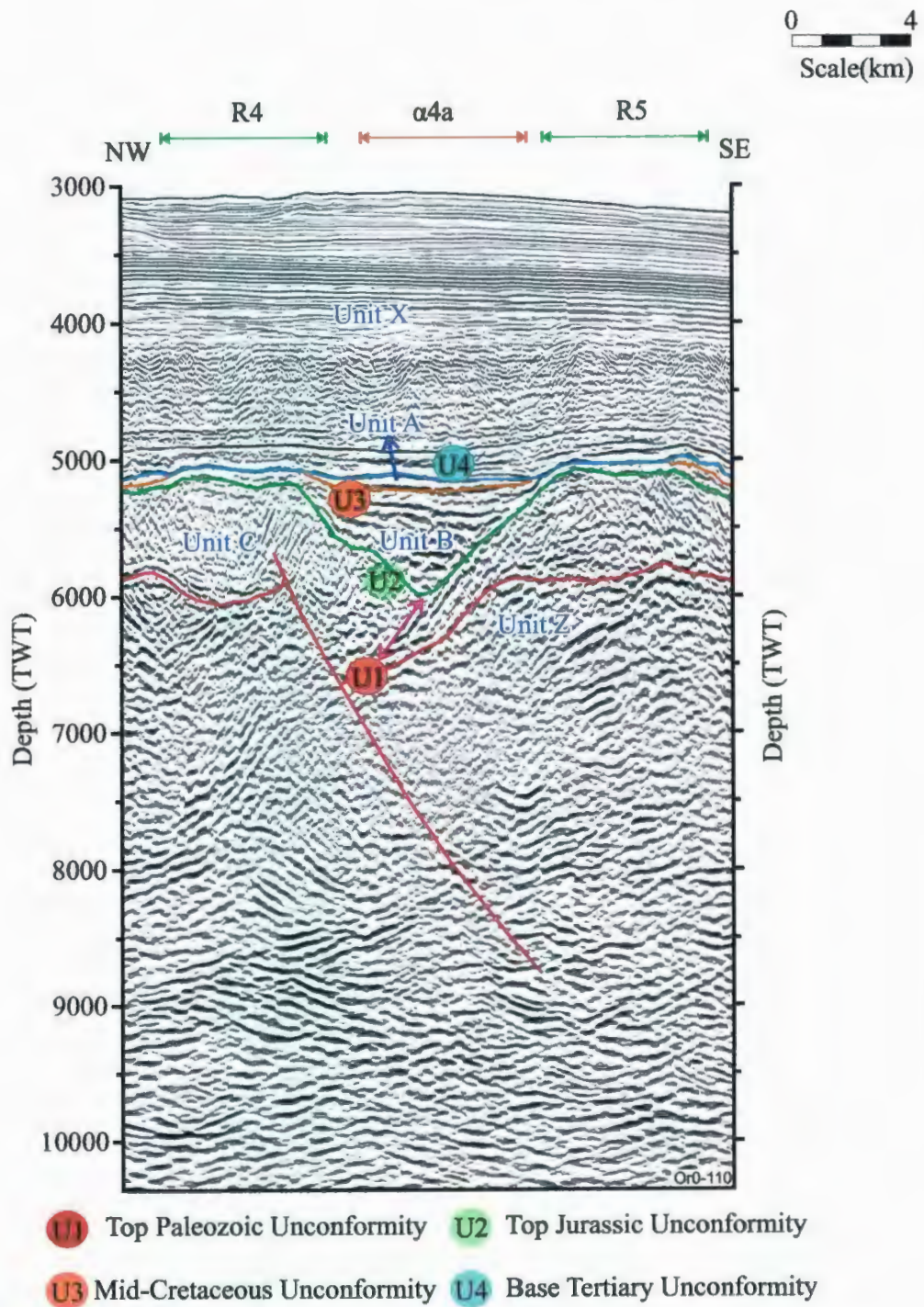


Figure 4.33. Multichannel seismic reflection (ORO-110) profile showing the subbasin $\alpha 4a$ depicts an asymmetrical cross-sectional geometry bounded by prominent ridges R4 and R5. Location shown in Figure 4.5.

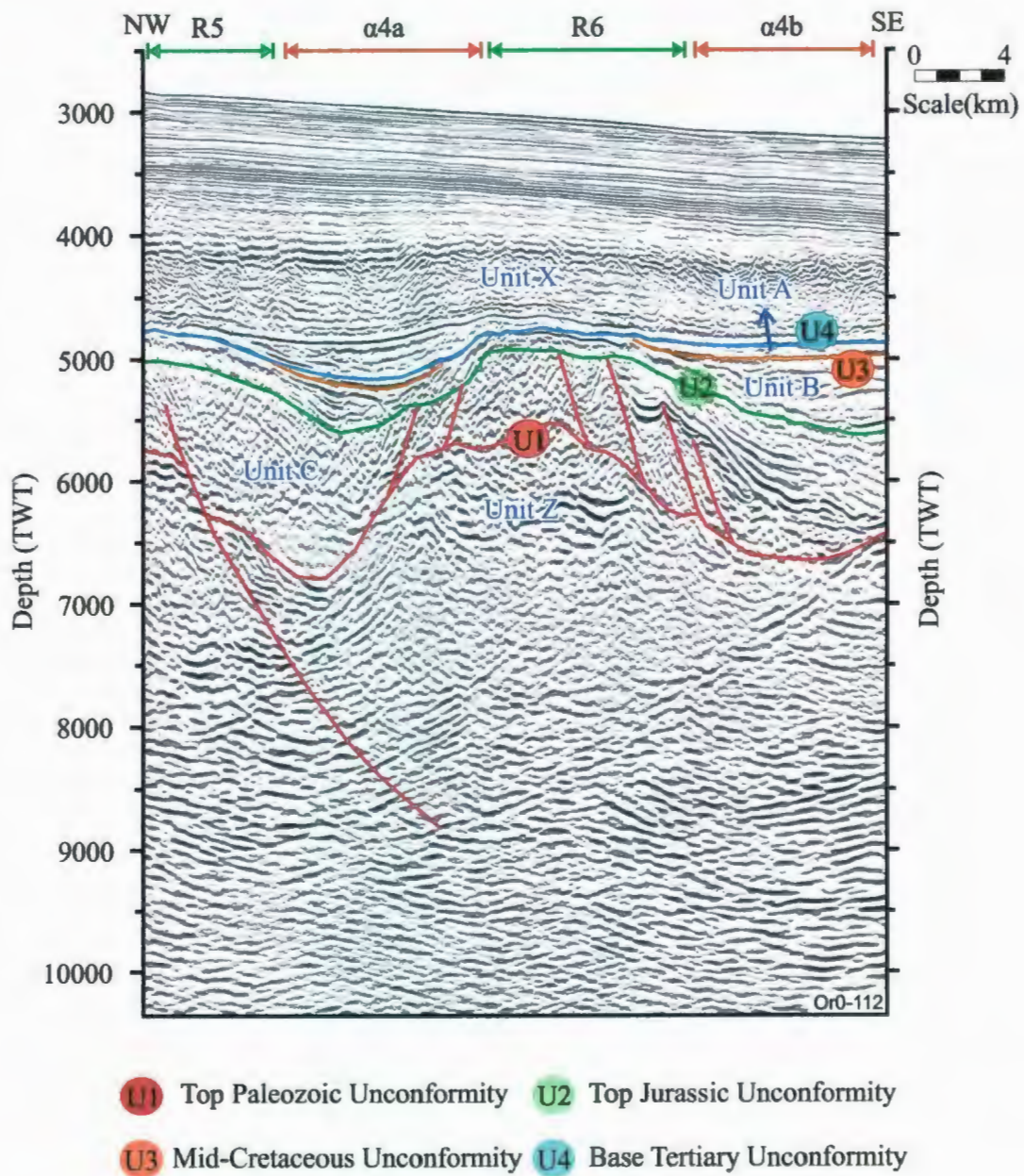


Figure 4.34. Multichannel seismic reflection (OR0-112) profile showing an asymmetrical subbasins $\alpha 4a$ and $\alpha 4b$ and their western boundary ridges R5 and R6. Location shown in Figure 4.5.

the axis of the subbasin which gradually thins to ~100-200 ms over the crest of ridges R5 and R6 (Fig. 4.34). This thinning is mostly accommodated by the convergence of progressive onlap of these successions. The upper Cretaceous successions form a nearly uniform, 50 ms-thick sediment pile in the subbasin with mild thinning towards the surrounding ridges. South of the region where subbasins $\alpha 4a$ and $\alpha 4b$ are merged to form basin $\alpha 4$, between 1200 to 1700 ms of Mesozoic sediments drape over the pre-rift basement unit Z (Fig. 4.30). The thin veneer (~100 ms) of upper Cretaceous successions gradually thins towards the ridges and is finally truncated at the Base Tertiary Unconformity. The floor of basin $\alpha 4$ is marked by a high amplitude continuous reflector bundle (Fig. 4.33). An intra Mesozoic reflector labeled in Fig 4.33 as X, shows that the locus of this basin was further to the northwest during the deposition of the Jurassic successions, but notably shifted toward the southeast during the deposition of the Cretaceous successions. The Mesozoic successions show a prominent thinning towards ridges R4 and R6 (Fig. 4.30).

Ridge R5 is a 10 km wide and 70 km long relatively small ridge (Figs. 4.3, 4.9). It displays an asymmetrical cross-sectional geometry, with the eastern flank being steeper than the west flank (Fig. 4.29). The upper Cretaceous successions define a uniform thickness (~100 ms) drape blanketing ridge R5. In some seismic reflection profiles (e.g., OR0-112) the lower Cretaceous successions gradually thin over the crest of the ridge and are largely truncated by a major composite unconformity that includes both the Mid-Cretaceous and the Base Tertiary Unconformities (Fig. 4.34). In this region, the Jurassic

successions appear to abut the western flank of ridge R5 (Fig. 4.34). The internal architecture of the core of ridge R5 is characterized by variably strong, often discontinuous chaotic reflections that give a corrugated appearance to the pre-rift basement Unit Z (Fig. 4.34). Further to the south, the crest of ridge R5 displays a dramatic plunge (4° at 190° plunge direction), and the structure becomes indistinguishable from the adjacent subbasins $\alpha 4a$ and $\alpha 4b$ (Fig. 4.9).

Ridge R6 is a large, generally double-crested anticlinal structure situated to the east of subbasin $\alpha 4b$ in the north and basin $\alpha 4$ in the south (Figs. 4.3, 4.9). The ridge has a relatively constant width of ~ 10 km, but thins to ~ 5 km towards the south (Fig. 4.9). Ridge R6 displays an asymmetrical cross-sectional geometry, rising >1600 ms and 2500 ms from the floor of the adjacent basins $\alpha 4$ and $\alpha 5$ (Figs 4.9, 4.34). It creates a major inflection in the Tertiary successions (Figs. 4.9, 4.34). Detailed examinations of seismic reflection profiles show that the nearly isopachous upper Cretaceous successions in surrounding basins $\alpha 4$ and $\alpha 6$ show progressive thinning by mainly convergence towards the ridge and that they are eventually truncated by the regional Base Tertiary Unconformity (Figs. 4.9, 4.34). The reflectors of lower Cretaceous and Jurassic successions appear to abut both flanks of ridge R6 (Fig. 4.34). The internal architecture of the core of the ridge R6 is defined by probably Jurassic successions in the upper part and pre-rift basement successions in the lower part.

4.5.2. Southern Portion of the West Basin and Ridge Province

In the southern part of the West Basin and Ridge Province, structures consist of at least three prominent northeast-southwest-trending ridges (R3, R4, R6) and two small intervening basins (i.e., α_3 , α_f). These structures are controlled by 3-5 northeast southwest-trending faults on their either western or eastern flanks (i.e., faults F5, F6, F7; Figs. 4.3, 4.9). These faults display normal-sense vertical stratigraphic separations. Faults F5 – F7 can be traced toward the south with some degree of confidence (Fig. 4.3): fault F5 abuts the Western and Southwestern Basin Margin, while faults F6 and F7 display a dramatic swing from a northeast-southwest trend to a northwest-southeast trend, eventually merging with the Western and Southwestern Basin Margin (Fig. 4.3). A new fault, F9 emerges from F7 in the southern part of this province and assumes a parallel trend with the White Sail Fault Zone. Another new fault, F10 is identified in the southeastern part of this province where it defines a short segment extending towards the southeast (Fig. 4.3).

In the southernmost region of this province ridge R3 displays a northeasterly plunge, thus rises toward the south, again becoming a major structural element. Fault F5 follows the structural style of ridge R3, and defines the western flank of this ridge. It is a northeast southwest trending, northwest-dipping structure. The lower Cretaceous succession in basin α_3 gradually thins towards the west flank of the basin (Fig. 4.35). In the southernmost region of this province basin α_3 is a small depocenter situated between ridges R3 and R4. It loses its expression toward the south as the basin axis progressively

rises (compare Fig. 4.35 with Fig. 4.36), reaching the elevation of the high-standing fault blocks defining the Western and Southwestern Basin margin (Figs. 4.3, 4.9). Limited seismic data in this region show that ridges R3 and R4 abut the northern fault that defines the Western and Southwestern Basin Margin (Figs. 4.3, 4.9).

4.6. East Basin Province

The East Basin is situated between the White Sail Fault Zone in the west, and the Eastern Basin Margin in the east (Fig. 4.3). It is bounded in the south by the southeastern segment of the Western and Southwestern Basin Margin. The Eastern Basin is a very broad depocenter, mainly delineated by the architecture and morphology of the Base Tertiary, Mid-Cretaceous and Top Jurassic Unconformities and the thickness of the overlying Tertiary succession (Figs. 4.27, 4.37). In detail, the East Basin emerges as a primary basin, α_{10} , and a series of small isolated and broadly northeast-southwest trending depocenters, which are separated from one another by a number of ridges. Some of these ridges are cored by basement yet others are developed within the lower Mesozoic successions, as further detailed below. Similar to what is observed in the West Basin and Ridge Province the margins of the ridges are often demarked by prominent northeast-southwest trending faults.

4.6.1. Northern Portion of East Basin Province

The northern portion of this tectonic province is characterized by three prominent broadly northeast-southwest trending ridges, R8, R9, R10 and two similarly trending

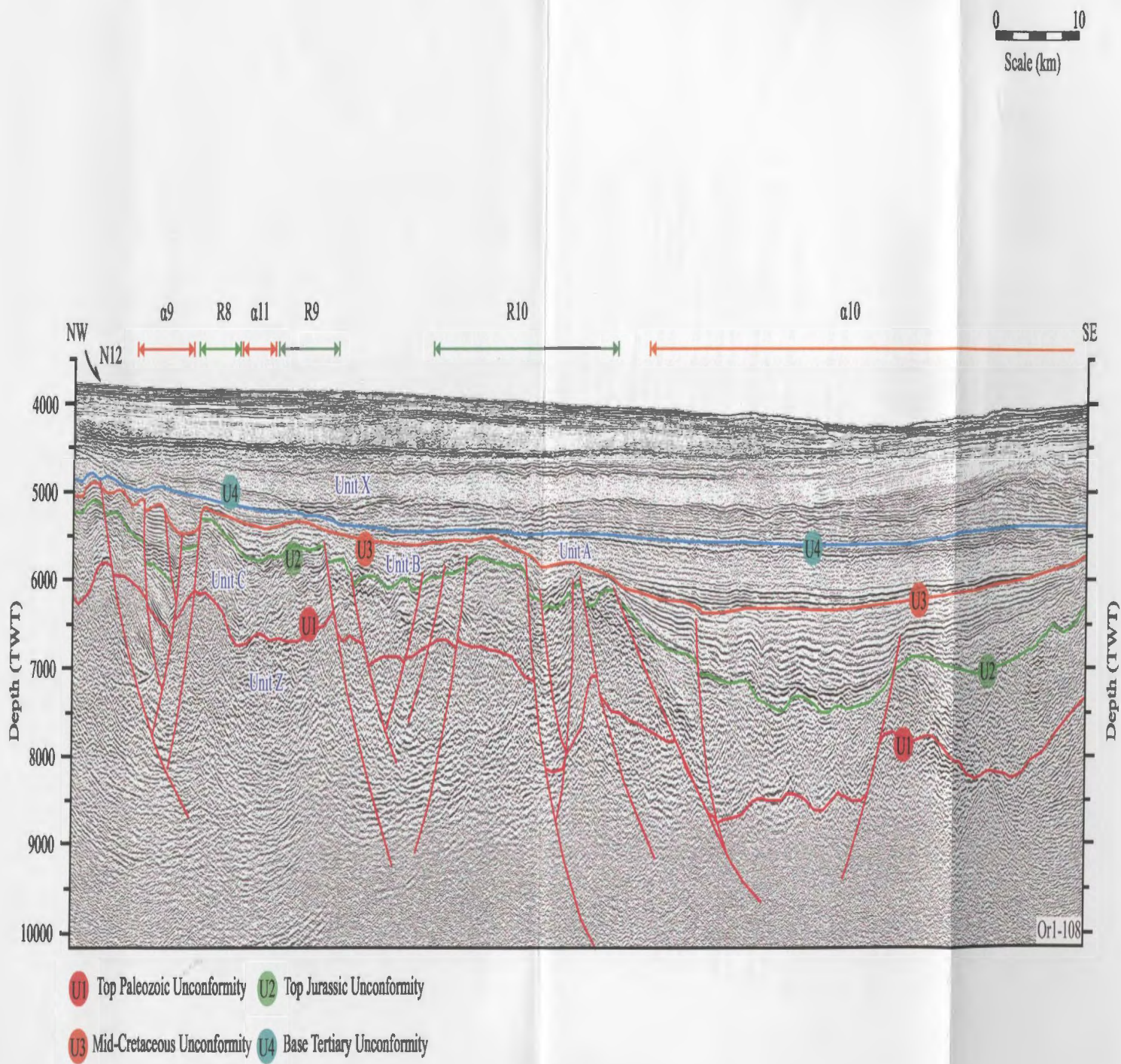


Figure 4.37. Multichannel seismic reflection (OR1-108) profile showing the prominent structures of the northern portion of the East Basin Province. Note the presence of the major depocenter, basin (a10) and its western boundary multi-crested ridge (R10). Location is shown in Figure 4.5.

basins: a large basin, α_{10} in the east and a very narrow basin, α_9 in the west (Figs. 4.9, 4.37). Seismic reflection profiles show that (i) major faults and their synthetic splays define the margins of the ridges, (ii) these faults show clear extensional stratigraphic separations and (iii) the fault planes exhibit listric trajectories. For example, the western margin of ridge R8 is delineated by fault F10, and the ridge occurs on the footwall of this fault. Similarly, the eastern margin of ridge R9 is depicted by fault F11, and ridge R9 actually forms the footwall block of this fault (Fig. 4.38). In this region, ridges R8 and R9 are situated close to one another, defining a broad double-crested horst structure. Seismic reflection profiles show that ridges R8 and R9 are largely cored by pre-rift basement successions of Unit Z, but may also include a significant Jurassic succession: difficulties in seismic correlations over the ridges preclude a reliable determination of the top of pre-rift basement rocks in these regions. A small depocenter (basin α_x) evolved between these two crests (Fig. 4.38). It is denoted by the thickness variations of the strata that are bounded by the Mid-Cretaceous and Top Jurassic Unconformities. The basin appears to have been completely filled, thus lost its character in the late Cretaceous (Fig. 4.38).

Basin α_9 occurs between faults F12 and F10 (Figs 4.3, 4.9). It is a ~10 km wide depocenter which contains ~1000-1100 ms thick Mesozoic successions. The basin is defined by the northeast-southwest trending and southeast-dipping major fault F12 and the similarly trending, but northwest-dipping fault F10 (Fig. 4.38). Fault F12 can be confidently shown to have a listric fault trajectory. It has several synthetic splays, which

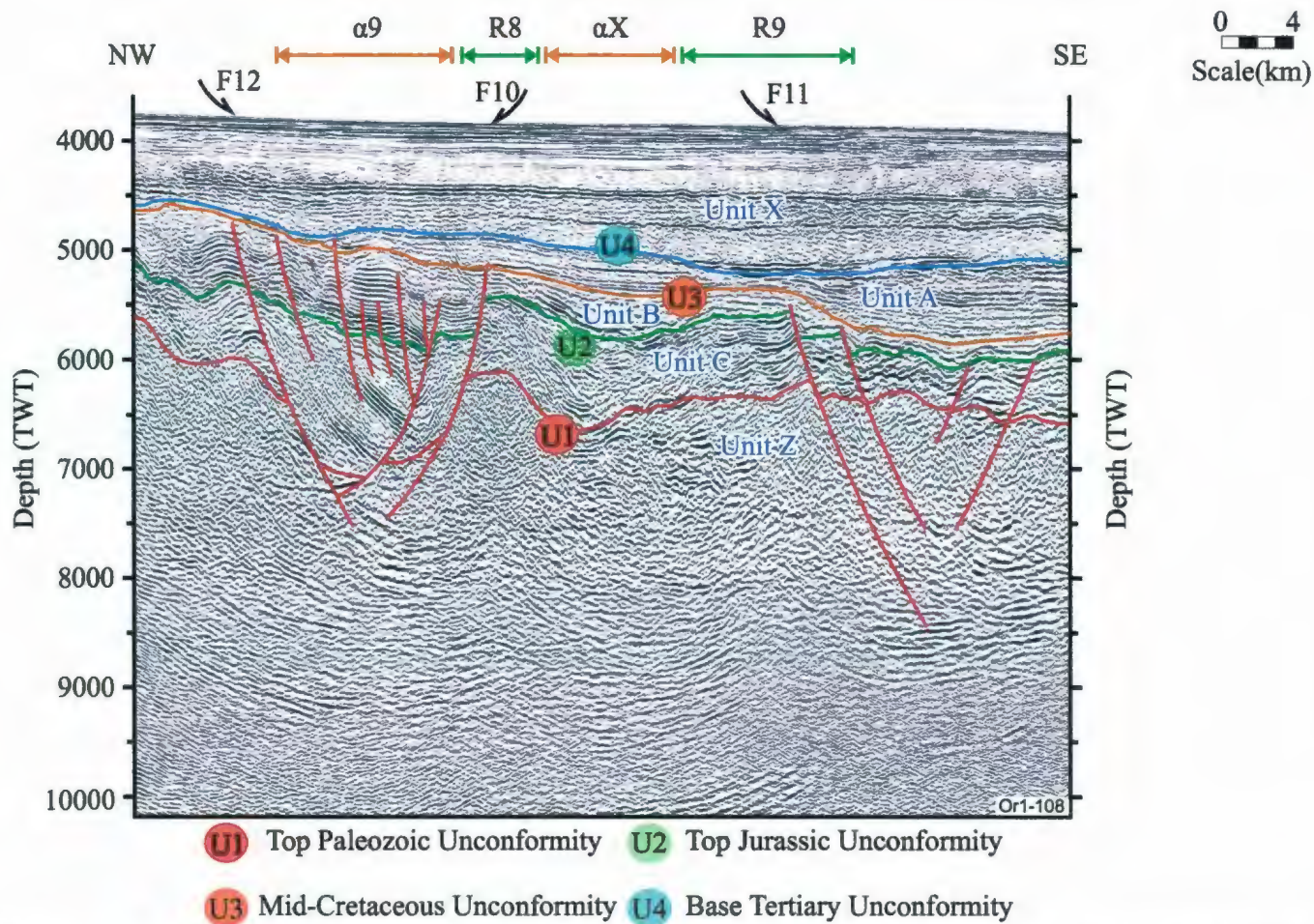


Figure 4.38. Blow-up of multichannel seismic reflection (OR1-108) profile showing the architecture of ridges R8 and R9, and their relationship to faults F10 and F11. Note that the ridges coincide with the footwall blocks of these faults. Further note that a thin upper Cretaceous succession is separated from the thicker lower Cretaceous succession by the Mid-Cretaceous Unconformity and that the latter unconformably overlies a thick ?Triassic-Jurassic succession. Location is shown in Figure 4.5.

run parallel to the fault and also show listric trajectories. Fault F10 and its synthetic splays also extend down section with listric trajectories, and abut the plane of fault F12 (Fig. 4.38). Fault F12 appears to be the master fault with fault F10 defining the antithetic splay. Seismic stratigraphy suggests that a thin (<50-300 ms) upper Cretaceous succession unconformably lies over an ~800 ms-thick lower Cretaceous succession, separated by the Mid-Cretaceous Unconformity. The lower Cretaceous succession, in turn, unconformably overlies an ~1200 ms-thick Jurassic succession, separated by the Top Jurassic Unconformity (Fig. 4.38).

Ridge R10 is situated ~10-15 km east of ridge R8. It is a northeast-southwest trending very broad structure that is ~10-15 km wide. Internally, the ridge is composed of a number of rotated and tilted fault blocks, most of which are cored by Jurassic successions, unconformably overlying the pre-rift basement Unit Z (Fig. 4.37). Several prominent northeast-southwest trending and mainly southwest-dipping normal faults dissect ridge R10. These faults have tip points that invariably lie within the lower Cretaceous succession, below the Mid-Cretaceous Unconformity, and extend with listric fault trajectories to depths greater than 9 seconds (Figs. 4.37, 4.39). Ridge R10 constitutes the western margin of the prominent basin α 10 (Figs. 4.9, 4.27, 4.37, 4.39). Basin α 10 is ~30-35 km wide and contains ~2500 ms of Mesozoic successions along its axial trough. The basin rests over the eastern faulted and tilted blocks of ridge R10 in the west and the faulted and tilted fault blocks that define the western margin of the Eastern Basin Margin. The internal stratigraphic architecture of the basin is such that 1000 ms-thick Jurassic strata largely abut the basin boundary faults, both in the east and west,

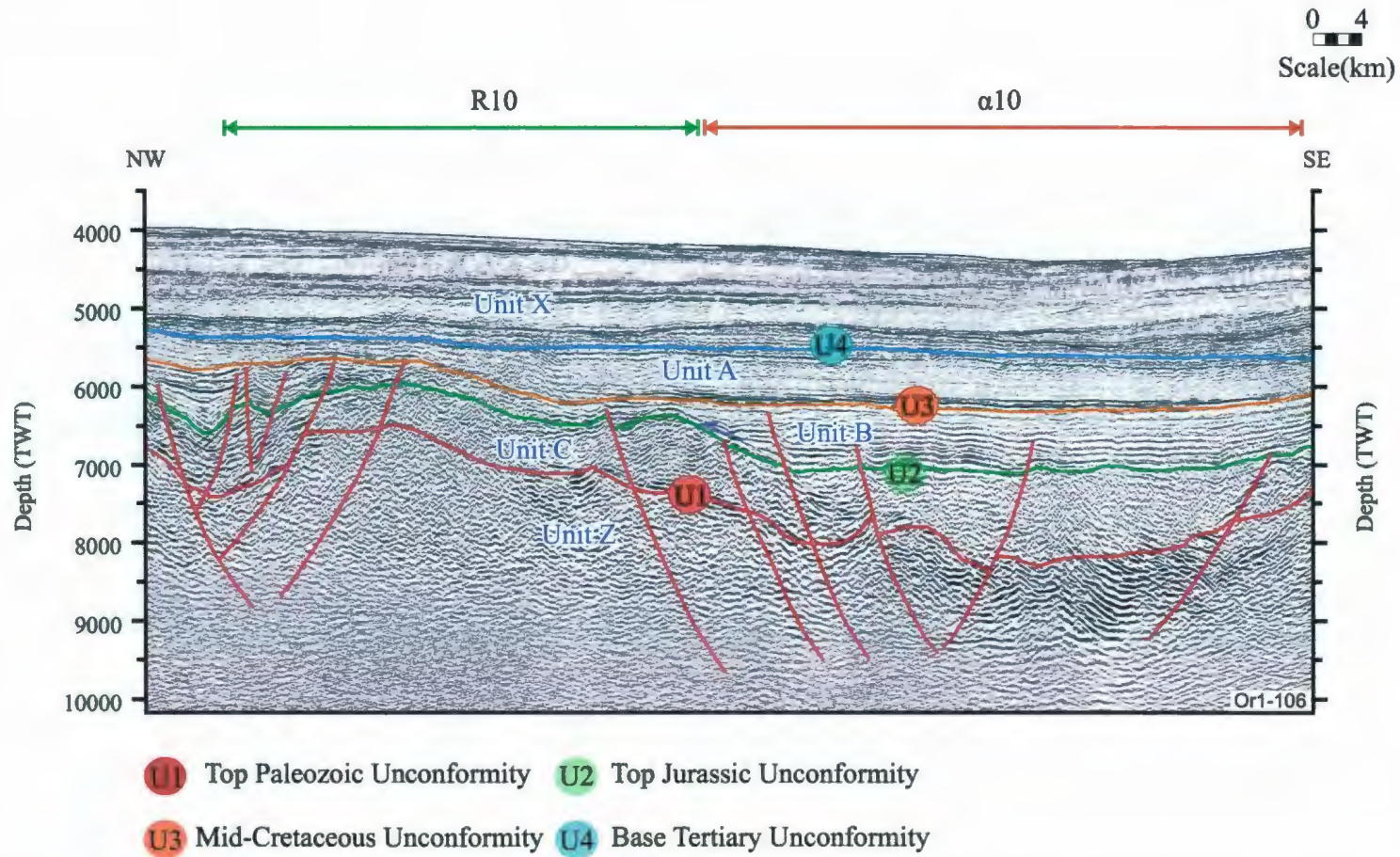


Figure 4.39. Multichannel seismic reflection (OR1-106) profile showing the prominent basin α 10 and ridge R10. Note the presence of mostly southwest-dipping normal sense faults that dissect ridge R10. This dissection creates a number of rotated and tilted fault blocks. The lower Cretaceous uppermost succession shows progressive onlap and eventually oversteps the tilted fault blocks of ridge R10 in the west. Location is shown in Figure 4.5.

whereas the 1100 ms-thick lower Cretaceous strata show notable thinning toward the basin margins (Fig. 4.37). This thinning is largely achieved by convergence of internal reflector, but also includes onlap and offlap reflection terminations. The uppermost 800 ms-thick section of the lower Cretaceous succession progressively onlap and eventually overstep the tilted fault blocks of ridge R10 in the west (Figs. 4.37, 4.39) and the faulted blocks of the Eastern Basin Margin in the east (Fig. 4.40).

4.6.2. Central Portion of the East Basin Province

Ridges R8, R9 and R10 and the major depocenter $\alpha 10$ can be readily traced southwards into the central portion of the Eastern Basin (Figs. 4.3, 4.9). In this region, another prominent ridge (R11) emerges between fault N3 and basin $\alpha 9$, and trends towards the southwest with an acute angle to the trend of fault N3. A small basin ($\alpha 13$) is developed between ridge R11 and the single merged fault that defines the White Sail Fault Zone in this region (see section 4.4). The double-crested structural high that encompassed ridges R8 and R9 in the northern portion of the East Basin Province progressively become two distinct structures as one moves southwards. This is accomplished as ridge R8 continues its northeast-southwest trend, but ridge R9 progressively swings in a counterclockwise sense to assume a north-south trend. This separation resulted in the development of a major basin, $\alpha 13$, which is currently nestled between ridges R8 and R9 (Fig. 4.41). Careful mapping show that the basin $\alpha 13$ is the southern continuation of the small depocenter basin αx described above.

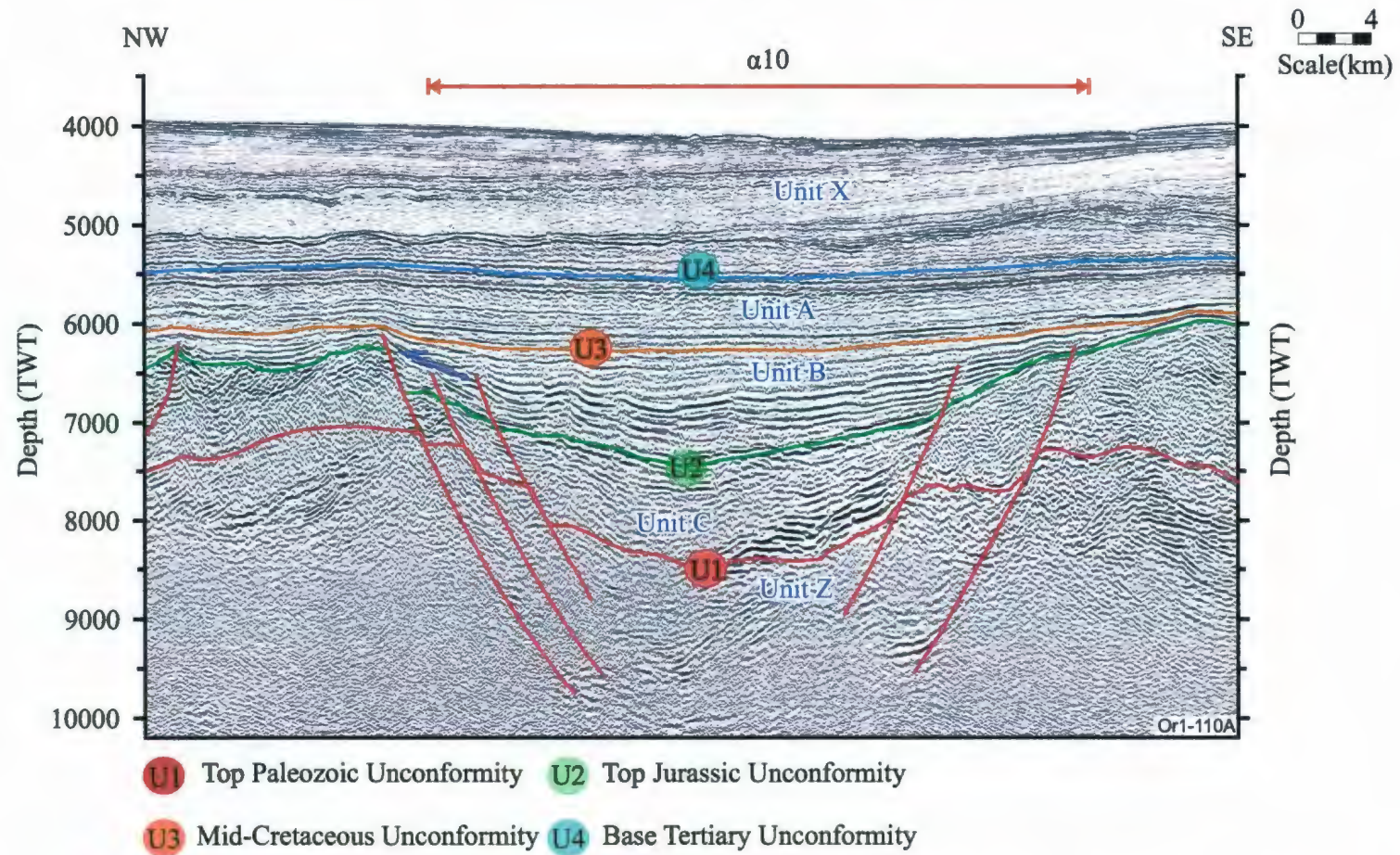


Figure 4.40. Multichannel seismic reflection (OR1-110A) profile showing basin $\alpha 10$ bounded by tilted and faulted blocks of the western margin of the Eastern Basin Margin in the east. Note the presence of progressive onlap and eventually overstep behaviour of the lower Cretaceous uppermost succession on this western margin of the basin $\alpha 10$. Location is shown in Figure 4.5.

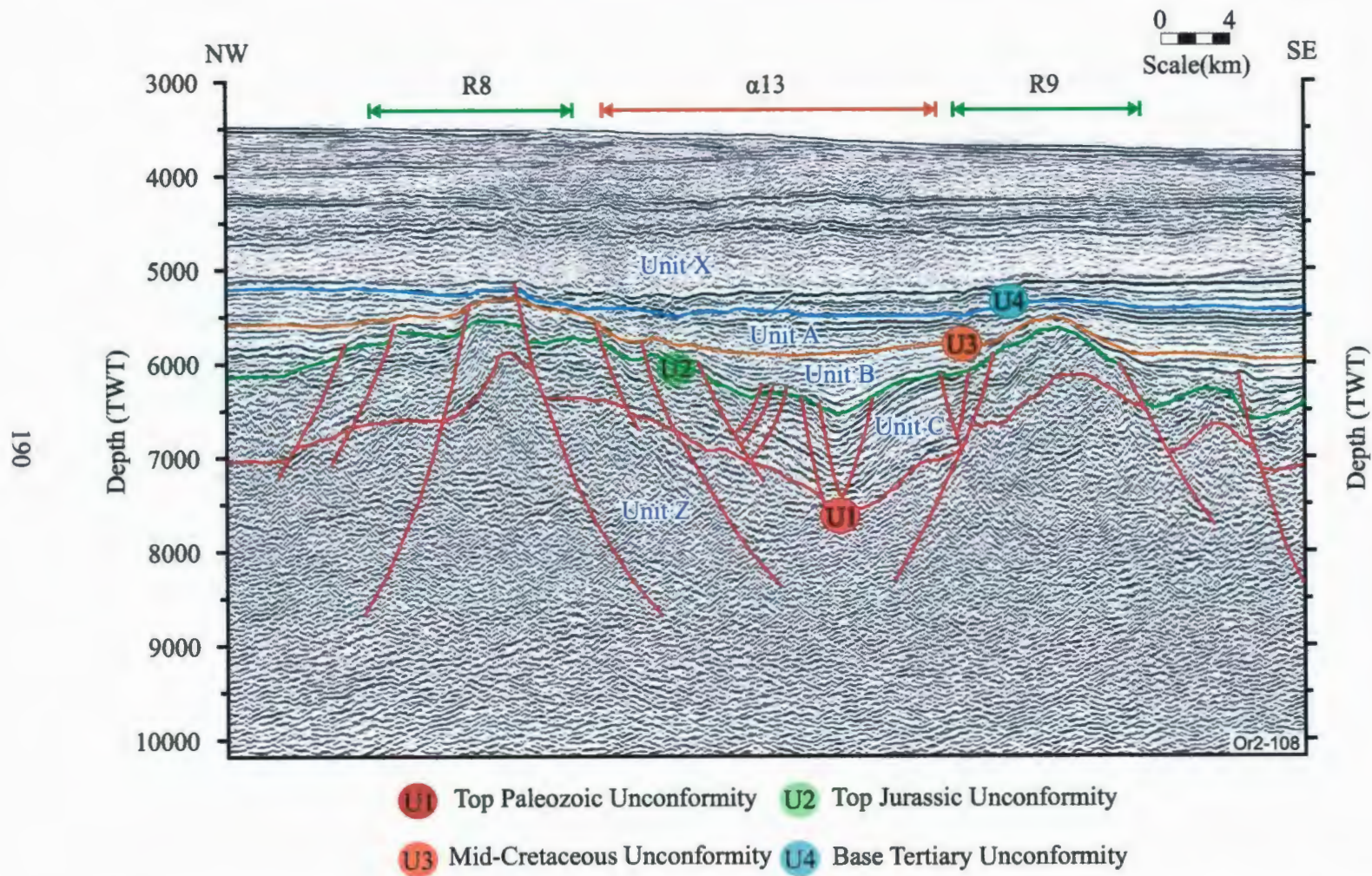


Figure 4.41. Multichannel seismic reflection (OR2-108) profile showing the central part of the East Basin Province. Note the presence of the prominent basin $\alpha 11$ that is situated between R8 and R9. Location is shown in Figure 4.5.

The western bounding fault of ridge R8 and its synthetic splays and the eastern bounding fault of ridge R9 and its synthetic splays can be readily identified in seismic reflection profiles and traced southwards (Figs. 4.3, 4.9). These faults display very similar structural style to those observed in the northern portion of the East Basin Province. However, new faults are developed marking the eastern margin of ridge R8 and western margin of ridge R9, as the double-crested nature of these two ridges is progressively replaced further south by the development of two prominent independent structures (Figs. 4.3, 4.41). For example, 3-4 roughly north-south trending, east-dipping major faults are imaged delineating the eastern margin of ridge 8 (Fig. 4.41). Similarly, 2-3 broadly north-south trending major faults are imaged forming the western margin of ridge R9 (Figs. 4.3, 4.41). These new faults all have tip points that are invariably situated within the upper Cretaceous succession, and extend down section with listric trajectories.

Basin $\alpha 11$ is an ~20-22 km wide depocenter situated between ridges R8 and R9 (Fig. 4.9). It displays a northeast-southwest trend in its northern portion, a north-south trend in its central portion and northwest-southeast trend in its southern portion, thus defining a west-convex arcuate map trace (Fig. 4.9). Along its axis basin $\alpha 11$ contains >1700 ms of Mesozoic successions deposited over the pre-rift basement (Fig. 4.41). In the deepest portion of the basin, inferred Jurassic successions are ~1000 ms-thick. They show little to no growth along the western margin of the basin, as they climb the fault panels toward ridge R8. However, the Jurassic succession shows a notable thinning of ~400 ms along the eastern margin of the basin toward ridge R9 (Fig. 4.41). A prominent unconformity marks the top of the Jurassic succession, where the unconformity is

delineated by the progressive onlap of the overlying lower Cretaceous package, both toward the eastern as well as the western margin of the basin (Fig. 4.41). This unconformity is believed to represent the wide-spread Top Jurassic Unconformity in the Orphan Basin. The lower Cretaceous succession is ~500 ms thick along the axis of the basin, but dramatically thins to ~50 ms over the crest of the adjacent ridges R8 and R9 (Fig. 4.41). The cause of the observed thinning of the lower Cretaceous succession is two fold: (i) the seismic data clearly show that the succession display progressive onlap and inter-stratal offlap toward the margins and (ii) there is considerable erosion along the flanks of the basin at the Mid-Cretaceous Unconformity (Fig. 4.41). The package situated between the Base Tertiary Unconformity and the Mid-Cretaceous Unconformity (i.e., inferred upper Cretaceous succession) also show progressive thinning toward the basin margins, but unlike the lower Cretaceous succession the upper Cretaceous reflections onlap and overstep the crests of ridge R9 and possibly R8 (Fig. 4.41). Mapping of the elevations of the basin axis along numerous east-west running seismic reflection profiles show that the axis of basin $\alpha 11$ displays a notable south-directed plunge, and that northwards the basin axis rises to almost the elevation of the ridges, becoming nearly indistinguishable from them.

Ridge R11 is a conspicuous structure in the central portion of the East Basin Province (Figs. 4.3, 4.9, 4.42). In its northern portion the structure has a northeast-southwest trend, but towards the south it shows a progression to assume a nearly north-south trend (Fig. 4.9). The structure is bounded to the west by a normal fault (N12), but the eastern margin of the ridge R11 is defined by the gently east-dipping western slope of

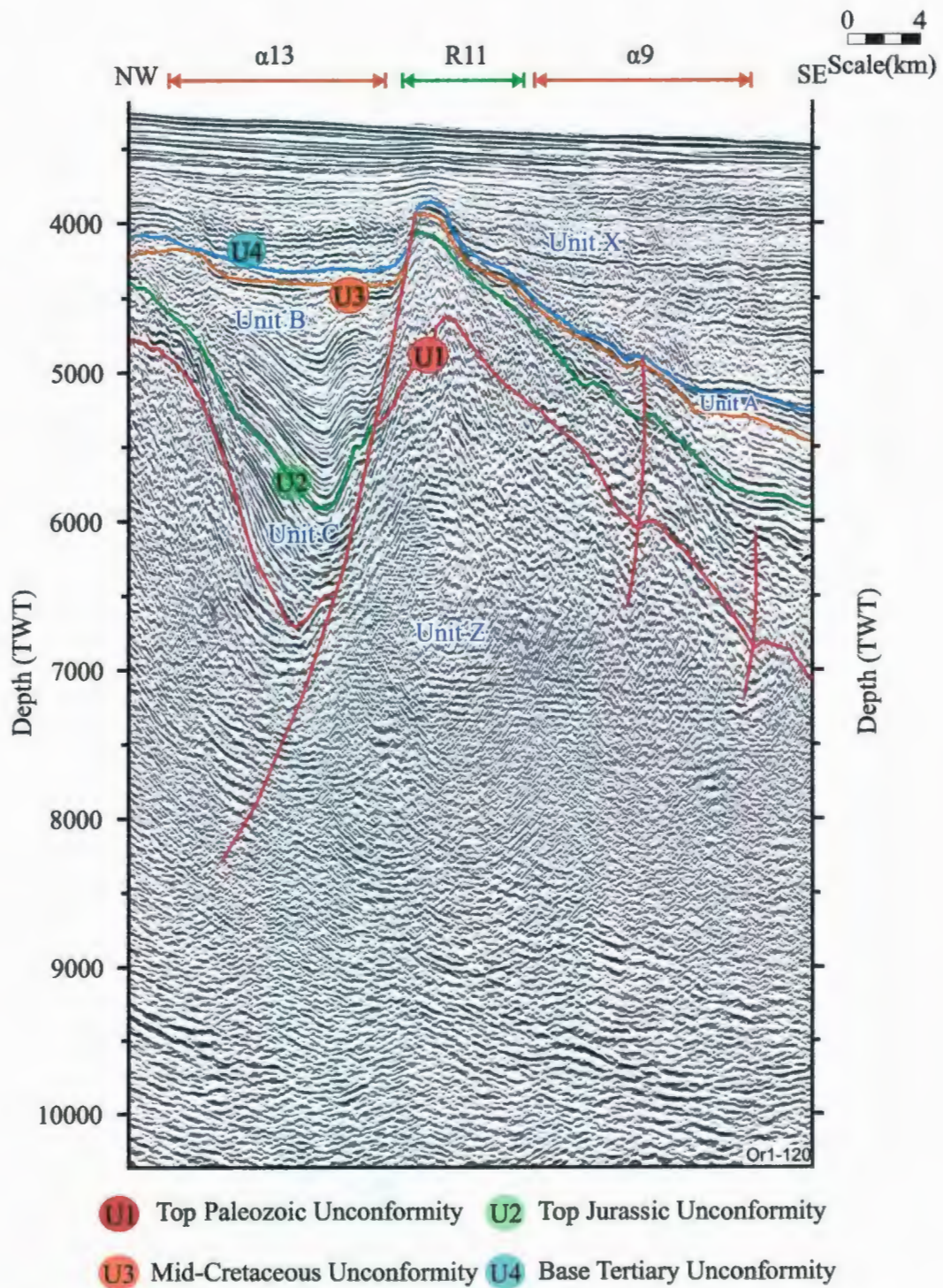


Figure 4.42. Multichannel seismic reflection (OR1-120) profile showing major ridge R11, and depocenter $\alpha 13$ of the East Basin Province. Location is shown in Figure 4.5.

basin $\alpha 9$ (Fig. 4.42). The internal architecture of ridge R11 is complex: it shows a series of low amplitude strong, but discontinuous reflections defining a broad anticlinal structure beneath the top of the pre-rift basement reflector. The inferred Jurassic succession can be readily traced from basin $\alpha 9$ westward toward ridge R11, where the succession forms a 300-400 ms thick blanket. The Top Jurassic, Mid-Cretaceous and Base Tertiary Unconformities converge over the crest of ridge R11, forming a major composite unconformity. The Mesozoic successions over the ridge must have remained as a major structure at the end of the Mesozoic Era, because the lower Tertiary reflections show a protracted onlap over the ridge with only the middle Tertiary strata overstepping the crest of Ridge R11.

The western margin of ridge R11 is notably steeper, and is cut by a northwest-dipping normal fault N12 (Fig. 4.42). The fault soles into the pre-rift basement, and shows tip point at the Base Tertiary Unconformity. Basin $\alpha 13$ is a narrow and deep depocenter developed between the White Sail Fault Zone and ridge R11. On map view, the basin displays a convex to the west trace, paralleling the general curvature of the White Sail Fault Zone (Figs. 4.3, 4.9). Internally, the basin contains an ~500 ms-thick Jurassic succession, which is unconformably overlain by ~1400 ms of Lower Cretaceous reflections, which are, in turn, unconformably overlain by a 100 ms-thick Upper Cretaceous succession (Fig. 4.42). These basinal strata show a remarkable west-directed onlap over the reflection that delineates the top of the pre-rift basement in the west,

whereas they abut the fault surface in the east, where they create a small roll-over structure (Fig. 4.42).

In the central portion of the East Basin Province, basin $\alpha 10$ is a very prominent, approximately 40-45 km-wide depocenter (Fig. 4.9). It is situated between the Eastern Basin Margin in the east and ridge R9 in the west. The deepest portion of the basin occurs at ~8 seconds depth in seismic reflection profiles (Fig. 4.43). In the central portion of the province, the western margin of the basin is delineated by 3-4 northeast-southwest trending southeast-dipping major extensional faults, which in turn define the eastern margin of ridge R9. Similarly, the eastern margin of the basin is delineated by 2-3 northeast-southwest trending, but northwest-dipping extensional faults, which define the western flank of the Eastern Basin Margin. Seismic reflection profiles show that these basin-bounding faults clearly cut the entire Mesozoic succession and sole into the pre-rift basement (Fig. 4.43). These faults show tip points invariably within the lower Cretaceous succession. Along its axis, basin $\alpha 10$ contains ~2400 ms of Mesozoic successions deposited over the pre-rift basement (Figs. 4.27, 4.43). In the deepest portion of the basin, the Jurassic succession is ~800 ms-thick, and similar to the depositional style observed within basin $\alpha 11$, the succession shows very little growth along the margins of the basin, even when the succession climbs across faults with significant throw (Fig. 4.43). Again, similar to the stratigraphic architecture observed in basin $\alpha 11$, the top of the Jurassic succession is marked by a prominent unconformity (i.e., the Top

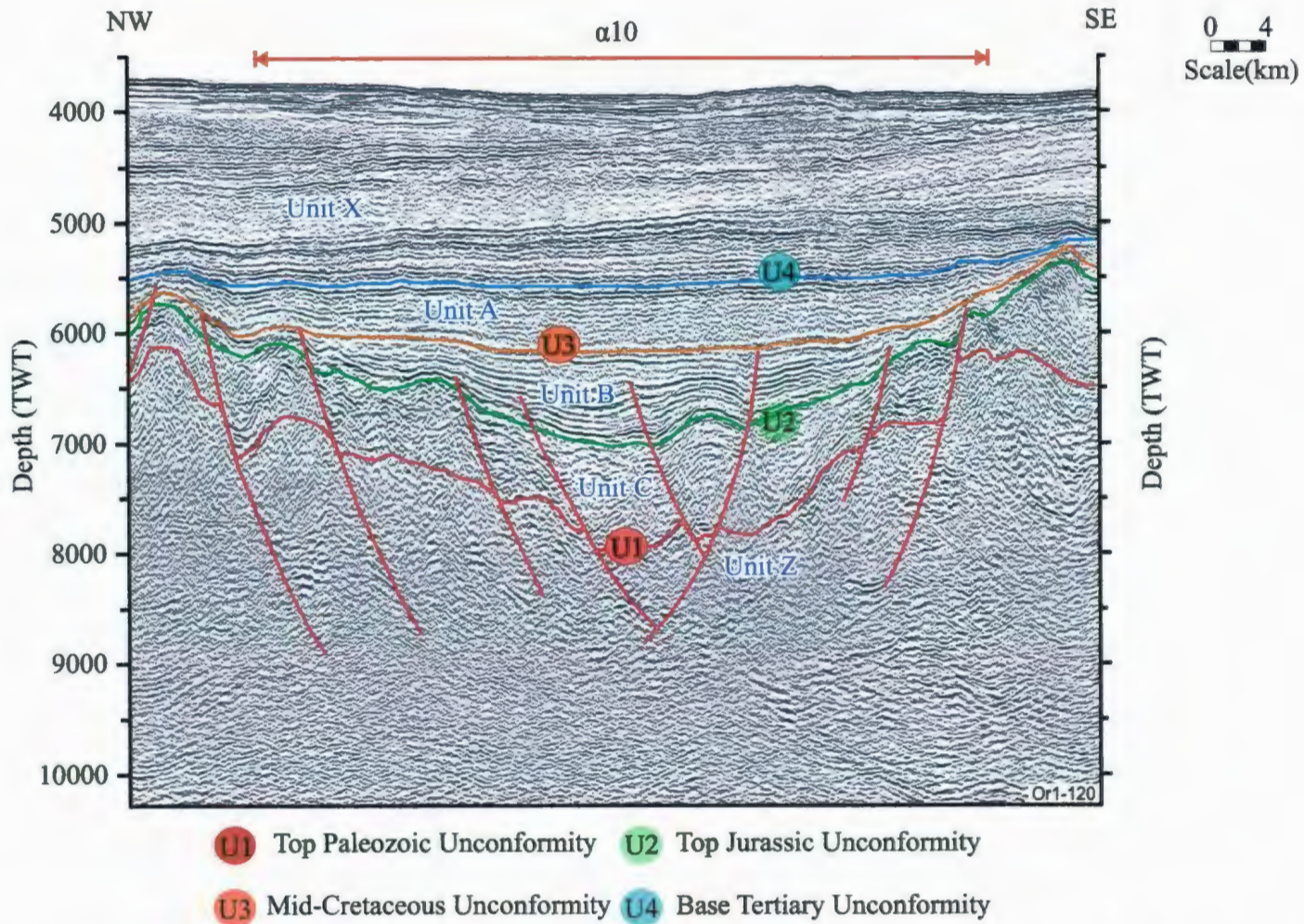


Figure 4.43. Multichannel seismic reflection (OR1-120) profile showing major depocenter basin $\alpha 10$ of the East Basin Province. Location is shown in Figure 4.5.

Jurassic Unconformity), where the overlying lower Cretaceous package shows a protracted onlap over the surface of the unconformity, both toward the eastern as well as the western margin of the basin (Fig. 4.43). Along the axis of basin $\alpha 10$ the lower Cretaceous succession is ~500 ms thick, but shows a very noticeable thinning over the crest of the adjacent ridge R9 in the west, as well as the faulted blocks that define the margin of the basin in the east (Fig. 4.43). The observed thinning is largely caused by progressive onlap of the Cretaceous strata over the Top Jurassic Unconformity, as well as mild erosion at the Mid-Cretaceous Unconformity (Fig. 4.43). The upper Cretaceous package is ~550 ms thick along the axis of the basin, but shows a protracted onlap over the Mid-Cretaceous Unconformity. Along the eastern margin of the basin the entire upper Cretaceous succession is lost to onlap, whereas along the western margin a 100-150 ms thick veneer oversteps the structures that define this region (Fig. 4.43).

4.6.3. Southern Portion of the East Basin Province

The progressive eastward swing of the White Sail Fault Zone to eventually assume a parallel trend with the east-southeast trending southern segment of the Western and Southwestern Basin Margin of the Orphan Basin is the single most important structure that controls the tectonic framework of the western portion of this region. All structures in the southwestern portion of the Eastern Basin Province, including basins $\alpha 13$ and $\alpha 9$, and the intervening ridge R11 are acutely convex to the west, and distinctly follow a parallel trend to the White sail Fault Zone. Basin $\alpha 13$ widens considerably toward the south as ridge R11 bounding its eastern margin assumes a northwest-southeast

trend (Fig. 4.9). The internal architecture of basin $\alpha 13$ is characterized by an ~ 2000 ms-thick Mesozoic succession deposited over the pre-rift basement (Fig. 4.40). The merged narrow single fault strand that defines the easternmost fault of the White Sail Fault Zone is a very prominent structure in this area and displays a listric fault trajectory that extends into the pre-rift basement strata, and becomes progressively shallower with depth exceeding ~ 7500 ms. The observed fault architecture created a very large roll-over structure in the Mesozoic successions within the rotated and tilted hanging wall block of this fault (Fig. 4.44). Several east-dipping normal faults cut the crestal region of the fault block, creating an apparent anticlinal structure in this region. The large crustal-scale rotated and tilted fault block appears to have partitioned the larger earlier Mesozoic depocenter into two smaller and younger Mesozoic depocenters. Careful inspection of the seismic reflection profiles show that the trough that defines the axis of the western basin has shifted through time from an easterly position to a more westerly position associated the evolution of the roll-over. The eastern younger Mesozoic basin is now perched between the slope of the rotated fault block in the west and the slopes of ridge R11 in the east. Internally, this small depocenter is filled with ~ 700 ms of Cretaceous successions, which show onlap over the basin margins in the east and west (Fig. 4.44).

Ridge R8 can be readily traced southwards where it abuts the east southeast trending structures of the White Sail Fault Zone (Figs. 4.3, 4.9). Basins $\alpha 9$ and $\alpha 13$ and the intervening ridge R11 cannot be confidently mapped in the southernmost regions of this province, thus their relationships with the Western and Southwestern Basin Margin and the White Sail Fault Zone cannot be fully determined.

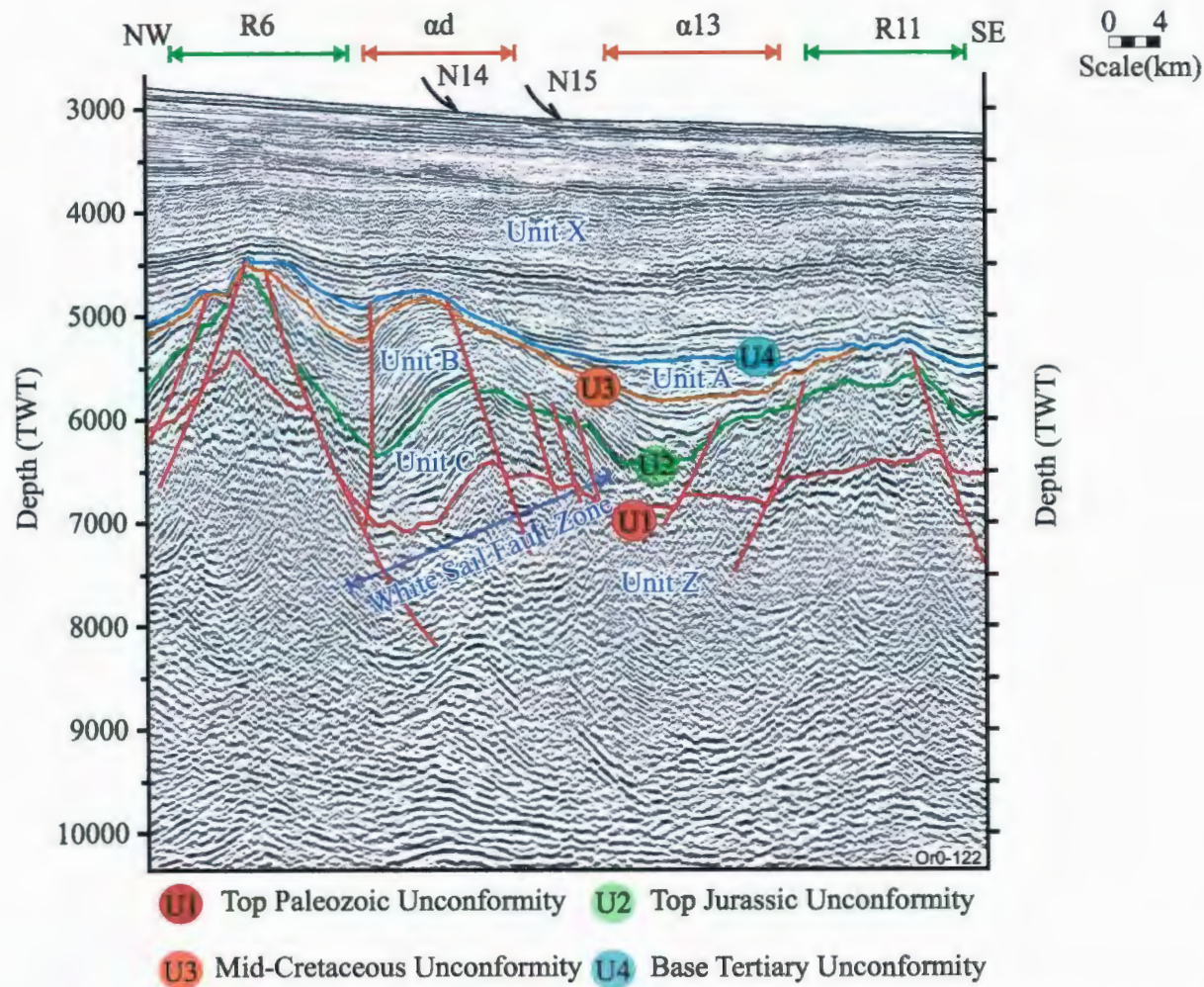


Figure 4.44. Multichannel seismic reflection (OR0-122) profile showing ridge R6 that defines the eastern margin of the White sail Fault Zone, the major depocenter basin $\alpha 13$ and ridge R11 in the East Basin Province. Location is shown in Figure 4.5.

Toward the southeastern corner of the study area, the Orphan Basin *sensu lato* progressively narrows and eventually closes as the northwest-southeast trending Western and Southwestern Basin Margin (as well as the now merged White Sail Fault Zone) meets the broadly north-south trending Eastern Basin Margin (Figs. 4.3, 4.9). This narrowing is entirely controlled by the northwest-southeast trending structures, and is not reflected in the orientation and architecture of the tectonic elements observed and mapped within the East Basin. Ridges R8 and R12 and basins $\alpha 10$ and $\alpha 11$, and their bounding faults can be confidently traced south into the south-easternmost regions of the Orphan Basin (Figs. 4.3, 4.9). These structures abut the northwest-southeast trending structures bounding the southern margin of the Orphan Basin.

In the southernmost region of the study area, ridge R8 is still mapped as a prominent structure bounded on its eastern and western flanks by major northeast-southwest trending and southeast- and northwest-dipping normal faults (respectively) that display listric fault trajectories, soling into the pre-rift basement unit Z (Fig. 4.45). The tip points of all faults bounding the structure as well as their synthetic and antithetic splays are invariably located below the Base Tertiary Unconformity. Preliminary seismic correlations suggest that the ridge is cored nearly entirely by the prerift strata, and that a 500 ms-thick veneer of Jurassic and 100-300 ms-thick Cretaceous strata overlie the crest of the structure.

Ridge 12 is also readily mapped in the southernmost regions as a major structure, which creates a significant inflection at the Top Jurassic, Mid-Cretaceous and Base

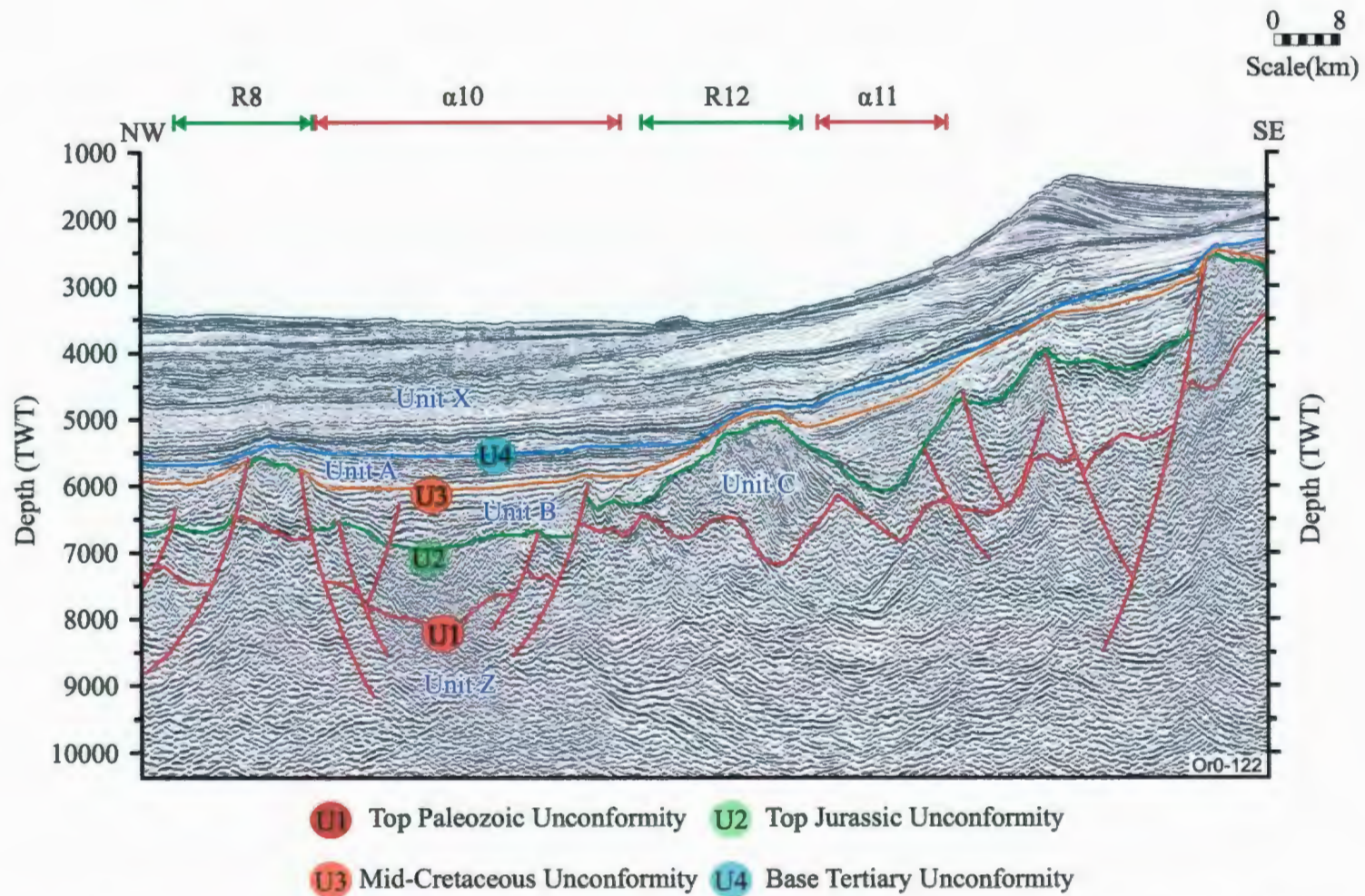


Figure 4.45. Multichannel seismic reflection (OR0-122) profile showing major basins $\alpha 10$ and $\alpha 11$ and ridges R8 and R12 in the East Basin Province. Location is shown in Figure 4.5..

Tertiary Unconformities (Fig. 4.45). It is mainly delineated by the Top Jurassic Unconformity, which rises ~900 ms from the adjacent basin floor to the ridge crest. The structure has a very distinctive core, characterized by a series of high-amplitude continuous reflections that show ~35° dip toward the southeast (Figs. 4.45, 4.46). Seismic stratigraphic correlations with existing exploration boreholes suggest that these high amplitude reflections are tilted Jurassic strata. Careful mapping shows that the reflector that defines the top of the pre-rift basement does not reflect the morphology of the ridge, as it represents a nearly horizontal surface. But, the morphology of the ridge is clearly reflected in the tilted, and ~1300 ms-thick Jurassic strata and the morphology of the Top Jurassic Unconformity (Figs. 4.45, 4.46).

Within the narrow basin that is developed between ridges R12 and R13 (or its southeast continuation into the merged structural highs that define the Eastern Basin Margin; Fig. 4.9). Here, the Lower Cretaceous succession (i.e., the package between the Top Jurassic Unconformity and the Mid-Cretaceous Unconformity) defines an ~900 ms-thick wedge that sharply abuts the fringes of ridge R12 in the west and shows a progressive onlap over the western margin of ridge R13 in the east (Figs. 4.45, 4.46). The upper Cretaceous package (i.e., the strata between the Base Tertiary and Mid-Cretaceous Unconformities) is ~350 ms thick within the trough of basin α 11 but rapidly thins to >100 ms over ridge R12.

Basin α 10 is an approximately 2500 ms thick wide basin in the southernmost segment of Orphan Basin. It includes a 1100 ms thick Jurassic succession deposited over

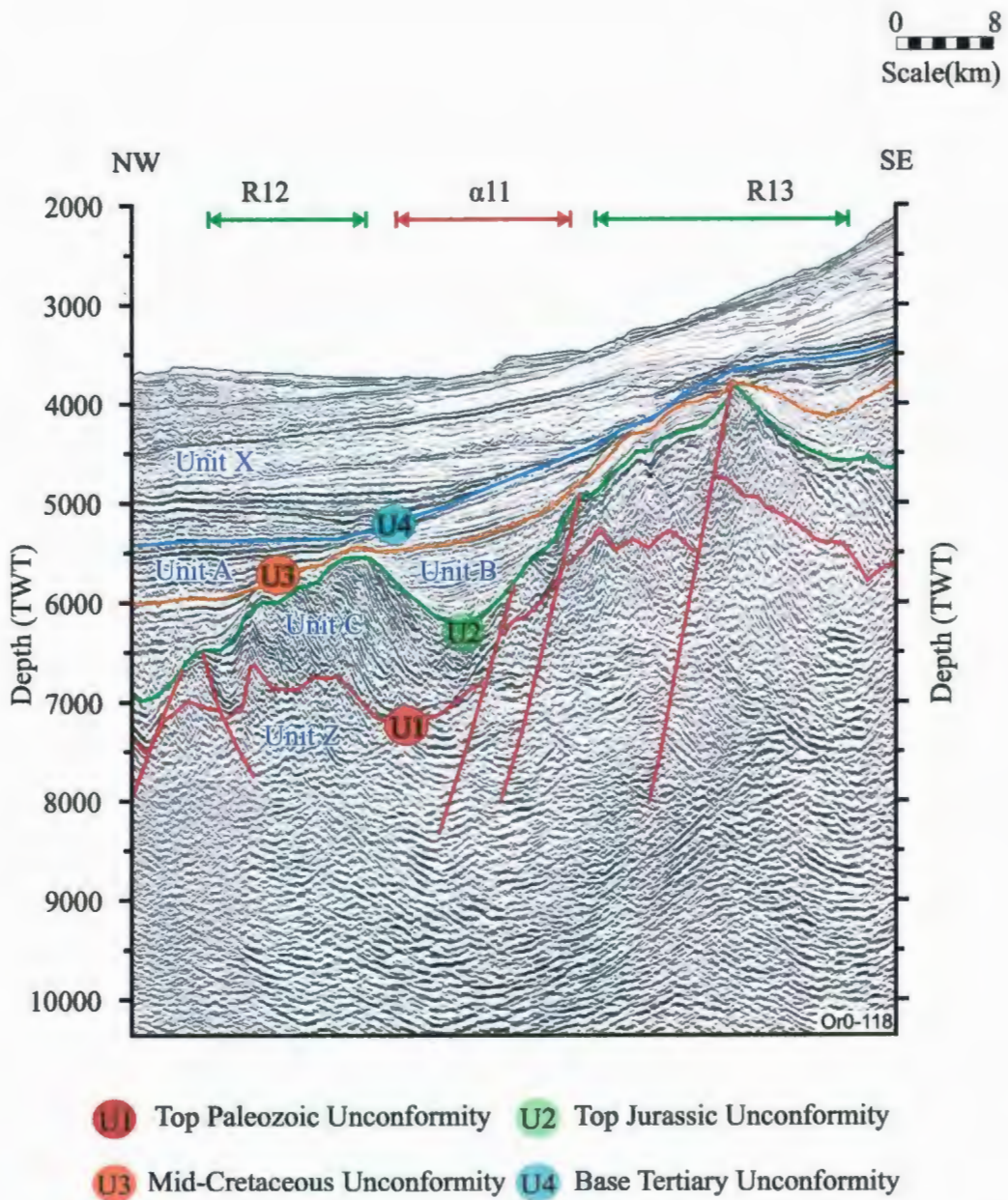


Figure 4.46. Multichannel seismic reflection (OR0-118) profile showing major basin $\alpha 11$ and ridges R12 and R13 in the East Basin and the East Basin Margin Provinces. Location is shown in Figure 4.5.

the pre-rift basement. This succession shows notable onlap over the western flank of ridge 12 in the east and the eastern flank of ridge R8. While the Jurassic succession occurs at the footwall of the fault block that defines the crest of ridge R8 (Fig. 4.45), a 1300 ms thick Jurassic succession is incorporated within the tilted fault block that defines the ridge R12 (Figs. 4.45, 4.46). Similar to that observed in basin $\alpha 11$, the 1500 ms thick Cretaceous succession shows a protracted progressive onlap over the basin margins, with the uppermost Cretaceous strata overstepping the crest of ridge R8 in the west (Fig. 4.45).

The triangular-shaped region developed between the southeastern segment of the Western and Southwestern Basin Margin and the Eastern Basin Margin is characterized by a series of northeast-southwest trending faults that define a prominent fault fan, which shows approximately 10-30° angle between the faults that define the Eastern Basin Margin (Fig. 4.3). These faults have listric trajectories, which progressively flatten to a bedding-parallel detachment surface within the pre-rift basement succession (Fig. 4.47). Several antithetic and synthetic fault splays are found developed in this fan. The tip points of these faults lies within the Upper Cretaceous succession (Fig. 4.47). Detailed examination of the seismic reflection profiles show that there is mild roll-over and notable growth on the hanging wall of many fault blocks within the Jurassic succession. The boundary between the Jurassic and Cretaceous successions is defined by a major angular unconformity surface, which is referred to as the Top Jurassic Unconformity. Although, it is structured by the fault fan, this surface is clearly tilted towards the southeast (Fig. 4.47). A 1300-300 ms thick Cretaceous succession fills the structural lows

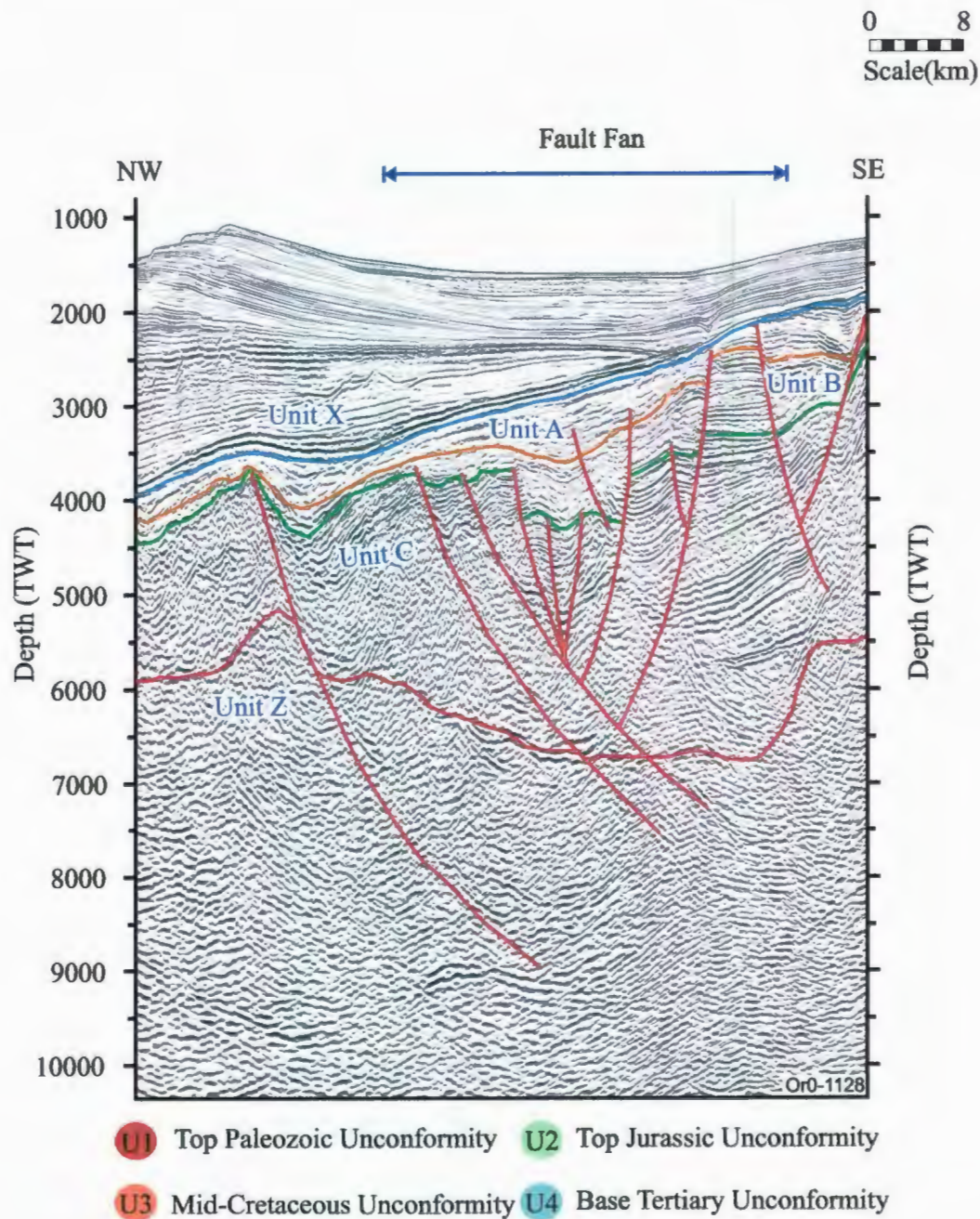


Figure 4.47. Multichannel seismic reflection (OR0-1128) profile showing the prominent fault fan situated at the southeastern corner of the Orphan Basin. Location is shown in Figure 4.5.

created by the fault fan, and the succession is capped by another angular unconformity surface (i.e., the Base Tertiary Unconformity; Fig. 4.47).

4.7. Possible Strike-Slip Faults within the Orphan Basin

There are two zones within the Eastern Basin Province where the seismic data reveals the possible presence of a sinistral strike slip faults that developed within the Mesozoic succession (Fig. 4.3). These zones are characterized by abrupt terminations of faults and other structural elements, such as the crests of ridges and troughs of basins along a linear zone and the re-appearance of these structures further south within a very short distance and with a notable left-lateral offset. It is unrealistic to assume that faults can show very sharp (5-10 km horizontal offset within 1-2 km distance) lateral shifts on map views other than being involved in significant strike-slip deformation.

For example, within discontinuity 1, ridges R8 and R9 and the intervening depression are sharply offset in the central portion of the East Basin by approximately 4.5 km. Similarly, in discontinuity 2, mapping shows that ridges R8 and R11, and the basin α 9, and possibly α 10 are sinistrally offset by 5-7 km. If detailed mapping of these structures is correct, then these discontinuities must represent significant left lateral strike slip activity within the Orphan Basin (Figs. 4.3, 4.9).

CHAPTER 5. INTERPRETATION AND DISCUSSION

5.1. Regional Tectonic Evolution

The deposition in the rift basins along the eastern Canadian continental margin occurred as a response to multiple episodes of rift-drift cycles associated with the break-up of the supercontinent Pangea (Tankard and Welsink 1987; Enachescu, 1987, and 1988; Sinclair, 1988; Ziegler, 1989; Enachescu et al., 2005). Each depositional cycle recorded the complex interaction between tectonics, eustatic sea-level changes, sediment supply and climate (Jansa and Wade 1975; Hubbard et al., 1985; Tankard and Welsink, 1987; Grant et al., 1988; Tankard et al., 1989; Tucholke, 1989; McAlpine, 1991).

The continental margin basement around the Grand Banks of Newfoundland consists of Precambrian and Paleozoic rocks of the Appalachian Orogen, which were rifted, eroded and buried during repeated Mesozoic-Cenozoic rifting episodes (Grant et al., 1988). Three consecutive episodes of rifting affected the region during the Triassic through mid-Cretaceous, followed by a final postrift period starting in the Late Cretaceous (Enachescu, 1987; Sinclair 1988, 1993; Deptuck, 2003).

Each rifting stage includes a period of extension characterized by normal faulting and minor basin subsidence, followed by a period of protracted uplift associated with sectoral break-up, and a period of sustained thermally-driven subsidence (i.e., postrift). In the following discussion, the stratigraphic architecture of the Orphan Basin described

in Chapter 3 and the tectonic framework of the region presented in Chapter 4 will be evaluated within the context of the evolution of the eastern Canadian continental margin.

5.1.1. Phase I

5.1.1.1. Rifting (Late Triassic – Early Jurassic)

The initial rifting between the North America and Europe/Northern Africa occurred during the Late Triassic to Early Jurassic. Deformation started in the Grand Banks of Newfoundland with a regional NW-SE extension creating a series of NE-SW-trending rift valleys (Arthur et al., 1982; Sinclair, 1988). Welford and Hall (2007) and Reston (2008) suggested that the rifting was notably asymmetric and involved a west-dipping mid-crustal detachment surface between the Galicia Margin in the east and the eastern Canadian margin in the west (Fig. 5.1). This detachment surface delaminated the continental crust and allowed the crustal thinning to take place as the Canadian margin moved westward along the detachment.

There are several models which explain the evolution of the eastern Canadian continental margin, particularly the Scotian shelf and Grand Banks of Newfoundland. These models are briefly described below so that the present study can be placed into a historical tectonic context. At the end of this discussion, an evolutionary model is proposed which explains the development of the northeastern segment of the Grand Banks of Newfoundland, particularly the Orphan and Flemish Pass basins.

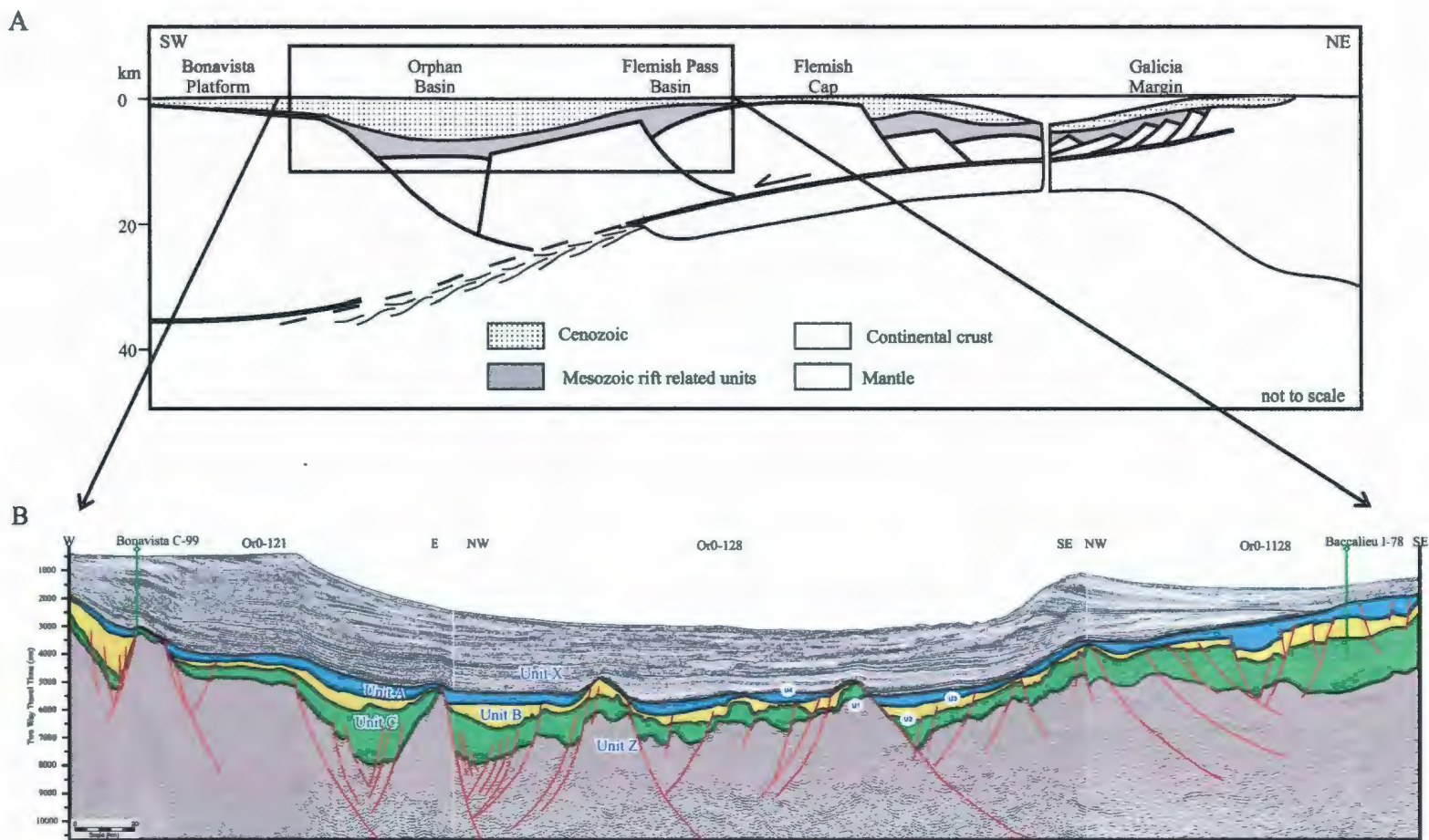


Figure 5.1. Schematic cross sections showing (A) the structure of the conjugate Grand Banks–Galicia margin pair. Note the presence of a west-dipping mid-crustal detachment surface between the two margins (modified from Tankard and Welsink, 1987 and Alves et al., 2003) and (B) regional seismic reflection profile C, across the Orphan and Flemish Pass basins.

Haworth and Keen (1979) used seismic refraction, gravity and magnetic data to suggest that the Jurassic opening produced a rifted margin adjacent to Nova Scotia and a transform margin along the southwestern Grand Banks. They further suggested that the width of the ocean-continent transition across the transform margin was approximately 50 km. They showed that (i) the eastern part of the transform margin is associated with a complex, Early Cretaceous volcanic province (i.e., the seamounts) and basement ridges showing evidence of subsidence, and (ii) the western portion of the transform margin is non-volcanic and lies within the 360 km wide Quiet Magnetic Zone floored by oceanic crust. Haworth and Keen (1979) showed that the development of the margin east of Newfoundland was more complicated with continental fragments separated from the shelf by deep water basins underlain by foundered and atypically thin continental crust. They argued that the crustal sections of the narrow Flemish Pass and the wide Orphan Basin suggest that the thinning was not simply due to stretching. They further argued that the Newfoundland Basin shows evidence for two-stage rifting between the Grand Banks and Iberia with both lateral separation and rotation of Spain. They suggested that the major sedimentary unconformities on the shelves (such as the Early Cretaceous unconformity on the Grand Banks) reflect uplift accompanying rifting.

Keen and Barrett (1981) used ocean bottom seismometers across the Orphan Basin and Flemish Pass. They used tau-*p* travel time inversion, synthetic seismogram analysis and conventional layered model calculations to show that these regions of the eastern Canadian continental margin are underlain by thinned continental crust, and that the M discontinuity is situated at about 22 km depth. They found two main crustal layers

with P-velocities of about 6.1 and 7.0 km s⁻¹, which are separated by sharp interfaces. These crustal layers are overlain by a layer with P-velocities of 5.5 km s⁻¹, which is interpreted to be Precambrian or Paleozoic basement. Mesozoic and Cenozoic sediments cover the basement rocks, and are over 4 km thick. They calculated a crustal thinning of 50% of the original crustal thickness, which occurred across a maximum horizontal extent of ~450 km. They further suggested that this extension can only satisfy the observed crustal structure and elevation of the margin during the rift phase if more extension took place in the lower lithosphere than in the upper lithosphere.

Srivastava et al. (2000) used magnetic data to determine the nature and origin of the thin crust across the ocean–continent transition between the Newfoundland and Iberia non-volcanic conjugate continental margins. The thin crust is usually found underlain by upper mantle with 7.2–7.4 km s⁻¹ velocities at shallow depths of 1–2 km. Previously, it had been proposed that such crustal material could have originated either by exhumation of the upper mantle during rifting or by slow seafloor spreading (White et. al., 1992). Srivastava et al. (2000) suggested that the ocean continent transition between the Newfoundland and Iberian margins is underlain by crustal material formed by slow seafloor spreading at a rate of 6.7 mm yr⁻¹ soon after Iberia separated from the Grand Banks of Newfoundland in the Late Jurassic. They showed the presence of weak magnetic anomalies in these margins and suggested that these regions may be underlain by oceanic crust formed during slow seafloor spreading. They further suggested that these data contradict the notion that the Sohm Abyssal Plain, Newfoundland and Iberia Basins were formed by un-roofing of the upper mantle during rifting.

Chian et al. (2001) used a single wide-angle seismic profile collected from the NE Newfoundland margin and existing multichannel seismic reflection profiles from the Orphan Basin and Flemish Cap to explain the opening of the NE Newfoundland Basin. They constructed a velocity model using 15 ocean bottom seismometers encompassing a considerable portion of the 400 km wide stretched continental crust which shows no evidence for the presence of a 5 km thick, 7.35 km s^{-1} layer modeled from an earlier experiment which is interpreted as magmatic under-plating (Keen and Barrett. 1981). Furthermore, their model illustrates that thinned continental crust extends seaward for ~360 km without under-plating, which in turn suggests non-volcanic rifting for the NE Newfoundland margin. They proposed that continental stretching continued from ~180 Ma to ~101 Ma when the final breakup between Canada and western Europe occurred, leaving a 400 km wide zone of thinned continental crust underneath the shelf and deep water area of the Orphan Basin. They also showed a zone of very thin (6-8 km) crust landward of the basin and suggested this to be a failed rift center formed as a result of the northward progression of non-volcanic rifting between Canada and Europe. They documented the presence of a sub-Moho reflector, and suggested that it indicates generally uniform stretching of the crust and upper mantle, and the absence of volcanics and under-plating is in contrast to the observations on related rift basins of the Grand Banks.

The uncertainties in the chronology of the successions imaged in deep basinal setting preclude a firm interpretation to be made regarding the presence of Triassic to Early Jurassic sediments in the Orphan Basin, as well as the amount of growth in the

faults bounding the horsts and graben. However, the hanging walls of several major faults, such as the faults associated with the Bonavista Fault Zone, as well as the White Sail Fault Zone, contain 1500-2500 ms thick successions, deposited above the pre-rift basement. In these areas, seismic correlation and several exploration wells show that the upper portion of this 1500-2500 ms thick succession is Late Jurassic age (e.g., Figs. 5.2, 5.3). Thus, it is conceivable that this thick succession contains Early Jurassic and older sediments.

In the southern and central portions of the Jeanne d'Arc Basin a NE-trending half-graben developed on the hanging wall of a major detachment basin-bounding fault, referred as the Murre-Mercury Fault system, with its associated antithetic and synthetic faults. Along the southeastern Jeanne d'Arc Basin, the Voyager Fault is also initiated at the first rifting. Further to the north in the Orphan Basin, the Bonavista and White Sail Fault Zones, as well as several large faults paralleling the White Sail Fault Zone (see Chapter 4) also developed during Late Triassic-Early Jurassic rifting phase, probably as a series of *en échelon* faults. This interpretation is based on the assumption that the 1500-2500 ms thick package of Unit C that occurs above the Paleozoic basement within the hanging walls of these faults contains Early Jurassic and possibly Triassic sediments. It is interpreted that both, the Bonavista and the White Sail Fault Zones and many associated faults constitute a series of crustal-scale, thick-skinned, east-dipping listric normal faults which sole deep into the crust. With the continuation of rifting during this initial rift stage, numerous antithetic and synthetic faults developed defining the flanks of a series of northeast-southwest trending horst and graben structures

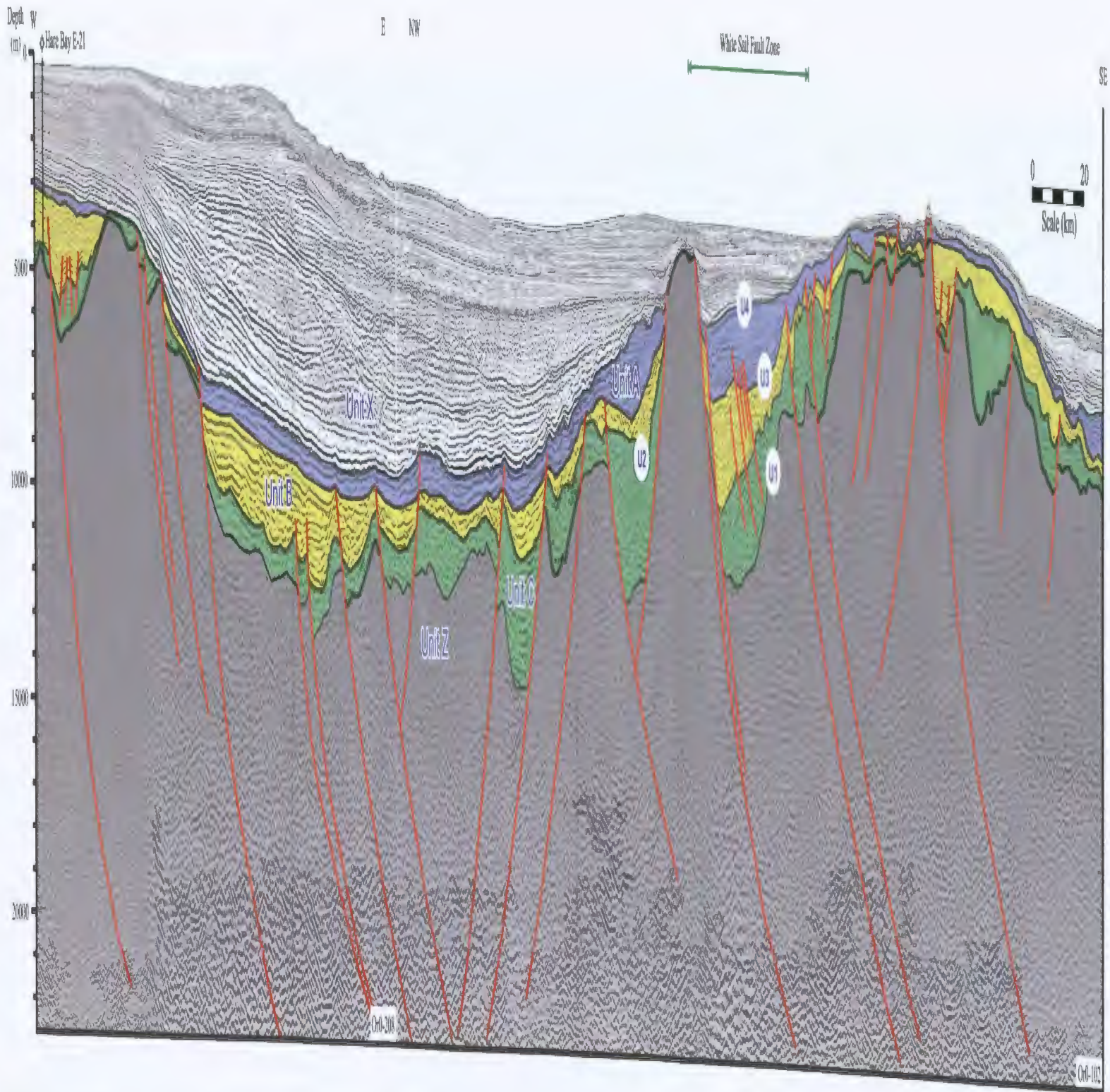


Figure 5.2. Depth converted regional composite seismic reflection profile A, across the Orphan Basin and environs, showing the hanging walls of several major faults, such as the faults associated with the White Sail Fault Zone (discussed in Chapter 4), were re-activated, as indicated by the development of growth strain in the Unit A, B and Unit C. Tilting of the Jurassic successions toward the fault planes suggest that the Orphan Basin continued to extend during this interval, causing significant rotation and tilting of the fault blocks and their sedimentary packages. Locations of the well Hare Bay E-21 and the composite seismic reflection profile are shown in Figure 4.5. Vertical scale given in depth (m).

(i.e., the ridges and troughs described in Chapter 4). These major faults must sole deep into the detachment surface.

During this extensional stage, the rifting propagated from south to north creating a numerous of NNE-SSW-trending basin-bounding faults. Regional mapping of the faults imaged in seismic reflection profiles from the Orphan Basin shows that the Bonavista Fault Zone defines a concave to the east map trace, which shows a very abrupt eastward swing near the boundary between the Orphan Basin and the Jeanne d'Arc Basin. The swing occurs within a narrow west northwest-east southeast trending belt of basement highs, and appears to sinistrally offset the Bonavista Fault Zone in the north from the Mercury Fault Zone in the south by approximately 45 km. This belt is also recognized by Welford and Hall (2007), where the authors used 3-D gravity inversion to suggest that the belt (referred to as the Cumberland Belt) represents a previously unrecognized structure that may form part of an extensive failed rift along the southern margin of the Orphan Basin. Cumberland Belt as a structural unit was first defined by Enachescu (1987) but its gravity and magnetic field expression was known from previous work. In this study, this narrow belt is interpreted to represent a prominent sinistral strike-slip zone, offsetting the Orphan Basin from the Jeanne d'Arc Basin (Fig. 5.4), which is not incompatible with the failed rift model proposed by Welford and Hall (2007). Comparison of the fault map from the Jeanne d'Arc Basin shows that there are several smaller but similar trending sinistral strike slip zones. For example, the narrow zone offsetting the Mercury Fault Zone from the Murre Fault Zone (i.e., the Nautilus Fault Zone; Fig. 5.4), and the zone that offsets the Murre Fault Zone in southern Jeanne d'Arc Basin (i.e., the Egret Fault

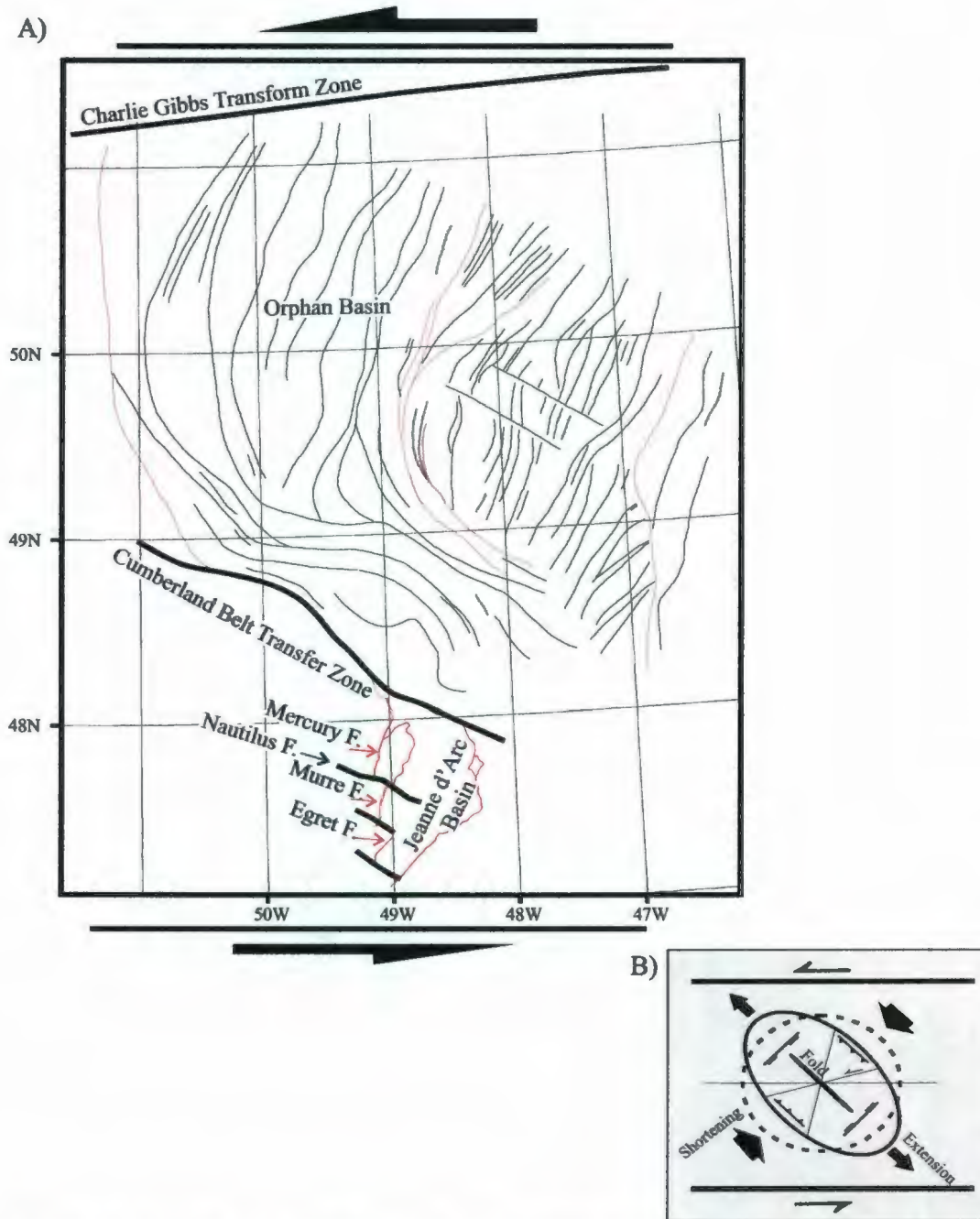


Figure 5.4. A) The schematic structural model showing the presence of two crustal scale, sinistral, strike-slip transfer zones, Cumberland Belt Transfer Zone and Charlie Gibbs Transform Zone, associated major faults across the Orphan Basin and several smaller but similar trending strike slip faults across the Jeanne d'Arc Basin. B) The angular relations between structures that tend to form sinistral simple shear under ideal conditions (modified after Wilcox et al., 1973)

Zone). Thus, the basins evolving during this early rift phase must have been partially separated from one another by regional strike-slip transfer faults (Fig. 5.4).

5.1.1.2. Uplift and Erosion (Early Jurassic)

The above period of crustal attenuation and initial basin formation was followed by the Early Jurassic (i.e., mid-Pliensbachian) break-up of the North American and African Plates. The break-up is associated with a protracted uplift and the ensuing erosion, which resulted in the development of a prominent unconformity on the Scotian shelf, as well as on the southern portion of the Jeanne d'Arc Basin (Sinclair, 1988).

Enachescu et al. (2005) stated that "... the East Orphan Basin contains a complete Jurassic sequence and possibly older sediments. Consequently, the basin is part of the initial Late Triassic-Early Jurassic intra-continental rift zone that scarred the Pangea supercontinent". The present study confirms some of the findings of Enachescu et al. (2005) but further suggests that the West Orphan Basin might contain a near complete Jurassic and possibly older successions. It is important to note that seismic reflection profiles from the Orphan Basin show no unequivocal evidence for the mid-Pliensbachian unconformity. Lower Jurassic successions are not encountered in any of the exploration wells drilled within the Orphan Basin. Therefore, the presence of the mid-Pliensbachian break-up unconformity cannot be confirmed in the Orphan Basin. There are two possible interpretations for the lack of the mid-Pliensbachian unconformity in the Orphan Basin:

- it may indicate that the region was not yet opened during the Triassic and Early Jurassic. However, this is contrary to the seismic stratigraphic data presented in this study, which show the presence of a 1500-2500 ms thick Jurassic and older successions within the hanging walls of many basin-bounding faults.
- it may suggest that an unknown thickness of Triassic to Early Jurassic succession was deposited but was subsequently completely eroded during the mid-Pliensbachian. This interpretation requires that the surface of the unconformity must have been deflated to coincide exactly with the top of the Paleozoic basement non-conformity. This option also does not seem very plausible for the following reasons. If the Orphan Basin had already opened by the early to mid-Pliensbachian, then the region is expected to have a prominent topography created by the tectonism associated with the early rifting. It is known that unconformities tend to preferentially erode the crests of existing topographic highs, leaving the successions in deeper basinal settings relatively unaffected. Therefore, the mid-Pliensbachian unconformity would have been visible in the seismic reflection profiles along the margins of the deep depressions, becoming conformable toward the center of the basins. The Jurassic and possibly older successions within the fault blocks are not well imaged, and often show poorly imaged, discontinuous and fuzzy reflections, making the identification of the unconformity very difficult.

The author believes that the Orphan Basin was formed during the Late Triassic – Early Jurassic rifting, and that future exploration wells from deep basins will provide the much needed data to confirm or deny the existence of Early Jurassic and possibly

Triassic successions in the Orphan Basin. The possible occurrence of stratified evaporates within the central portion of the Orphan Basin (see Chapter 3) and the suggestion of stratified evaporates in East Orphan Basin (Enachescu et al., 2005) similar to sequences encountered in the conjugate Porcupine Basin await confirmation by exploration drilling. If confirmed, these will provide unequivocal evidence for the Late-Triassic to Early Jurassic stretching of the Orphan Basin area.

5.1.1.3. Postrift (Early Jurassic – mid-Jurassic)

Following the initial rifting episode, the Orphan Basin and environs experienced a period of sustained regional thermal subsidence. Associated with this subsidence a thick package of possibly Jurassic rocks was deposited in the evolving half-grabens. Prominent growth stratal wedges observed in Unit C in the hanging walls of the fault blocks suggest that these faults were active and tectonic activity continued throughout the post rift interval. Tilting of the Jurassic successions toward the fault plane observed within these fault blocks indicates that the Orphan Basin continued to extend during this interval, causing significant rotation and tilting of the fault blocks and their sedimentary packages (Figs. 5.2, 5.3, 5.5-5.7). Two distinctly different styles of rotation are observed in the Jurassic successions of Unit C. One style involves the tilting of the fault blocks toward the fault plane, with growth strata developed within the hanging walls (e.g., Fig. 5.7, the Blue H-28 structure). Another style involves a wholesale rotation of the entire hanging wall succession with little evidence for growth development (e.g., Fig. 5.7, the rotated block in the east). The latter resembles in structural architecture and stratigraphic

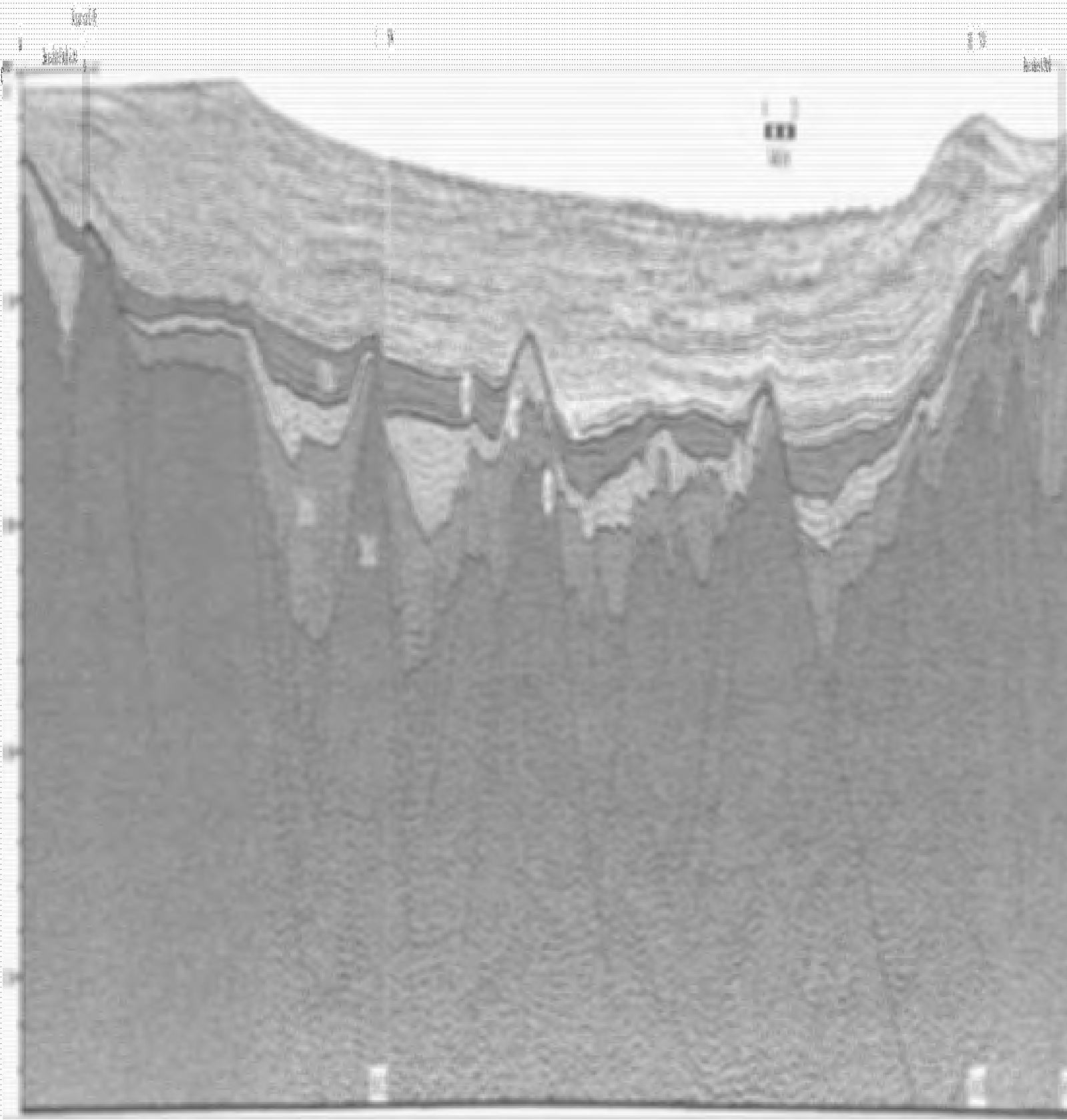


Figure 8. A geological cross-section showing sedimentary layers. The top part shows a relatively flat surface with some small structures. Below, the layers are folded into a series of downward-pointing, rounded folds. The layers are clearly defined by their varying shades of gray, indicating different rock types or sedimentation stages. The overall structure is a classic example of a synclinal fold.

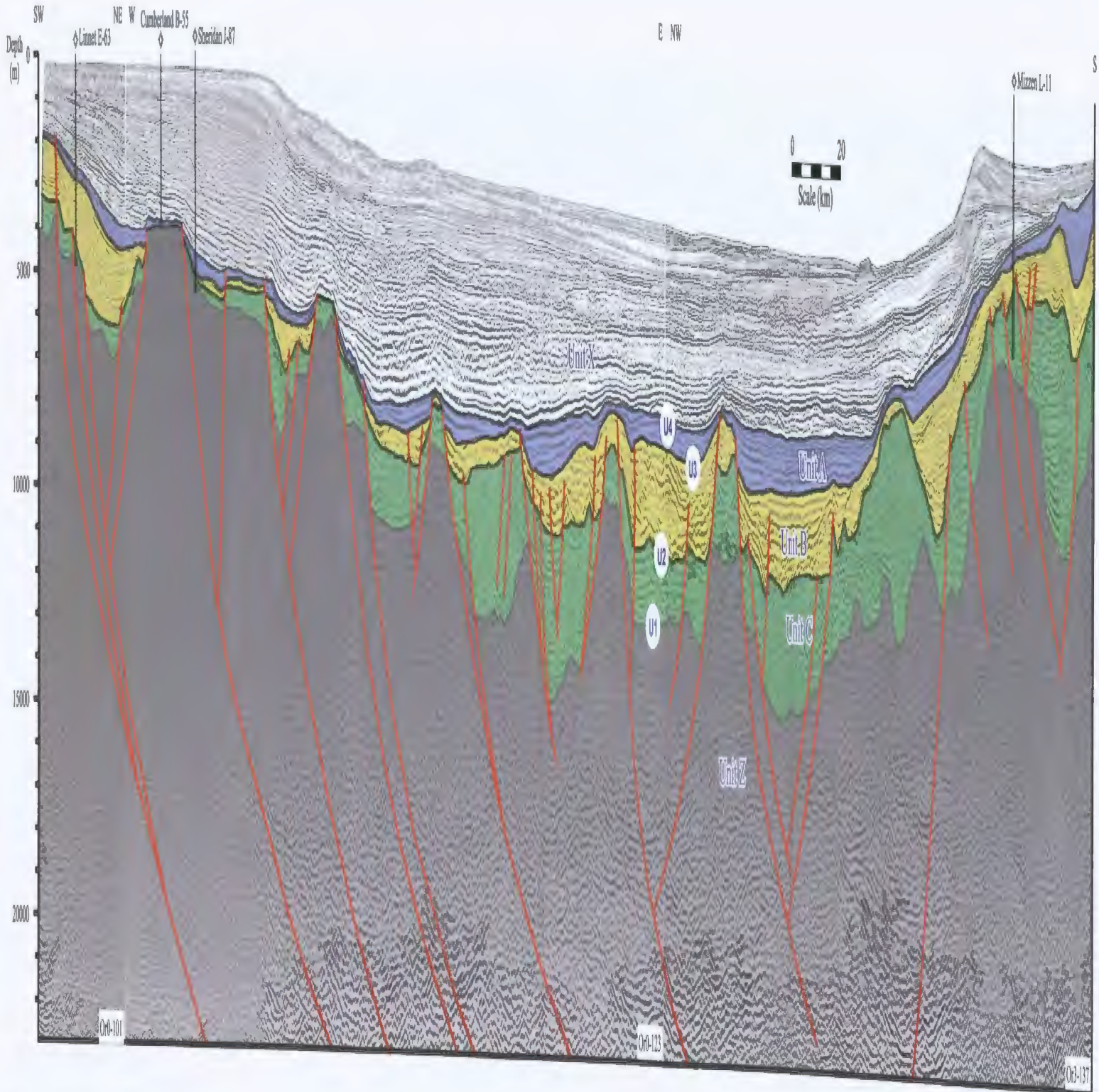


Figure 5.6. Depth converted regional composite seismic reflection profile D, across the Orphan Basin and environs, showing the hanging walls of several major faults (discussed in Chapter 4), were re-activated, as indicated by the development of growth strata in the Unit A, B and Unit C. Tilting of the Jurassic successions toward the fault plane suggest that the Orphan Basin continued to extend during this interval, causing significant rotation and tilting of the fault blocks and their sedimentary packages. Locations of the wells Linnet E-63, Cumberland C-55 and Sheridan L-87, Mizzen L-11 and the composite seismic reflection profile are shown in Figure 4.5. Vertical scale given in depth (m).

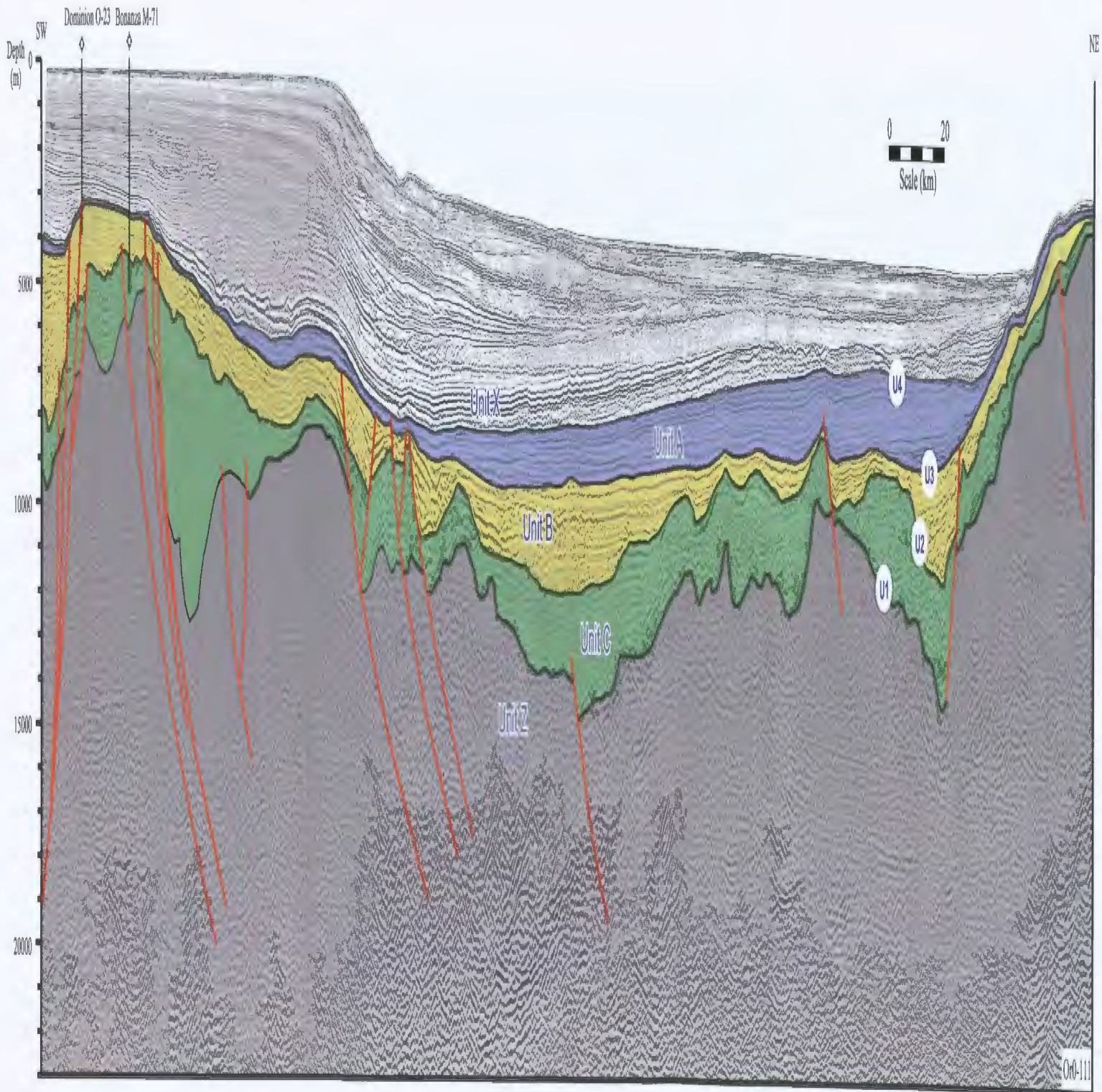


Figure 5.7. Depth converted regional composite seismic reflection profile E, across the Orphan Basin and environs, showing the hanging walls of several major faults (discussed in Chapter 4), were re-activated, as indicated by the development of growth strata in the Unit A, B and Unit C. Tilting of the Jurassic successions toward the fault plane suggest that the Orphan Basin continued to extend during this interval, causing significant rotation and tilting of the fault blocks and their sedimentary packages. Location of the wells Dominion O-23, Bonanza B-27 and the composite seismic reflection profile is shown in Figure 4.5. Vertical scale given in depth (m).

style the Flying Foam structure of the northwestern Jeanne d'Arc Basin, and exemplifies the magnitude of the block rotation that occurred in the Orphan Basin.

5.1.2. Phase II

5.1.2.1. Rifting (Late Jurassic – Early Cretaceous)

The period of prolonged regional thermal subsidence was interrupted by the uplift and ensuing erosion associated with the second phase of rifting. The Top Jurassic Unconformity marks the transition from the postrift of Phase I to the rift of Phase II. Previous studies show that during the Late Jurassic-Early Cretaceous, the NW-SE-oriented extension that prevailed during Phase I deformation was replaced by a predominantly E-W extension in the Jeanne d'Arc Basin (Enachescu, 1987). This phase of deformation resulted in the development of a series of mainly N-S-trending normal faults. The mid-Kimmeridgian unconformity marks the initiation of the Avalon Uplift and renewed E-W extension in the Jeanne d'Arc Basin (Sherwin, 1973; Jansa and Wade; 1975; Sinclair et al., 1994).

In the Orphan Basin, the Phase II rifting is marked as a significant tectonic episode, when the pre-existing NNE-SSW trending tectonic elements were re-activated, as indicated by the development of growth strata in the lower portion of Unit B (Figs. 5.2, 5.3, 5.5-5.7). The Top Jurassic (i.e., Tithonian) Unconformity is a widespread seismic marker separating Unit C below from Unit B above (Figs. 5.2, 5.3, 5.5-5.7). The prominent growth strata wedges imaged within the hanging walls of many major faults

suggest that the initial faults developed during Phase I rifting were reactivated during the second phase of rifting. However, the internal seismic stratigraphic architecture of Unit B is somewhat dissimilar to that of Unit C in that the top of Unit B does not display strong evidence for tilting, thus, shows little evidence for rotation of the fault blocks during this time (Figs. 5.2, 5.3, 5.5-5.7). Several new faults developed during this rifting phase, which are characterized by little to no growth in Unit C strata, but variable growth in Unit B strata.

During this period several north-plunging valleys developed in the southern portion of the Jeanne d'Arc Basin, variably cutting into the underlying Rankin Formation (e.g., Gambo N-70 well; Swift and Williams, 1980; Enachescu, 1993, Sinclair et al., 1994). The horsts and graben that initiated in the Orphan Basin during the Phase I rifting, became prominent during the Late Jurassic-Early Cretaceous (i.e., the basins and ridges described in Chapter 4). However, the data from the Orphan Basin show no evidence for the Jurassic successions being incised by large paleovalleys, as in the southern portion of the Jeanne d'Arc Basin.

Thick siliciclastic successions were deposited in evolving half graben in many basins along the entire Grand Banks of Newfoundland, including the Jeanne d'Arc Basin (McAlpine, 1990, Enachescu, 1992), as well as the Orphan Basin (this study). In the Jeanne d'Arc Basin, the mainly Neocomian tectonic activity was also affected by the initiating of northwest-trending Labrador rift and the associated volcanic activity (Hubbard et al., 1985; McAlpine, 1990).

5.1.2.2. Uplift and Erosion (mid-Valanginian – mid-Aptian)

The second episode of rifting between the North American and European Plates occurred in the latest Jurassic – Early Cretaceous (i.e., Neocomian). In the Jeanne d'Arc Basin, the end of this period is represented by the Mid-Cretaceous Unconformity. In the Orphan Basin, this unconformity is represented by a moderately strong reflector within Unit B. Only a limited number of seismic profiles show any evidence for this unconformity surface. For example, in Figures 5.7 and 5.8 the surface of unconformity is marked by a mild onlap of the overlying succession only within the central portion of the Orphan Basin. Traced toward the ridges and the eastern and western margins of the basin, the reflector defining the unconformity is truncated by the Mid-Cretaceous (i.e., the Cenomanian) Unconformity. Whereas, in many seismic reflection profiles, the reflector defining the surface of this unconformity appears perfectly conformable (e.g., Figs. 5.7, 5.9). This unconformity is not mapped across the entire study area.

Correlations with the sedimentary successions drilled in the exploration wells suggest that the surface of the unconformity and its correlative conformity is broadly Valanginian-Aptian in age. A recent M.Sc. thesis at Memorial University of Newfoundland, also reports the occurrence of this unconformity in other parts of the Orphan Basin (i.e., the K2 unconformity of Hardy, 2007). In this study, the mild unconformity surface U2 (top Jurassic and/or Tithonian Unconformity) is correlated with the episode of uplift and erosion associated with the break-up between the North American and European Plates in the latest Jurassic to Early Cretaceous, and defines the

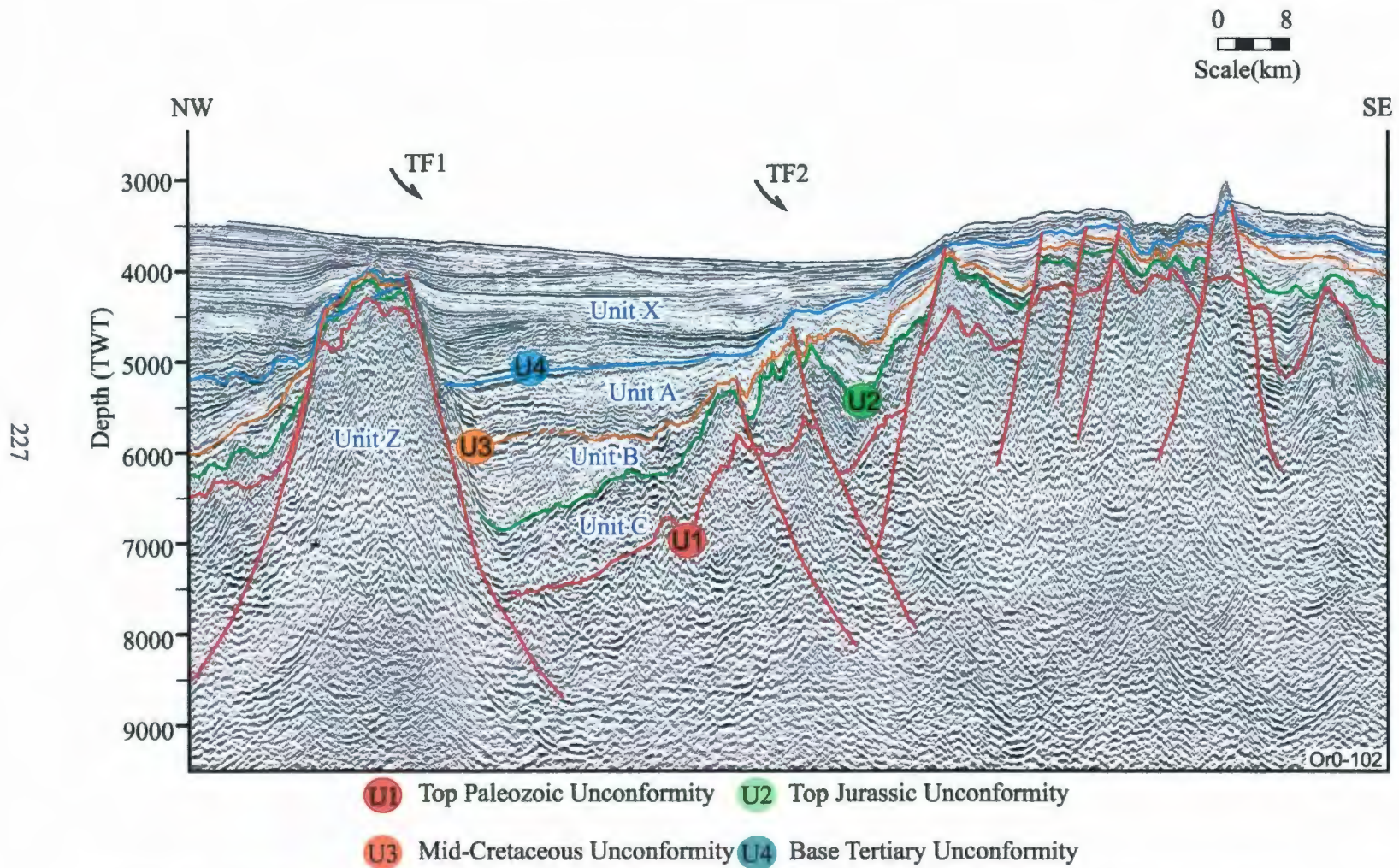


Figure 5.8. Multichannel seismic reflection (OR0-102) profile showing significant growth within the Unit A (Early Cretaceous) and Unit B Late Cretaceous on the hanging walls of TF1 and TF2. Location shown in Figure 4.5.

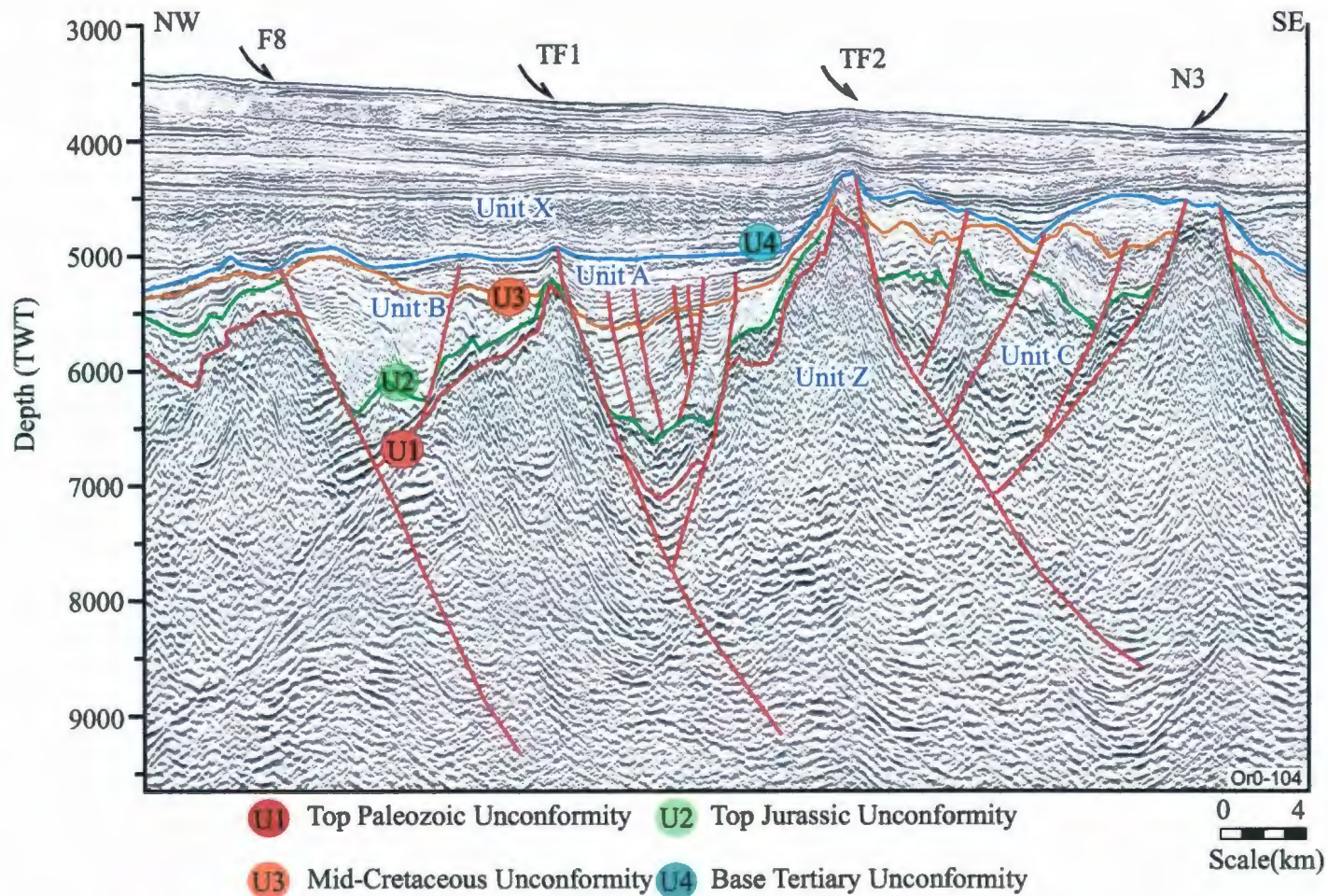


Figure 5.9. Multichannel seismic reflection (OR0-104) profile showing remarkable growth stratal wedges on the hanging walls of major listric faults; TF1, TF2, N3 and F8. Note the presence of large amounts of rotation and tilting of the growth strata wedges. Location of the seismic profile shown in Figure 4.5.

separation between the rift and postrift phases. Additional exploration wells and their biostratigraphic dating are needed to delineate the duration of the hiatus represented by this unconformity.

5.1.2.3. Postrift (Early Cretaceous – Valanginian to Aptian)

The postrift phase lasted from the Valanginian to Albian and is represented by the deposition of mixed siliciclastic- and carbonate-dominated successions in the Jeanne d'Arc Basin (Enachescu, 1987; Sinclair et al., 1994 and Driscoll et al., 1995). In the Orphan Basin, many of the faults, which were active during the preceding Late Jurassic- Early Cretaceous rifting, became inactive during the postrift period. Yet, several faults retained their tectonic activity as indicated by the growth strata wedges developed within the upper portion of Unit B.

5.1.3. Phase III

5.1.3.1. Rifting (mid-Cretaceous – Albian to Aptian)

The above phase of basin subsidence was followed by the onset of the Phase III rifting, which culminated in the eventual break-up of Iberia and the Grand Banks starting in the southern Grand Banks (e.g., Tail of the Bank, Carson, Bonniton basins) during the mid-Valanginian (Enachescu, 1986 and 1987; Sinclair, 1988), moving northward into the Jeanne d'Arc during the mid-Aptian (Jansa and Wade, 1975; Wade, 1978; Hubbard et al., 1985; Hubbard, 1988; Tankard and Welsink, 1987, 1989; Tankard et al., 1989; Hiscott et al., 1990; McAlpine, 1990; Driscoll et al., 1995). The final break-up is associated with a

period of regional uplift and erosion, resulting in the development of a prominent unconformity in the Albian/Aptian in the Jeanne d'Arc Basin, which is referred to as the Avalon Unconformity or the Mid-Cretaceous Unconformity (Koning et al., 1988 and Enachescu et al., 2005). In the Orphan Basin, the regional Mid-Cretaceous Unconformity is also a prominent marker, but it occurs mainly in the Cenomanian, suggesting a diachroneity of approximately 15-20 Ma in tectonics and sedimentation between the Jeanne d'Arc and Orphan Basins.

In the Jeanne d'Arc Basin, the Late Barremian/Early Aptian unconformity marks the onset of the third phase of rifting (Driscoll et al., 1995). In the Late Barremian, the E-W directed extension was replaced by the NE-SW directed extension, creating a transtensional regime in the Jeanne d'Arc Basin (Enachescu, 1988; Tankard and Welsink, 1989; Sinclair 1993, Sinclair et. al., 1994). The NW-SE trending trans-basin faults developed as a result of this transtensional regime in the mid-Aptian-late Albian, and created numerous smaller subbasins and intervening ridges. By the end of the Cretaceous, rifting propagated to the northeast and then to the northwest into the Labrador Sea (Sinclair, 1988; Enachescu et al., 2005).

In the Orphan Basin, the Phase III rifting is clearly documented as a significant tectonic episode, when most of the pre-existing tectonic elements were re-activated as NNE-SSW trending structures, as indicated by the development of prominent growth strata wedges in the upper segment of Unit B (Figs. 5.2, 5.3, 5.5-5.7). During this period, Orphan Basin became wider, as shown by the rotation and tilting of many of the fault

blocks. Several new faults developed during this time, particularly within the central portions of deeper basins. These faults show no growth in Units C and lower Unit B, but mild growth in the upper portion of Unit B and the entire Unit A. Careful mapping of structures in Orphan Basin shows that there is no difference in the orientation of the faults exhibiting growth strata wedges in Units C, B or A. The overall NNE-SSW orientation of the faults in Orphan Basin suggests that the region experienced a predominantly ESE-WNW extension, which is broadly similar to the E-W extension observed in the Jeanne d'Arc Basin during the pre-Late Barremian. The data and fault mapping in the Orphan Basin do not favour a switch in the orientation of the tectonism from a predominantly E-W directed extension to a NE-SW directed extension as observed in the Jeanne d'Arc Basin to the south.

5.1.3.2. Postrift (Late Cretaceous – Paleocene)

The last phase of thermal subsidence occurred in the Late Cretaceous-Paleocene. It represents the transition from rift to drift processes. The Late Cretaceous and Base Tertiary unconformities observed in the Jeanne d'Arc Basin were developed as a response to the break-up between Labrador and Greenland and Greenland and northern Europe (McAlpine, 1990). The regional, Base Tertiary Unconformity overlies the Dawson Canyon Formation. Increased thermal subsidence in the Tertiary caused the tilting of the basin and resulted in the thickening of the postrift succession toward the northern Jeanne d'Arc Basin (Enachescu, 1987; Sinclair et al., 1992).

In seismic reflection profiles from the Orphan Basin, the Base Tertiary Unconformity occurs as a prominent marker showing mild erosion of the underlying Cretaceous successions of Unit A and onlap/downlap of the overlying Tertiary successions of Unit X (Figs. 5.2, 5.3, 5.5-5.7). Unlike the Late Cretaceous and Base Tertiary unconformities observed in the Jeanne d'Arc Basin, only the Base Tertiary Unconformity is identified in the Orphan Basin. There are several potential explanations for this observed discrepancy:

- During the Late Cretaceous, the entire region may have had a north-directed tilt, leaving the Jeanne d'Arc Basin sub-aerially exposed, but the Orphan Basin below the depositional base. Thus, an unconformity developed in the Jeanne d'Arc Basin, while the Orphan Basin received uninterrupted sedimentation;
- Alternatively, both the Late Cretaceous and Base Tertiary unconformities were developed in the Jeanne d'Arc and Orphan Basins. However, the Base Tertiary Unconformity in the Orphan Basin may have decapitated a much thicker succession, removing all the evidence for two separate unconformities.
- It is also conceivable that the Late Cretaceous Unconformity in the Jeanne d'Arc Basin may have been a very local and regionally restricted event.

Additional chronostratigraphic data are needed from both basins to resolve this issue.

The Tertiary represents a tectonically quiet period; with readjustment of minor small block and minor halokinetic movements, and fault rejuvenations associated with compaction (McAlpine, 1990).

5.2. Tectonic Model of the Flemish Cap Rotation

The seismic and exploration borehole data suggest that the tectonic evolution of the Orphan Basin is associated with a protracted ESE-WNW extension between the broadly NE-SW trending Charlie-Gibbs Fracture Zone in the north and the similarly trending Cumberland Belt Transform Zone (Figs. 5.4, 5.10). The Charlie-Gibbs Fracture Zone and Cumberland Belt Transform Zone are transfer zones (e.g., Welsink et al., 1989; Tankard et al., 1989; Enachescu et al., 2004a; Welford and Hall, 2007) bounding the northern and southern margins of the Orphan Basin, respectively. The present study suggests that both transfer zones must have considerable sinistral strike-slip components. Thus, the Orphan Basin appears to be a large extensional basin developed between two major crustal-scale transfer faults. The predominantly NNE-SSW ($\sim 020^\circ$) trending extensional faults which define the primary architecture of the basins and ridges in Orphan Basin (see Chapter 4) form an acute angle of $\sim 45^\circ$ with the broadly NE-SW trending ($\sim 065^\circ$) transfer faults, confirming that the Orphan Basin developed as an extensional basin between the Charlie-Gibbs Fracture Zone and the Cumberland Belt Transform Zone (Fig. 5.4).

The separation between Orphan Basin and Flemish Cap started in Late Jurassic-Early Cretaceous. Reconstructions based on magnetic and gravity data suggest that the

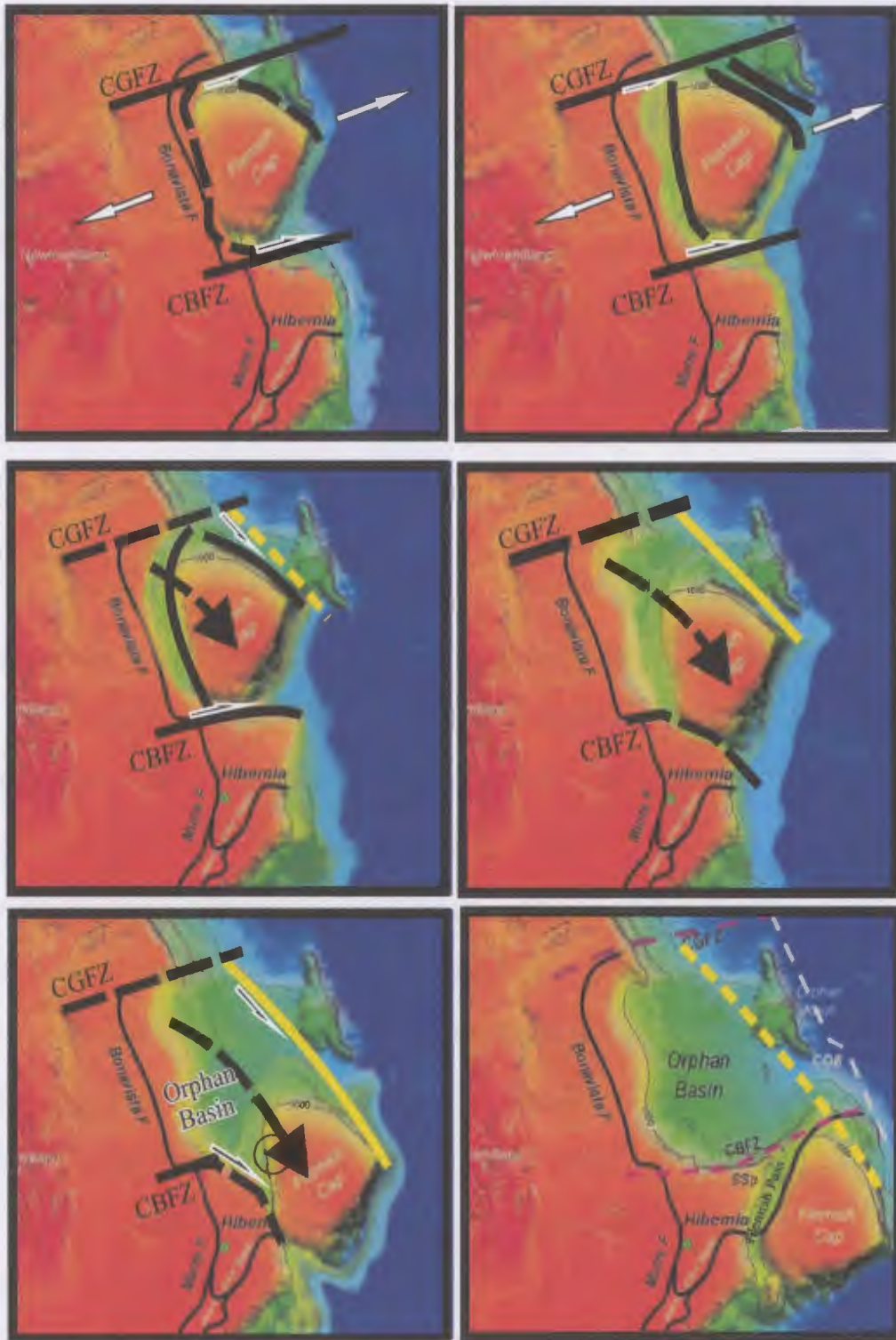


Figure 5.10. Schematic reconstruction model of the separation of the Flemish Cap from Orphan Basin. Note the presence of two major transfer zones accommodating the southeast migration and clockwise rotation of the Flemish Cap. The 1000 m-interval bathymetric contours shown in black. Tectonic framework from Enachescu et al., 2004a and bathymetry from Tucholke et al., 2004.

Flemish Cap was nestled within the Orphan Basin in the Jurassic, and that it began to rotate clockwise and migrate toward the southeast during the Late Jurassic and Early Cretaceous (Srivastava et al., 2000, Enachescu et al., 2005; Sibuet et al, 2007). Three lines of evidence from the Orphan Basin seismic reflection data support this interpretation, as explained below: (i) the geographic position of significant growth in the upper portion of Unit B and the entire Unit A, (ii) the location of the prominent rotation and tilting in the faults showing the above growth, and (iii) the fan-shaped separation of the White Sail Fault Zone from a 5-10 km wide narrow zone in the central Orphan Basin to a 60-75 km wide zone in the northern Orphan Basin.

Examination of the seismic reflection profiles clearly shows that the NNE-SSW trending faults in the northern and northeastern segment of the Orphan Basin exhibit noticeably greater amounts of growth within the entire Units B and A (Figs. 5.2, 5.3, 5.5-5.7). For example, along lines OR0-102, OR0-104 faults labeled as F8, TF1, TF2, N3 show remarkable growth strata wedges on the hanging walls (Figs. 5.8, 5.9). The magnitude of growth in these faults is much greater than that observed in the western and southern portions of Orphan Basin. Similarly, these faults display the largest amounts of rotation and tilting of the growth strata wedges (Figs. 5.8, 5.9). The preferential growth in the faults in the northeastern portion of Orphan Basin, and the significantly larger rotation and tilting collectively imply the greater degree of stretching in the northern and northeastern portions of the Orphan Basin, relative to the southern segment of the basin. The large fan-shaped fault splays coming out of the White Sail Fault Zone, also support the preferential stretching of the northern portion, and further suggest a 25-35° clockwise

rotation. The shape of the Orphan Basin is also distinct in that it is much broader in the north, becoming narrow and tapered toward the southeast. This distinct basin shape also suggests that the northern portion of the basin was subjected to a larger amount of extension.

The separation of the Flemish Cap from Orphan Basin has broad tectonic ramifications. For example, the clockwise rotation and migration of the Flemish Cap necessitates the development of two transfer zones, which must have accommodated the southeast slip of the Flemish Cap relative to the Orphan Knoll to the north and the Jeanne d'Arc Basin to the south (Fig. 5.10). The transfer zone in the northeast, separating the Orphan Knoll from the Orphan Basin and Flemish Cap requires a sinistral system, whereas the zone separating the Orphan Basin from the Jeanne d'Arc Basin must be a dextral system (Fig. 5.10). Of these, the Cumberland Belt Transfer Zone must have acted as the southern transfer zone. However, the displacement between the Bonavista Fault Zone in the north and the Mercury Fault Zone in the south appears to have a sinistral component, with the Bonavista Fault Zone being displaced 75-100 km west of the Mercury Fault Zone (Fig. 5.4). It is possible that the original displacement in the Cumberland Belt Transfer Zone was sinistral during the Triassic-Jurassic, but the system was overprinted with a dextral component as the eastern segment of the transfer zone accommodated the southeast migration and clockwise rotation of the Flemish Cap. The faults associated with the boundary between the Orphan Basin and the Jeanne d'Arc Basin have a predominantly WNW-ESE trend swinging southward to a more NW-SE trend. This architecture suggests that the southeastern portion of the Cumberland Belt

Transfer Zone defined the hard boundary along which the Flemish Cap traveled away from the Orphan Basin into its present day position southeast of the Orphan Basin.

In addition to the above boundary conditions, the wholesale rotation and travel of the Flemish Cap continental fragment from the Late Jurassic to Late Cretaceous requires the development of a crustal-scale detachment across Orphan Basin. It is possible that this detachment lies within the upper crust. For example, within the 9-10 seconds range of the seismic reflection profiles, there is at least one major surface of detachment in Orphan Basin. Most of the listric normal faults mapped in the study area sole into this surface. For example, the fault plane that floors the rotated fault block within the Jurassic succession dips further into the basin and defines a major surface of detachment (i.e., Fig. 5.3.). It is also possible that the detachment lies within the lower crust (?upper mantle), well below the successions imaged in the seismic reflection profiles.

The literature is mute about the eastern margin of the Orphan Basin, particularly the zone along which the inferred sinistral motion of the travel associated with the Flemish Cap has taken place. The present study sheds light to this issue. The structural architecture of the Eastern Basin Margin Province describes a set of prominent broadly N-S trending and mainly west-dipping normal faults (Fig.5.4; also see Chapter 4). These faults show considerable growth in Units B and A. It is speculated that this extensional fault fan defines the western margin of the sinistral strike slip zone that facilitated the southeast relative movement of the Flemish Cap during the Cretaceous.

The above simplistic model requires that there was space in the southeastern regions of the Flemish Cap to accommodate the southeasterly migration of the continental fragment.

5.3. Regional Paleogeography and Sedimentary Evolution

5.3.1. Phase I

5.3.1.1. Rifting (Late Triassic – Early Jurassic)

In the Scotian Basin and the southern portion of the Jeanne d'Arc Basin, this phase of rifting was accompanied by the deposition of fluvial to lacustrine sandstones and mudstones identified as the Eurydice Formation (Jansa and Wade 1975; Enachescu 1987, 1988; Tankard and Welsink 1989; McAlpine, 1990; Driscoll, 1995). As rifting developed, repeated marine incursions occurred from the Tethys Sea, into the rift basins and subbasins and led to the deposition of evaporite successions known as the Argo and Osprey formations (McAlpine, 1990). In the Jeanne d'Arc Basin, this rifting episode was also associated with igneous activity, which resulted in the development of a thin unit of subaerial basalt flows between the Argo and Osprey formations (Mc Alpine, 1990; Pe-Piper, Jansa and Lambert 1992). The interbedded carbonates and evaporites of the Iroquois Formation represent a progressive transition from non-marine to coastal sabkhas, to restricted lagoons and finally to a shallow warm sea in the Early Jurassic (Fig. 5.11.A, B; McAlpine, 1990).

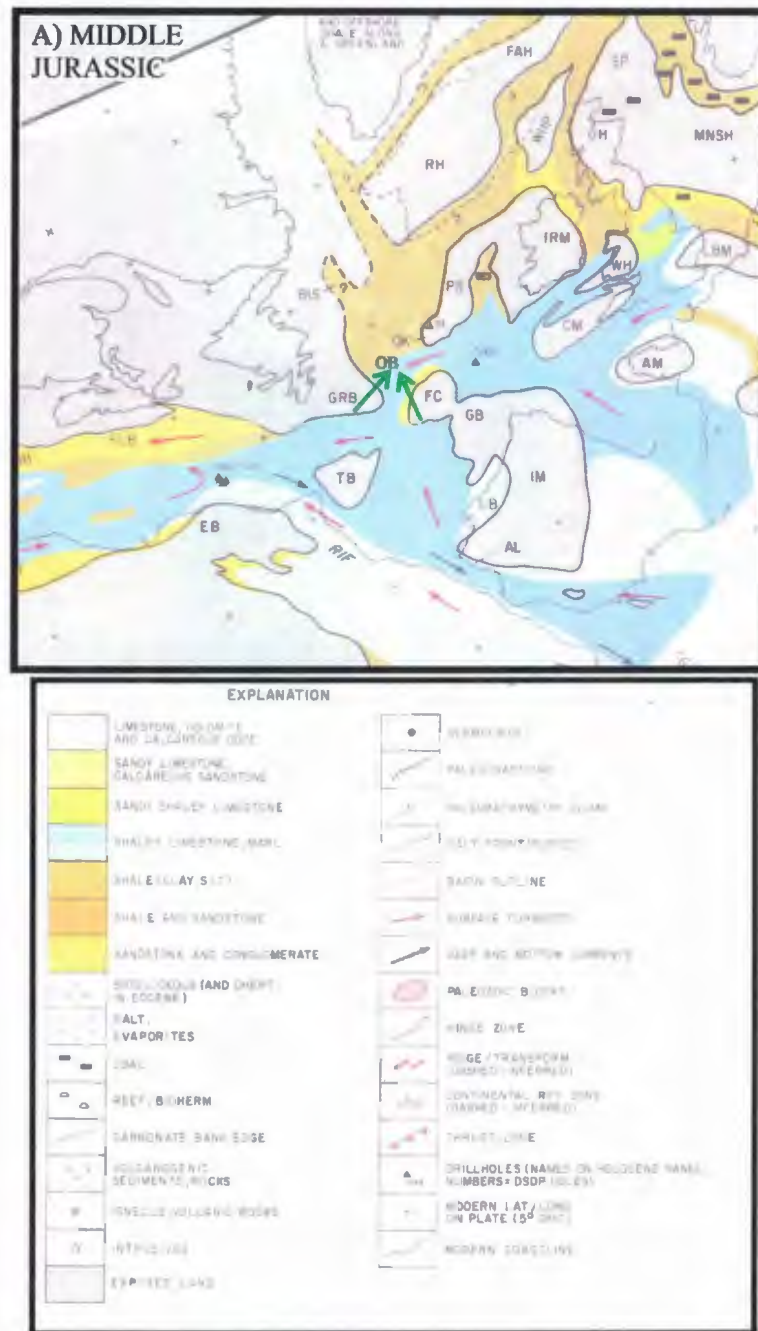


Figure 5.11. A. Lithological - Paleogeographic maps of the north Atlantic East Coast Margin showing the relative position of the paleocontinents, sedimentary deposition, current directions and modern coastline. FC= Flemish Cap, OK= Orphan Knoll, SCB= Scotia Bank, GRB= Grand Banks, PB= Porcupine Basin, IRM= Irish Margin, OB= Orphan Basin. Green arrows show the direction of sedimentary input (modified from Tucholke and McCoy, 1986). See next figures for the later maps.

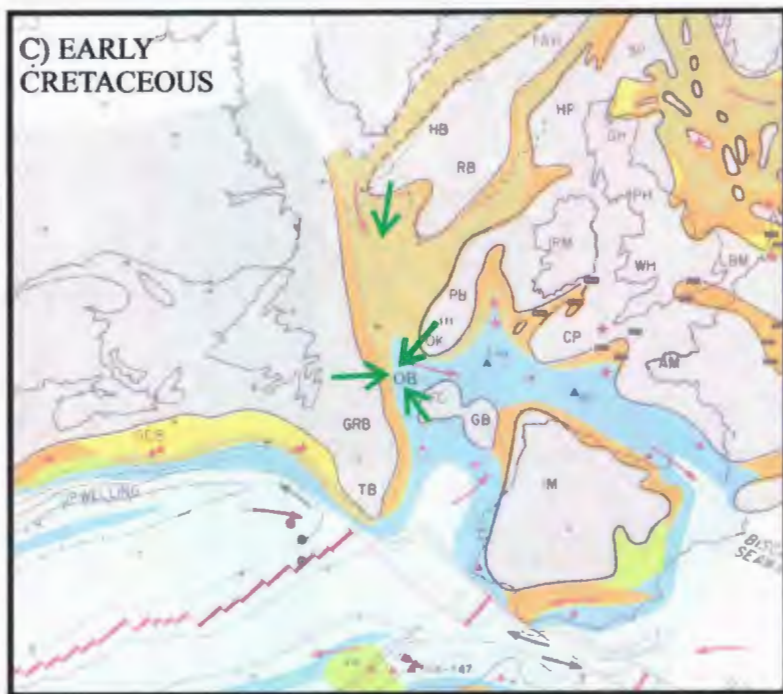
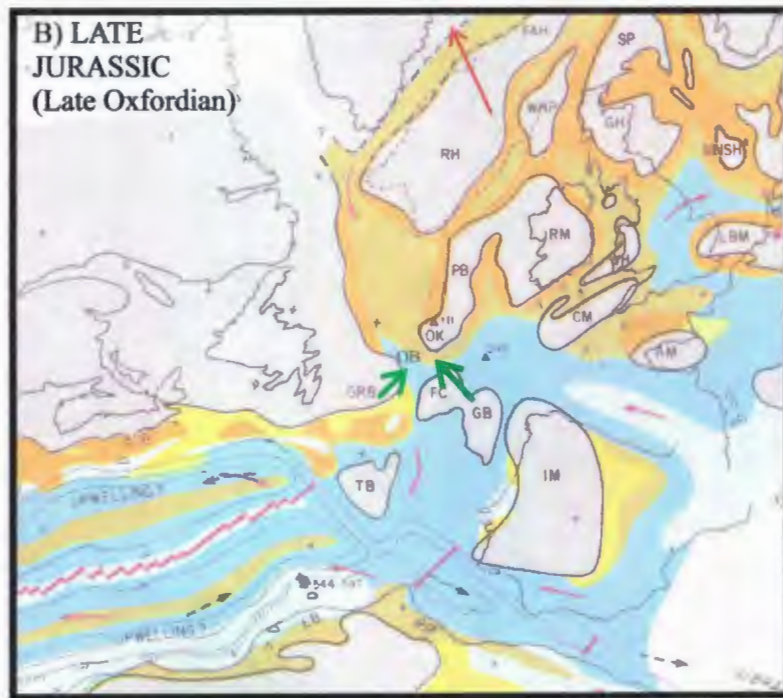


Figure 5.11.B,C. See figure 5.11.A. for the figure caption and details.

Exploration borehole data do not corroborate the presence of any Triassic or Early Jurassic successions in the Orphan Basin. However, seismic stratigraphy show the presence of a thick package of sediments older than Late Jurassic age. The style of tectonism of the sedimentary successions confined to the fault-bounded deep depressions confirm that sequences older than Late Jurassic (i.e., those encountered in the boreholes) are deformed in extensional settings, thus they must be younger than Paleozoic age. Future exploration drilling is needed to confirm (or deny) the existence of Early Jurassic and possibly older successions in Orphan Basin.

5.3.1.2 Uplift and erosion (Early Jurassic)

As discussed in section 5.1.1.2 above, there is no evidence in the seismic reflection profiles for the Early Jurassic (i.e., mid-Pliensbachian) unconformity associated with the break-up of the North American and African Plates.

5.3.1.3 Postrift (Early Jurassic – mid-Jurassic)

During the Early Jurassic, a broadly east-west trending narrow seaway developed between Africa in the south and North America/Europe in the north (Fig. 5.11.A, 5.11.B). From the Early to Late Jurassic (Kimmeridgian), continental-marine sandstones, mudstones, shales and limestones were deposited in this broad epeiric sea in the Jeanne d'Arc Basin (Tankard and Welsink, 1987; Grant and McAlpine, 1990). Here, the Downing Formation was deposited during the Early to Middle Jurassic (Pliensbachian-Callovian, McAlpine, 1990). The Downing Formation consists of marine mudstones and

carbonates deposited in a shallow, low-energy epicontinental environment. The Whale Member of the Downing Formation is a regional limestone unit, which shows a period of quiescence in the progressively deepening marine environment. The Voyager Formation conformably overlies the Downing Formation. It consists of a Late Bathonian-early Oxfordian-age, fine-grained sandstone-shale succession with coal stringers and limestone interbeds, and represents a deltaic near-shore to marginal - marine environment (Bujak Davies Group, 1988 a, b; McAlpine, 1990). The overlying Rankin Formation consists of organic-rich shales, limestones and marlstones, representing a deeper marine environment (McAlpine, 1990). The Egret Member of the Rankin Formation also consists of organic rich-shales and represents a low energy, restricted-marine environment (McAlpine, 1990).

In the Orphan Basin and its environs, the mid to Late Jurassic successions are only encountered in the Mizzen L-11, Baccalieu I-78 and possibly in the Great Barasway F-66 (data not yet released) wells, in addition to the Bonanza B-27 well drilled over the Cumberland Belt Transfer Zone. No well in western Orphan Basin ever encountered sediments of similar age. However, this is not surprising because these three wells are drilled over either roll-over anticlines or the crest of small horst blocks created by faulting of the Jurassic and Cretaceous successions (Units C to A) within NNE-SSW trending basins; whereas many wells in western Orphan Basin such as the Blue H-28, Bonavista C-99, Linnet E-63 are drilled over the crest of basement-cored ridges. Thus, the absence of mid to Late Jurassic successions in the exploration wells drilled in the west does not preclude the existence of this age succession in western Orphan Basin.

Paleogeographic reconstructions based on scanty well data suggest that the siliciclastic successions encountered in the Mizzen L-11 and the Baccalieu I-78 wells originated from a southeasterly and easterly source, possibly located in the Flemish Cap region (Fig. 5.11.A, 5.11.B).

5.3.2. Phase II

5.3.2.1. Rifting (Late Jurassic – Early Cretaceous)

During the Late Jurassic – Early Cretaceous rifting, the northwest trending seaway between the eastern Canadian continental margin and western Europe broadened and received considerable siliciclastic input from the adjacent landmasses (Fig. 5.11.C). Across the Grand Banks of Newfoundland, the Jeanne d’Arc, Fortune Bay and Hibernia formations represent this synrift sequence and contain some of the most important reservoir rocks. During this time, a braid and alluvial plain developed in southern Jeanne d’Arc Basin, leading to the deposition of a coarse siliciclastic succession referred to as the Jeanne d’Arc Formation (Tankard and Welsink, 1987; Grant et al., 1988; Bujak Davies Group, 1988a; Tankard and Welsink 1989; McAlpine, 1990; Sinclair et al., 1994). The maximum flooding surface of the Portlandian transgression defines the boundary between the Jeanne d’Arc Formation and the overlying pro-delta shales and siltstones of the Fortune Bay Formation (Late Tithonian; Posamentier et al., 1988; Sinclair and Riley, 1995). The deposition of the Jeanne d’Arc Formation ceased during the Portlandian transgression (Mackay and Tankard, 1990). The overlying Hibernia Formation thickens toward the north within northerly-trending fault-bounded depressions of the Jeanne d’Arc

Basin (Arthur et al., 1982, Tankard and Welsink, 1987; Brown et al., 1989; Hurley, 1992). It mainly consists of thin, very fine-grained delta-front sandstones and pro-delta siltstone and shale interbeds (Sinclair et.al., 1994).

In the southern Orphan Basin, the Flemish Pass and northernmost portion of the Jeanne d'Arc Basin, the Late Jurassic – Early Cretaceous sediments are recovered in the Baccalieu I-78, Mizzen L-11 and Bonanza B-27 wells. In these wells, the rift successions were represented by the predominantly siliciclastic Rankin and Jeanne d'Arc Formations. Paleogeographic reconstructions show that by the Neocomian, the rift separating North America and Europe extended well into the Labrador Sea, with terrigenous input provided from the adjacent land masses, both from east and west (Fig. 5.11.C). Micropaleontological data from the Rankin Formation and Jeanne d'Arc Formations suggest a middle/inner neritic to lagoonal environment for the southern portion of the Orphan Basin. In the northern and central portions of the Orphan Basin, Late Jurassic – Early Cretaceous sediments are not recovered in the exploration wells. The absence of these successions in the exploration wells drilled exclusively over the crests of structural highs does not preclude their presence in the central and northern Orphan Basin. This interpretation is further corroborated by the seismic stratigraphic correlations (Chapters 3 and 4).

5.3.2.2. Uplift and Erosion (mid-Valanginian – mid-Aptian)

This mid-Valanginian – mid-Aptian uplift and erosion is marked by a mild unconformity in the Orphan Basin, as explained in section 5.1.2.2.

5.3.2.3. Postrift (Early Cretaceous – Valanginian to Aptian)

During Valanginian, the deposition of the B Marker Member marks the initiation of the second thermal phase in the Jeanne d'Arc Basin (Bujak Davis Group, 1988c; McAlpine, 1990). Here, the B Marker Member consists of oolitic/skeletal limestones deposited in a warm and shallow-water environment in the Jeanne d'Arc Basin. The Catalina and Eastern Shoal formations and their distally equivalent Whiterose Formation collectively form a thick, postrift succession above the B Marker Member (Sinclair, 1988; McAlpine, 1990). In the Hibernia Field, the Catalina Formation is dominated by sandstones, shales and calcareous sandstones. It was deposited in an interdistributary bay and shallow marine shoreface environment (Sinclair, 1988; McAlpine, 1990). Elsewhere, siltstones and shales of the Whiterose Formation were deposited. The Eastern Shoal Formation locally overlies the Whiterose Formation, and represents a transgressive, shallowing-upward succession. The development of shallow marine limestones (i.e., A Marker Member) overlaps the postrift succession (McAlpine, 1990).

In the southern and southeastern Orphan Basin, the Early Cretaceous – Valanginian to Aptian postrift episode is represented by the deposition of the Whiterose/Hibernia Upper Zone Equivalent. These successions are drilled in the Kyle L-11, Mizzen L-11 and Baccalieu I-78 wells, where sediments were deposited in a shallow marine setting with sediments probably originating from then emergent Orphan Knoll and Flemish Cap areas (Fig. 5.11.C).

5.3.3. Phase III

5.3.3.1. Rifting (mid-Cretaceous – Albian to Aptian)

In the Jeanne d'Arc Basin, the base of the synrift succession is marked by a regional limestone and calcareous sandstone sequence (i.e., the A Marker Member; Mackay and Tankard, 1990). It is deposited within a shallow marine environment. The stratigraphic position of the A Marker Member is controversial: Sinclair (1988) places the A Marker within the Avalon Formation, whereas McAlpine (1990) places it within the Eastern Shoals Formation. In the western and northern parts of the Jeanne d'Arc Basin (e.g., the Whiterose and Hibernia oil fields), the A Marker occurs above the Whiterose Formation. In the central and southern parts of the basin, a thick succession of oolitic limestone and calcareous sandstone (i.e., A Marker Member) is assigned to the Eastern Shoal Formation (McAlpine, 1990). The succeeding Avalon Formation consists of lagoonal and tidal flat mudstones and fine grained estuarine sandstones. They were deposited during late Barremian to early Aptian time and are associated with a regional uplift of the Atlantic margin (Enachescu et al., 2005) or renewed arching to the southern portion of the Jeanne d'Arc Basin (Sinclair, 1988). The erosion during this uplift (i.e., the Avalon Uplift of Jansa and Wade, 1975; Enachescu, 1987; Sinclair, 1988; Deptuck, 2003) resulted in the development of a widespread angular unconformity known as the Avalon Unconformity or Mid-Cretaceous Unconformity (Koning et al., 1988; Enachescu et al., 2005) or the Late Aptian Unconformity (Mackay and Tankard, 1990; McAlpine,

1990). It is associated with the final continental break-up between the Grand Banks of Newfoundland and Iberia.

No exploration well drilled in the Orphan Basin ever encountered the A Marker Member. However, a number of successions associated with the synrift deposition occur in the region, including the Avalon Formation and the Barremian Shales, which are the distal equivalents of the Eastern Shoal Formation. Based on micropaleontologic studies from exploration wells, a paralic to shallow marine environment for the Avalon Formation and intertidal to marginally marine, deltaic environment for the Barremian Shales are strongly suggested.

In the Jeanne d'Arc Basin, the overlying syntectonic Ben Nevis Formation consists of a fining upward, sandstone-dominated terrigenous sequence (McAlpine, 1990). It is deposited during the late Aptian to late Albian, and represents the last fault-controlled deposition in the Jeanne d'Arc Basin (McAlpine, 1990; Sinclair, 1993; Sinclair et. al., 1994). The Ben Nevis Formation is overlain by the late Albian Unconformity, which marks the end of extensional events (McAlpine, 1990). The shales of the Nautilus Formation are deposited in a low energy, open marine shelf environment (Sinclair, 1988; McAlpine, 1990). In the northeastern portion of the Jeanne d'Arc Basin, the Nautilus Formation is the lateral equivalent of the Ben Nevis Formation, but in the southwestern Jeanne d'Arc Basin, it displays a vertical stratigraphic contact overlying the Ben Nevis Formation.

In the Orphan Basin, the mid-Cretaceous – Albian to Aptian period is represented by the Nautilus Formation. In the Linnet E-63 and Blue H-28 wells, this formation consists of a thick succession of shales with sandstone interbeds, indicating deposition within a shallow marine environment. The predominance of fine-grained sediments and the paucity of sandstones suggest that there were no large point-sources during the deposition of this succession in the immediate surroundings of the Orphan Basin. The relationship between the siliciclastic successions encountered in the Jeanne d'Arc Basin and Orphan Basin is not clear. The Cumberland Belt Zone was developing as a large ridge separating these two basins during this period. It is speculated that this ridge formed a large structural high south of Orphan Basin, preventing large quantities of sediment reaching the Orphan Basin from the sources in the Jeanne d'Arc Basin and environs. It is further speculated that the sediments encountered in the Nautilus Formation must have been supplied from a predominantly northwestern source(s), as also implied by Ziegler (1999; Fig.11.D).

In the Jeanne d'Arc Basin, the Dawson Canyon Formation (Cenomanian to Maastrichtian; Fig. 5.11.E) mainly consists of transgressive marine shales. It includes a limestone unit (the Petrel Member), a shale-prone unit (the Red Island Member), a deltaic sandstone unit (the Otter Bay Member), a shale-dominated unit (the Bay Bulls Member), a sandstone unit (the Fox Harbour Member; Jansa and Wade, 1975; Boudreau et al., 1986; Sinclair, 1988; McAlpine, 1990; Deptuck, 2003). The lateral equivalent Wyandot Formation (Deptuck, 2003) (or Wyandot Member, de Silva, 1993) consists of pelagic chinks and marlstones.

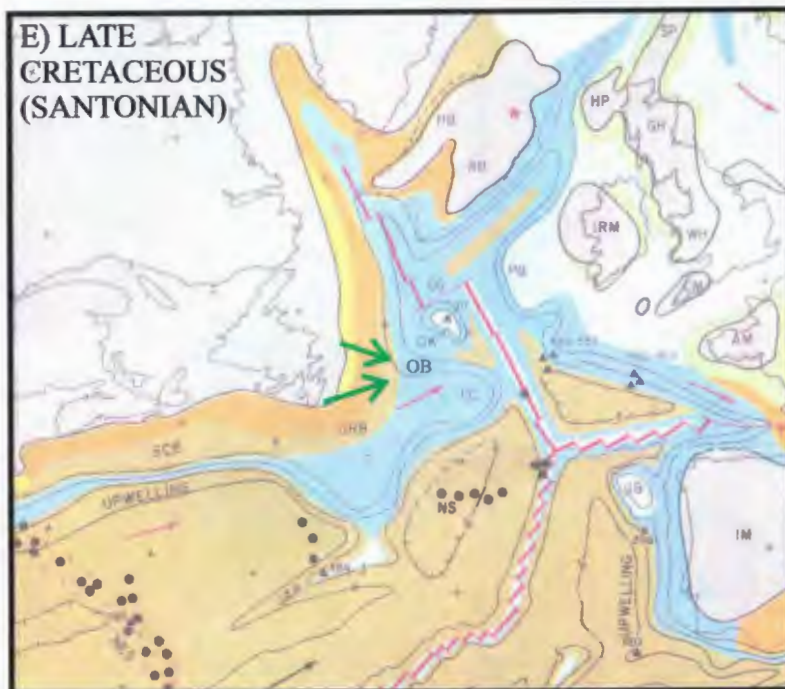
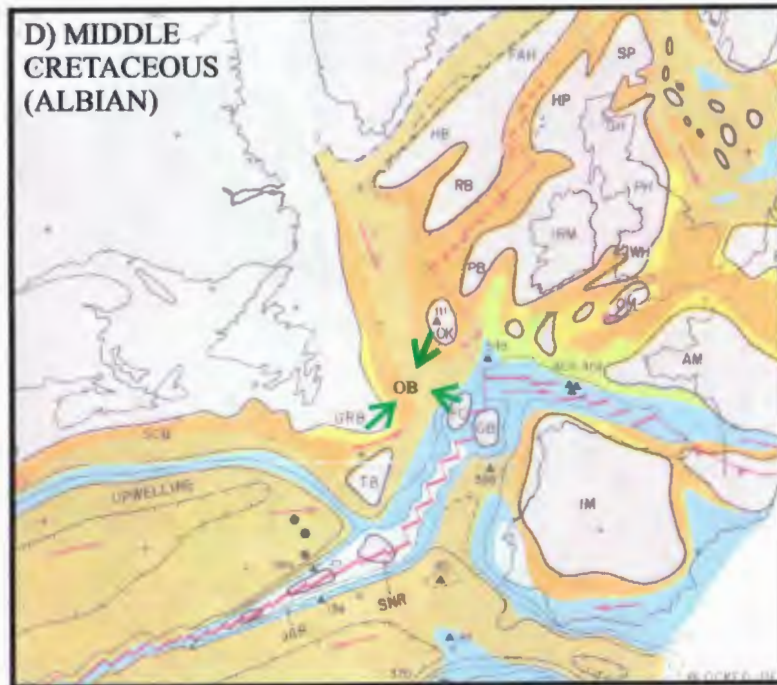


Figure 5.11.D,E. See figure 5.11.A. for the figure caption and details.

In the Orphan Basin the Dawson Canyon Formation is well represented as a medium- to coarse-grained sandstone succession, interbedded with shales and marls. Micropaleontological data, particularly planktonic foraminifera suggest that this succession was deposited in an open shelf and/or deeper slope environment in the northern portion of the Orphan Basin and deltaic with marine influence in the southern Orphan Basin (Fig. 5.11.E; Koning et al., 1988). It is speculated that the coarse-grained siliciclastic sediments were supplied from the west, probably at point sources (such as deltas) flowing east across the Bonavista Platform.

5.3.3.2. Postrift (Late Cretaceous – Paleocene)

The Tertiary marine shale and mudstone sequences form a thick prism along the eastern Canadian continental margin. The Paleocene aged-South Mara Member of the Banquereau Formation contains sandstones and pro-delta turbidites (McAlpine, 1990). In the Grand Banks of Newfoundland and Orphan Basin, the tectonic activity lasted until the Eocene, but the final, long-lasting thermal sag phase continued (McAlpine, 1990; Enachescu et al., 2005). Continued thermal sag phase and seaward tilting of the passive margin led to the deposition of shales, chalks, siliceous mudstones, siltstones and sandstones in the Orphan and Jeanne d'Arc basins (Sinclair, 1988; McAlpine, 1990).

CHAPTER 6. IMPLICATIONS FOR PETROLEUM SYSTEMS

6.1. Foreword

The Newfoundland passive margin includes a series of sedimentary basins situated in shallow to deep water settings. Since the early 70's, the oil and gas industry has had significant interest in this margin, with the exploration efforts gradually shifting toward the deeper water plays during the last two decades. The Orphan Basin is one such basin, with increasing exploration activity; it is situated immediately north of the prolific Jeanne d'Arc Basin. The exploration interest in this basin is stimulated by the recent oil discovery in the adjacent Flemish Pass Basin in the Mizzen O-16 well, and the discovery of potential source rock and oil shows in other wells in this region.

One hundred and thirty three exploration wells were drilled in the offshore Newfoundland and Labrador, and 21 oil and gas discoveries have been reported from various basins. These discoveries suggest the presence of ~ 2.1 billion barrels of oil, 10 trillion cubic feet of natural gas and 450 million barrels of natural gas liquids in this region (C-NLOPB, 2009). In 1979, the Blue H-28 was drilled on the slope of Orphan Basin at a water depth of 1486 m, to a total depth of 6100 m. The well cut through the Paleozoic age pre-rift basement successions, Early Cretaceous (Neocomian) age sandstone dominated strata, Late Cretaceous (Maastrichtian) age shale dominated successions and finally Paleocene age predominantly shale-mudstone strata. It encountered no hydrocarbons and no source rocks. The oil and gas industry regained interest in the deeper, but lesser-explored Orphan Basin and seven additional exploration

wells were drilled over basement-cored structural highs in the western portion of the Orphan Basin between 1974 and 1985. These wells revealed no oil show or source rock, but showed the presence of good potential reservoir rocks with up to 19% porosities in the Linnet E-63, Bonavista C-99 and Blue H-28 wells. The exploration focus shifted recently to the deeper eastern portion of the Orphan Basin. A modern regional seismic grid acquired by GSI comprising over 20,000 km of seismic reflection data, a record land sale in 2003, several large 3D seismic surveys acquired between 2003 and 2006 are the result of the new attention given to deepwater Orphan Basin (Enachescu et al., 2005).

Within the context of this thesis, seismic regional correlations between the Orphan Basin and the Jeanne d'Arc and Flemish Pass basins provide a better understanding of the petroleum system in the study area.

6.1.1. Considerations for the Petroleum System

Paleogeographic reconstructions of the pre-Mesozoic show that the Grand Banks of Newfoundland formed a broad sedimentary platform developed as part of the Appalachian Orogeny. Some of the basins on the Grand Banks of Newfoundland and the Labrador Shelf contain good-quality reservoir rock of Paleozoic carbonates and metasediments, such as seen in the Labrador Basin and western Newfoundland. During the Late Triassic-Early Jurassic, a narrow rift (Tethys Rift) expanded from the Gulf of Mexico to Northern Europe (Enachescu et al., 2005). During the thermal subsidence in Late Jurassic – Early Cretaceous (Atlantic Rift), a shallow sea with euxinic conditions led to the deposition of potential oil source rock along the eastern Canadian continental

margin (See Chapter 5; Powell, 1985). This source rock is known as the Egret Member of the Rankin Formation and is dated as Kimmeridgian.

During Early Cretaceous, shallow marine sandstones with good porosity and permeability were deposited in the eastern Canadian sedimentary basins, including the Orphan, Jeanne d'Arc, and Flemish Pass basins (e.g., Blue H-28). The Late Cretaceous successions drilled in the Bonavista C-99 and Linnet E-6 wells document the reservoir quality sandstones in the Orphan Basin.

6.2. Potential Reservoir Rocks in the Orphan and Flemish Pass Basins

The northeast-southwest trending ridges mapped within the West Basin and Ridge Province and East Basin Province (see Chapter 4) were periodically exposed to subaerial erosion, which locally created coarse siliciclastic sedimentary input into the adjacent, similarly trending troughs and basins. These coarse siliciclastics probably formed basinward-tapering sedimentary wedges. It is possible that these marginal wedges form variable quality reservoir rocks in the Orphan Basin (*sensu lato*). The predominant source of the siliciclastic sediments into the general region of Orphan Basin was land-derived material transported into the basin via major rivers from the south and west (see Chapter 5). These rivers likely formed significant delta sequences along the western and southern fringes of the Orphan Basin, potentially creating reservoir successions in these areas.

6.3. Types of Hydrocarbon Traps

Critical evaluation of individual structures with respect to the presence or absence of closure are not made in this study. However, the ubiquitous occurrence of large horsts, rotated blocks, ridges and their intervening basins (see Chapter 4) offers possibilities for structural closures to exist within the study area. In addition, growth stratal wedges developed on the hanging walls of many listric normal faults, and the rotation and tilting of the successions within the hanging walls have created significant apparent structural closures. Syn-sedimentary, large roll-over structures are also prospective closures (e.g., Great Barasway F-66). These are evident in 2D views, offering the possibility of 3D closures on regional scales. The protracted progressive onlap successions together with pervasive erosional unconformities on basin margins offer numerous regions with potential for stratigraphic traps in the region. All these require a denser data grid than the one used in this study. Careful examination and evaluation of 3D data should prove the structural leads shown in previous chapters.

6.4. Distribution and Maturity of the Source Rock

The presence of oil shows in exploration wells in the Flemish Pass Basin clearly suggests that (i) there exists a local Late Jurassic source rock within the study area, and that (ii) the source rock went into the oil-generative window. The lithologies identified as the potential source rock in the Flemish Pass Basin include Kimmeridgian-age organic rich shales (Egret Member of Rankin Formation; e.g., Mizzen O-16, Baccalieu I-78). Seismic stratigraphic correlations with the Flemish Pass and Orphan basins strongly

suggest that rocks with similar acoustic character and extent which are correlated with the Jurassic source rocks in the Flemish Pass Basin also occur within the north-south and/or northeast-southwest trending deep basins of the Orphan Basin. Whether or not similar lithologies also exist in the Orphan Basin is conjectural, and awaits drilling and ground-truthing of the deep basinal successions. The successions drilled (but not yet released) in the Great Barasway F-66 well might provide the much needed information regarding the presence of potential source rock in the Orphan Basin, and the quality and nature of the organic matter stored within the potential source rock. These data will further enlighten the community regarding the degree of exposure to thermal maturation of the source rock. The geothermal gradient along the northern portion of the Grand Banks of Newfoundland is relatively high ($\sim 25^\circ \text{ km}^{-1}$) and the depth of burial of the pre-Early Cretaceous successions within the Orphan Basin (*sensu lato*, east and west) is deep (4-5 km); therefore, it is very likely that the potential source in these regions entered the oil generative window.

6.5. Recommendations For Future Work

There are several important questions regarding the oil and gas potential of the Orphan Basin that await answers:

- What is the source of the oil shows reported in the Flemish Pass Basin? Can we unequivocally determine that it is exclusively Late Jurassic Egret equivalent rocks? Also, is it possible to have a mature Paleozoic source rock in the region? Are any younger source rocks present?

- When did the potential source rock within the deep Orphan Basin (*sensu lato*) enter the oil generative window? Can we use a predictive approach to estimate the timing of oil and gas generation (also see below)?
- Were large-scale structures already formed when the source rock entered the oil generative window? Is so, there exists the potential for major oil accumulation within the region.
- What were the conduits for the evolving oil and gas? Were faults originally leaky, but tight later in their evolution?

The answers for these questions were beyond the scope of this thesis. However, the following recommendations for future work can be made.

- The exploration wells in the Orphan and Flemish Pass Basins have bottom hole temperatures measured. A study should be carried out which uses a) the bottom hole temperatures to determine the thermal structure of the Orphan and Flemish Pass basins and b) the sedimentary and stratigraphic information from exploration wells to determine the subsidence history, so that the timing of the oil generative window can be predicted. This information can then be used to better understand the timing of migration into traps and the risk of trap preservation.
- When the new borehole data from Great Barssasway F-66, Mizzen L-11 and O-16 become public, petrophysical analysis can be done on the well logs to determine the characteristics and quality of the source and

reservoir rocks. Also geochemical studies can be done on the collected cores and thin sections to determine the distribution of source and reservoir rocks.

CHAPTER 7. CONCLUSIONS

The interpretation of approximately 25,000 km of multi-channel seismic reflection profiles, evaluated using the stratigraphy and sedimentary data from nine key exploration wells revealed the following salient conclusions:

1. The evolution of the Orphan Basin and environs is recorded in five seismic stratigraphic units (Z, A, B, C, X), each separated from one another by widespread regional markers U1-U4, representing prominent unconformities.
 - Unit Z is characterized by a variable seismic signature, and includes Precambrian and Paleozoic basement successions, consisting of diverse lithologies ranging from metasedimentary to intrusive rocks. This unit is bounded at its top by the regional marker U1 which is correlated with the top Paleozoic Unconformity.
 - Unit C is characterized by either parallel to sub-parallel reflections or an internal configuration marked by steeply dipping reflections, which are the result of the rotation and tilting of major extensional fault blocks. This unit is comparatively well developed in the southeastern portion of the study area. The correlation with the borehole data suggests that Unit C successions are predominantly of Jurassic age. The upper boundary of this unit is correlated to be the top Jurassic (Tithonian) Unconformity).
 - Unit B is often represented by high amplitude, strong and continuous reflections. It is thickest in the east and thins along the western margin of the

Orphan Basin. This unit includes mainly Early Cretaceous age successions which are mostly covered by the regional Mid-Cretaceous (Cenomanian) Unconformity.

- Unit A is characterized by strong high amplitude reflections, which show notable lateral continuity across the study area. This unit is thickest in the eastern portion of the Orphan Basin. Unit A successions are correlated to be Late Cretaceous in age and are capped by the regional Base Tertiary Unconformity.
 - Unit X represents the uppermost Tertiary age strata within the study area. It is characterized by strong to very strong high amplitude reflections. The top of Unit X corresponds to the sea floor. Unit X is generally thickest on the shelf but progressively thins toward the basin.
2. The regional correlation between the key wells from the Orphan, Flemish Pass and Jeanne d'Arc Basins indicated that the Jurassic is well developed in the eastern Orphan and Flemish Pass Basins. The data further suggest that Jurassic sediments may be widespread in the deep basinal settings of the western portion of the Orphan Basin. The structural architecture of the basement Unit Z and the seismic character of the overlying successions with steeply dipping tilted and rotated reflections within fault blocks also provide circumstantial support for the presence of Jurassic successions in the western portion of the Orphan Basin.
 3. The extensional tectonic activity continued in the study area throughout the Cretaceous, but slowly culminated in the late Cretaceous/early Tertiary as

indicated by the absence of growth strata within the Tertiary succession associated with the faults, and tip points of these faults being situated in the Early Tertiary successions.

4. The tectonic architecture of the Orphan Basin and environs reflects a long and multi-phase rifting history, including both extensional and strike-slip tectonism. On the basis of stratigraphic and structural architecture, the successions below the Base Tertiary Unconformity in the Orphan Basin are broadly divided into five tectonic provinces; (1) the Western and Southwestern Basin Margin, (2) the Eastern Basin Margin, (3) the White Sail Fault Zone, (4) the West Basin and Ridge Province, and (5) the East Basin.
 - The Western and Southwestern Basin Margin is characterized by a broad wide zone consisting of several roughly north-south trending east-dipping listric normal faults, which separate the Bonavista Platform in the west from the Orphan Basin in the east. The southern portion of this zone progressively swings toward the southeast, and forms a major zone, the Cumberland Belt Transfer Zone, separating the Orphan and Flemish Pass Basins in the north from the Jeanne d'Arc Basin in the south. This zone sinistrally offset the Orphan Basin from the Jeanne d'Arc Basin. Regional correlations with the Jeanne d'Arc Basin reveal the presence of a number of smaller, but similar trending strike-slip zones such as, the Nautilus Fault Zone and the Egret Fault Zone. This interpretation suggests that the northward propagation of the Late

Triassic Early – Jurassic Rifting separated the basins from one another by regional strike-slip transfer faults.

- Eastern Basin Margin is characterized by 4-5 northeast-southwest trending listric normal faults. The hanging wall of many of these faults show prominent growth stratal wedges in Units B and A (i.e., the Cretaceous) within rotated and tilted blocks. These faults display a progressively westward-increasing extensional separation on the Top Jurassic Unconformity, creating a staircase morphology along the easternmost boundary of the Orphan Basin.
 - The White Sail Fault Zone is a major listric normal fault zone. It partitions the Orphan Basin into two morpho-tectonic provinces, referred to as the West Basin and Ridge Province and the East Basin Province. The significant growth of some of the Mesozoic successions and major rotated and tilted fault blocks over the pre-rift basement successions collectively suggest that this fault zone became reactivated numerous times since the Jurassic, with tectonically quiet intervals in between.
 - The West Basin and Ridge and the East Basin Provinces are characterized by numerous basement-cored ridges and their intervening basins bounded by major faults. Moreover, the East Basin Province also displays the growth strata and faulted block rotation and tilting evidence of reactivation.
5. The tectono-stratigraphic and morphological examinations of the study area suggest that during the Middle Jurassic, the Flemish Cap was situated within the

Orphan Basin (*sensu lato*), but began to progressively rotate in a clockwise direction during the Late Jurassic, migrating into its present position during the Late Cretaceous, with a 25°-35° of total rotation. The following lines of evidence are presented for this migration:

- The morphology of the Orphan Basin is distinctly skewed: it is ~60-75 km wide in the north, but becomes tapered to ~5-10 km wide towards the south and southeast;
- The hanging walls of faults in the northern and northeastern portion of the Orphan Basin show noticeably greater amounts of growth of Early to Late Cretaceous successions, than the faults in the southern portion of the basin;
- The observed preferential growth is complemented by much larger amounts of rotation and tilting of the fault blocks. This style is best observed in the northern segment of the White Sail Fault Zone as well as the northern segment of the East Basin Province.

REFERENCES

- Aksu, A. E., and Hiscott, R. N., 1992.** Shingled Upper Quaternary debris flow lenses on the NE Newfoundland slope. *Sedimentology* 39, p. 193–206.
- Arthur, K. R., Cole, D. R., Hendersong., G. L. & Kushnird, . W., 1982.** Geology of the Hibernia Discovery. In: *The Deliberate Search for the Subtle Trap* (Ed. by M. T. Halbouty), Mem. AAPG, vol. 32, p. 181-195.
- Alves, T.M., Motta, C., Sandnes, F., Cunha, T., Monteiro, J.H. Pinheiro, L.M. 2006.** Mesozoic-Cenozoic evolution of North Atlantic continental-slope basins: the Peniche basin, western Iberian margin. *AAPG Bulletin*, vol. 90 (1), p. 31–60.
- Bally, A. W., 1983.** Seismic expression of structural styles: *AAPG Studies in Geology* 15, p. 1-2.
- Berggren, W.A., Kent, D.V., Swisher, C.C., Aubry, M.-P. 1995.** A revised Cenozoic geochronology and chronostratigraphy. In: Berggren, W.A., Kent, D.V., Aubry, M.-P., and Hardenbol, J. (eds.), *Geochronology, Time Scales and stratigraphic correlation*. SEPM special publication No. 54, p. 129-212.
- Bowen, I.N.A., and Griffiths, P., 1979.** Well History – Abandonment Report, BP et al. Hare Bay E-21, December 1979.
- Boudreau, A. E., Mathez, E. A., and McCallum, I. S., 1986.** Halogen geochemistry of the Stillwater and Bushveld complexes: Evidence for transport of the platinum-group elements by Cl-rich fluids: *Journal of Petrology*, v. 27, p. 967–986.
- BP et al., 1974.** Well History – Suspension Report, BP Columbia Bonavista C-99.

- BP et al., 1975.** Well History – Abandonment Report, BP Columbia Bonavista C-99.
- BP Exploration, 1991.** Biostratigraphic study of Flemish Pass wells. Kyle L-11, British Petroleum Exploration. (C-NOPB File Number 8932-B003-001E).
- Brown, D. M., K. D. McAlpine, and R. W. Yole, 1989.** Sedimentology and sandstone diagenesis of the Hibernia Formation in the Hibernia oil field, Grand Banks of Newfoundland: AAPG Bulletin, v. 33, p. 557 –575.
- Bujak, J.P., Barss, M.S., and Williams, G.L., 1977a.** Offshore eastern Canada—Part I and II: Organic type and color and hydrocarbon potential. Oil Gas J. 75 No. 15, p. 96–100.
- Bujak, J.P., Barss, M.S., and Williams, G.L., 1977b.** Offshore eastern Canada—Part I and II: Organic type and color and hydrocarbon potential. Oil Gas J. 75 No. 15, p. 198–202.
- Canada-Newfoundland Offshore Petroleum Board, 2003.** Schedule of wells, Newfoundland offshore area. Available from <http://www.cnlopb.nl.ca>.
- Canada-Newfoundland and Labrador Offshore Petroleum Board (C-NLOPB), 2008.** Schedule of Wells index [online]. Available from <http://www.cnlopb.nl.ca>.
- Chadwick, R. A., 1985.** Seismic reflection investigations into the stratigraphy and structural evolution of the Worcester Basin. Journal of the Geological Society, London, 142, p. 187-202.
- Chaplin, C.E., Van Elsberg, J.N., Gourlay R.C.B., 1982.** Comparative lithologic and petrographic analyses of petroleum basement or adjacent rocks in: Mobil et al

Linnet E- 63, Mobil et al Sheridan J-87, Mobil et al Cumberland B-55, Mobil in house report, December 1982.

Chian, D., Marillier, F. Hall, J. and Quinlan, G., 1998. An improved velocity model for the crust and upper mantle along central mobile belt of the Newfoundland Appalachian orogen and its offshore extension, *Can. J. Earth Sci.*, 35, p. 1238-1251.

Chian, D., Reid, I. and Jackson, H., 2001. Crustal structure beneath Orphan Basin and implications for nonvolcanic continental rifting, *J. Geophys. Res.*, 106(B6), p. 10923–10940.

Chough, S. K., and Hesse, R., 1976. Submarine meandering talweg and turbidity currents flowing for 4,000 km in the Northwest Atlantic Mid-Ocean Channel, Labrador Sea: *Geology*, v. 4, no. 9, p. 529-533.

Chough, S.K. and Hesse, R., 1980. The Northwest Atlantic mid-ocean channel of the Labrador Sea: III. Head spill vs. body spill deposits from turbidity currents on natural levees. *J. sedim. Petrol.*, 50, p. 227–234.

Coe, A., and K.D. Church, 2003. Sequence stratigraphy, in A. Coe, ed., *The sedimentary record of sea-level change*: Cambridge, Cambridge University Press, chapter 4, p. 57–98.

Davies, S.C., 1979. BP Research Centre, Exploration and Production Division, Paleontology Branch, The Biostratigraphy and paleoenvironments of the Hare Bay E-21 well, offshore Newfoundland, Canada, November 1979.

- de Voogd, B., C. E. Keen, and W. A. Kay, 1990.** Fault reactivation during Mesozoic extension in eastern offshore Canada: *Tectonophysics*, v. 173, p. 567–580.
- Deon, G. and Timmons, G., 2003.** Well history report, Mizzen L 11.
- Deptuck, M.E., 2003.** Post-rift geology of the Jeanne d'Arc basin, with a focus on the architecture and evolution of early Paleogene submarine fans, and insights from modern deep-water systems. Unpublished Ph.D. thesis, Dalhousie University, 241p.
- Deptuck, M.E., Steffens, G.S., Barton, M., and Pirmez, C., 2003.** Architecture and evolution of upper fan channel-belts on the Niger Delta slope and in the Arabian Sea, *Marine and Petroleum Geology* 20 (6–8), p. 649–676.
- DeSilva, N., 1993.** Sequence stratigraphy and hydrocarbon potential of Cenomanian–Eocene interval, Jeanne d'Arc Basin, offshore Newfoundland: *The Leading Edge*, v. 12, p. 694–697.
- DeSilva, N.R., 2000.** Flemish Pass basin; hydrocarbon prospectivity and potential deep water development, *Journal of Canadian Petroleum Technology* ; vol. 39; Issue: 6, p. 22-25.
- Dow, W. G., 1979.** Geochemical analysis of Texaco Shell et al Blue H-28 well, offshore Newfoundland: Robertson Research (U.S.) Inc. Report No. 90, Project: RUS/790/II/28 (Open file available from Canada Oil and Gas Lands Administration Branch, Dept. of Energy, Mines and Resources, Canada).

- Dow, W.G., Robertson Research (U.S.) Inc., 1982.** Geochemical Evaluation of the B.P. Hare Bay H-31 well, offshore Newfoundland, May 1982.
- Driscoll, N. W., J. R. Hogg, N. Christie-Blick, and G. D. Karner., 1995.** Extensional tectonics in the Jeanne d'Arc Basin, offshore Newfoundland: Implications for the timing of break-up between Grand Banks and Iberia, in R. A. Scrutton, R. A. Stoker, G. B. Shimmield, and A. W. Tudhope, eds., The tectonics, sedimentation and palaeoceanography of the North Atlantic region: Geological Society (London) Special Publication 90, p. 1-28
- Enachescu, M.E., 1986.** Integrated geophysical study of Newfoundland continental margin (East Coast Canada). Society of Exploration Geophysicists, 56th annual meeting, SEG Abstracts, p. 488-492.
- Enachescu, M. E., 1987.** Tectonic and structural framework of the Northeast Newfoundland continental margin, Sedimentary basins and basin-forming mechanisms, (Eds) Beaumont, Christopher and Tankard, Anthony J. Basins of Eastern Canada and worldwide analogues, CSPG Memoir 12, Atlantic Geoscience Society Special Publication, vol. 5, p. 117-146.
- Enachescu, M. E., 1988.** Extended basement beneath the intracratonic rifted basins of the, Grand Banks of Newfoundland, Journal of the Canadian Society of Exploration Geophysicists, vol. 24, no. 1, p. 48-65.
- Enachescu, M.E., 1992.** Enigmatic basins offshore Newfoundland: Can. J. Expl. Geophys., vol. 28, p. 44-61.

- Enachescu, M.E., 1993.** Amplitude interpretation of 3-D reflection data, *The Leading Edge* 12, p. 678–685.
- Enachescu, M.E., Meyer, K.E., and Hogg, J.R., 2004a.** The East Orphan Basin, offshore Newfoundland and Labrador: A deepwater super extended rift with hydrocarbon potential. Canadian Society of Petroleum Geology Conference, Calgary, AB, Expanded Abstract.
- Enachescu, M.E., Hogg, J.R., and Meyer, K.E., 2004b.** Orphan Basin, offshore Newfoundland, Canada: Structural and tectonic framework, petroleum system and exploration potential. Canadian Society of Exploration Geophysicists, Annual Meeting, Calgary, AB, Expanded Abstract.
- Enachescu, M.E., Kearsey, S., Hogg, J., Einarsson, P., Nader, S., and Smee, J., 2004c.** Orphan Basin, offshore Newfoundland, Canada: Structural and tectonic framework, petroleum system and exploration potential. SEG 74th Annual Meeting and Exposition, Denver, Colorado, Expanded Abstract.
- Enachescu, M.E., Kearsey, S., Hardy, V., Srivastava, S., Sibuet, J., Hogg, J., Meyer, K., Fagan, P., and Thompson, T. and Ferguson, R., 2005.** Evolution and petroleum potential of Orphan Basin, offshore Newfoundland, and its relation to the movement and rotation of Flemish Cap based on plate kinematics of the North Atlantic. GCSSEPM Perkins Conference, Petroleum Systems of Divergent Continental Margin Basins, paper on CD-Rom, 25 figs, 1 table, p. 75-131

- Enachescu, M.E., 2006.** Structural setting and petroleum potential of the Orphan Basin, offshore Newfoundland and Labrador, *Recorder*, 31(2), p. 5–13.
- Esso Parex et al., 1986.** Well history reports. Kyle L-11(C-NOPB File Number 10275).
- Falvey, D. A., 1974.** The development of continental margins in plate tectonic theory: *APEA Jour.*, v. 14, p. 95-10.
- Falvey, D. A., and Middleton, M. F., 1981.** Passive continental margins: Evidence for a pre-breakup deep crustal metamorphic subsidence mechanism. *Oceanologica Acta*, 1981, Proceedings of 26th International Geological Congress, Geology of Continental Margins Symposium, Paris, 7–17 July, p. 103–114.
- Geochem Laboratories Ltd., 1985.** Hydrocarbon Analysis on BP Baie Verte, Prepared for BP.
- Gradstein, F.M., Thomas, F.C., 1983.** Stratigraphy and depositional environment of Texaco Blue H-28. Report No. EPGs-PAL.1-83FMG/FCT, 3 p.
- Gradstein, F.M., Jansa, L. F., Srivastava, S.P., Williamson, M.A., Bonham-Carter, G., and Stam, B., 1990.** Aspects of north Atlantic paleo-oceanography. In *Geology of the continental margin of Eastern Canada*. Edited by M.J. Keen and G.L. Williams.
- Gradstein, F. M., Agterberg, F. P., Ogg, J. G., Hardenbol, J., van Veen, P., Thierry, J., and Huang, Z., 1995.** A Triassic, Jurassic, and Cretaceous time scale, in W. A. Berggren, D. V. Kent, and J. Hardenbol, eds., *Geochronology, time scales, and global stratigraphic correlations: SEPM Special Publication 54*, p. 129-212.

- Grant, A.C., 1972.** The continental margin off Labrador and eastern Newfoundland--Morphology and geology: Canadian Jour. Earth Sci., v. 9, p. 1394-1430.
- Grant, A.C., Jansa, L.F., McAlpine, K.D., and Edwards, A., 1988.** Mesozoic-cenozoic geology of the eastern margin of the Grand Banks and its relation to the Galicia Bank. In Boillot, G., Winterer, E.L., et al., Proc. ODP, Sci. Results, 103, College Station, TX (Ocean Drilling Program), p. 787-808.
- Grant, A.C. and McAlpine, K.D. 1990.** The Continental margin around Newfoundland, In Geology of the Continental Margins of Eastern Canada, M.J. Keen and G.L. Williams (eds.); Geological Survey of Canada, Geology of Canada, no. 2, p. 239-292.
- Grant, A.C. and McAlpine, K.D., 1990.** The continental margin around Newfoundland--la marge continentale autour de terre-neuve. In Geology of the continental margin of Eastern Canada--Geologie de la marge continentale de l'est du Canada Edited by M.J. Keen and G.L. Williams.
- Hardy, V., 2007.** Cretaceous evolution and seismic stratigraphy of the Orphan Basin. MSc Thesis (Geophysics), Memorial University of Newfoundland.
- Haworth, R., and Keen, C., 1979.** The canadian atlantic margin, a passive continental margin encompassing an active past, 59, p. 83-126.
- Hesse, R. 1992.** Continental Slope sedimentation adjacent to an Ice Margin. I. Seismic facies of Labrador Slope. Geo-Marine Letters , 12, p. 189-199.

- Hiscott, R.N., Wilson, R.C.L., Gradstein, F.M., Pujalte, V., García-Mondéjar, J., Boudreau, R.R., and Wishart, H.A., 1990.** Comparative stratigraphy and subsidence history of Mesozoic rift basins of North Atlantic. AAPG Bull., 74, p. 60-76.
- Hubbard, R. J., Pape, J., and Roberts, D. G., 1985.** Depositional sequence mapping to illustrate the evolution of a passive continental margin: AAPG Memoir 39, p. 93-115.
- Hubbard, J., 1988.** Age and significance of sequence boundaries on Jurassic and Early Cretaceous rifted continental margins. Bull. Am. Ass. Petrol. Geol., 72, p. 49-72.
- Jansa, L.F., Gradstein, F.M., Harris, I.M., Jenkins, W.A., and Williams, G.L., 1976.** Stratigraphy of the Amoco-IOE Murre G-67 well, Grand Banks of Newfoundland. In Geological Survey of Canada, Paper 75-30, p. 1-14.
- Jansa, L.F., Gardner J.V., and Dean, W.E., 1977.** Mesozoic sequences of the central North Atlantic. In: Y. Lancelot, E. Seibold et al. Initial Reports of the Deep Sea Drilling Project, v **vol. XLI**, U.S. Government Printing Office, Washington, p. 991-1010.
- Jansa, L.F. and Pe-Piper, G., 1986.** Geology and Geochemistry of middle Jurassic and early Cretaceous igneous rocks on the eastern north American continental shelf. Geological Survey of Canada Open File Report No. 1351, 104p.

- Jansa, J. F., and Wade, J. A., 1975.** Geology of the continental margin off Nova Scotia and Newfoundland. In: Offshore Geology of Eastern Canada, Geological Survey of Canada, Paper 74-30, 2, p. 51-105.
- Keen, C.E., and Barrett, D.L., 1981.** Thinned and subsided continental crust on the rifted margin of eastern Canada: crustal structure, thermal evolution and subsidence history: *Geophysical Journal of the Royal Astronomical Society*, v. 65, p. 443-465.
- Keen, C.E., Stockmal, G.S., Welsink, H., Quinlan, G., and Mudford, B., 1987.** Deep crustal structure and evolution of the rifted margin northeast of Newfoundland; results from Lithoprobe East. *Canadian Journal of Earth Sciences = Journal Canadien des Sciences de la Terre*, 24, p.1537-1549.
- Keen, C.E., Loncarevic, B.D., Reid, I., Woodside, J., Haworth, R.T., and Williams, H., 1990.** Tectonic and geophysical overview--tectonique et geophysique regionales. In *Geology of the continental margin of Eastern Canada--Geologie de la marge continentale de l'est du Canada* Edited by M.J. Keen and G.L. Williams. Geological Society of America, United States (USA),
- Keen, C.E., Beaumont, C., 1990.** Geodynamics of rifted continental margins. In: Keen, M.J., Williams, G.U. (Eds.), *Geology of the Continental Margin of Eastern Canada*. Geological Survey of Canada, *Geology of Canada* 2, p. 393-472
- Kennard, C. Schafer and L. Carter, 1990.** Late Cenozoic evolution of Sackville Spur; a sediment drift on the Newfoundland continental slope, *Canadian Journal of Earth Sciences* 27, p. 863-878.

King, E.L., Fader, G.B.J., Sonnichsen, G.V., 2001. Contrasts in glacial regimes on the northern Grand Banks of Newfoundland and northeast Newfoundland Shelf, Vol. 26. GAC-MAC Joint Annual Meeting, St. John's, Newfoundland, May 27–30, 2001, p. 78 (Abstracts).

Koning, T., Campbell, R.H., Hibbs, D.C., Leonhardt, G.W., and Williams, A., 1988. An exploration case study of a world record deepwater wildcat well drilled in the Orphan Basin, Newfoundland; Blue H-28. Twentieth annual Offshore Technology Conference, Proceedings - Offshore Technology Conference, 20: 395-406. Houston, Texas.

Louden, K., 2002. Tectonic evolution of the east coast of Canada. Canadian Society of Exploration Geophysicists Recorder p. 37-48

Mackay, A.H. and Tankard, A.J., 1990. Hibernia oil field – Canada, Jeanne d'Arc Basin, Grand Banks offshore Newfoundland: Structural Traps III, Tectonic Fold and Fault Traps, Treatise of Petroleum Geology, Atlas of Oil and Gas Fields, p. 145-175.

McAlpine, K.D., 1990. Mesozoic stratigraphy, sedimentary evolution, and petroleum potential of the Jeanne d'Arc Basin, Grand Banks of Newfoundland. Paper - Geological Survey of Canada, vol: 50, p. 89-17.

McIver, N. L., 1972. Cenozoic and Mesozoic Stratigraphy of the Nova Scotia Shelf; Canadian Journal of Earth Sciences = Revue Canadienne des Sciences de la Terre, 1972, Vol. 9, Issue 1, p. 54-70.

- McKenzie, D., 1978.** Some remarks on the development of sedimentary basins: Earth and Planetary Sci. Letters, v. 40, p. 25-3.
- McKenzie, D. P., 1980.** The variation of temperature with time and hydrocarbon maturation in sedimentary basins formed by extension. Earth Planet. Sci. Lett., 55, p. 87-98.
- Mitchum, Jr. R.M., Vail P.R. and Thompson, S., 1977a.** Seismic stratigraphy and global changes of sea-level, part 2: the depositional sequence as a basic unit for stratigraphic analysis. In: C.E. Payton, Editor, Seismic Stratigraphy—Applications to Hydrocarbon Exploration American Association of Petroleum Geologists Bulletin vol. 26, Society for Sedimentary Geology, p. 53-62.
- Mitchum, R. M., Jr., Vail, P. R. and Sangree, J. B., 1977b.** Seismic stratigraphy and global changes of sea level, part 6: stratigraphic interpretation of seismic reflection patterns in depositional sequences, in C. E. Payton, ed., Seismic stratigraphy--applications to hydrocarbon exploration: AAPG Memoir 26, p. 117-133.
- Mobil et al., 1983.** Biostratigraphy and paleecology report for Linnet E-63.
- Myers, K.J. and Milton, N.J., 1996.** Concepts and principles of sequence stratigraphy. In: D. Emery and K.J. Myers, Editors, Sequence Stratigraphy, Blackwell Science, p. 11-44.
- Myers, R.A., and Piper, D.J.W., 1988.** Seismic stratigraphy of late Cenozoic sediments in the northern Labrador Sea: a history of bottom circulation and glaciation. Can. J. Earth Sci. 25, p. 2059-2074.

- Piper, D.J.W. and Hundert, A.T., 2002.** Stratigraphic record on the Sohm Abyssal Plain of detritus from the Wisconsinan glaciation in eastern Canada, *Geo-Mar. Lett.* 22, p. 75–85.
- Piper, D.J.W., 2005.** Late Cenozoic evolution of the continental margin of eastern Canada, *Norwegian J. Geol.* 85 (2005), p. 305–318.
- Pocock, A.J.S., 1986.** Palynology of samples from the Baccalieu I-78 Well. 48 00 N: 46 00 W. Additions and Corrections to March 16 1986.
- Posamentier, H.W., Jervey, M. T., and Vail, P. R., 1988.** Eustatic controls on clastic deposition I—Conceptual framework, in Wilgus, C. K., et al., eds., *Sealevel changes: An integrated approach: Society of Economic Paleontologists and Mineralogists Special Publication 42*, p. 109-124.
- Powell, T. G., 1985.** Paleogeographic implications for the distribution of Upper Jurassic source beds: offshore eastern Canada: *Bulletin of Canadian Petroleum Geology*, v. 33, p. 116-119.
- Reston, T.J., 2008.** The structure, evolution and symmetry of the magma-poor rifted margins of the North and Central Atlantic: A synthesis. In press in *Tectonophysics*.
- Robertson Research Canada Limited; Dolby, G., Oliver, E.M., and Thorne, B.V.A., 1979.** Exploration Report No. 205 for Texaco Canada Inc., The micropaleontology, palynology and stratigraphy of the Texaco et al. Blue H-28 well, October 1979.

- Robertson Research (U.S.) Inc; Dow, W. G., 1979.** Report No. 90, prepared for Texaco Canada Inc., Geochemical Analysis of the Texaco Blue H-28 well, offshore Newfoundland, October 1979.
- Robertson Research (U.S.) Inc., Dow, W.G., 1982.** Geochemical Evaluation of the B.P. Hare Bay H-31 well, offshore Newfoundland, May 1982.
- Robertson Research Canada Limited; Charnock, M.A., Robertson, A.G., Shipp, D.J., Tooby, K.M., Varol, O., 1985.** The biostratigraphy of Baie Verte J-57 well, Offshore eastern Canada.
- Shaw, J., 2006.** Palaeogeography of Atlantic Canadian Continental Shelves from the Last Glacial Maximum to the present, with an emphasis on Flemish Cap. *J. Northw. Atl. Fish. Sci.* 37, p. 119–126.
- Sherwind, . F., 1973.** Scotian Shelf and Grand Banks. In: *Future Petroleum Provinces Canada* (Ed. by R. G. McCrossan), Mem. Can. Soc. Peiml, 1, p. 519-559.
- Shimeld, J.W., MacRae, R.A., Wielens, J.B.W., 2000.** Sequence stratigraphy and hydrocarbon potential of regional Upper Cretaceous limestone units, offshore eastern Canada. *GeoCanada 2000*, Calgary, Alberta, Abstract 784.
- Sibuet, J.-C., Srivastava S. and Manatschal, G., 2007.** Exhumed mantle-forming transitional crust in the Newfoundland–Iberia rift and associated magnetic anomalies, *J. Geophys. Res.* 112, p. B06105

- Sinclair, I.K., 1988.** Evolution of Mesozoic-Cenozoic sedimentary basins in the Grand Banks area of Newfoundland and comparison with Falvey's (1974) rift model. *Bulletin of Canadian Petroleum Geology*, 36, p. 255-273.
- Sinclair, I. K., 1992.** Sequence stratigraphic response to Aptian-Albian rifting in conjugate margin basins: a comparison of the Jeanne d'Arc Basin, offshore Newfoundland and the Porcupine Basin, offshore Ireland. In: Programme with Abstracts. The Tectonics, Sedimentation and Palaeoceanography of the North Atlantic Region, Conference, Edinburgh, p. 28-29.
- Sinclair, I.K., McAlpine, K.D., Sherwin, D.F., McMillan, N.J., Taylor, G.C., Best, M.E., Campbell, G.R., Hea, J.P., Henao, D., and Procter, R.M., 1992.** Petroleum resources of the Jeanne d'Arc Basin and environs, Grand Banks, Newfoundland--Ressources petrolieres du Bassin de Jeanne d'Arc et des environs, Grand Bancs, Terre-Neuve. 92-08, Geological Survey of Canada, Ottawa, ON, Canada (CAN), Canada (CAN).
- Sinclair, I. K., 1993.** Tectonism: the dominant factor in mid-Cretaceous deposition in the Jeanne d'Arc Basin, Grand Banks. *Mar. petrol. Geol.*, 10, p. 530-149.
- Sinclair, I.K., Shannon, P.M., Williams, B.P.J., Harker, S.D., and Moore, J.G., 1994.** Tectonic control on sedimentary evolution of three North Atlantic borderland Mesozoic basins, *Basin Research*, 6: 193-217.
- Sinclair, I.K., 1995.** Sequence stratigraphic response to Aptian-Albian rifting in conjugate margin basins: a comparison of the Jeanne d'Arc Basin, offshore

Newfoundland and the Porcupine Basin, offshore Ireland. In: Scrutton, R.A., Stoker, M.S., Shimmeld, G.B., and Tudhope, A.W. (Eds), *The Tectonics, Sedimentation and Palaeoceanography of the North Atlantic Region*, Geol. Soc. Lond. Sp. Publ. 90, p. 29-49.

Sinclair, I. K. and Riley, L. A., 1995. Separation of Late Cimmerian rift and drift megasequences: a comparison of the Jeanne d'Arc Basin, Grand Banks and the Outer Moray Firth, North Sea, In: *Sequence Stratigraphy on the Northwest European Margin* (Eds R. J. Steel, V. L. Felt, E. P. Johannessen and C. Mathieu), Spec. Publ. Norm Petrol Soc. No. 5, p. 347–363.

Skogseid, J., Barnwell, A., Aarseth, E.S., Alsgaard, P.Co., Briseid, H.C., and Zwach, C., 2004. Orphan basin: Multiple failed rifting during early opening of the north Atlantic. *Eos. Trans., AGU*, Vol. 85, 2004 (17, Joint Assembly Suppl., Abstract T41B-03).

Sonderholm, M., Christiansen, F.G., Olsen, J.C., Planke, S., Bojensen-Koefoed, J.A., Dalhoff, F., Nielsen, R., Myklebust, R., and and Nohr-Hansen, H., 2003. Early rifting of the Labrador Sea and Baffin Bay: A new evidence from seismic, well and sea-bed data. AAPG International Conference and Exhibition Technical Program, Barcelona, (supplement), Abstract.

Smee, J.S., 2003. Hydrocarbon potential of parcels 1-12, C-NOPB call for bids NL, 03-1, Orphan Basin, offshore Newfoundland [online]. Available from <http://www.nr.gov.nl.ca/mines&en/oil/callforbids/contents.pdf>.

- Smee, J.S., Nader, S., Einarsson, P., Hached, R., and Enachescu, M., 2003.** Orphan Basin, offshore Newfoundland: New seismic data and hydrocarbon plays for a dormant frontier basin. CSEG/CSPG, Abstract.
- Srivastava, S.P., 1978.** Evolution of the Labrador Sea and its bearing on the early evolution of the North Atlantic. *Geophysical Journal of the Royal Astronomical Society*, 52, 313-357.
- Srivastava, S.P.; Sibuet, J.-C.; Cande, S.; Roest W.R. and Reid, I.D., 2000.** Magnetic evidence for slow spreading during the formation of the Newfoundland and Iberian margins, *Earth Planet. Sci. Lett.* **182** (2000), p. 61-76.
- Stanley, D. J., Swift, D. J. P., James, N. P., Sutton, R. G., 1972.** Late Quaternary progradation and sand "spillover" on the outer continental margin off Nova Scotia, southeast Canada: *Smithsonian Contr. Earth Sci.*, v. 8, 88 p.
- Stockmal, G.S. and Waldron, J.W.F., 1990.** Structure of the Appalachian deformation front in western Newfoundland: implications of multi-channel seismic reflection data. *Geology*, v. 18, p. 765-768.
- Swift, J. H., and J. A. Williams., 1980.** Petroleum source rocks: Grand Banks area, in A. D. Miall, ed., *Facts and principles of world petroleum occurrence: Canadian Society of Petroleum Geologists Memoir 6*, p. 567-587.
- Tankard, A.J. and Welsink, H.J., 1987.** Extensional tectonics and stratigraphy of Hibernia oil field, Grand Banks, Newfoundland, *AAPG Bulletin*, 71: 1210-1232.

- Tankard, A.J., and Welsink, H.J., 1988.** Extensional tectonics, structural styles and stratigraphy of the Mesozoic Grand Banks of Newfoundland. In Manspeizer, W. (Ed.), *Triassic-Jurassic Rifting: Continental Breakup and the Origin of the Atlantic Ocean and Passive Margins (Pt. A)*: Amsterdam (Elsevier), *Devl. in Geotect.*, 22:129-165.
- Tankard, A.J. and Welsink, H.J., 1989.** Mesozoic extension and styles of basin formation in Atlantic Canada; Extensional tectonics and stratigraphy of the North Atlantic margins. *AAPG Memoir*, 46 p. 175-195.
- Tankard, A.J. and Balkwill, H.R., 1989.** Extensional tectonics and stratigraphy of the North Atlantic margins; Introduction; Extensional tectonics and stratigraphy of the North Atlantic margins. *AAPG Memoir*, 46: 1-6.
- Tucholke, B.E., Austin, J. A. JR and Uchupi, E., 1989.** Crustal structure and rift-drift evolution of the Newfoundland Basin. In: *Extensional tectonics and stratigraphy of the North Atlantic Margin* (Ed. by A. J. Tankard and H. R. Balkwill), *Mem. Am. Ass. petrol. Geol.*, 46, p. 247-263.
- Tucholke, B.E., and McCoy, F.W., 1986.** Paleogeographic and paleobathymetric evolution of the North Atlantic Ocean. In Vogt, P.R, and Tucholke, B.E. (Eds.), *The Western North Atlantic Region. Geol. Soc. Am., Geol. of North Am. Ser.*, p. 589-602.
- Tucholke, B.E., Sibuet, J.-C., and Klaus, A., 2004.** *Proceedings of the Ocean Drilling Program, Initial reports, Volume 210.*

- Uchupi, E., 1968.** Atlantic continental shelf and slope of the United States Physiography. Prof. Pap. U.S. geol. Surv. 529-C, 30 p.
- van der Velden, A.J., van Staal, C.R., and Cook, F.A., 2004.** Crustal structure, fossil subduction and the tectonic evolution of the Newfoundland Appalachians: Evidence from a reprocessed seismic reflection survey: Geological Society America Bulletin, v. 116, p. 1485-1498.
- Wade, J. A., 1978.** The Mesozoic-Cenozoic history of the northeastern margin of North America: Offshore Technology Conf. Proc, v. 3, p. 1849-1858.
- Warren, J.S., 1976.** The morphology of two transverse channels on the northeast Newfoundland Shelf. Maritime Sediments 12, p. 19-32.
- Welford, J.K., and Hall, J., 2007.** Crustal structure across the Newfoundland rifted continental margin from constrained 3-D gravity inversion: Geophysical Jour. International, v.171, p.890-908.
- Welsink, H.J., Dwyer, J.D., and Knight, R.J., 1989.** Tectono-stratigraphy of the passive margin off Nova Scotia. In: Extensional Tectonics and Stratigraphy of the North Atlantic Margins A.J. Tankard and H.R. Balkwill, Editors, AAPG Mem. 46, p. 215-231.
- White, R.S., McKenzie, D.P., O'Nions, R.K., 1992.** Oceanic crustal thickness from seismic measurements and rare earth element inversion, J. Geophys. Res. 97, p. 19683-19715

- Wilcox, R. E., Harding, T.P., Seeley, d. R., 1973.** Basic wrench tectonics: American Association of Petroleum Geologists Bulletin, v. 57, p. 74-96.
- Williams, H., 1979.** Appalachian Orogen in Canada: Canadian Journal of Earth Sciences, v. 16, p. 792-807.
- Williams, H., 1995.** Geology of the Appalachian-Caledonian Orogen in Canada and Greenland: Geological Survey of Canada, Geology of Canada No. 6, 944 p.
- Williams, H., 2003.** Geologic Ancestors to the Atlantic: The Geology of Newfoundland, Quarterly, V.96, Issue 410, <http://www.newfoundlandquarterly.ca/fall03/rock.php>.
- Williams, H. and Hatcher, R.D., Jr., 1983.** Appalachian suspect terranes; contributions to the tectonics and geophysics of mountain chains. Memoir - Geological Society of America, 158, p. 33-53.
- Williams, H., Colman-Sadd, S.P., and Swinden, H.S. 1988.** Tectonic -stratigraphic subdivisions of central Newfoundland. In Current Research, Part B, Geological Survey of Canada, Paper 88-1B, p. 91-98.
- Williams, H., Dehler, S. A., Grant, A. C., and Oakey, G. N., 1999.** Tectonics of Atlantic Canada, Geoscience Canada, vol. 26, no. 2, p. 51-70.
- Williams, H., Dehler, S.A., Grant, A.C., and Oakey, G.N., 1999.** Tectonics of Atlantic Canada, Geoscience Canada, 26, p. 51-70.
- Williams, H., and Grant, A.C., 1998.** Tectonic Assemblages, Atlantic Region, Canada: Geological Survey of Canada, Tectonic Assemblages, Atlantic Region, Canada, Open File 3657, scale: 1:3,000,000.

- Williams, H., and Hiscott, R.N., 1987.** Definition of the Iapetus rift-drift transition in western Newfoundland: *Geology*, v. 15, p. 1044-1047.
- Williams, B.P.J., Shannon, P.M., and Sinclair, I.K., 1999.** Comparative Jurassic and Cretaceous tectono-stratigraphy and reservoir development in the Jeanne d'Arc and Porcupine basins. *Petroleum geology of Northwest Europe; Proceedings of the 5th Conference, Petroleum Geology of Northwest Europe: 5: 487-499.*
- Williams, G.L., Ascoli, P., Barss, M.S., Bujak, J.P., Davies, E.H., Fensome, R.A. and Williamson, M.A. 1990.** Biostratigraphy and related studies: Offshore eastern Canada. Chapter 3 in M.J. Keen and G.L. Williams (eds.), *Geology of the Continental Margin off Eastern Canada. Geological Survey of Canada, Geology of Canada, no. 2, p. 89-137 (also Geological Society of America, The Geology of North America, v. I-1).*
- Williams, G.L., 1975.** Palynological analysis of B.P. Bonavista C-99, East Newfoundland. Report No. EPGs-PAL.34-75GLW, 4 p
- Wilson, R.C.L., Hiscott, R.N., Willis, M.G., and Gradstein, F.M., 1989.** The Lusitanian Basin of west-central Portugal: Mesozoic and Tertiary tectonic, stratigraphic and subsidence history. In Tankard, A.J., and Balkwill, H.R. (Eds.), *Extensional Tectonics and Stratigraphy of the North Atlantic Margins. AAPG Mem., 46, p. 341-361.*

Ziegler, P.A., 1989. Evolution of the North Atlantic—an overview In: A.J. Tankard and H.R. Balkwill, Editors, Extensional Tectonics and Stratigraphy of the North Atlantic Margins, AAPG Memoir 46 (1989), p. 111–129.

Ziegler, P.A., 1999. Evolution of the Arctic–North Atlantic and the Western Tethys, AAPG Bulletin 1999, 43, p. 164–196.

APPENDIX A

List of exploration companies involved in the drilling of wells in the Orphan and Jeanne d'Arc Basins, listed according to wells, and the company responsible for the drilling.

A.1.1 Blue H28 – Texaco et al., 1979

Texaco Canada Incorporated

Shell Canada Limited

Petro-Canada Incorporated

Home Oil Corporation Limited

Dome Petroleum Limited

Hudson's Bay Oil and Gas Company Limited

A.1.2 Hare Bay E-21 – BP et al., 1979

British Petroleum Canada Energy Company

Gulf Canada Resources Limited

Chevron Canada Resources

Columbia Gas Development of Canada

Petro-Canada Incorporated

A.1.3 Baie Verte J-57 – BP et al., 1985

British Petroleum Canada Energy Company

Chevron Canada Resources

Columbia Gas Development of Canada

Beau Canada Exploration Limited

A.1.4 Bonavista C-99 – BP and Columbia Gas, 1974

British Petroleum Canada Energy Company

Columbia Gas Development of Canada

A.1.5 Linnet E-63 – Mobil Oil et al., 1982

Mobil Oil Canada Limited

Petro-Canada Incorporated

Gulf Canada Resources Limited

Pan-Canadian Oil

Norcen Energy Resources Limited

Canterra Energy Limited

Roxy Petroleum

A.1.6 Mizzen L-11 – Petro-Canada et al., 2003

Petro-Canada Incorporated

ExxonMobil Canada

Chevron Canada Resources

Texaco Canada Incorporated

EnCana Corporation

Norsk Hydro Canada Oil and Gas Incorporated

A.1.7 Baccalieu I-78 – ESSO et al., 1985

ESSO Resources Canada Limited

Parex Production Incorporated

AT&S Exploration Limited

Trillium Exploration Corporation

Canterra Energy Limited

Mobil Oil Canada Limited

Norcen Energy Resources Limited

North Canadian Oil Limited

Roxy Petroleum

Beau Canada Exploration Limited

Alberta Energy Company Limited

MLC Oil and Gas

Comaplex Minerals Corporation

Voyager Energy Limited

A.1.8 Kyle L-11 – ESSO, 1986

ESSO Resources Canada Limited

A.1.9. Bonanza M-71 Mobil et al, 1983

Mobil Oil Canada Limited

Gulf Canada Resources Limited

Petro-Canada Incorporated

Pan-Canadian Oil

Norcen Energy Resources Limited

Canterra Energy Limited

Roxy Petroleum

APPENDIX B

Table of wells in Orphan, Flemish Pass and Jeanne d'Arc basins showing the depths of formation tops and bottoms (mbsf). The depth informations collected from C-NLOPB Schedule of Wells (2007) and C-NLOPB Database (2007, 2008). These lithological picks were loaded into Landmark Software for time-depth conversions, creating synthetic seismograms and seismic sequence interpretation purposes.

Well Name	Depth Type (mbsf)		Formation / Unconformity
	Top	Bottom	
Blue H-28			
		4910	BANQUEREAU FM
	4910	4910	<i>(BASE TERTIARY UNCONFORMITY)</i>
	4910	5281	DAWSON CANYON FM
	4910	5124	FOX HARBOUR/OTTER BAY MB
	5281	5281	<i>(FAULT OR UNCONFORMITY)</i>
	5281	6103.1	METASEDIMENTS BASEMENT
Baie Verte J-57			
		3964	BANQUEREAU FM
	3964	3964	<i>(BASE TERTIARY UNCONFORMITY)</i>
	3964	4911	DAWSON CANYON FM
	3964	4667	FOX HARBOUR/OTTER BAY MB
Bonavista C-99			
		3628.5	BANQUEREAU FM
	3628.5	3628.5	<i>(BASE TERTIARY UNCONFORMITY)</i>
	3628.5	3679	DAWSON CANYON FM
	3634.5	3652	FOX HARBOUR/OTTER BAY MB
	3652	3676	(LIMESTONE)
	3676	3679	(MAROON SHALE)
	3679	3679	<i>(CENOMANIAN UNCONFORMITY)</i>
	3679	3779	GRANITEPEGMATITE ?GRANITE WASH BSMNT

Cumberland B-55			
		3685	BANQUEREAU FM
	3652	3685	(PALEOCENE CHALK)
	3685	3685	(<i>BASE TERTIARY UNCONFORMITY</i>)
	3685	3706.5	FOX HARBOUR/OTTER BAY MB
	3685	3706.5	DAWSON CANYON FM
	3706.5	3706.5	(<i>CENOMANIAN UNCONFORMITY</i>)
	3706.5	3728	WEATHERED ? BASEMENT
	3728	4136.5	METASEDIMENTS BASEMENT
Hare Bay H-21			
		3241	BANQUEREAU FM
	3241	3241	(<i>BASE TERTIARY UNCONFORMITY</i>)
	3241	3398	DAWSON CANYON FM
	3241	3362	FOX HARBOUR/OTTER BAY MB
	3398	3398	(<i>CENOMANIAN UNCONFORMITY</i>)
	3398	4874	BARACHOIS (PENNSYLVANIAN)
Linnet E-63			
		2542	BANQUEREAU FM
	2514	2542	TILTON MB
	2542	2542	(<i>BASE TERTIARY UNCONFORMITY</i>)
	2542	2913	DAWSON CANYON FM
	2586	2913	FOX HARBOUR/OTTER BAY MB
	2913	2913	(<i>CENOMANIAN UNCONFORMITY</i>)
	2913	4175	NAUTILUS FM
	3758	4084	SANDSTONE & SHALE
	4084	4175	SHALE
	4175	4520.2	METASEDIMENTS BASEMENT
Sheridan J-87			
		4509	BANQUEREAU FM
	4424	4509	TILTON MB
	4509	4509	(<i>BASE TERTIARY UNCONFORMITY</i>)
	4509	4539	DAWSON CANYON FM
	4539	4667	WYANDOT FM

	4667	4678	PETREL MB
	4857	4857	(CENOMANIAN UNCONFORMITY)
	4857	5486.4	METASEDIMENTS BASEMENT
Baccalieu I-78			
		1706	BANQUEREAU FM
	1706	2120	BARREMIAN SHALES & THIN SANDSTONES
	1706	1706	(BASE TERTIARY UNCONFORMITY)
	2120	2257	AVALON EQUIV
	2257	3190	WHITEROSE/HIBERNIA UPPER ZONE EQUIV
	3190	3274	HIBERNIA LOWER ZONE EQUIV
	3274	3727	FORTUNE BAY EQUIV
	3727	3770	JEANNE D'ARC EQUIV
	3770	3770	(TITHONIAN UNCONFORMITY)
	3770	5135	RANKIN FM
	4398	4804	(UPPER KIMMERIDGIAN SOURCE ROCK)
	4975	5135	(LOWER KIMMERIDGIAN SOURCE ROCK)
Dominion O-23			
		3173	BANQUEREAU FM
	3133.5	3173	(PALEOCENE CHALK)
	3173	3173	(BASE TERTIARY UNCONFORMITY)
	3173	3997.8	FORTUNE BAY FM
Bonanza M-71			
		3460	BANQUEREAU FM
	3451	3460	(PALEOCENE CHALK)
	3460	3460	(BASE TERTIARY UNCONFORMITY)
	3460	4240	FORTUNE BAY FM
	4240	4240	(TITHONIAN UNCONFORMITY)
	4240	4462	(UPPER KIMMERIDGIAN SOURCE ROCK)
	4240	5282	RANKIN FM
	4462	4568	("LOWER TEMPEST" SANDSTONES)
	4690	5282	(LOWER KIMMERIDGIAN SOURCE ROCK)
	5282	5282	(FAULT OR UNCONFORMITY ?)
	5282	5294.7	(METASEDIMENTS BASEMENT)

Kyle L-11			
		1946	BANQUEREAU FM
	1946	2368	(BARREMIAN SHALES & MARLSTONES)
	1946	1946	(<i>BASE TERTIARY UNCONFORMITY</i>)
	2368	2627	AVALON EQUIV
	2627	3207	WHITEROSE/UPPER ZONE HIBERNIA EQUIV
	3207	3379	HIBERNIA LOWER ZONE EQUIV
	3379	3517	FORTUNE BAY EQUIV MARLSTONES
	3517	4200	(METASEDIMENTS BASEMENT)
	3517	3517	(<i>TITHONIAN UNCONFORMITY</i>)
Mizzen L-11			
	2522	2522	(<i>BASE TERTIARY UNCONFORMITY</i>)
	2522	2581	NAUTILUS EQUIV
	2581	3335	WHITEROSE EQUIV
	3335	3508	("BACCALIEU SANDSTONE")
	3508	3598	(LATE JURASSIC)
	3598	3741	(LATE JURASSIC SANDSTONE)
	3741	3823	RANKIN EQUIV
Panther P-52			
		2653	BANQUEREAU FM
	2642	2653	(PALEOCENE CHALK)
	2653	2653	(<i>BASE TERTIARY UNCONFORMITY</i>)
	2653	2835	FORTUNE BAY FM
	2835	2835	(<i>TITHONIAN UNCONFORMITY</i>)
	2835	4203.2	RANKIN FM
	2969	3256	("UPPER TEMPEST" SANDSTONES)
	3256	3566	(UPPER KIMMERIDGIAN SOURCE ROCK)
	3576	3758	("LOWER TEMPEST" SANDSTONES)
	3794	4003	(LOWER KIMMERIDGIAN SOURCE ROCK)
Lancaster G-70			
		3207	BANQUEREAU FM
	3200	3207	(TERTIARY LIMESTONE)
	3207	3207	(<i>BASE TERTIARY UNCONFORMITY</i>)

	3207	5194	RANKIN FM
	3207	3761	(UPPER KIMMERIDGIAN SOURCE ROCK)
	3764	3789	("LOWER TEMPEST" SANDSTONES)
	4736	4856	(LOWER KIMMERIDGIAN SOURCE ROCK)
	5194	5292	(SHALE TONGUE)
	5194	5701	VOYAGER FM
Gabriel C-60			
		2498	BANQUEREAU FM
	2498	2498	(<i>BASE TERTIARY UNCONFORMITY</i>)
	2498	2505	DAWSON CANYON FM
	2498	2505	WYANDOT
	2505	2505	(<i>CENOMANIAN UNCONFORMITY</i>)
	2505	2940	WHITEROSE EQUIV
	2875	2875	(<i>FAULT OR UNCONFORMITY</i>)
	2940	4553	HIBERNIA EQUIV
	4553	5171	FORTUNE BAY EQUIV
Conquest K-9			
		3225	BANQUEREAU FM
	3137	3225	TILTON MB
	3225	3225	(<i>BASE TERTIARY UNCONFORMITY</i>)
	3225	3883	DAWSON CANYON FM
	3316	3513	WYANDOT
	3556	3718	PETREL MB
	3883	3883	(<i>CENOMANIAN UNCONFORMITY</i>)
	3883	4968.3	FORTUNE BAY FM



